

Ph.D. in Medicine

Genetic determinants of ATR inhibitor sensitivity and resistance in Gastric Cancer

Marta Jessica Llorca Cardeñosa



Supervisors: Prof. Andrés M. Cervantes Ruipérez
Dra. Gloria Ribas Despuig

Valencia, April 2019



The **ROYAL MARSDEN**
NHS Foundation Trust

The co-Supervisors of the present doctoral Thesis, Dr. Andrés M. Cervantes Ruipérez, full professor of Medicine at the Faculty of Medicine of the University of Valencia and Dra. Gloria Ribas Despuig, Senior Associate Researcher of the Cancer Functional Genomics Group within the Department of Medical Oncology at the Biomedical Research Institute-INCLIVA certify that,

Marta Jessica Llorca Cardeñosa, graduated in Biology at The University of Valencia, Masters in “Molecular Approaches in Biomedical Sciences” at The University of Valencia and, funded by the Instituto de Salud Carlos III (Ministerio de Economía y Competitividad, FI16/00246), has carried out the present Doctoral Thesis “**Genetic determinants of ATR inhibitor sensitivity and resistance in Gastric Cancer**” and that, to their judgement, meets all the necessary requirements in order to qualify for the **PhD in Medicine** for which purpose it will be presented at the University of Valencia. The work has been done under their supervision, authorising its presentation before the Qualifying Court. And for this purpose, this certificate is extended.

Valencia, March 2019.

Thesis supervisors:

Prof. Andrés M. Cervantes Ruipérez
Faculty of Medicine,
University of Valencia

Dra. Gloria Ribas Despuig
Cancer Functional Genomics group
Biomedical Research Institute
INCLIVA

"I have not Failed. I have found a thousand ways that won't work"
Thomas Edison

Acknowledgements:

To my supervisors Gloria Ribas and Andres Cervantes for giving me the opportunity to join their group when I first started, and supporting me all this time;

to my Labo 3 colleagues Maider I., Maria P., Sara O., Maite M. and Pepa C., for all the good times we spent together, and for always supporting me and helping me in everything I needed;

to Irene Chong, for your generosity, positivity, support, and for believing in me when I needed it the most;

to Chris Lord, for sharing your always bright scientific vision, and for helping me to become more resilient and learn how to “roll with the punches”;

to my Gene Function colleagues and ICR friends for making special the time I've spent there, and helping me in the development of this thesis; Specially to Lauren A., Drago K., Roman C., Inger B., Feifei S., Katy D., Steve P., Rachel B., Saira K. and the pub quiz crew;

to María M., Elen B., Katya K., Marta H., Gema P., Barbara G., Elena y David, for being my family in London;

to my friends Sonia P., and Silvia B. for always being there;

to my family, for giving me everything that I have, always supporting me in all ways, showing me how to love, and how to live, and for forgiving all my defects;

to God, for giving me life every day, and a purpose to live it;

without you, this thesis would not be possible,

Thank you!

Index

List of abbreviations	5-7
List of tables	9
List of figures	11-12
List of Appendix tables and figures	13
Abstract	17
Introduction	19-40
Gastric cancer incidence and mortality.....	19
Gastric cancer subtypes (clinical and molecular characterisation).....	19-21
Current treatment of gastric cancer.....	21-24
SWI/SNF complex and cancer.....	24-26
<i>ARID1A</i> and its significance in gastric cancer.....	26-28
DNA damage repair processes in cancer.....	28-30
Double Strand Break repair.....	30-31
ATR structure.....	31-34
Synthetic lethality.....	34-35
<i>ARID1A</i> and DNA damage repair inhibitors.....	35-37
Current clinical use of ATR inhibitors.....	37-38
High-Throughput CRISPR/Cas9-based genetic screens to detect mechanisms of synthetic lethality	38-39
Aims and approaches.....	40
Materials and Methods	41-56
Cell lines.....	41
Microsatellite instability determination.....	41-42
Genomic DNA extraction from cell lines.....	42
Polymerase Chain Reaction and gel electrophoresis.....	42
TOPO cloning and sanger sequencing.....	42-43
Chemicals.....	43-44
Western blotting and antibodies.....	44
Cellular viability assays.....	45
Cell proliferation experiment.....	45
RNA extraction and Real time-PCR (RT-PCR).....	45-46
Reverse siRNA transfection Knockdown experiments.....	46
<i>In vivo</i> assessment of ATR inhibitor efficacy in gastric cancer Patient-Derived Xenografts (PDXs).....	47-48
YCC6 VX970 resistant cell lines.....	48
Proteomic analysis by mass spectrometry in ATRi...resistant clones.....	48-49
Next generation sequencing.....	49
Analysis of cell cycle distribution by FACS.....	49-50
<i>ARID1A</i> CRISPR/Cas9 mutagenesis.....	50
Positive selection genome-wide CRISPR screen.....	50-53

Dense Tiling ATR CRISPRx screen.....	54-56
Statistical analysis.....	56
Results.....	57-127
ATR sensitivity in ARID1A deficient gastric cancer models.....	57-80
Characterisation of <i>ARID1A</i> status and mutational signature in gastric tumour cell lines.....	57-64
Sensitivity to ATR inhibition in gastric tumour cell lines.....	64-66
PARP inhibitor sensitivity in gastric tumour cell lines.....	67-68
Small molecule inhibition to PI3K, HDAC6 and EZH2 in gastric cancer tumour cell lines.....	67-71
ATR and PARP inhibitors combination screens.....	72-74
ATR and PI3K inhibitors combination screens.....	72-76
Creation of ARID1A isogenic models to assess ARID1A-driven ATR inhibition sensitivity.....	72-80
 <i>In vivo</i> assessment of ATRi efficacy in gastric cancer Patient-Derived Xenografts.....	81-91
 VX970 positive selection genome-wide CRISPR/Cas9 mutagenesis Screen.....	93-107
 Creation and characterisation of YCC6 ATR inhibitor resistant clones.....	109-119
 Dense Tiling ATR CRISPRx screen.....	121-127
Discussion.....	129-148
Rationale of this thesis.....	129
 Summary of the work presented in this thesis.....	129-147
ARID1A and ATR are synthetically lethal <i>in vitro</i> and <i>in vivo</i>	129-132
<i>In vivo</i> assessment of ATR inhibitors efficacy in gastric cancer PDXs.....	133-134
ATRi resistance mechanisms in gastric cancer.....	134-135
Positive selection genome-wide CRISPR/Cas9 mutagenesis screen reveals ATR inhibitor resistance-mediating genes.....	135-143
ATR inhibitor resistant isogenic cells.....	143-145
Dense tiling ATR CRISPRx screen.....	145-147
 Biological implications of the results and future perspectives.....	147-148
Conclusions.....	149
References.....	151-170
Appendix (supplementary information).....	171-184
Resumen en castellano.....	185-196

List of Abbreviations

5-FU	5-Fluoracil
ACRG	Asian Cancer Research Group
ANOVA	Analysis Of Variance
ATCC	American Type Culture Collection
AUC	Area Under the Curve
BER	Base Excision Repair
BID	Twice a day
C	Celsius
CAT	Catalytic
cDNA	Complementary cDNA
CGC	Cancer Gene Census
CIN	Chromosomally Instable
crDNA	CRISPR RNA
CRISPR	Clustered Regularly Interspaced Short Palindromic Repeats
Ct	Cycle threshold
CTG	CellTitre Glo
DE	Drug Effect
DDR	DNA Damage Response
DMSO	Dymethyl Sulphoxide
DNA	Deoxyribonucleic Acid
DSB	Double Strand Break
dsDNA	Double-Stranded DNA
EBV	Epstein-Barr Virus
ECF	Epirubicin, Cisplatin, and 5-FU
EdU	5-ethynyl-2'-deoxyuridine
EMT	Epithelial-to-Mesenchymal Transition
FACS	Fluorescence-Activated Cell Sorting
FDA	Food and Drug Administration
FFPE	Formalin-Fixed Paraffin Embedded
FW	Forward
g	gram
GC	Gastric Cancer
gDNA	Genomic DNA
GEJ	Gastro-Oesophageal Junction
GERD	Gastroesophageal Reflux Disease
GFP	Green Fluorescent Protein
GS	Genomically Stable
GTP	Guanosine Triphosphate
gRNA	guide RNA
HDR	Homology-Directed Repair
HR	Homologous Recombination
HPLC	High-Performance Liquid Chromatography
i	inhibitor(s)
ICL	Inter-and Intrastrand Crosslink Repair
ICR	Institute of Cancer Research
IFN	Interferon
IHC	Immunohistochemistry

Indel	Short Insertion/Deletion
IR	Ionizing Radiation
IRF	Interferon Regulatory Factor
ISG	Interferon Stimulated Genes
KCLB	Korean Cell Line Bank
KDa	Kilo Dalton
L	Litre
LOF	Loss of Function
M	Molar
m	mili
MAD	Mean Absolute Deviation
MAGeCK	Model-based Analysis of Genome-wide CRISPR/Cas9 Knockout
MMR	Mismatch-Repair
MOI	Multiplicity Of Infection
MS	Mass Spectrometry
MSI	Microsatellite Instability
MSS	Microsatellite Stability
mRNA	messenger RNA
n	nano
NER	Nucleotide Excision Repair
NGS	Next-Generation Sequencing
NHEJ	Non-Homologous End Joining
OS	Overall Survival
PAM	Protospacer Adjacent Motif
PCR	Polymerase Chain Reaction
PDX	Patient-Derived Xenograft
PI	Propidium Iodide
pptm	parts per ten million
r^2	Spearman's rank correlation coefficient
RFP	Red Fluorescent Protein
RNA	Ribonucleic Acid
RNA seq	RNA sequencing
ROS	Reactive Oxygen Species
RT-PCR	Reverse-Transcription Polymerase Chain Reaction
Rv	Reverse
sgRNA	Single-guide RNA
SL	Synthetic Lethality
SF ₅₀	Survival Fraction 50% concentration
siCON	Small Interfering ribonucleic acid control (non-targeting)
SID	Once a day
siRNA	Short interfering RNA
SRB	Sulphorhodamine B
SSB	Single-Strand Breaks
ssDNA	Single-stranded DNA
T	Time
TCGA	The Cancer Genome Atlas
TLS	Trans Lesions Synthesis
TSG	Tumour Suppressor Gene
UCSF	University College of San Francisco
UV	Ultraviolet

v	Version
VE	Viability Effect
WHO	World Health Organisation
WB	Western Blot
WT	Wyld type
μ	micro

List of Tables

Table 1. Summary of PCR and Sanger sequencing primers used in this thesis.....	43
Table 2. Drugs used in this thesis.....	43-44
Table 3. Western blot antibodies used in this thesis.....	44
Table 4. Mutation categories identified from Exome sequencing of gastric tumour cell lines and HCT 116 ARID1A colorectal isogenic cell line.....	59
Table 5. Exome sequencing mutations listed in the Cancer Genome Census found in our panel of cell lines.....	60-63
Table 6. <i>ARID1A</i> mutations and characteristics identified from exome sequencing of gastric tumour cell lines and HCT 116 colorectal ARID1A isogenic pair.....	64
Table 7. Information about the PDX models.....	82
Table 8. sgRNA detected in the picked resistant colonies from the genome-wide CRISPR/Cas9 mutagenesis screen in YCC6 gastric tumour cell line.....	101
Table 9. Mutations found in the CRISPRx screen VX970 resistant YCC6 cells.....	125

List of Figures

Introduction:

Figure 1. Incidence and mortality of gastric cancer (data extracted from GLOBOCAN 2018).....	21
Figure 2. Molecular classification of gastric cancer.....	22
Figure 3. SWI/SNF complex.....	25
Figure 4. Frequency of <i>ARID1A</i> mutations amongst cancer types.....	26
Figure 5. Mechanisms of DDR.....	30
Figure 6. Mechanisms of DSB Repair.....	32
Figure 7. ATR Structure.....	34
Figure 8. Synthetic lethality.....	35
Figure 9. CRISPR/Cas9 mediated gene edition.....	39

Results:

Figure 1. Characterisation of <i>ARID1A</i> status in GC tumour cell lines.....	65
Figure 2. Sensitivity to ATR inhibition in <i>ARID1A</i> deficient GC tumour cell lines.....	66
Figure 3. PARP inhibition in GC tumour cell lines.....	68
Figure 4. PI3K inhibition in GC tumour cell lines.....	70
Figure 5. HDAC6 and EZH2 inhibition in GC tumour cell lines.....	71
Figure 6. ATR and PARP inhibitors combination in GC tumour cell lines.....	73-74
Figure 7. ATR and PI3K inhibitors combination in GC tumour cell lines.....	75-76
Figure 8. Enhanced ATRi sensitivity in SNU 484 <i>ARID1A</i> deficient isogenic GC tumour cell lines.....	78-79
Figure 9. Sensitivity to ATR inhibition in combination with PARP inhibition in <i>ARID1A</i> deficient isogenic GC tumour cell lines.....	80
Figure 10. PDX experimental design.....	83
Figure 11. GC1 <i>ARID1A</i> deficient PDX is highly sensitive to ATR inhibition.....	85
Figure 12. GC2 <i>ARID1A</i> deficient PDX is highly sensitive to ATR inhibition.....	86
Figure 13. GC3 <i>ARID1A</i> deficient PDX is highly sensitive to ATR inhibition.....	87
Figure 14. GC4 <i>ARID1A</i> deficient PDX is highly sensitive to ATR inhibition.....	88
Figure 15. GC5 <i>ARID1A</i> proficient PDX is mildly sensitive to ATR inhibition.....	89
Figure 16. GC6 <i>ARID1A</i> proficient PDX is mildly sensitive to ATR inhibition.....	90
Figure 17. GC7 <i>ARID1A</i> proficient PDX is highly sensitive to ATR inhibition.....	91
Figure 18. Genome-wide SF ₀ positive selection CRISPR/Cas9 screen workflow.....	94
Figure 19. Preparation of the models, dose optimisation and genome-wide CRISPR/Cas9 screen workflow.....	96
Figure 20. Genome-wide CRISPR/Cas9 screen computational Analysis.....	99
Figure 21. Genome-wide CRISPR/Cas9 YCC6 screen validation pipeline.....	100
Figure 22. Validation CRISPR/Cas9 mini-screen.....	102
Figure 23. Validation of <i>IRF9</i> as a candidate for ATRi resistance in IRF1 isogenic cells.....	103
Figure 24. Validation of <i>HUWE1</i> as a candidate for ATRi resistance in HUWE1 isogenic cells.....	105
Figure 25. Candidate ATRi resistance causing genes identified from GW CRISPR screens of 5 cell lines (including data from Wang <i>et al.</i> , 2018).....	106
Figure 26. YCC6 ATRi resistant cell experiment design.....	110
Figure 27. Detection of morphological changes in YCC6 ATRi resistant clones.....	111

Figure 28. ATRi resistant clones' data analysis workflow.....	113
Figure 29. Mass spectrometry transcriptomic data reveals common differentially expressed proteins in all YCC6 ATRi resistant clones.....	114
Figure 30. Mass spectrometry transcriptomic data reveals common differentially expressed proteins in H1/H2/H3/H4/H6 YCC6 ATRi resistant clones.....	115
Figure 31. Mass spectrometry transcriptomic data reveals common differentially expressed proteins in H5/M1 YCC6 ATRi resistant clones.....	118
Figure 32. Silencing of SMG1 re-sensitises the resistant clones H3 to VX970.....	119
Figure 33. CRISPRx screen workflow.....	122
Figure 34. Ion Torrent CRISPRx Sample preparation.....	123
Figure 35. The majority of the ATRi-resistance causing mutations locate in the FAT or catalytic domains.....	126

List of appendix tables and figures

Supplementary Table 1. sgRNA and target genes used in the genome-wide screen validation experiment.....171-176

Supplementary Table 2. Table of ATR tiling primers for CRISPRx PCR 1.....174-176

Supplementary Table 3. List of overlapping resistance hits with Z-Score >2 comparing our YCC6 CRISPR screen results with the TOV21G screen and the 293A, HCT 116 and MCF10A cell lines extracted from Wang *et al.*, 2018.....177-181

Supplementary Figure 1. Mass spectrometry transcriptomic data reveals common differentially expressed proteins in all YCC6 ATRi resistant clones.....182

Supplementary Figure 2. Mass spectrometry transcriptomic data reveals common differentially expressed proteins in H1/H2/H3/H4/H6 YCC6 ATRi resistant Clones.....183

Supplementary Figure 3. Mass spectrometry transcriptomic data reveals common differentially expressed proteins in H5/M1 YCC6 ATRi resistant clones.....184

Abstract

Synthetic lethal approaches in identifying genetic determinants of drug response is a powerful method in selecting patients for targeted cancer therapies. Ataxia-Telangiectasia Mutated (ATM) and Rad3-related protein kinase (ATR) is a valuable target to inhibit the DNA damage repair (DDR) pathway, that has been shown to be particularly effective in cancer cells harbouring other DDR defects, including truncating mutations in *ARID1A*, found in the 20% of gastric cancer (GC) patients. Although ATR inhibitors (ATRi) are emerging as promising cancer therapies, resistance mechanisms inevitably arise from these drugs as monotherapy, emphasising the importance of identifying genetic determinants of response and resistance to inform drug combinations that result in durable clinical responses.

In this thesis, an integrated functional genomics approach was undertaken in order to identify genetic determinants to ATRi sensitivity and resistance in GC. First, I show that *ARID1A* defective GCs *in vitro* and *in vivo* models exhibit enhanced sensitivity to ATRi. Second, I have comprehensively identified and validated genetic determinants of ATRi-resistance by undertaking a genome-wide (GW) CRISPR/Cas9 screen and created ATRi resistant isogenic models, including *CDC25B*, *HUWE1*, *CARD10*, *SMG8*, *SMG9*, *SMG1*, *HNRNPF*, *IRF9*, and *STAT2*. Lastly, I have shown for the first time that mutations in the ATR FAT domain cause resistance to ATRi.

These findings inform us about the biological mechanisms of ATRi sensitivity and resistance in GC. Furthermore, this data provides the preclinical rationale for assessing ATRi such as VX970, AZD6738 or M4344 in clinical trials, for patients with GC.

Introduction

Gastric cancer (GC) incidence and mortality

GC is the third leading cause of cancer-related deaths, accountable for over 1,000,000 new cases in 2018 and an estimated number of 783,000 deaths (1 of every 12 deaths worldwide), which makes it the fifth most frequently diagnosed cancer, globally (**Figure 1**). GC is more common in men than in women (1:2) and incidence rates are especially high in Eastern Asia (Japan, Korea, Mongolia etc.), South America and Eastern Europe. The aetiology of GC is strongly linked to the environment (Kolonel, Hankin et al. 1985, Bertuccio, Chatenoud et al. 2009), as *Helicobacter pylori* (*H. pylori*) infection constitutes the main risk factor for GC (1994, Plummer, Franceschi et al. 2015). Dietary factors (e.g. high salt content, low fruit intake), Epstein-Barr virus infection (EBV), smoking and alcohol consumption are also established risk factors (Humans 2012, Cancer Genome Atlas Research 2014, Mayne, Playdon et al. 2016). The incidence of GC is related to the location within the stomach; non-cardia GC (localised in a more distal region of the stomach) have decreased in prevalence over the past years largely due to *H. pylori* eradication, while GC arising from the cardia (gastro-oesophageal junction, GEJ) have increased especially in high-income countries. In part, this may be due to its association with obesity, gastroesophageal reflux disease (GERD) and a small percentage of Barrett's oesophageal cases (Howson, Hiyama et al. 1986, Ngoan, Mizoue et al. 2002).

Gastric cancer subtypes (clinical and molecular characterisation)

The vast majority of GC are adenocarcinomas, which have been traditionally classified according to histopathological factors, using either Lauren classification, that divides GC into diffuse gastric and intestinal subgroups (Lauren 1965), or the world Health Organization classification, dividing it in papillary, tubular, mucinous and poorly cohesive carcinomas (WHO classification of Tumours of the Digestive System, 2010). However, these histological-based classification systems have demonstrated little prognostic or clinical utility in terms of treatment stratification (Cervantes, Roda et al. 2013, Cancer Genome Atlas Research 2014). In contrast, molecular-based

classifications aim to identify disease-specific genetic alterations that are potential therapeutic targets (Kim, Barzi et al. 2018).

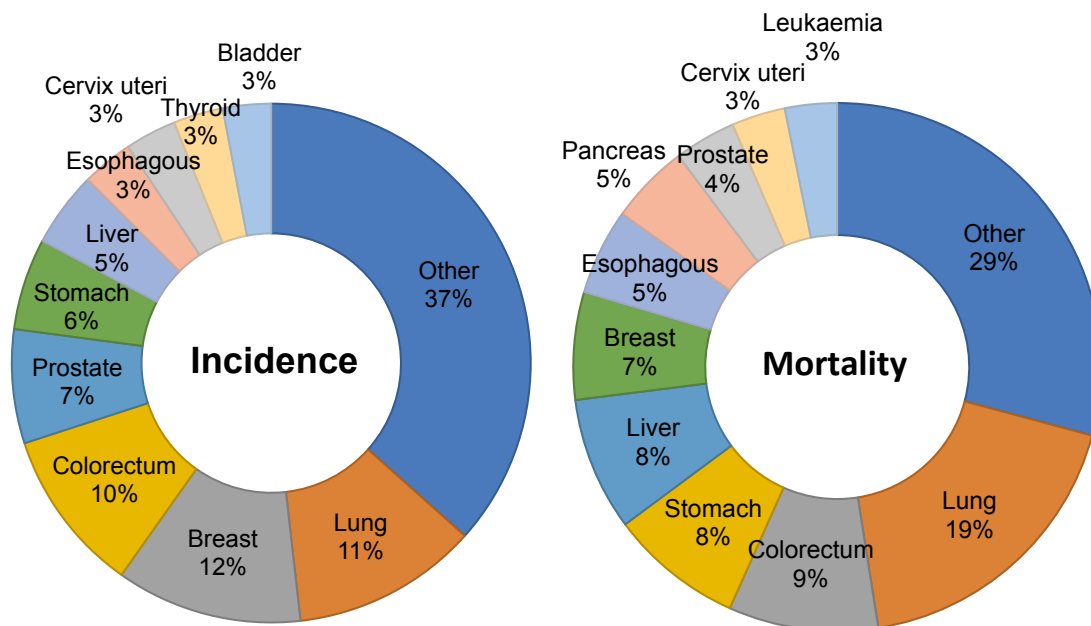


Figure 1. Incidence and mortality of GC (data extracted from GLOBOCAN 2018). The incidence of GC (stomach) represents the 5.7% of the incidence of all cancers in the general population, being in the 5th position in the ranking with over 1,000,000 new cases reported in 2018. According to the mortality, GC is the 3rd most common cause of cancer-related deaths, responsible of 1 of 12 deaths worldwide.

The implementation of whole genome sequencing and high-throughput techniques in cancer research has enabled the development of molecular classifications, including the classification published in 2014 by the Cancer Genome Atlas Research Network, describing four distinct molecular subgroups (**Figure 2**). The most frequently occurring subgroup, the chromosomally instable GC (CIN, 50%) is characterised by chromosomal instability, where gene amplifications are very frequent and involve diverse tyrosine kinase receptors or associated pathways (Human Epidermal Growth Factor Receptor 2, *ERBB2*; *Epidermal Growth Factor Receptor*, *EGFR*, *Epidermal Growth Factor Receptor 3*, *ERBB3*; *Janus Kinase 2*, *JAK2*; *Fibroblast Growth Factor Receptor 2*, *FGFR2*; *MET Proto-Oncogene*, *Receptor Tyrosine Kinase*, *MET*; *Phosphatidylinositol-4,5-Bisphosphate 3-Kinase Catalytic Subunit*, *PIK3C*; *KRAS Proto-Oncogene GTPase*, *KRAS*; and *NRAS Proto-Oncogene GTPase*, *NRAS*). The microsatellite instability group (MSI, 22% of the cases), is the second most frequent group and it is characterised by high genomic instability due to DNA mismatch repair

machinery deficiencies, resulting in a very high mutation rate with hotspot mutations within genes including *ERBB2*, *EGFR*, *ERBB3*, *JAK2*, *Fibroblast Growth Factor Receptor 2 (FGFR)*, *MET*, *AT-Rich Interactive Domain 1A (ARID1A)*, *Phosphatidylinositol-4,5-Bisphosphate 3-Kinase Catalytic Subunit A (PIK3CA)* and high levels of the Programmed Death-Ligand 1 (PD-L1) expression. Genomically stable (GS) GCs, that represent the 20% of the cases are associated with diffuse histology according to Lauren's classification, and show a high frequency of *E-Cadherin (CDH1)* mutations (26%) and *Ras Homolog Family Member A (RHOA)* (15%). Finally, the Epstein-Barr virus positive (EBV) related group comprises 9% of the cases of GC and these tumours are mainly located in the gastric fundus, showing a promoter hypermethylator phenotype and the highest frequency of *PIK3CA* mutations (80%), as well as amplification of *JAK2* and *PD-L1* genes. A similar classification was also determined by the Asian Cancer research group (ACRG), that took into account the *Tumour Protein P53 (TP53)* activity and epithelial-to-Mesenchymal transition (EMT), thus dividing GC into four groups comprising the MSS/EMT, MSI, MSS/TP53^{WT}, MSS/TP53^{-/-} (Cristescu, Lee et al. 2015). These new molecular classifications have widened the view of gastric carcinogenesis and have focused research in the discovery of genetic actionable targets, that have the potential to improve the outcome of patients with GC (Hartgrink, Jansen et al. 2009).

Current treatment of gastric cancer

Surgical resection of GC is the best curative option, although the risk of relapse following resection remains high. For that reason, clinical trials such as MAGIC and FLOT4 have reported a benefit from adding perioperative or neoadjuvant chemotherapy to patients with operable oesophagogastric cancers, even when diagnosed at early stages of the disease (Cunningham, Allum et al. 2006, Al-Batran, Hofheinz et al. 2016). More specifically, the MAGIC trial revealed a survival benefit from the administration of perioperative epirubicin, cisplatin, and 5-FU (ECF) for patients with operable oesophagogastric cancer (Cunningham, Allum et al. 2006). Building on this data, the FLOT4 trial showed that the FLOT triplet regimen (oxaliplatin, infusional 5-FU, and docetaxel) improves the outcome of patients with localised oesophagogastric cancer compared with the ECF triplet (Al-Batran, Hofheinz et al. 2016). Despite these advances in clinical research, the overall survival for patients

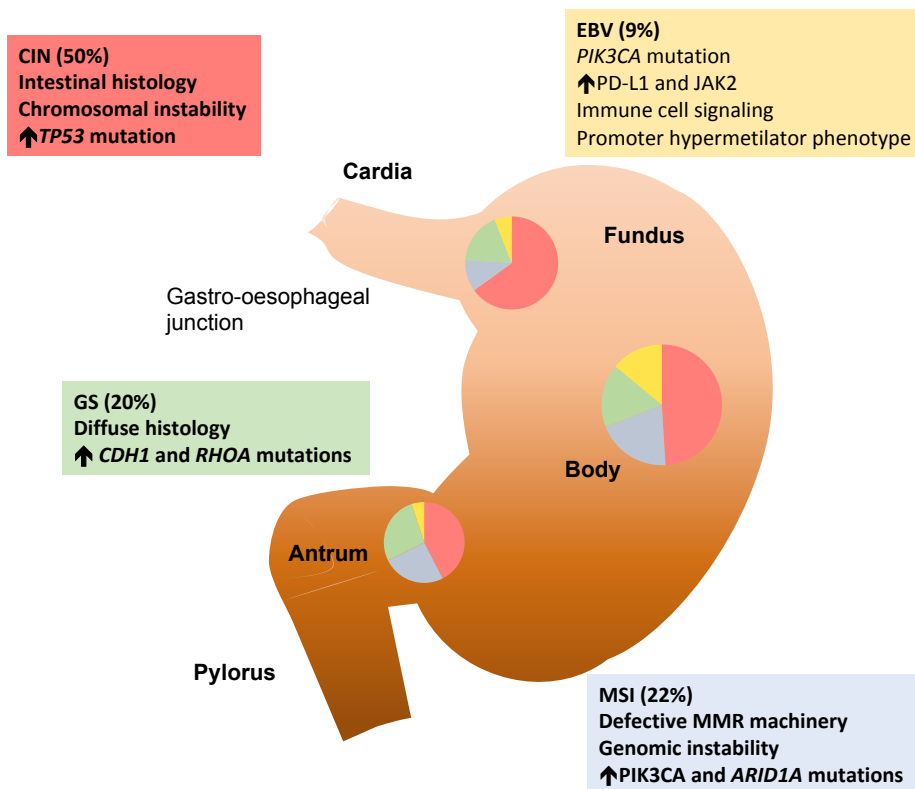


Figure 2. Molecular classification of GC. Comprehensive molecular characterisation of gastric adenocarcinoma done by the Cancer Genome Atlas Research in 2014 defined four major genomic subtypes of GC: The EBV-infected tumours, tumours presenting microsatellite instability (MSI), genomically stable tumours (GS) and chromosomally unstable tumours (CIN) (adapted from GC Genome Atlas, 2014).

with GC remains poor. Due to the vague presenting symptomatology of GC, the majority of the cases are diagnosed at an advanced stage where treatment is mainly restricted to platinum based chemotherapy. However, platinum resistance is inevitable and new treatment options are required (Cunningham, Oliveira et al. 2008, Cunningham, Starling et al. 2008, Okines, Chau et al. 2008, Rao, Starling et al. 2008). Many clinical trials using targeted therapies have been undertaken in the last few years, but only a modest improvement in OS has been achieved. Currently, there are only three approved targeted treatments in GC. The first targeted therapy in GC that was clinically implemented in 2010 was Trastuzumab, a monoclonal antibody targeting *ERBB2*, in *ERBB2* amplified cases (HER2-positive). Up to 22 % of gastric adenocarcinomas and gastroesophageal tumours show an overexpression in *HER2* (Bang, Van Cutsem et al. 2010, Van Cutsem, Bang et al. 2015). Trastuzumab is given in the first-line treatment of *HER2*-positive advanced or metastatic GC

adenocarcinoma in combination with platinum-based chemotherapy. Trastuzumab binds to the extracellular domain of the *HER2* receptor, inhibiting proliferation of tumour cells that overexpress *HER2* by preventing the activation cell cycle progression pathways and has proved to prolongate survival in *HER2*-positive patients. However, the median OS advantage was observed to be no more than three months, due to the development of resistance (ToGA trial) (Bang, Van Cutsem et al. 2010, Croxtall and McKeage 2010). The anti-angiogenic, anti-*VEGFR2* (*Vascular Endotelial Growth Factor receptor 2*) monoclonal antibody ramucirumab, has also been approved by the food and drug administration (FDA) to be used in the second-line setting as monotherapy or in combination with paclitaxel, as significant survival benefits in patients with advanced GC who had progressed on first-line chemotherapy have been observed in the RAINBOW and REGARD trials (Fuchs, Tomasek et al. 2014, Wilke, Muro et al. 2014). The last FDA approved targeted therapy in GC consists in the tight-junction protein Claudin18.2 (*CLDN18.2*) antibody, IMAB352. Combined with chemotherapy, IMAB352 has shown to enhance T-cell infiltration and pro-inflammatory cytokines (FAST study), increasing OS when used in first-line treatment of GC (Lordick, Mariette et al. 2016, Lordick and Terashima 2016).

Additionally, promising phase III trials assessing the effectiveness of immunotherapy and immune checkpoint inhibitors in GC are being conducted (Sclafani, Brown et al. 2016, Kang, Boku et al. 2017, Fuchs, Doi et al. 2018). For example, pembrolizumab, a PD-L1 antibody has been approved by the FDA to be used in third line setting on advanced GC and is currently being evaluated in combination with chemotherapy (Fuchs, Doi et al. 2018), or nivolumab, a *program death 1*, PD-1 antibody that has been approved for its use in Japan and that is currently being tested in combination with an anti-CTLA4 (*Cytotoxic T-Lymphocyte Associated Protein 4*) antibody (Ipilimumab) in a phase I/II study, showing promising results so far (Kang, Boku et al. 2017, Janjigian, Bendell et al. 2018).

Despite the extensive efforts and the large number of clinical trials undertaken, effective targeted therapies, that can improve the OS in patients with resectable and non-resectable GC cancers are still urgently required (reviewed in (Kim, Barzi et al. 2018). This underlines the importance of; firstly, assessing methods for accurate the selection of the candidate population; second, the need of further research into the

identification of reliable biomarkers for targeted therapies to be able to predict patients who will benefit from treatment, and; lastly exploiting the potential of new treatment approaches, such as immunotherapy treatments in monotherapy or combination with chemotherapy or other therapies.

SWI/SNF complex and cancer

The Switch/Sucrose non-fermentable chromatin remodelling complex (SWI/SNF), comprises a large protein complex, in charge of the activation of gene expression by modulating nucleosomes at gene promoters (Imbalzano, Kwon et al. 1994) (Liu, Balliano et al. 2011) and is found widely dysregulated in cancer (Shain and Pollack 2013). The SWI/SNF complex is capable of unwinding the DNA around histone cores, providing access to DNA that regulates transcription, DNA repair and replication, in an ATP dependent way (Imbalzano, Kwon et al. 1994, Kwon, Imbalzano et al. 1994). This complex has been related to a variety of essential processes in eukaryotic cells, such as differentiation, proliferation, DNA repair and tumour suppression (Reisman, Glaros et al. 2009). In humans, the SWI/SNF complex can form two different configurations, denominated as BAF or polybromo-associated BAF (PBAF). This allows the complex to have a broad role of activities, depending on the genetic context (Shain and Pollack 2013).

SWI/SNF complex includes one of the two mutually exclusive ATPases, SMARCA2 (BRM) and SMARCA4 (BRG1); and one of the three mutually exclusive functionality-conferring proteins (i.e. DNA binding, histone binding), ARID1A (BAF250A), ARID1B (BAF250B) or PBRM1 (BAF180). Usually, ARID1A and ARID1B are associated with BAF complexes, which can work with either BRM, or BRG1 ATPases, while PBRM1, together with ARID2 (BAF200) and BRD7 are only found in pBAF complexes, which are associated to only BRG1. Additionally, there are some other core and accessory subunits that are associated with all versions of the complex (BAF or PBAF), like SMARCB1 (BAF47/SNF5), SMARCC1 (BAF155), SMARCC2 (BAF170), SMARCE1 (BAF57); and SMARCD1 (BAF60A), SMARCD2 (BAF60B), SMARCD3 (BAF60C), PHF10 (BAF45A), DPF1 (BAF45B), DPF2 (BAF45D), DPF3 (BAF45C), ACTL6A (BAF53A) and ATL6B (BAF53B), respectively (Shain and Pollack 2013) (**Figure 3**).

SWI/SNF mutations are widely spread in several tumour types, occurring, most frequently in the subunits with enzymatic activity (SMARCA4 and SMARCA2) or in the ones that confer functionality to the complex (ARID1A, ARID1B, ARID1 and PBRM1). The fact of SWI/SNF mutations, being described across several units of the complex, indicates that the whole functional activity of it might be compromised, even when only one of the subunits its mutated, conferring a tumour suppressor role to the complex itself (Shain and Pollack 2013). This observation has been described in a comprehensive study of protein level variation in colorectal tumour cells, where when the downregulation of several proteins, either in the BAF o PBAF configuration of the SWI/SNF complex, resulted in the downregulation of other subunits of the complex (Roumeliotis, Williams et al. 2017).

From all proteins of the complex, *ARID1A* (*AT-rich interactive domain-containing 1A protein*), is localised in chromosome 1p36.11, and it constitutes one of the most-frequently altered proteins across all cancers (Wu, Wang et al. 2014). *ARID1A* encodes for a key DNA binding protein involved in a wide range of cellular processes, including gene expression regulation, cell development, differentiation, proliferation, apoptosis and DNA repair (Reisman, Glaros et al. 2009, Wu and Roberts 2013, Wu, Wang et al. 2014, Wu, Zhang et al. 2016, Sun, Wang et al. 2018).

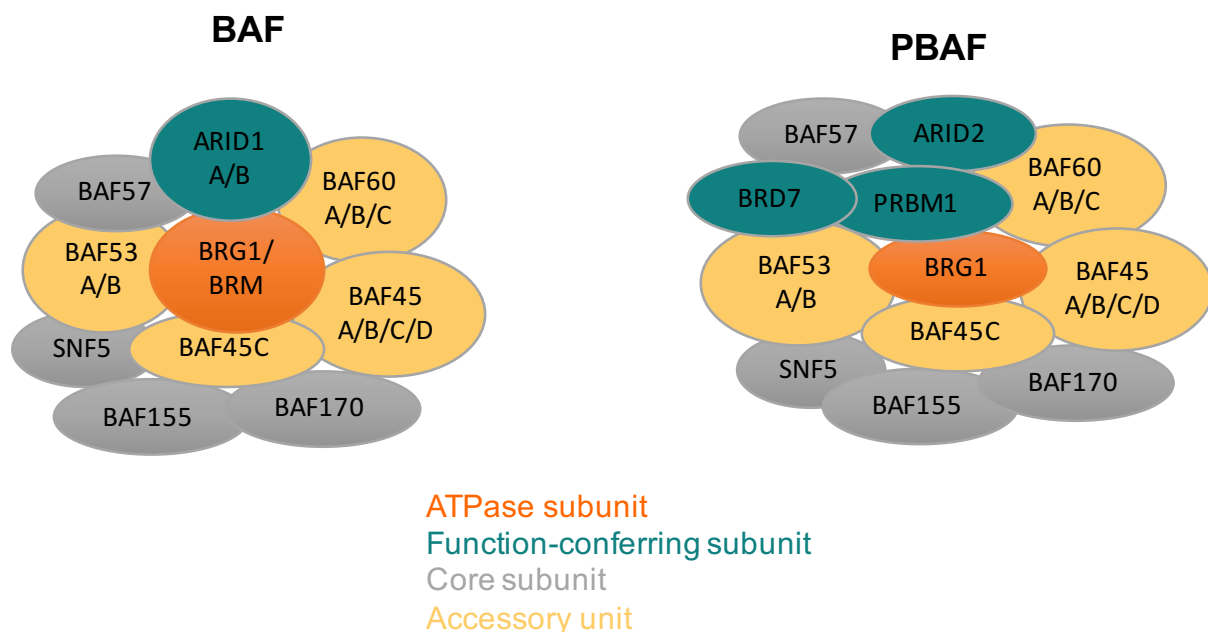


Figure 3. SWI/SNF complex. The SWI/SNF can form two different configurations, denominated as BAF and PBAF. SWI/SNF complex contains one of the two mutually exclusive

ATPases, SMARCA2 (BRM) and SMARCA4 (BRG1); and one of the three mutually exclusive functionality-conferring proteins, ARID1A (BAF250A), ARID1B (BAF250B) or PBRM1 (BAF180). Additionally, the core and accessory subunits are SMARCB1 (BAF47/SNF5), SMARCC1 (BAF155), SMARCC2 (BAF170), SMARCE1 (BAF57); and SMARCD1 (BAF60A), SMARCD2 (BAF60B), SMARCD3 (BAF60C), PHF10 (BAF45A), DPF1 (BAF45B), DPF2 (BAF45D), DPF3 (BAF45C), ACTL6A (BAF53A) and ATL6B (BAF53B), respectively.

ARID1A and its significance in gastric cancer

ARID1A is found to be mutated in around the 20% of all cancer cases, being highly mutated in ovarian clear cell carcinomas (Jones, Wang et al. 2010) (46-57%), uterine endometroid carcinomas (33-49%) (Guan, Mao et al. 2011, Liang, Cheung et al. 2012, Cancer Genome Atlas Research, Kandoth et al. 2013), ovarian endometroid carcinomas (30%) (Wiegand, Shah et al. 2010), gastric carcinomas (8-27%) (Wang, Kan et al. 2011, Jones, Li et al. 2012, Zang, Cutcutache et al. 2012) and oesophageal adenocarcinoma (9-19%) (Wang, Nagl et al. 2004, Chong, Cunningham et al. 2013, Streppel, Lata et al. 2014), amongst others (**Figure 4**).

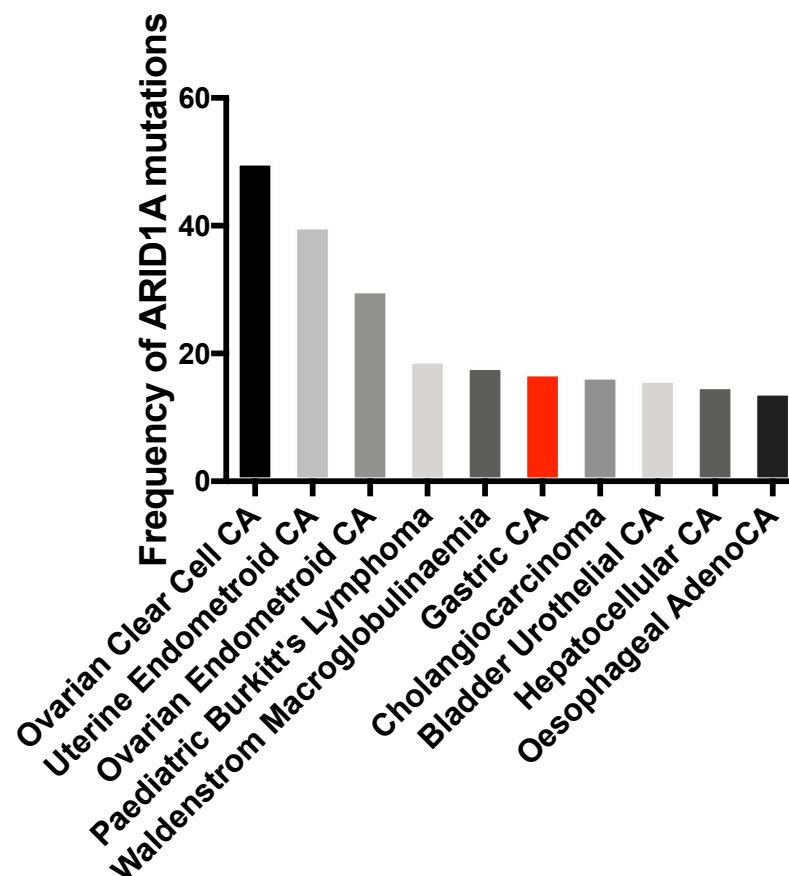


Figure 4. Frequency of *ARID1A* mutations amongst cancer types. *ARID1A* is one of the most frequent altered proteins across all cancers. Figure shows a histogram with the cancer types with highest rates in *ARID1A* mutations according to cBioPortal data (2018).

ARID1A mutations are mutually exclusive to p53 mutations and are highly prevalent in tumours with MSI. This observation has been reported in several histologies, including GC (Wang, Kan et al. 2011, Kim, Je et al. 2012, Allo, Bernardini et al. 2014, Cancer Genome Atlas Research 2014, Chou, Toon et al. 2014). Furthermore, *ARID1A* has recently been found to physically interact with the mismatch repair (MMR) protein MSH2, and it seems that *ARID1A* is involved in the recruitment of the latter to chromatin during replication, contributing to impaired MMR and a mutator phenotype in cancer (Shen, Ju et al. 2018).

Additionally, *ARID1A* loss has been found to frequently coexist with activating mutations of *PIK3CA* (Yamamoto, Tsuda et al. 2012, Zang, Cutcutache et al. 2012, Cancer Genome Atlas Research 2014), loss of *PTEN* expression (Bosse, ter Haar et al. 2013), and an increase in the phosphorylation of AKT1 at Ser-473 (Liang, Cheung et al. 2012), all events leading to a downstream overactivation of the PI3K/AKT pathway. These observations strongly suggest an inter-dependency between *ARID1A* mutations and PI3K/AKT pathway activation, indicating that tumour cells with loss of *ARID1A* expression may be dependent on constitutive activation of the PI3K/AKT-pathway and therefore may also be synthetically lethal to its inhibition (Samartzis, Noske et al. 2013). This could be of considerable clinical relevance since loss of *ARID1A* expression may be predictive for a favourable treatment response to small molecule inhibitors of the PI3K/AKT-pathway, which are currently under clinical investigation in GC (Samartzis, Gutsche et al. 2014, Zhang, Yan et al. 2016, Lee, Yu et al. 2017)

In parallel, studies undertaken in ovarian cancer models have found the *ARID1A* deficiency to be synthetically lethal to the inhibition of the catalytic subunit of polycomb repressive complex 2, *EZH2* due to its agonistic regulation of PI3K/AKT pathway, through the modulation of *PIK3IP1* expression (Bitler, Aird et al. 2015). This indicates that inhibiting *EZH2* methyltransferase activity through the use of *EZH2* inhibitors in *ARID1A*-mutated cancers could potentially represent a novel synthetic lethal therapeutic strategy (Bitler, Aird et al. 2015). Furthermore, as *ARID1A* deficiency has been linked to an increase in the expression of *HDAC6* protein which results on apoptotic suppression through the inactivation of p53, *HDAC6* has been proposed to be an alternative synthetic lethal partner for *ARID1A* (Bitler, Wu et al. 2017). These

affirmations have been extended to the use of pan-HDAC inhibitors, in monotherapy or combination with *EZH2* inhibitors, following the rationale that ARID1A loss confers sensitivity to HDAC inhibitors, due to co-repression of *EZH2*, suppressing the expression of *EZH2/ARID1A*, as well as target tumour suppressor genes such as *PIK3IP1*, thereby inhibiting proliferation and promoting apoptosis in cancer cells (Fukumoto, Park et al. 2018).

To the date, other *ARID1A* described synthetic lethality resulting from the exposure to small molecule inhibitors comprise dasatinib and the *ARID1A* homolog in the SWI/SNF complex, *ARID1B*. Dasatinib, a multi-target kinase inhibitor was identified in a high throughput drug screen performed in 12 Ovarian clear tumour cell lines to enhance apoptosis in *ARID1A* mutant cells in a p21 and RB dependent manner (Miller, Brough et al. 2016). In the case of *ARID1B*, a large cohort of tumour cell lines used to discover essential genes, showed a mutually exclusivity of *ARID1A* and *ARID1B*, where at least one of the copies of *ARID1B* was necessary for *ARID1A* deficient cells to survive (Cheung, Cowley et al. 2011). This *ARID1A-ARID1B* synthetic lethality has been previously described by other authors, although its clinical utility has not yet been exploited (Helming, Wang et al. 2014).

DNA damage repair (DDR) processes in cancer

Eukaryotic cells have a complex machinery that allows them to maintain the DNA integrity through every round of replication. Genomic instability can arise from several agents and processes like the ultraviolet radiation, ionizing radiation, reactive oxygen species (ROS), environmental agents, and some chemicals and drugs (Lindahl and Barnes 2000, Hoeijmakers 2009). The non-efficient repair of these lesions increases the risk of mutagenesis in an exponential way, potentially leading to the development of tumours (Hoeijmakers 2009). The whole set of pathways involved in the repair of DNA lesions is known as the DNA Damage Response (DDR). The DDR machinery encompasses a large variety of proteins and pathways, that operate in one way or another, depending on the type of damage that needs to be repaired (Lord and Ashworth 2012).

The main DDR pathways comprise nucleotide excision repair (NER), the base excision repair (BER), the mismatch repair (MMR), the trans lesion synthesis (TLS),

the inter- and intrastrand crosslink repair (ICL), DNA single strand break repair and DNA double strand break repair (**Figure 5**). Ultraviolet (UV) light from the sun, reactive ROS or numerous chemicals can cause lesions in nucleotides that lead to a distortion in the DNA helix. This kind of alterations are repaired by the NER pathway that enables unwinding of DNA around the lesion, DNA excision, removal of approximately 30 base pairs (bp) around the lesion, reassembling of nucleotides to the gap by the DNA polymerase and ligation of DNA strands (Masutani, Sugasawa et al. 1994, Wakasugi, Kawashima et al. 2002, Marteijn, Lans et al. 2014). BER enables the correction of bases damaged by oxidation, alkylation, deamination and depurination/depurimidination. The damaged bases are removed and single nucleotides or DNA stretches are cleaved and replaced by a DNA polymerase and a DNA ligase (Robertson, Klungland et al. 2009). MMR machinery is responsible for correcting the incorporation of inappropriate nucleotides during replication. Inactivation of this repair pathway (frequently due to germline mutations or promoter hypermethylation of the *MLH1*, *MSH2*, *MSH6*, or *PMS2* genes) causes MSI and hypermutation in the genome. It has been widely studied and linked to Lynch syndrome and colorectal cancer predisposition, although it has also been studied in other histologies (Fishel, Lescoe et al. 1993, Leach, Nicolaides et al. 1993, Bak, Sakellariou et al. 2014, Cancer Genome Atlas Research 2014). TLS prevents forks stalling by bypassing damaged or missing bases, reassuring an efficient completion of DNA replication (Chang and Cimprich 2009). To accomplish this, TLS polymerases display with a lower fidelity than normal replicative polymerases, increasing the mutation frequency, although they only synthesize short stretches of DNA (Sale, Lehmann et al. 2012, Sharma, Helchowski et al. 2013). ICL are caused by the formation of covalent bonds of proteins or DNA due to the presence of two reactive groups in the two adjacent bases on the same strand (intrastrand crosslink) or between the two complementary DNA strands (interstrand crosslinks). To remove these undesired bonds, proteins involved in the Fanconi Anemia pathways are required, as well as homologous repair (HR), NER and TLS pathways (Clouston, Scharer et al. 2013). Single strand breaks (SSBs) can arise as a result of ionizing radiation or the ROS generation by the cellular metabolism. SSBs are efficiently recognized by the poly (ADP) ribose polymerase (PARP). PARP (mainly PARP1) binds to the SSB sites and synthesizes PAR-chains that binds to target proteins (including itself), activating its catalytic activity and resulting in the initiation of de DNA

repair cascade, mainly through the BER pathway. Although PARP1 plays a pivotal role in BER, it is also involved in other DDR processes, like the switch from non-homologous end joining repair to homologous repair at stalled replication forks (explained below) (Schultz, Lopez et al. 2003, Hochegger, Dejsuphong et al. 2006, Fisher, Hochegger et al. 2007, Bryant, Petermann et al. 2009, Langelier, Planck et al. 2012). Lastly, double strand break (DSB) repair is essential, as its inefficient reparation can lead to mutations and chromosomal rearrangements that can be lethal to cells. DSBs can arise as a result of ionizing radiation or from the collapse of replication forks, and it can be repaired by several specialised mechanisms.

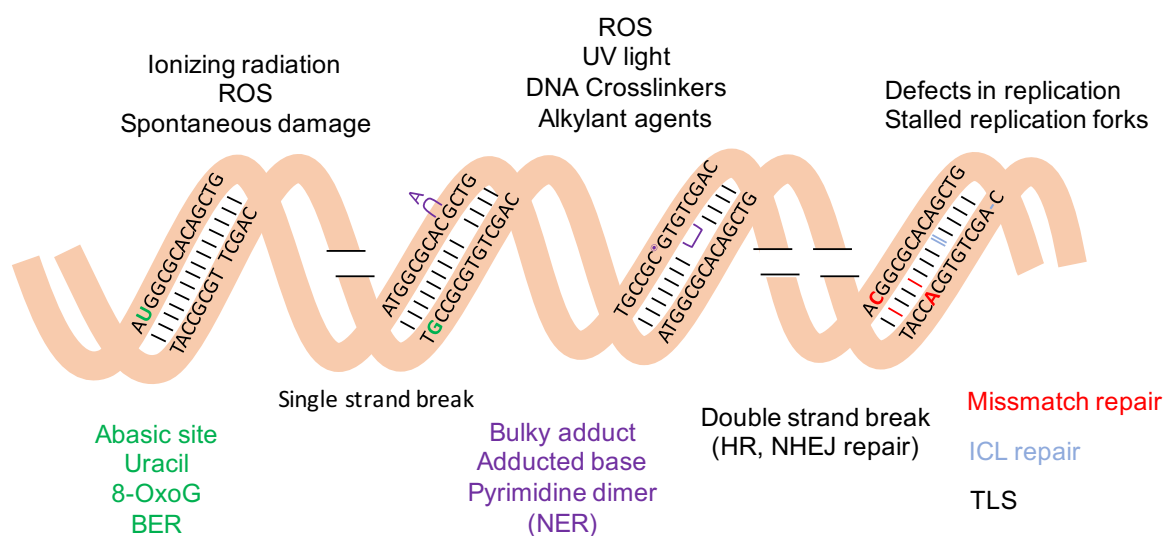


Figure 5. Mechanisms of DDR. Genomic instability can arise from several agents and processes like the ultraviolet radiation, ionizing radiation, reactive oxygen species (ROS), environmental agents, and some chemicals and drugs. The main DDR pathways include the nucleotide excision repair (NER), the base excision repair (BER), the mismatch repair (MMR), the trans lesion synthesis (TLS) the inter and intrastrand crosslink repair (ICL), the DNA single strand break (SSB) repair and the DNA double strand break (DSB) repair.

Double Strand Break repair

DSBs represent the most lethal type of DNA lesions and it is repaired by two main mechanisms; homologue recombination (HR) and non-homologous end joining (NHEJ), although alternative-NHEJ and single-strand annealing pathways have also been described. HR pathway relies on the intact sister chromatid as a template for accurate repair, resulting in faithful replication, and it is relatively error free (Hartlerode and Scully 2009, Brandsma and Gent 2012). Briefly, HR is triggered by Mre11-RAD50-NSB1 (MRN) complex, which activates and recruits ataxia–telangiectasia, mutated

(ATM) to the DSB, which interacts with CtIP and other exonucleases, that generate a single strand DNA (ssDNA) tail (Wyman and Kanaar 2006, Heyer, Ehmsen et al. 2010, Stracker and Petrini 2011). Then, the ssDNA is coated by the Replication Protein A (RPA) to remove the secondary structures (Sugiyama, Zaitseva et al. 1997), while BRCA2 mediates the replacement of RPA by RAD51 to mediate a strand invasion of several proteins, including ATM and Rad3-related (ATR) and ATR interacting protein (ATRIP), to repair DNA using the correct strand as a template (Williams, Williams et al. 2007, Cimprich and Cortez 2008, Pardo, Gomez-Gonzalez et al. 2009). Finally, the junctions are resolved resulting in correctly repaired DNA (Pardo, Gomez-Gonzalez et al. 2009). Therefore, DNA lesions are detected by sensor proteins, where ATM and ATR play a central role, by phosphorylating several mediator proteins (like the cell cycle checkpoint kinases 1 and 2, CHK1 and CHK2), that amplify the DDR by recruiting several effector substrates (Zhou and Elledge 2000). Both pathways work in a orchestrated way and are required for NHEJ, HR, ICL and NER repair pathways, as well as for replication fork stability during replication (Ciccio and Elledge 2010) (**Figure 6A**). On the other hand, NHEJ is considered an error-prone pathway, as it consists of the ligation of the DNA ends without using the intact sister chromatid template (Mahaney, Meek et al. 2009, Brandsma and Gent 2012). NHEJ enables binding of Ku70/80 heterodimer to the DSB where it recruits and activates the catalytic subunit of the DNA dependent protein kinase (DNA-PK) to mediate the creation of compatible ends that can then be ligated (Ciccio and Elledge 2010, Lieber 2010) (**Figure 6B**).

An improved understanding of how DDR contributes to tumorigenesis has informed the synthesis of DDR small molecular inhibitors that have had a large impact in the clinical practice, based upon the principal of the high-speed replication rate, genomic instability and inefficiency of cancer cells to repair DNA damage, making them sensitive to these DNA-defect causing drugs that can also be used in combination with chemotherapy or radiotherapy.

ATR structure

ATR is a large protein (2644 amino acids) and a member of the phospho-inositide 3-kinase related kinases (PIKK) family which is essential for cell viability and embryonic development (Brown and Baltimore 2000, Cortez, Guntuku et al. 2001). ATR is in

charge of monitoring the progression of replication forks in S phase, maintaining genomic stability and promoting a complete and accurate replication of the genome by mediating the phosphorylation of a large number of substrates and preventing premature mitotic entry (Casper, Nghiem et al. 2002, Cimprich and Cortez 2008, McNees, Tejera et al. 2010, Flynn and Zou 2011). Structurally, it contains several HEAT (*Huntington, Elongation factor 3, Protein phosphatase 2A, and PI3K TOR1*) repeats, close to the N-terminal, (Ball, Myers et al. 2005, Chen, Zhao et al. 2007, Rubinson, Gowda et al. 2010), and a C-terminal catalytic kinase domain (PI3K/PI4K),

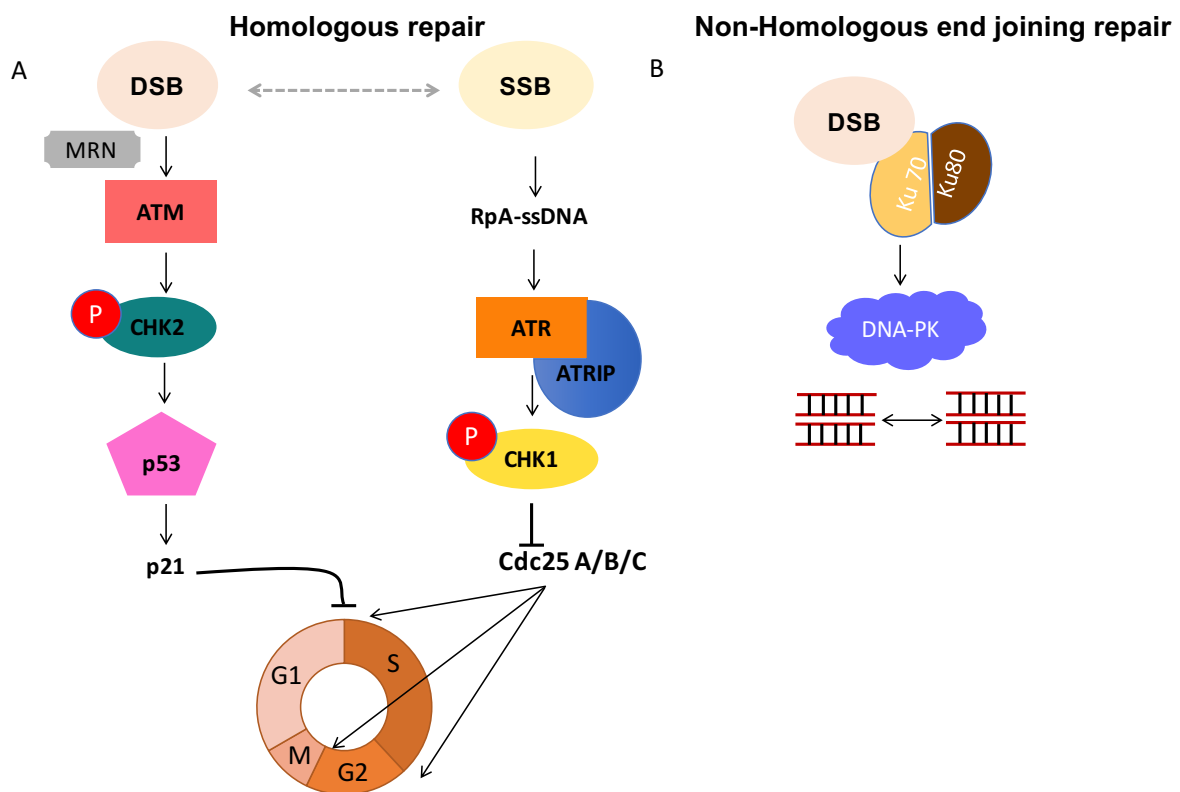


Figure 6. Mechanisms of DSB repair. Double strand breaks are mainly repaired through homologous repair (HR) or by non-homologous end joining (NHEJ). **A.** In HR, ATM is mainly activated by the MRN complex in a DSB context, resulting in the activation of CHK2 and p53 that cause G1 cycle arrest through *CDKN1A* (p21). Alternatively, single stranded DNA (ssDNA) originated in SSB activates ATR, that forms a complex with ATRIP, that phosphorylates CHK1, among other targets, causing a G2/M arrest and also S phase progression control. **B.** NHEJ enables binding of Ku70/80 heterodimer to the DSB where it recruits and activates the catalytic subunit of the DNA dependent protein kinase (DNA-PK) to mediate the creation of compatible ends that can then be ligated.

flanked by FAT (*FRAP, ATM, TRRAP*) and FATC (*FAT-C*) domains (Mordes and Cortez 2008, Mordes, Glick et al. 2008). An additional PIKK regulatory domain (PRD)

has been described by some authors, located in between the catalytic and FATC domains (residues from 2483 to 2597) (Mordes and Cortez 2008, Mordes, Glick et al. 2008) (**Figure 7**). Some regions of the protein have been described to be implicated in important protein-protein interactions, such as the heterodimerisation with ATRIP (ATR-interacting protein) through its HEAT repeats (Ball, Myers et al. 2005, Chen, Zhao et al. 2007); or its activation by its autophosphorylation in the threonine 1989 (located in the FAT domain) and the FATC/PRD C-terminal domains, mediated by its interaction with TopBP1 (Topoisomerase (DNA) II Binding Protein 1) and, to a lower extent with ETAA1 (Ewing tumor-associated antigen 1), which are stabilised by its heterodimerisation with ATRIP (Mordes and Cortez 2008, Mordes, Glick et al. 2008, Liu, Shiotani et al. 2011, Marechal and Zou 2013, Bass, Luzwick et al. 2016, Haahr, Hoffmann et al. 2016). Additionally, ATR is known to orchestrate the DDR cascade through its binding and phosphorylation to several proteins like CHK1 (Liu, Guntuku et al. 2000, Cortez, Guntuku et al. 2001, Ball, Myers et al. 2005, Mordes, Glick et al. 2008, Bass, Luzwick et al. 2016, Haahr, Hoffmann et al. 2016), although little is known about the specific functions of each region of ATR protein in this complex process. Furthermore, due to its large size, ATR high-resolution structure has only been partially revealed (Rao, Liu et al. 2018).

Mutations in ATR have been associated with Seckel syndrome, a rare condition characterised by growth retardation and microcephaly (O'Driscoll, Ruiz-Perez et al. 2003). Interestingly, deletion of the FATC domain is known to abolish all kinase activity of ATR and this is thought to be due to the impairment of ATR activation by its interaction with TopBP1, as well as a disruption of the adjacent kinase or FAT domain folding (Mordes and Cortez 2008, Mordes, Glick et al. 2008). In contrast, mutations in the PRD region do not abolish the PIK kinase activity but they cause impairment in kinase regulation (Mordes and Cortez 2008, Mordes, Glick et al. 2008). Mutations in the FAT domain have been described in an autosomal dominant oropharyngeal cancer (p.Gln2144Arg), which caused an inhibition of ATR-dependent responses to DNA damage (Tanaka, Weinel et al. 2012). Although FAT domain function has not yet been determined, it is possible that it could have a tumour suppressor role as well as mediate protein-protein interactions in the same way as other PIKKs (i.e. ATM), as looping of the FAT domain results in a direct physical interaction with the kinase domain, thereby stabilising the c-terminal end of the protein and being implicated in

downstream regulatory activities (Bosotti, Isacchi et al. 2000, Lempiainen and Halazonetis 2009).



Figure 7. ATR structure. ATR is a phospho-inositide 3-kinase related kinase (PIKK) that contains several N-terminal HEAT (*Huntington, Elongation factor 3, Protein phosphatase 2A, and PI3K TOR1*) repeats, and a C-terminal catalytic kinase domain (PI3K/PI4K) (2322aa-2567aa), flanked by a FAT (*FRAP, ATM, TRRAP*) (residues 1640-2185) and FATC (*FAT-C*) (residues 2612-2644) domains. An additional PIKK regulatory domain (PRD) has been described by some authors, located in between the catalytic and FATC domains (residues from 2483 to 2597).

Synthetic lethality (SL)

The concept of synthetic lethality has been widely used as an approach to target genetic deficiencies in tumours and it describes a context where the defect of one individual gene is compatible with cell viability, but the perturbation of a combination of genes results in cell death (**Figure 8**) (Brough, Frankum et al. 2011, Ryan, Bajrami et al. 2018), providing an approach that can be used to selectively target tumour cells (Ashworth and Lord 2018). The first clinical application of SL allowed the use of PARP inhibitors (PARPi) for the treatment of breast and ovarian cancers with *BRCA1* and *BRCA2* gene defects (Farmer, McCabe et al. 2005, Tutt, Lord et al. 2005). The recent advances in high-throughput screening techniques have enabled the extension of SL to other histologies, in order to find new actionable target genes that can specifically sensitize cancer cells to drugs that are genotype-specific (Ashworth and Lord 2018). Using the concept of SL as an approach to treat cancer is specifically useful in a tumour suppressor context (as the case of *ARID1A*), where the restoration of the protein loss is not usually possible, but, the detection of the specific tumour dependencies upon that loss can be targeted with a determined treatment, and this can constitute an effective alternative.

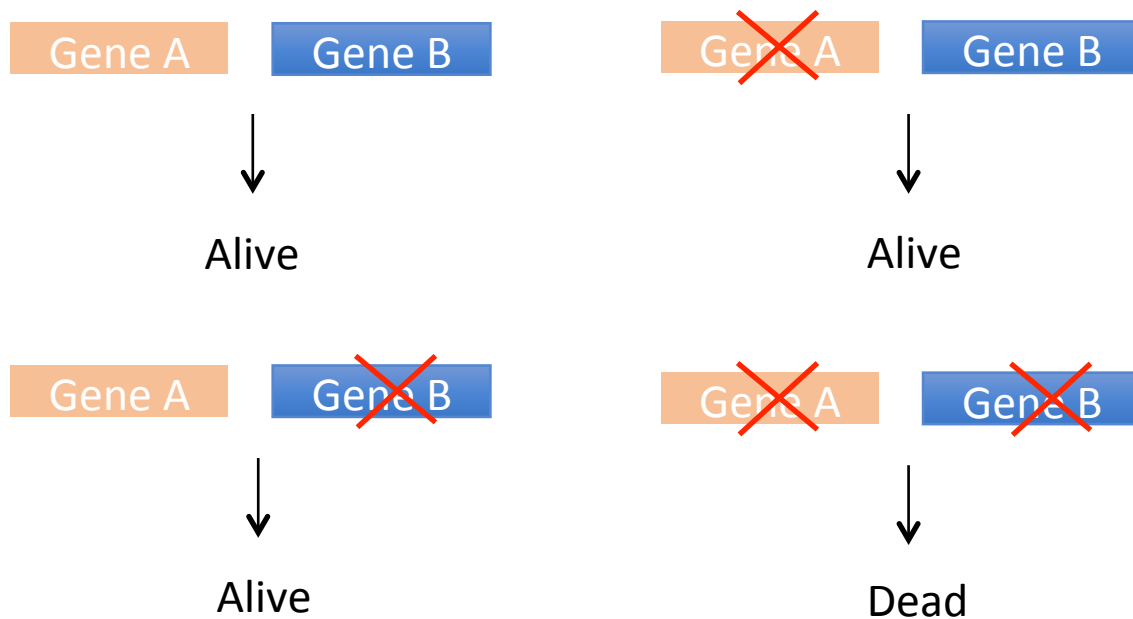


Figure 8. Synthetic lethality. SL described a context where the defect of one individual gene is compatible with cell viability, but the perturbation of a combination of genes results in cell death.

ARID1A and DNA damage repair inhibitors

One of the multiple roles of *ARID1A*, and the SWI/SNF complex itself, consists of the maintenance of genome integrity. *ARID1A* is known to participate in the DNA decatenation process, facilitating DDR of DSB by its interaction with *Topoisomerase II α* (*TOP2A*) during mitosis, which is in charge of decatenating the sister chromatids to permit chromosome segregation (Lou, Minter-Dykhouse et al. 2005, Dykhuizen, Hargreaves et al. 2013, Williamson, Miller et al. 2016). *ARID1A* has been reported to be recruited to DSBs through its interaction with ATR, facilitating DSB end processing to generate RPA-coated ssDNA, and sustaining ATR activity in response to DSB (Shen, Peng et al. 2015). Therefore, loss of *ARID1A* has been linked to an impaired checkpoint activation and a sensitization of cells to several DSB-inducing agents like PARPi and ATRi (Bitler, Aird et al. 2015, Bitler, Fatkhutdinov et al. 2015, Shen, Peng et al. 2015, Bitler, Aird et al. 2016, Williamson, Miller et al. 2016, Bitler, Wu et al. 2017, Jones, Fleuren et al. 2017, Fukumoto, Park et al. 2018).

Although *ARID1A* is currently not being used as a biomarker in any on-going clinical trial, recent studies have demonstrated its clinical importance and suggested that should be taken into consideration as a biomarker for a number of small molecule

inhibitors including ATR, PARP, HDAC, EZH2 and PI3K inhibitors, amongst others (Bosse, ter Haar et al. 2013, Samartzis, Noske et al. 2013, Samartzis, Gutsche et al. 2014, Bitler, Aird et al. 2015, Bitler, Fatkhutdinov et al. 2015, Shen, Peng et al. 2015, Wang, Li et al. 2016, Wang, Wang et al. 2016, Williamson, Miller et al. 2016, Bitler, Wu et al. 2017, Jones, Fleuren et al. 2017, Fukumoto, Park et al. 2018, Yang, Yang et al. 2018). Moreover, the use of antibodies to detect ARID1A expression by immunohistochemistry (IHC), has been carried out by Khalique and colleagues, which will allow patients to be stratified based on their ARID1A status into early phase clinical trials (Khalique, Naidoo et al. 2018).

There are already three early phase studies retrospectively taking in account *ARID1A* mutational status and its association with therapy response. First, the OLAPCO trial takes in account *ARID1A* status to treat patients with a combination of olaparib (PARPi) and the AKT inhibitor AZD5363 (NCT02576444). Secondly, the randomised phase II study of nintedanib (*Vascular Endothelial Growth Factor, VEGF, FGFR* and *Platelet Derived Growth Factor Receptor, PDGFR* inhibitor) is being carried on in patients with ovarian or endometrium carcinoma, and will assess *ARID1A* status retrospectively (2013-002109-73). Finally, a trial due to start recruiting patients soon will assess the chemotherapeutic agent dasatinib in patients with recurrent or persistent ovarian, fallopian tube, endometrial or peritoneal carcinoma and will retrospectively compare *ARID1A* mutational and IHC status (NCT02059265) (Khalique, Naidoo et al. 2018). Moreover, a Phase II Proof of Concept Study is due to start in the Royal Marsden Hospital (NCRI) with the objective of assessing the Activity of the ATRi, AZD6738, as a single agent and in combination with the PARPi olaparib in *ARID1A* stratified gynaecological cancers (ATARi trial). The results of this trial will be highly informative and might encourage further stratification of patients taking in account *ARID1A* as biomarkers in other histologies if improvements in survival outcomes are seen.

With regards to clinical trials assessing the effectivity of DDR inhibitors in GC, a translational phase II study using the PARPi olaparib or the ATRi AZD6738 will soon start recruiting patients with advanced oesophageal, gastro-oesophageal and GC (SOIAR trial), with one of the objectives of assessing ARID1A status as a candidate predictive biomarkers of both inhibitors response.

Although not many GC-specific studies have been carried out, the use of several DDR-involved proteins inhibitors has been explored in other histologies before, and it is currently the focus of many investigations (Brandsma, Fleuren et al. 2017, Lord and Ashworth 2017). More specifically, because of the crucial role of ATR in the DDR process, and considering published preclinical data showing SL in particular molecular contexts, ATRi are being assessed in preclinical and clinical studies, in monotherapy or combination with other drugs (Sundar, Brown et al. 2017).

Current clinical use of ATR inhibitors (ATRi)

One of the first described ATRi was the selective and potent VE821 (Vertex pharmaceuticals), which showed significant synergistic effects in cell lines when combined with chemotherapeutic agents and radiation (Prevo, Fokas et al. 2012, Huntoon, Flatten et al. 2013, Josse, Martin et al. 2014, Abdel-Fatah, Middleton et al. 2015). VE821 was demonstrated to have an enhanced effect in cell lines with p53 or ATM defects (Reaper, Griffiths et al. 2011). AZ20, and its improved oral version, AZD6738, were developed by AstraZeneca, showing similar features and compared with VE821 (Foote, Blades et al. 2013, Guichard, Brown et al. 2013, Sarris, Trantas et al. 2013). Both of these compounds are currently being tested in phase I clinical trials being VE821 now labelled as VX970/M6620. Preliminary data from the VX970 and AZD6738 clinical trials monotherapy and combination with several chemotherapy regimens reviewed in (Sundar, Brown et al. 2017) have revealed some good responses, especially in patients with tumours presenting defects in DDR (like for example loss of ATM) (O'Carrigan, Luken et al. 2016, Shapiro, Wesolowski et al. 2016, Yap, Krebs et al. 2016). AZD6738 is being evaluated in combination with PARPi in several trials (NCT03330847, NCT03682289, NCT03462342, NCT03428607, NCT02264678, NCT02576444) and partial responses have been reported (Yap, Krebs et al. 2016). Another trial studying the combination of VX970 with the PARPi veliparib and cisplatin is ongoing (NCT02723864). Additionally, a new oral version of the vertex ATRi (VX803/M4344) is currently undergoing a phase I dose escalation study in advanced solid tumours as monotherapy and in combination with carboplatin chemotherapy (NCT02278250).

ATR is becoming a popular druggable target along the DDR pathway, and further clinical trials, evaluating these compounds in monotherapy or in combination with other therapies such as PARPi or immunotherapy, are needed to fully exploit the

potential of ATRi (Sundar, Brown et al. 2017). Additionally, the discovery of robust biomarkers that allow an effective stratification of the patients will help to achieve better results.

High-throughput CRISPR/Cas9-based genetic screens to detect mechanisms of synthetic lethality

Cas9 nuclease is a DNA endonuclease enzyme from the prokaryotic CRISPR immune system that is able to cleave DNA at a NGG sequence (also known as PAM site), to form DSBs (Deveau, Garneau et al. 2010, Garneau, Dupuis et al. 2010, Horvath and Barrangou 2010, Bhaya, Davison et al. 2011) (**Figure 9**). Cas9 can be recruited to PAM sites by a short 20 nucleotides guide RNA (gRNA) molecule, that specifically binds to a determined sequence of the genome (Mali, Yang et al. 2013). Once recruited to the gRNA sequence, Cas9 cleaves the DNA a few base pairs (bp) 5' from the PAM site, generating a DSB. This mechanism has been exploited to precisely edit the genome, since the repair of the DSB can be carried out by HR, maintaining the original sequence or can alternatively be repaired using the NHEJ pathway, which is an error-prone pathway, that will cause the insertion or deletion of nucleotides in the area where the DNA has been cleaved, potentially resulting in a gene loss of function and defective protein expression (Mali, Yang et al. 2013). This approach is known as the Clustered Regularly Interspersed Short Palindromic Repeat Associated 9 (CRISPR/Cas9) gene editing technology (Ran, Hsu et al. 2013). Genome-wide (GW) CRISPR/Cas9 screens represent the high-throughput application of the CRISPR/Cas9 system, where thousands of mutations over the whole genome are caused in one reaction, in order to investigate potential synthetically lethal interactions. Nowadays, several approaches have been described to induce modifications in the DNA using CRISPR/Cas9 screens. CRISPRn (nuclease) libraries are available to induce knockout expression of genes, while CRISPRi (inhibition) libraries are used to induce repression of genes, and CRISPRa (activation) are used to cause gene activation (Miles, Garippa et al. 2016). Other further modifications of the CRISPR/Cas9 methodology have been described, as for example, the use of dead Cas9 proteins that lack the catalytic activity to make DSB, but maintain the ability to bind the DNA and form single-stranded bubbling structure, where DNA modifying enzymes (i.e. deaminases) can be added to alter the DNA, typically causing point mutations (mostly missense mutations) around a 5-nucleotide window (CRISPRx approach)(Hess,

Fresard et al. 2016) (**Figure 9**). Screens can also be classified into positive or negative selection screens. Positive selection screens are useful to identify resistance-causing genes to a particular drug, where cells are exposed to high doses of drug (Surviving fraction of 0, SF_0), and only cells with a resistance-conferring mutation are able to proliferate. One is able to detect an enriched population of certain sgRNA in the resistant population, compared with a time=0 sample. In contrast, negative selection screens are carried out using low drug concentrations (SF_{50} - SF_{80}), thus favouring the death of the cells with certain sensitivity-conferring mutations, consequently detecting a lack in certain sgRNAs representation in the final population, compared with T=0 sample (Miles, Garippa et al. 2016).

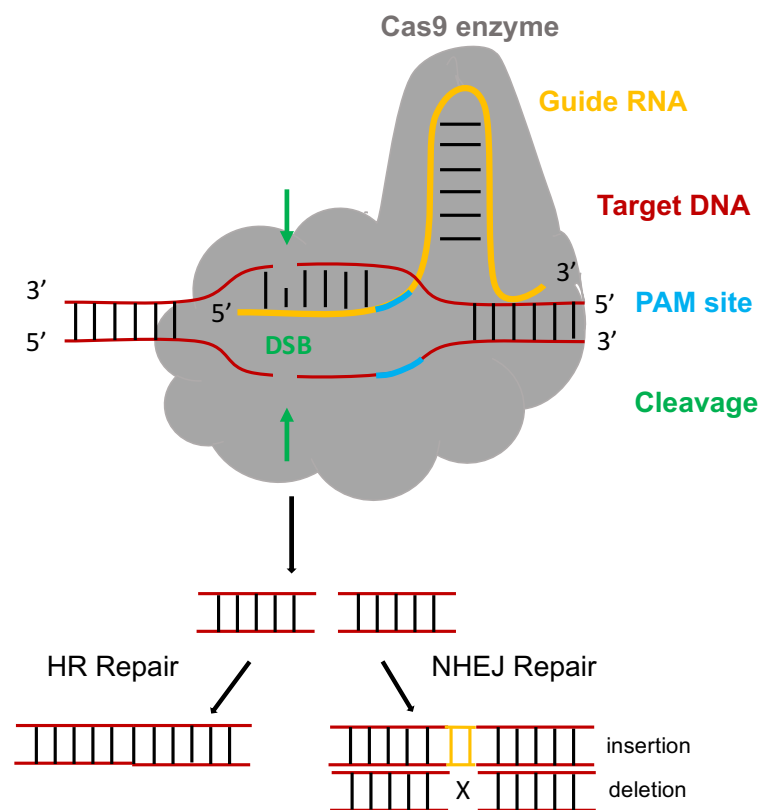


Figure 9. CRISPR/Cas9 mediated gene editing. Mechanism of Cas9-induced gene targeting. Cas9 interacts with a specific 20bp guide RNA that binds to the complementary genomic sequence adjacent to a *NGG* (PAM) site. Cas9 cleaves the DNA few base pairs from the PAM site, generating a double strand break (DSB). The repair of the DSB can be then carried out by HR, maintaining the original sequence or can alternatively be repaired using the NHEJ pathway, which is an error-prone pathway, that will cause the insertion or deletion of nucleotides in the area where the DNA has been cleaved, potentially resulting in a gene loss of function and defective protein expression.

Aims and approaches

Due to the increasing number of studies confirming the high frequency of *ARID1A* mutations in GC, efforts to identify targeted therapies towards this genetic alteration are clinically relevant. Furthermore, preclinical data demonstrating synthetic lethality with DDR inhibitors such as ATRi or PARPi, that have already been approved or are being tested in clinical practice in other histologies, provides a rationale to test these compounds in *ARID1A* deficient GC models. Moreover, determining potential resistance mechanisms to these therapies will allow the design of effective combinatorial approaches to achieve improved responses in GC patients with who have extremely limited treatment options.

Therefore, the aims of this project are:

1. To identify genetic dependencies for *ARID1A* deficiency through monotherapy or combination drug testing experiments, in a panel of gastric tumour cell lines.
2. To validate genetic dependencies for *ARID1A* deficiency in GC *in vitro* models (patient derived-xenografts).
3. To identify mechanisms of resistance to ATRi in GC through the use of high throughput CRISPRn, CRISPRx screens and the characterisation of ATRi resistant models.

As part of these work I have (i) demonstrated the previously described synthetic lethality involving ATR inhibitors in *ARID1A* deficient cancers can be extended to GC models, both *in vitro* and *in vivo*, (ii) identified and validated a list of genetic determinants to ATRi resistance, including *HUWE1*, *SMG8*, *SMG9*, *SMG1*, *HNRNPF*, *IRF9*, *CARD10*, *CDC25B* and *STAT2* iii) created ATRi resistant models that have allowed me to validate previous hypothesis, and added additional information about the resistance mechanisms that can arise from ATRi treatment (iv) identified mutations localised in the FAT domain of ATR, that cause resistance to ATRi.

Materials and Methods

Cell lines

AGS, HEK 239T and NCI N87 cell lines were obtained from American Type Culture Collection (ATCC). SNU 1, SNU 5, SNU 484 and SNU 638 were purchased from Korean Cell Line Bank (KCLB). YCC6 cell line was a gift from Professor Sun Young Rha from the Yonsei Cancer Center in South Korea. ARID1A HCT 116 isogenic cell lines were obtained from Horizon Discovery. HCT 116 cells were grown in McCoys medium and DMEM was used for HEK2 39T cells. The rest of the cells were grown in regular RPMI 1640. All medium was supplemented with 10% FBS. No antibiotics were added to the media. Cell line identity was confirmed regularly by STR typing using the StemElite Kit (Promega), analysing eight ATR loci: vWA, TH01, CSF1PO, D16S539, D7S820, D13S317, D5S818 and amelogenin (for gender identification). Mycoplasma testing was carried out periodically using MycoAlert Mycoplasma Detection Kit (Lonza).

Microsatellite instability determination

Microsatellite instability determination was carried out by the Molecular Diagnostics Departments (The Centre for Molecular Pathology, The Royal Marsden NHS Foundation Trust, Sutton, UK). Briefly, the Type-it Microsatellite PCR kit (Qiagen, Hilden, Germany) was used to co-amplify five markers (NR27, NR21, NR24, BAT25 and BAT26) in a standard multiplex PCR. The PCR conditions were: denaturation at 95 °C for 5 minutes, 28 cycles of melting at 95 °C for 30 seconds, annealing at 60 °C for 90 seconds, and extension at 72 °C for 30 seconds, followed by a final extension phase at 60 °C for 3 minutes. The PCR products were denatured and separated by capillary electrophoresis using an ABI PRISM 310 DNA sequencer and were further analysed with the GeneMapper software (Applied Biosystems, Paisley, UK). MSI status was confirmed when two or more markers presented instability and microsatellite stable (MSS) status was confirmed when one or none of the markers presented instability.

In the case of the PDX *in vivo* experiment the studied markers were NR21, BAT26, BAT25, NR24 and MONO27, using penta-C and D as controls, which serve as internal controls.

Genomic DNA extraction from cell lines

Genomic DNA was extracted from cell lines using the QIAamp DNA Blood Mini Kit (Quiagen), according to the manufacturer's instructions, eluted in 30 µl of nuclease-free H₂O and stored at -20°C. DNA concentrations were determined by measuring absorbance at 260nm using a the NanoDrop1000.

Polymerase Chain Reaction (PCR) and gel electrophoresis

Generally, PCR Amplicons were generated using 100ng of DNA in 50 µl reactions, using the New England BioLabs Q5® High-Fidelity DNA Polymerase set, according to manufacturer's protocol, using specific primers listed in **Table 1**. PCR was carried out on a thermocycler as follows: 98°C for 2', followed by 30 cycles of 98°C for 30'' (melting), 60°C for 30'' (annealing) and 72°C for 20'' (elongation), followed by a final 72° for 2' step. Annealing temperature and elongation were adjusted for each reaction according to the primer requirements and length of the product, respectively. All primers were ordered from Integrated DNA technologies (IDT) or Thermo Fisher scientific as lipolysed powder, which were resuspended in nuclease-free H₂O (Ambion) to a concentration of 100 µM and stored at -20°C. Primers were then diluted to 10 µM for use in each PCR reaction. PCR products were analysed by agarose gel electrophoresis by mixing with 6x loading dye (New England Biolabs) and separation by gel electrophoresis. Agarose gels were made as follows: 1-2% ultra-pure agarose (Life Technologies) dissolved in 1x TAE buffer + 1/10,000 GelRed nucleic acid stain (Biotium). Hyperlader 1 (Bioline) was used to estimate length of the PCR products. DNA was then visualised using an ultraviolet transilluminator (Syngene).

TOPO cloning and sanger sequencing

100ng PCR products from genomic DNA extracted from CRISPR-Cas9 targeted SNU 484 cells or GW-CRISPR/Cas9 mutagenesis screen YCC6 resistant colonies were cloned into the pCR-Blunt II-TOPO vector, using the Zero Blunt TOPO PCR Cloning kit (Invitrogen) following manufacturer's protocol. The final mix was incubated 1h at room temperature and prepared for transformation. For transformation, 150 µl of

competent cells were placed into a sharp-bottom Eppendorf and mixed gently with 5 µl of cloned product. After 30 minutes of ice incubation, tubes were heated at 42°C for 45 seconds and cooled back on ice. 300 µl of outgrowth SOC media were added and the tubes were placed in the shaker for 1h at 37°C. After incubation, tubes were spanned and plated in petry plates. Petry plates were then incubated upside down overnight at 37°C. Next day; colonies were picked, expanded in antibiotic selective media and DNA was extracted after 18h of incubation, using the Qiaprep Spin Miniprep kit from Quiagen. PCR purification was carried out using the QIAquick PCR Purification Kit.

Table 1. Summary of PCR and sanger sequencing primers used in this thesis

Reagent	Sequence	Supplier
HUWE1 CRISPR Forward primer	CCATGTAAACAGTCATAGCCAC	IDT
HUWE1 CRISPR Reverse primer	GGACAGGGCAGAGCTATAAG	IDT
IRF9 Forward primer	CACGCCTGTAAAGCCAGTCC	IDT
IRF9 Reverse primer	GGACAGGGCAGAGCTATAAG	IDT
U6-F	GGCCTATTTCCCATGATTCCTTC	IDT
CRISPR-scaf-R	ACTCGGTGCCACTTTTTCAA	IDT
ARID1A CRISPR Forward primer	AGGGGGGGAGAAGACGAAGA	Thermo Fisher
ARID1A CRISPR Reverse primer	AGGCCAGGGCTTTGTTGT	Thermo Fisher

For the sanger sequencing, 15 µl of purified DNA, was mixed with 2 µl of 10 µM forward or reverse primers for the target gene sequence and prepared at a final concentration of 100 ng/µl in the case of plasmidic DNA, or 10ng/µl for PCR purified DNA. Samples were outsourced to Eurofins Genomics (<https://www.eurofinsgenomics.eu>) and results were analysed using the sequence alignment tool of ApE Plasmid Editor free software.

Chemicals

Information about all chemicals used is listed in **Table 2**.

Table 2. Drugs used in this thesis

Drug	Code	Supplier
VX970 (VE822)	S7102	Selleckchem
AZD6738	S7693	Selleckchem
Olaparib	S1060	Selleckchem
Talazoparib	S7048	Selleckchem
BKM120 (buparisisb)	S2247	Selleckchem
MK2206 (-2HCL)	S1078	Selleckchem

ACY1215 (ricolinostat)	S8001	Selleckchem
GSK126	S7061	Selleckchem
Puromycin solution	Ant-pr-1	Invitrogen
Blasticidin solution	And-bl-05	Invitrogen
Doxycycline hyclate	D9891	Sigma-Aldrich
M4344 (PDX)		Merck

Western blotting and antibodies

Whole cell lysates were extracted using lysis buffer (1% Sodium deoxycholate, 1% TritonX-100, 1% Nonident P-40, 0.1% SDS, 150nM NaCl, 5mM EDTA, 50mM Tris, 30mM NaF and water), supplemented with proteinase inhibitor (10X) and phosphatase inhibitor (100x), and separated using 3-8% Tris-Acetate gels (Invitrogen) or 4%–12% sodium dodecyl sulfate-polyacrylamide gel electrophoresis (SDS-PAGE) Bis-Tris gel, transferred to nitrocellulose membrane, blocked in 5% milk or BCA and blotted with primary antibody in Milk or BCA overnight. Next day, a fluorescent secondary antibody was added, following 3 x 5 minutes' washes with TBST. Membrane was again washed with 3 TBST x 5 minutes' washes, and signal was then read using the Li-core (odyssey) system. Information about the antibodies used is shown in **Table 3**. All WB were performed by triplicate. Only the best result is represented in the figures.

Table 3. Western Blot antibodies used in this thesis

Gene	Protein size (KDa)	Primary antibody dilution (BSA/Milk)	Secondary antibody dilution (Milk)	Specie	Company	Product code
ARID1A	242	1:1000 (BSA)	1:5000	Rabbit	CST	12354
β-Actin	44	1:2000 (Milk)	1:10000	Mouse	CST	3700
IRF9 (ISGF3)	48	1:500 (BSA)	1:1000	Mouse	SC	sc-135953
HUWE1 (lasu/ureb1)	490	1:500 (BSA)	1:1000	Rabbit	Bethyl	A300-486A-T
SMG1	410	1:1000 (BSA)	1:2000	Rabbit	CST	9149
UPF1	141	1:5000 (BSA)	1:5000	Rabbit	CST	12040
Ezrin	81	1:1000 (Milk)	1:5000	Rabbit	CST	3145
CRISPR-Cas9	158	1:2000 (Milk)	1:5000	Mouse	Diogenode	C15200203-100
IRDye 800CW donkey anti-Rabbit IgG					Li-cor	926-32213
IRDye 800CW Goat anti-Mouse IgG					Li-cor	925-32210
Anti-Mouse IgG					CST	7076
Anti-Rabbit IgG					CST	7074

Cellular viability assays

5-days survival assays were performed in 384-well plates. Cells were plated at a concentration of 500 cells per well and drugged for 5 days, 24h after seeding. Viability was estimated using CellTitre-Glo luminescence reagent (Promega). Cell-based assays were performed by triplicate. Final number of cells was normalised to DMSO median and surviving fractions of cells were plotted in GraphPad Prism, where lines of best fit were drawn using a four-parameter nonlinear regression. SF₅₀ (Surviving Fraction 50 = the concentration of drug required to cause a 50% inhibition of the cell population) or AUC (Area Under the Curve) values were calculated from these curves using GraphPad Prism software. Comparisons of dose-response curves were performed using two-way ANOVA testing. Comparisons of SF₅₀ or AUC data were performed using the Mann-Whitney test for non-parametric samples.

Cell proliferation experiment

2000, 4000 and 6000 cells were seeded in a clear well 6-well plate and live-analysed for 7 days using the IncuCyte Zoom Live Cell Analysis System (Essenbio) at 37°C, 5% CO₂. Final number of cells was estimated through image analysis, and mean and standard deviation was calculated for each well and compared in between samples. Proliferating experiment was repeated more than three times, only the best result is shown in the figures.

RNA extraction and Real time- PCR (RT-PCR)

RNA was extracted using RNeasy Mini Kit (Quiagen) and RNA concentration was measured using the NanoDrop1000. cDNA conversion was carried out from 1 µg of RNA using iScript Kit (Bio-Rad). Quantitative PCR was first optimised carrying out a standard curve as an initial run, to determine the optimal primer concentration for ARID1A (Fw probe: 5'-TCATGCCCAACCTTCGTATC-3'; Reverse probe: 5'-GATGGCTGCTGGGAGTATG-3'), used at a final concentration of 900 nM. β-Actin was used as an endogenous control, using a final primer concentration of 300 nM (Fw probe: 5'-CCCTGGCACCCAGCAC-3': Rv Probe: 5'-GCCGATCCACACGGAGTAC-3'). The experiment was done by triplicate in MicroAmp Optical 96-Well Reaction Plate from Thermo Fisher, and ran in the QuantStudio 6 Flex (Thermo Fisher), following the next temperature steps: 50°C for 2', 95°C for 2min and 40 cycles of 15°C for 15'' and 60°C for 1'.

Raw data from the RT-PCR machine is presented as Cycle threshold (Ct), which indicates the number of PCR cycles required for fluorescence to reach a defined threshold. The difference in Ct values for the *ARID1A* (FAM) and *ACTIN* (VIC) signals were calculated to define the Δ Ct, which indicates the level of *ARIDA* expression relative to the endogenous control *ACTIN*. The fold-change for each replica well was used to define the median and standard deviation of the *ARID1A* expression levels in every cell line.

Reverse siRNA transfection knockdown experiments

Reverse transfections using the siRNA SMARTpool, siCON2 negative control (DE dharmacon) or the siAllstar negative control (Quiagen) were carried out in 6 well-plates using 5 μ l of the siRNA (20 μ M), mixed with 250 μ l of optiMEM and incubated at RT for 10 minutes. 5 μ l of RNAiMax (Invitrogen) were incubated with 250 μ l of optiMEM for 10 minutes. Total volume of the transfection mix was added to the siRNA mix and incubated at RT for 30 minutes. Lysates were retrieved after 3 days, and proteins were extracted to test for protein expression by western blot. In the cases where a higher number of cells was needed experiments were performed in 10 cm plates, where quantities of the reagents were scaled to a final volume of 10 ml. Viability assays were performed as described in cellular viability assays section. The de-convoluted siRNA target sequences used are as follows: siARID1A_1 GCAACGACAUGAUUCCUAU, siARID1A_2 GAAUAGGGCCUGAGGGAAA, siARID1A_3 AGAUGUGGGUGGACCGUUA, siARID1A_4 UAGUAUGGCUGGCAUGAUC, siSMG1_1: GCAAAGAGCUGUUCAGGAA, siSMG1_2: GCGAAAGAUUGACAUCAUA, siSMG1_3: GUCAAGAGCUCUAUAGGAA, siSMG1_4: GUUAGAGCUUCGUUUUAUUA. All siRNA experiments were done by triplicate. Only the best result is shown in the figures.

Cells plated in wells transfected with the siRNA of interest were compared with cells in the wells transfected with the negative control siRNA (siCON2 or siAllstar). The surviving fraction was the calculated as follows:

Surviving fraction = (Luminescence in siRNA of interest treated well)/(Luminescence in siAllstar treated wells).

***In vivo* assessment of ATRi efficacy in gastric cancer Patient-Derived Xenografts (PDX).**

In vivo efficacy study testing the M4344 oral ATRi (Merck) was carried out by CrownBio company, in an agreed academic collaboration with Merck Serono, in gastric adenocarcinoma PDX models (CrownBio HuPrime GC xenografts) implanted in female BALB/c Nude mice. Seven PDX were selected from CrownBio database, according to its *ARID1A* mutational status, which was provided by the company (exome sequencing and RNA sequencing information) and additionally validated in-house. *ARID1A* protein expression testing was done by Saira Khalique and The Breast Cancer Now laboratory (The Institute of Cancer Research, London, UK) by IHC and *ARID1A* DNA sequencing was done the Tumour Profiling Unit (The Institute of Cancer Research, London, UK), using the PGM 318 Chip (IonTorrent) using a previously designed panel of genes, containing *ARID1A*, created by Saira Khalique as previously described (Khalique, Naidoo et al. 2018). Briefly, *ARID1A* loss of protein expression was tested through IHC of Formalin-fixed paraffin-embedded (FFPE) sections across all the tumour samples, using the D2A8U *ARID1A* antibody at a 1:250 dilution, (Cell Signalling Technology) and the Dako-Autostainer Link 48 with the EnVision FLEX kit as per manufacturer's instructions (Agilent Technologies). HCT 116 *ARID1A* WT and deficient cell pellets were used as positive and negative controls, respectively, and two independent pathologists' who were blinded to the mutational status of the sample determined the results obtained. Additionally, microsatellite instability status was determined as described above.

For the *in vivo* experiment, M4344, rather than VX970 has been used, as M4344 is an oral compound that has previously been observed in other tumour models to have superior *in vivo* efficacy and it is currently being assessed in phase I clinical trials in monotherapy or in combination with PARPi. Although single agent M4344 delivered at 20mg/kg daily is largely well tolerated in other *in vivo* tumour models, an additional single agent M4344 arm at a reduced dose of 10mg/kg daily was included as a precaution in the event that tolerability issues are experienced in the mice.

Therefore, to assess the sensitivity of the PDXs to M4344, six experimental arms were designed, where seven randomised distributed mice, bearing tumours with an approximate size of 100-200mm³, were treated with either: M4344 20mg/kg twice a day (BID), twice per week; M4344 10mg/kg once a day (SID), twice per week; ATRi M4344 3mg/kg daily, Talazoparib 0.1 mg/kg 2x daily and ATRi M4344 3mg/kg daily +

Talazoparib 0.1 mg/kg 2x daily, all treatments given by oral gavage. Model GA2148 was used to escalate the doses, that were lessened in the rest of the models, due to severe body weight loss in mice receiving the highest doses of the ATRi. The other models were treated with 10mg/kg twice a week or 5 mg/kg M3433 daily instead of 20 and 10 mg/kg. Sample sizes for treatment groups were calculated on Cohen principle (1998), considering the following basics: Effect on 75% are measured as significant, assuming normal distribution, p-value (α) <0.05 and a β of 0.95. Calculation of the variance is assumed to be about 40% for a randomised population (tumours are randomised to have equally distributed standard variations within the treatment groups). Plasma samples were retrieved from each animal at 2 and 6 hours after treatment for pharmacokinetic studies. Furthermore, for the cases where reduced tumour growth has been observed, mice were continued to be treated until the tumour developed acquired resistance and re-grown. Those tumours were then harvested for further molecular characterisation through whole exome sequencing, RNA sequencing and mass spectroscopy-based proteomic profiling (**Figure 10**).

YCC6 VX970 resistant cell lines

To generate YCC6 VX970 resistant cells, two independent 20-30% confluent flasks were treated with increasing concentrations of VX970, starting from SF₈₀ and steadily increasing dose every week, for a total of 5 consecutive months, until they became resistant to 5 or 8 times-fold the initial SF₅₀ (from 54nM to 230nM and 460nM, respectively). Then, single cells were sorted in 96 well-plates by flow cytometry, using the FACS Aria (Becton Dickinson). 8 proliferating colonies (6 of them resistant to 460 nM flask, and two of them resistant to 260nM VX970), were then expanded and treated, with same concentrations of drug for 2 weeks, before testing for ATRi (VX970 and AZD6738) sensitivity, compared with parental YCC6 cell line. Cells were expanded and lysates were retrieved to simultaneously extract DNA, RNA and proteins for exome sequencing, RNA sequencing or Mass spectrometry, respectively.

Proteomic analysis by mass spectrometry in ATRi resistant clones

Protein extraction, preparation and mass spectrometry processing and analysis was carried out by the Proteomics & Metabolomics Laboratory (Institute of Cancer Research, London, UK). Briefly, cell pellets were lysed by probe sonication/boiling, and protein extracts were subjected to trypsin digestion. The tryptic peptides were

labelled with the Amine-reactive TMT10plex Isobaric Label reagent set (Thermo Fisher Scientific), which enables multiplexed protein identification (9,410 proteins) and quantitative analysis by tandem mass spectrometry (MS). Labelled products were then combined at equal amounts, and fractionated with high-pH C18 high-performance liquid chromatography (HPLC). LC-MS analysis was performed on the Dionex Ultimate 3000 system coupled with the Orbitrap Fusion Mass Spectrometer. Data analysis was carried out using online Perseus software (Marx Plank institute).

Next Generation Sequencing (NGS)

Exome sequencing was carried out by Tumour Profiling Unit (The Institute of Cancer Research, London, UK). Briefly, DNA extracted from cells from the GC panel was exome sequenced using the HiSeq2500 (v4, Illumina), after preparing the samples according to manufacturer's instructions, using the Agilent SureSelectXT V6 exome library kit (Illumina) and using PE 100 cycles to a median depth of >100X for all samples. FastQ files were generated and further processed by the Breast Cancer Research Bioinformatics Group (The Institute of Cancer Research, London, UK).

Analysis of cell cycle distribution by FACS

For the cell cycle analysis, 60,000/ml cells were seeded in 6-well plate and incubated 48h before VX970 or DMSO control was added to the media in two different concentrations (75nM and 150nM). Cells were then exposed to the drug for 24 or 48h, stained with 20µM EdU (5-ethynyl-2'-deoxyuridine, a nucleoside analog to thymidine, incorporated into DNA during active DNA synthesis) for one hour, when they were harvested and fixed overnight with cold ethanol 70%. Staining was then carried out using the Click-IT EdU kit (Thermo Fisher Scientific). Next day, cells were permeabilised and Alexa647 was added to the media. Cells were then digested with RNase A (Sigma Aldrich), before propidium iodide (PI, a DNA intercalating agent that allows us to measure cell viability or DNA content in the cells) was added to the cells (Sigma Aldrich). Detection of EdU or PI staining was analysed on a BD LSR II flow cytometer (BD Biosciences). EdU was measured with the red laser detecting Alexa647 blue at 635 nm and using the 60/20 filter, while PI was measured at 488nm detecting PE/Texas red using the 610/20 filter. Debris and doublets were gated out from a FSC/SSC dot plot and DNA dye area/width dot plot, respectively and the selected population was analysed regarding its cell distribution on the cell cycle using the FACS

diva software. Flow cytometry analysis was supervised by Radhika Patel and the flow cytometry unit (The Institute of Cancer Research, UK).

ARID1A CRISPR/Cas9 mutagenesis

60% confluent cells were transfected in 6-well plates, following a standard forward transfection protocol using 2500ng Geneart Platinum Cas9 nuclease (Invitrogen) per well, 5µl of Lipofectamine Cas9 Plus Reagent, 7.5µl Lipofectamine CRIPRMAX Reagent (Invitrogen) and 650ng of *ARID1A* sgRNA, previously generated with the GeneArt Precision sgRNA Synthesis Kit (Invitrogen) (sgRNA sequence ARID1A.1: AAGAACTCGAACGGGAACGC: sgRNA sequence ARID1A.2: CGGACCTGAAGAACTCGAAC: sgRNA sequence ARID1A.3: GAAGAACTCGAACGGGAACG). A sgRNA with no homology to any known mammalian gene was used as a negative control. Single cells were sorted with FACS Aria (Becton Dickinson) in 96-well plates and left to proliferate. Colonies were harvested and tested for ARID1A protein expression by western blot, and for mutations, by PCR and Sanger sequencing using the following primer sequences, amplifying the region surrounding the gRNA target sequence (Forward: AGGGGGGAGAGAAGACGAAGA; Reverse: AGGCCAGGGCTTTGTTGT).

Positive selection genome-wide CRISPR/Cas9 screen

Doxycycline (Dox) inducible-Cas9 expressing cells were generated by transduction of YCC6 cells with the Edit-R Inducible Lentiviral hEF1a-Blast-Cas9 Nuclease (Dharmacon) and selected in 7µg/ml blasticidin for five days (YCC6^{iCas9}). Cas9 catalytic activity was tested using a two-fluorescence protocol, transducing cells with a GFP (Green Fluorescent Protein)/RFP (Red Fluorescent Protein, Cherry) expressing construct (GFP/RFP/empty), or with the same construct carrying an additional gRNA sequence towards GFP protein (GFP/RFP/gfp-sgRNA). Cells were then treated with Dox for at least 2 days, retrieved, and green and red fluorescence was analysed by flow cytometry using the BD LSRII cell analyser. More than 50% of the cells showing a decrease in green fluorescence, in the cells infected with the GFP/RFP/gfp-sgRNA construct, compared with the empty one was considered as a positive result for Cas9 catalytic activity.

Next, cells were seeded aiming a 1000x representation per sgRNA in the library, and infected at a multiplicity of infection (MOI) of 0.3, to avoid multiple sgRNA infections

per cell, with a previously published and validated GW human lentiviral CRISPR library (Kosuke Yusa, Human GW CRISPR guide RNA library V1)(Koike-Yusa, Li et al. 2014). Efficiently transduced cells were selected twice with 5 µg/ml puromycin for two and five days, consecutively, when a sample T=0 was taken (<1000x sgRNA representation number of cells). After the T=0 sample was taken, 1 million cells were plated per each 15-cm plate, maintaining the 1000x sgRNA representation, and 100 nM VX970 (SF0) was added to the cells. Cells were fed and drugged twice a week for three weeks, before T=1 was taken. Additionally, twenty-four surviving colonies were picked and analysed for the presence of sgRNA sequences by PCR and Sanger sequencing, as described above.

DNA from sample T=0 and T=1 was extracted and PCR of the CRISPR guide regions were carried out. Guides in each sample were sequenced by the Tumour Profiling Unit (The Institute of Cancer Research, London, UK), using a U6 custom primer on the HiSeq (Illumina), which sequences the CRISPR sgRNA to generate gRNA count data. Bioinformatic analysis were performed by the Breast Cancer Research Bioinformatics Group (The Institute of Cancer Research, London, UK). MAGeCK (Model-based Analysis of GW CRISPR/Cas9 Knockout) software was used to generate sgRNA counts according to the sequences present in the GW CRISPR library. Using the normalised read count data from MAGeCK, quality checks (QC) were performed (read counts per guide, distribution of read counts), to confirm the robustness of the data. For downstream analysis of gRNA read count data, two approaches were used: Z-score analysis and MAGeCK analysis.

For the Z-score analysis (where Z=0 represents no effect on viability and positive Z scores represent gain of viability), the guides with a maximum read count of zero in the T=0 sample were firstly identified and removed from the analysis. Then, the raw read counts were converted to parts per ten million (pptm) counts to account for variation in the amounts of DNA sequenced. The raw pptm counts were further converted to pseudocounts by adding a factor of 0.5 and then were log₂ transformed before calculating the viability effect (VE) and drug effect (DE) Z-scores (equation 1 and 2). VE is defined as the rate of decrease in abundance of each gRNA in the population over time in the absence of drug treatment (DMSO) while DE is defined as the difference in abundance of each gRNA between VX970 and vehicle (DMSO) treated samples at a specified time point during the experiment. To remove variation in DE that can be attributed to VE, a linear model of DE~VE was fitted and then

adjusted DE using equation 3 to give corrected DE. I considered a threshold of Z-score larger than 2 for resistant sgRNAs and Z-score ranks for positive selection were generated by sorting results based on their Z-score.

Equation 1:

$$\text{Viability Effect (VE)} = \frac{(DMSO(T1) - DMSO(T0)) - \text{median}(DMSO(T1) - DMSO(t0))}{MAD(DMSO(T1) - DMSO(T0))}$$

Equation 2:

$$\text{Drug Effect (DE)} = \frac{(Drug(T) - DMSO(T)) - \text{median}(VX970) - DMSO(T))}{MAD(VX970(T) - DMSO(T))}$$

Equation 3:

$$DE' (DE \text{ corrected}) = (DE - c) - (VE \times m)$$

*Being DMSO: log2 PPTM count of DMSO samples at time points T=1 and T=0; Drug: log2 PPTM counts of drug samples at time point T; MAD: mean absolute deviation; C: intercept; m: slope.

In addition to our Z-score analysis, MAGeCK analysis was also used for the analysis. Briefly, MAGeCK algorithm normalises read counts according to the median, in order to adjust for the effect of the library size and read count distribution. Then, the variance of read counts is estimated and a negative binomial model is used to test whether sgRNA abundance differs significantly between treatment and control arms. SgRNAs are ranked according to the p-values calculated from the negative binomial model, and used to identify positively or negatively selected genes, using modified robust ranking aggregation algorithm (RRA). Additionally, positively and negatively regulated pathways can be reported, by applying RRA algorithm to the rankings of genes in a particular pathway.

A final rank list of hits was generated by consolidating results from both Z-scores and MAGeCK approach by calculating a single score using the product of their rank values (sqrt (Z-score rank) * (MAGeCK rank)).

An initial validation of the hits was carried out in single 96 well CRISPR/Cas9 arrayed reaction plate using 5 or more parallel crRNA per targeted gene, plus 2 negative control sgRNAs (with no homology towards any human gene). Cell growth after mutagenesis and treatment was monitored using the IncuCyte Zoom Live Cell Analysis System (Essenbio) along time, at 37°C, 5% CO₂. In each well, 1500 YCC6^{iCas9} cells were reversely transfected with 5 µl of 2µM sgRNA and 5 µl of 2uM

tracrRNA in 20 μ l of OptiMEM, using 3.5 μ l of 1:10 diluted RNAiMAX (Invitrogen), and incubated for 24h. Next day, media was removed and fresh media, containing 80nM VX970 was added (dose high enough to kill all cells in a normal condition). Plates were left in the IncuCyte for two weeks, until negative control cells were all dead and cells were fed twice a week with fresh drug. Drug-free media was then added to the cells, that were left to recover for one week, prior IncuCyte growth graphs were generated. Additionally, CellTitre Glo (CTG) analysis was carried out to measure the number of living cells in each well, and these results were compared with the growth graphs to determine which crRNAs caused resistance to the lethal doses of VX970.

In parallel, I sanger sequenced the DNA of the picked resistant colonies and determined the sgRNAs that were inserted in the cells. This was done by extracting DNA and PCR amplification, using the U6 forward primer (GGCCTATTTCCCATGATTCCTTC) and a Scaf modified reverse primer (ACTCGGTGCCACTTTTTCAA), which are located next to the sgRNA sequence in the constructs, using 10 μ l of Q5 buffer, 1 μ l 10mM dNTPs, 2 μ l 10 μ M U6 primer, 2 μ l 10 μ M Scaf primer, 0.5 μ l Q5 polymerase, 32.5 μ l Nuclease-free water and 100ng DNA. The program used comprised an initial incubation of 98°C for 2 minutes, 30 cycles of 98°C for 20 seconds (melting), 60°C for 30 seconds (annealing), 72 °C for 30 seconds (elongation), and a final extension step of 72°C for two minutes. The PCR product was then purified using the QIAquick PCR Purification Kit (Quiagen) and sent for sanger sequencing (Eurofins). For the colonies with more than one sgRNA inserted, I did a TOPO cloning experiment to generate ssDNA copies (see above).

Colonies with a single sgRNA insertion, validated in the previous experiment, were selected for further analysis. The resistant colonies were then tested for protein expression loss by WB (see above for protocol), using specific antibodies (**Table 3**). Then, ATR inhibition resistance of the colonies was checked by 5-days survival assays performed in 384-well plates (as described before). For the colonies presenting ATRi resistance, ssDNA was generated through TOPO cloning and bacterial transformation (see above) and final product was sent to sanger sequence surrounding the sgRNA targeting region, using specific primers listed in **Supplementary Table 1**. Additionally, cell cycle experiments were carried on (see section above), and siRNA or CRISPR/Cas9 mutated clones were generated to validate the hits that were not represented in the picked colonies.

Dense Tiling ATR CRISPRx Screen

In order to find out which mutations along the ATR sequence confer resistance to the ATRi VX970, a two-arm CRISPRx screen was carried out. In these screen, I used base editors to generate point mutations by promoting the direct and irreversible conversion of one base pair to another at a target genomic locus (lead by the sgRNA) without requiring double-stranded DNA breaks (DSBs), homology-directed repair (HDR) processes, or donor DNA templates (Komor, Kim et al. 2016, Nishida, Arazoe et al. 2016, Komor, Zhao et al. 2017).

For the first arm, a dense CRISPR library comprising 552 guides targeting all ATR sequence was synthesised (Twist biosciences) and cloned into the BbsI site of pKLV5-U6gRNA5-PGKPuroBFP. Ten million YCC6 cells were infected at a low MOI (to assure single guide insertion per cell) and selected in 5 µg/ml puromycin for 5 days. Afterwards, the cells were seeded in 10 cm plates and transfected when 80% confluent with 10µg of plasmidic DNA constructs carrying regular Cas9 (pCW-Cas9, Addgene #50661) or, the following base editors: SaBE4-Gam (Addgene, #100809) as a cytosine deaminase, and ABE7.10 (Addgene, #102919), an Adenine deaminase. GFP expressing plasmid, pEGFP-N1 (Clontech) was used as a negative control and forward transfection was carried out following the regular Lipofectamine 2000 protocol (Invitrogen) following the principal described by (Gaudelli, Komor et al. 2017). Media was changed after 5 hours and cells were left incubating for 48h, before they were seeded at a concentration of 50,000 cells/ml in a new 10-cm plate, the day before the VX970 treatment started. Cells were treated twice a week for 2 weeks with 100 nM VX970, until negative control cells were all dead. Resistant cells were then expanded and retrieved for further analysis.

In the second approach, the same 552 sgRNA library was cloned into a pGH224_sgRNA_2xMS2_Puro (Addgene, #85413) construct, and transduced into deadCas9 (dCas9) expressing YCC6 cells (YCC6^{dCas9}). To create YCC6^{dCas9} cells, YCC6 cells were transduced with a pGH125_dCas9-Blast lentiviral construct (Addgene, #85417), carrying a dead form of Cas9, with no catalytic activity to make DSB, but with the capacity to bind the DNA and form single-stranded bubbling structures described in (Hess, Fresard et al. 2016), where the base editors will deaminate a cytosine or adenosine, causing point mutations (mostly missense mutations) around a 5-nucleotide window. Then, cells were infected with the gRNA tiling library at a low MOI and selected in puromycin for 5 days, prior they were

transfected with 10µg of plasmidic constructs carrying the following base editors: pGH156_MS2-AID-Hygro (Addgene, #85415) and pGH183_MS2-AIDΔDead-Hygro (Addgene #85414), as a negative control. Transfection was carried out following the regular Lipofectamine 2000 protocol (Invitrogen) in 10 cm plates, and left 48 hours to cause mutations along the ATR gene. Next, cells were seeded at a concentration of 50,000 cells/ml in new 10-cm plates and fed with 100 nM VX970 for two weeks. Resistant colonies were harvested and retrieved for further analysis.

RNA was extracted from resistant cells of both arms, using the RNAeasy mini kit (Quiagen), and cDNA was prepared using three ATR specific primers and the SuperScript III Reverse transcriptase kit (Invitrogen) with the following conditions: Mixed in TUBE 1 (per sample): 1µg RNA, 1 µl of 10mM dNTPs, 1µl of 10µM primer (ATR specific) and 6µl of nuclease-free H₂O, in a total volume of 10µl. Tube 1 was then incubated at 65°C for 5 minutes and immediately put on ice for 1-2 minutes. Mixed in TUBE 2 (per sample): 4µl of 5x buffer, 0.5µl of SSIII (reverse transcriptase), 1µl of 1MDTT and 4.5 µl of H₂O, in a total volume of 10 µl. I then added tube 2 to tube 1 and heated the mix at 25 °C for 10 minutes, 50°C for 50 minutes and 75°C for 15 minutes. Next, I carried out a tiling ATR PCR (PCR1), where I amplified the whole ATR sequence in amplicons no longer than 300bp. I used 36 primer pairs (listed in **Supplementary Table 2**) that included an PB3 sequence, used as a bridge to add a barcoded IonA sequence in the second PCR (Forward primer), and an IonP1 tail (reverse primer). All PCR1 reactions were checked on a 2% agarose gel and mixed for PCR purification, using the AMPure XP beads (Auto Q Biosciences) following manufacturer's protocol. DNA resulting from PCR1 was then mixed in one reaction and amplified in PCR2, when the 5' barcoded Ion torrent tail was added. Final product was purified again following the same beads protocol used before, and processed using the Ion Chef PGM Hi-View templating kit (IonTorrent). Samples were then sequenced using the PGM 318 Chip v2 at a 45pM molarity (IonTorrent). Sample processing from PCR purification 2 and sequencing was performed by the Tumour Profiling Unit (Institute of Cancer Research, London, UK). FastQ files were generated and aligned to ATR cDNA sequence by Steven Pettitt (The Breast Cancer Now laboratory, The Institute of Cancer Research, London, UK) using Novoalign (Novocraft technologies). Coverage was calculated per base using samtools pileup with a maximum depth of 50,000 (github.com/samtools). Bam files were then compared with consensus ATR cDNA sequence and mutations were listed and localised in the protein

structure of ATR using the Integrative Genome Viewer (Broad institute) and the Chimera software (UCSF), respectively.

Statistical analysis:

Statistical analysis was performed using Microsoft Excel or GraphPad Prism. All tests were two-sided unless otherwise stated Mann-Whitney tests were used to compare non-parametric datasets and Student's t-tests used for parametric datasets. Additionally, GW CRISPR/Cas9 mutagenesis screen data and next-generation sequencing (NGS) data was analysed by the Breast Cancer Research Bioinformatics Group (The Institute of Cancer Research, London, UK), using R and following the above specifications. Venn-diagrams for the cross referencing with Wang *et al* was carried out using the online software described in (Heberle, Meirelles et al. 2015). See above for technique-specific analysis methodology.

Results

1. ATR sensitivity in ARID1A deficient gastric cancer models

Characterisation of *ARID1A* status and mutational signature in gastric tumour cell lines.

Recent studies have demonstrated that defects in *ARID1A* sensitise tumour cells to ATRi, both *in vivo* and *in vitro*, by triggering premature mitotic entry, genomic instability and apoptosis (Williamson, Miller et al. 2016). This SL has been established in the context of ovarian clear carcinomas, where loss of *ARID1A* is a common event (Katagiri, Nakayama et al. 2012, Lowery, Schildkraut et al. 2012). One of the multiple functions attributed to *ARID1A* consists in its recruitment to double strand breaks (DSB), via its interaction with the upstream DNA damage checkpoint kinase ATR. *ARID1A* seems to facilitate efficient processing of DSB to single-strand ends and sustains DNA damage signalling (Shen, Peng et al. 2015). *ARID1A* mutations have been reported in around 20% of GCs (Wang, Kan et al. 2011, Cancer Genome Atlas Research 2014, Wu, Wang et al. 2014, Cristescu, Lee et al. 2015), being associated with MSI, upregulation of the PI3K pathway, and wild type TP53 status (Cancer Genome Atlas Research 2014, Cristescu, Lee et al. 2015, Kim, Jung et al. 2015, Han, Kim et al. 2016, Lee, Yu et al. 2017). Whether *ARID1A*, through its interaction with ATR, plays a role in maintaining genomic integrity that could be exploited as a therapeutic liability by the use of ATRi, remains unresolved in GC.

To assess if the previously described synthetic lethal effect of ATR inhibition in *ARID1A* deficient models (Williamson, Miller et al. 2016), was also applicable to GC, I characterised a panel of six commonly available gastric tumour cell lines, as well as the isogenic HCT 116 *ARID1A* WT and null colorectal tumour cell lines, that represent controls for *ARID1A* expression and ATRi sensitivity.

Additionally, I included the YCC6 gastric tumour cell line, as a gift from Professor Sun Young Rha from the Yonsei Cancer Center in South Korea. First, I undertook

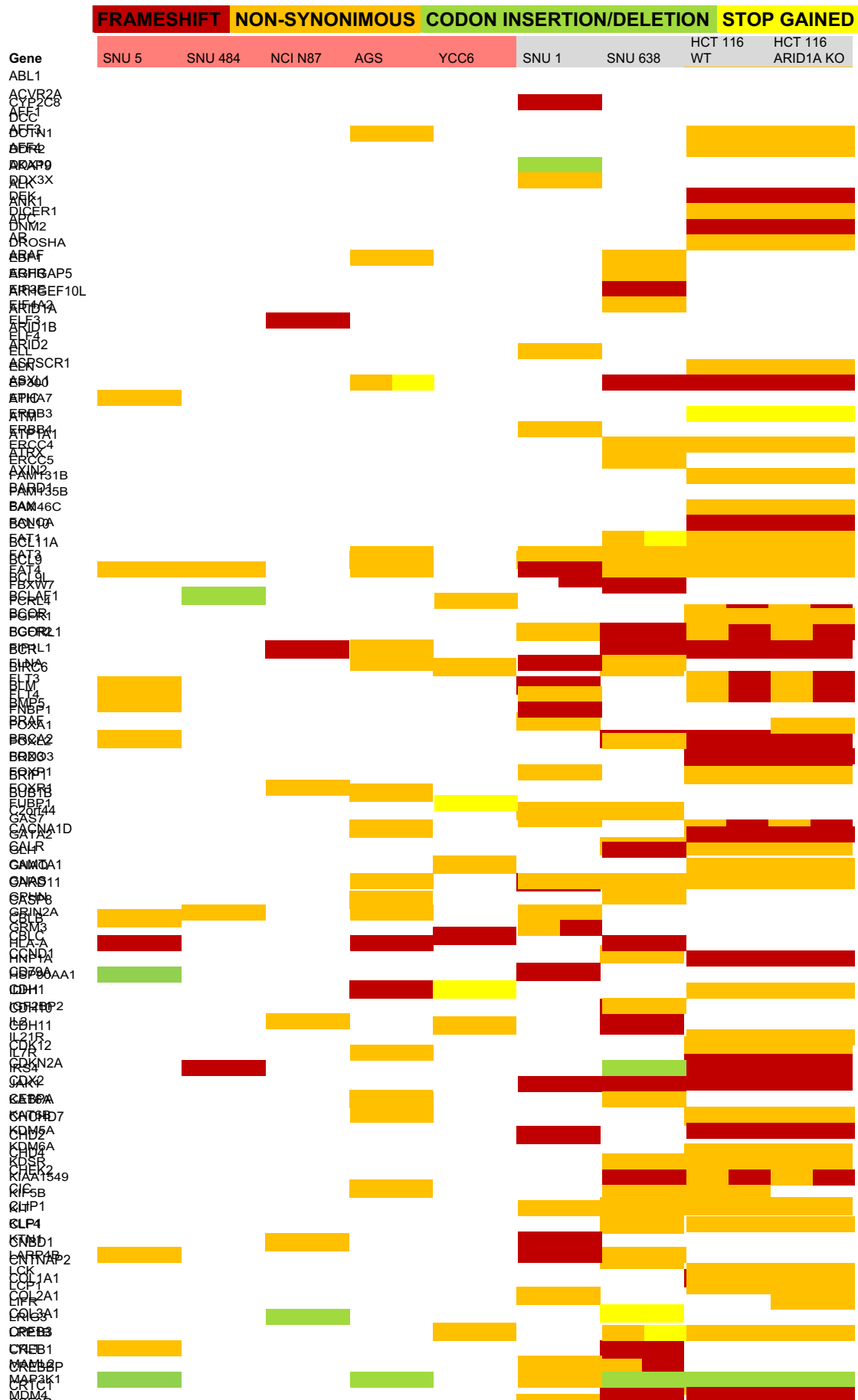
microsatellite analysis of these tumour cell lines. Five microsatellite markers (NR27, NR21, NR24, BAT25 and BAT26) were assessed using a multiplex PCR assay system (Buhard, Cattaneo et al. 2006, Patil, Bronner et al. 2012, Pagin, Zerimech et al. 2013). This analysis revealed MSI in SNU 1, SNU 638 and HCT 116 cell lines (**Table 4**). Next, I performed whole-exome DNA sequencing to identify the mutational profile across this panel of tumour cells line (**Table 4 and Table 5**). Generally, MSI cells were found to harbour a larger number of mutations compared with the microsatellite stable ones (MSS), as expected from cells with the inability to repair mismatch defects that can arise from DNA duplication. Information about cancer genome census gene mutations of all cell lines can be found in **Table 5**. More specifically, our exome-sequencing results confirmed the presence of *ARID1A* loss of function mutations in SNU 1, SNU 5, YCC6 and the HCT 116 *ARID1A* deficient cell line (*ARID1A* deficient group). SNU 638 possessed a heterozygous frameshift mutation in *ARID1A*, while no *ARID1A* mutations were detected in SNU 484, NCI N87, AGS and HCT 116 WT cells (*ARID1A* proficient group) (**Table 6, Figure 1A**). The *ARID1A* loss of function mutations detected in the GC tumour cell lines comprised truncating mutations; large deletions or frameshift indels that resulted in premature stop codons (**Table 6**). The variation of *ARID1A* expression was confirmed by qPCR mRNA measuring (**Figure 1B**), and protein expression was determined by western blotting (**Figure 1C**). Reduced mRNA levels and loss of protein expression were found in the GC tumour cell lines harbouring homozygous loss of function *ARID1A* mutations, although these two features were not highly correlated in a quantitative way (**Figure 1B and Figure 1C**), consistent with a model of post-transcriptional regulation of *ARID1A* previously reported by others (Wiegand, Shah et al. 2010, Wu, Wang et al. 2014, Kartha, Shen et al. 2016, Roumeliotis, Williams et al. 2017). Even though the SNU 638 GC tumour cell line showed to have a heterozygous frameshift deletion, I found normal *ARID1A* protein expression levels, as well of mRNA levels, compared with the *ARID1A* “Deficient” models and was thus included in the *ARID1A* proficient group.

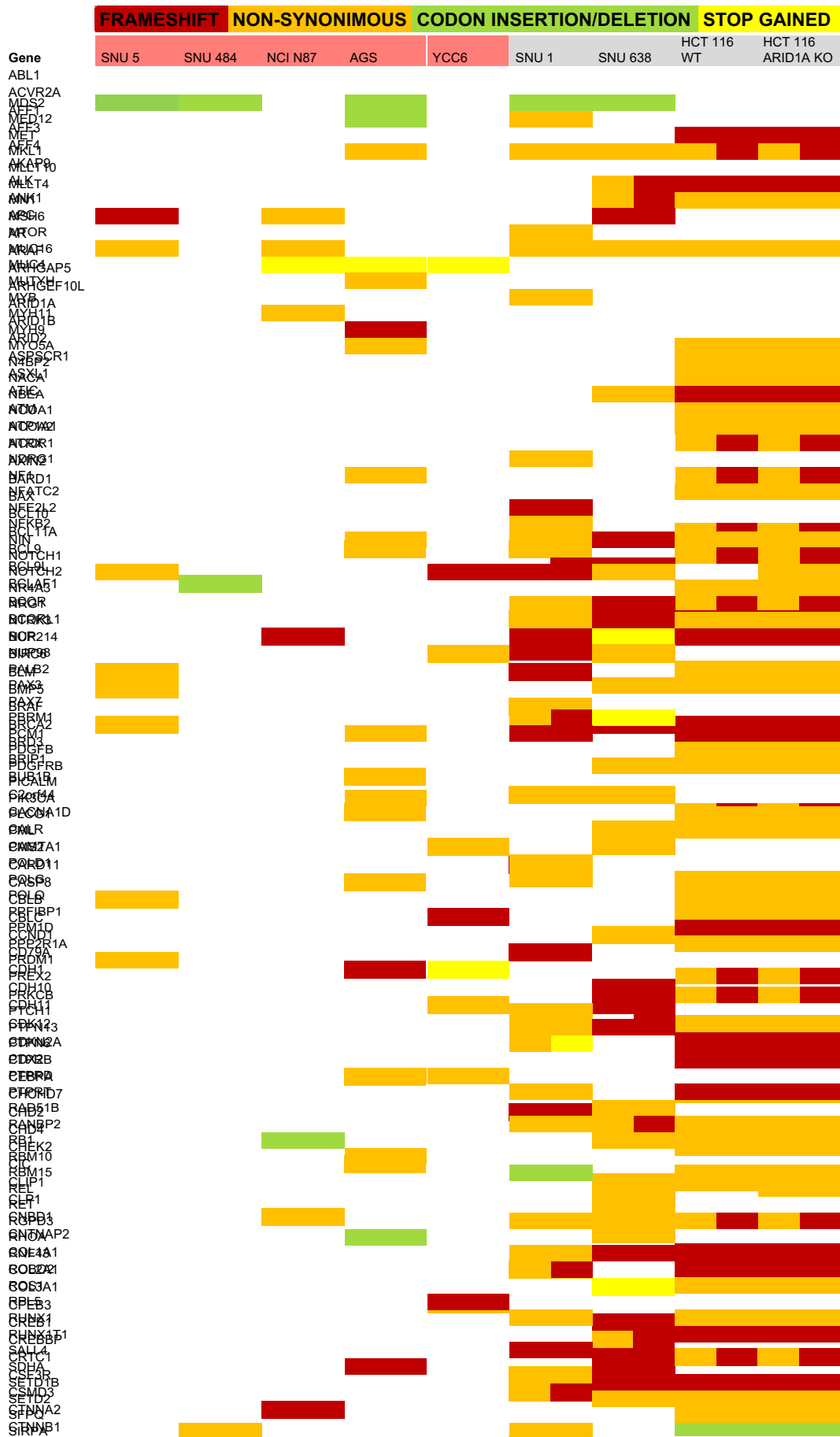
Table 4. Mutation categories identified from exome sequencing of gastric tumour cell lines and HCT 116 ARID1A colorectal isogenic cell line. Microsatellite unstable cell lines in red, microsatellite stable cell lines in black. WT, Wild type; KO, Knock out.

Cell line	Synonymous	Frameshifts	Non-synonymous	Codon change	Start gained	Start lost	Stop gained	Stop lost	Total
SNU 1	489	658	1079	288	6	6	52	3	2581
SNU 5	136	166	242	249	1	0	13	1	808
SNU 484	111	148	196	219	3	1	4	1	683
SNU 638	546	752	1219	293	13	5	55	3	2886
NCI N87	113	179	217	264	4	14	0	2	793
AGS	279	179	725	246	10	0	25	3	1467
YCC6	108	152	201	226	1	0	9	2	699
HCT 116 WT	907	1048	1921	284	17	3	98	1	4279
HCT 116 ARID1A KO	962	1076	2069	284	17	5	104	1	4518

Table 5. Exome sequencing mutations listed in the Cancer Genome Census found in our panel of cell lines. WT, Wild type; KO, Knock out. See table key for type of mutation.

Gene	FRAMESHIFT		NON-SYNONIMOUS		CODON INSERTION/DELETION		STOP GAINED		
	SNU 5	SNU 484	NCI N87	AGS	YCC6	SNU 1	SNU 638	HCT 116 WT	HCT 116 ARID1A KO
ABL1									
ACVR2A									
AFF1									
AFF3									
AFF4									
AKAP9									
ALK									
ANK1									
APC									
AR									
ARAF									
ARHGAP5									
ARHGEF10L									
ARID1A									
ARID1B									
ARID2									
ASPSR1									
ASXL1									
ATIC									
ATM									
ATP1A1									
ATRX									
AXIN2									
BARD1									
BAX									
BCL10									
BCL11A									
BCL9									
BCL9L									
BCLAF1									
BCOR									
BCORL1									
BCR									
BIRC6									
BLM									
BMP5									
BRAF									
BRCA2									
BRD3									
BRIP1									
BUB1B									
C2orf44									
CACNA1D									
CALR									
CAMTA1									
CARD11									
CASP8									
CBLB									
CBLC									
CCND1									
CD79A									
CDH1									
CDH10									
CDH11									
CDK12									
CDKN2A									
CDX2									
CEBPA									
CHCHD7									
CHD2									
CHD4									
CHEK2									
CIC									
CLIP1									
CLP1									
CNBD1									
CNTNAP2									
COL1A1									
COL2A1									
COL3A1									
CPEB3									
CREB1									
CREBBP									
CRTC1									
CSF3R									
CSMD3									
CTNNA2									
CTNNB1									
CTNND2									
CUL3									
CUX1									
CXCR4									





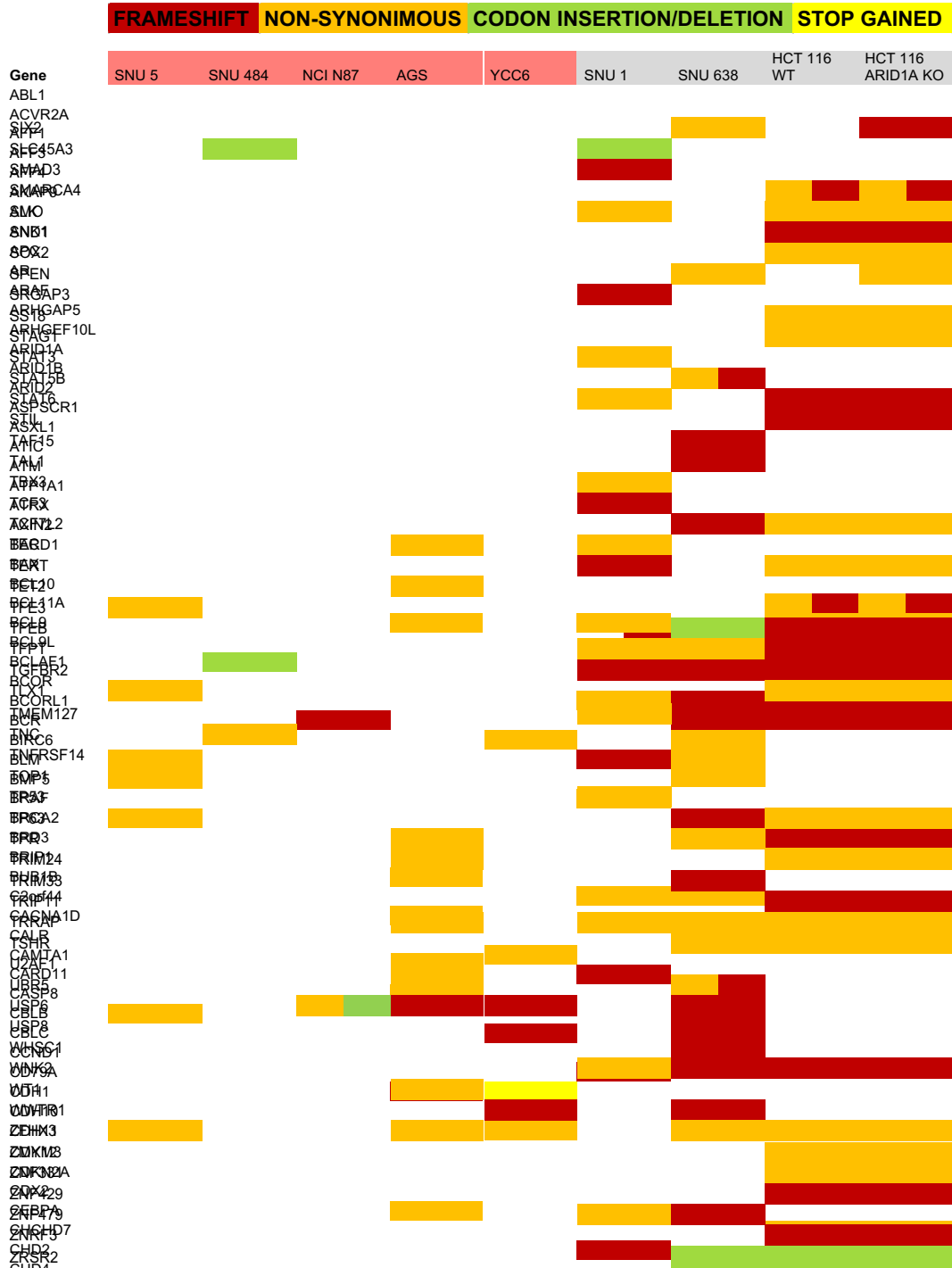


Table 6. *ARID1A* mutations and characteristics identified from exome sequencing of gastric tumour cell lines and HCT 116 colorectal *ARID1A* isogenic pair. Large deletions in SNU 5 and YCC6 were defined by the absolute lack of reads along the deleted area.

ARID1A mutations (Cell line)	MUTATION (genomic position)	TYPE	CHANGE	ZYGOSITY	PROTEIN CHANGE
SNU 1	1:27101267	Frameshift deletion Frameshift insertion	GC>G	Heterozygous	X1517X
	1:27105930		T>TG	Heterozygous	X1848X
SNU 5	Complete deletion	Deletion	-	Homozygous	-
SNU 484	-	-	-	-	-
SNU 638	1:27092739	Frameshift del	AG>A	Heterozygous	X921X
NCI N87	-	-	-	-	-
AGS	-	-	-	-	-
YCC6	Deletion from aa 900	Deletion	-	Homozygous	-
HCT 116 WT	-	-	-	-	-
HCT 116 <i>ARID1A</i> KO	1:27057658	Stop gained	C>T	Homozygous	Gln456*

Sensitivity to ATR inhibition in gastric tumour cell lines.

To test if *ARID1A* deficient tumour cell lines showed an enhanced sensitivity to ATR inhibition, compared with the *ARID1A* proficient tumour cell lines, 5-day drug exposure dose-response sensitivity curves were carried out in 384-well plates. Cells were exposed to one of two different small molecule ATRi, VX970 and AZD6738. I found that the HCT 116 isogenic *ARID1A* deficient cell line was sensitive to both VX970 and AZD6738, compared with the HCT 116 *ARID1A* proficient cell line (two-way ANOVA p-value < 0.001 for both ATRi) (**Figure 2A and 2B**). Furthermore, YCC6 and SNU 5 GC tumour cell lines, both of which harbour large homozygous *ARID1A* deletions and complete loss of protein expression, displayed profound sensitivity to both small molecule ATRi (SF₅₀ = 0.054nM and 0.082nM respectively), whereas SNU 1, harbouring two frameshift *ARID1A* mutations, showed moderate sensitivity (SF₅₀ = 0.297nM). The *ARID1A* proficient cell lines were relatively resistant to ATRi compared

with the GC tumour cell lines with *ARID1A* deletions (AGS SF₅₀ = 0.452nM, SNU 484 SF₅₀>1µM, NCI N87 SF₅₀ = 260nM) (**Figure 2C, Figure 2E**). I also analysed the area under the curve (AUC) values for GC tumour cell lines with proficient *ARID1A* expression compared with those that are *ARID1A* deficient and noticed a trend to higher sensitivity levels in the *ARID1A* deficient models, although this difference was not statistically significant (VX970 Mann Whitney p-value = 0.057, AZD6738 Mann Whitney p-value = 0.114) (**Figure 2D and Figure 2F**).

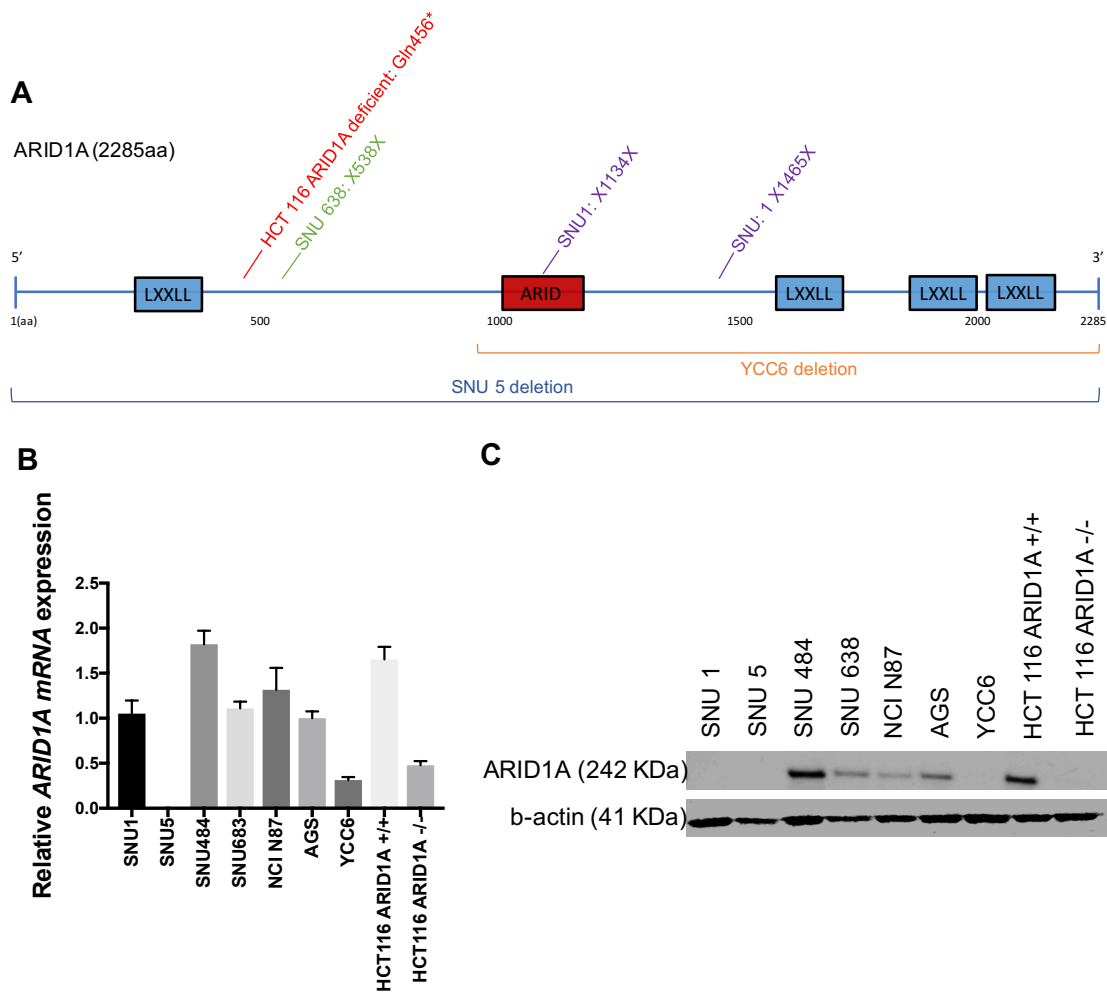


Figure 1. Characterisation of *ARID1A* status in GC tumour cell lines. **A.** Representation of protein coding sequences and major domains in *ARID1A*. *ARID1A* gene deletions in YCC6 and SNU 5 GC tumour cell lines are illustrated in orange and blue, respectively. The *ARID1A* mutations in SNU 638 and SNU 1 GC tumour cell lines are shown in green and purple, respectively. The location of the *ARID1A* frameshift mutation in the *ARID1A* deficient HCT 116 isogenic colorectal cell line is illustrated in red. **B.** Relative levels of *ARID1A* mRNA expression measured by quantitative PCR in GC tumour cell line panel. HCT 116 *ARID1A* WT (+/+) and *ARID1A* deficient (-/-) isogenic colorectal tumour cell lines are positive and negative controls. **C.** Western blot showing loss of *ARID1A* protein expression in the GC tumour cell lines harbouring truncating mutations or gene deletions in *ARID1A*. HCT 116 *ARID1A* +/+ and *ARID1A* -/- are positive and negative controls.

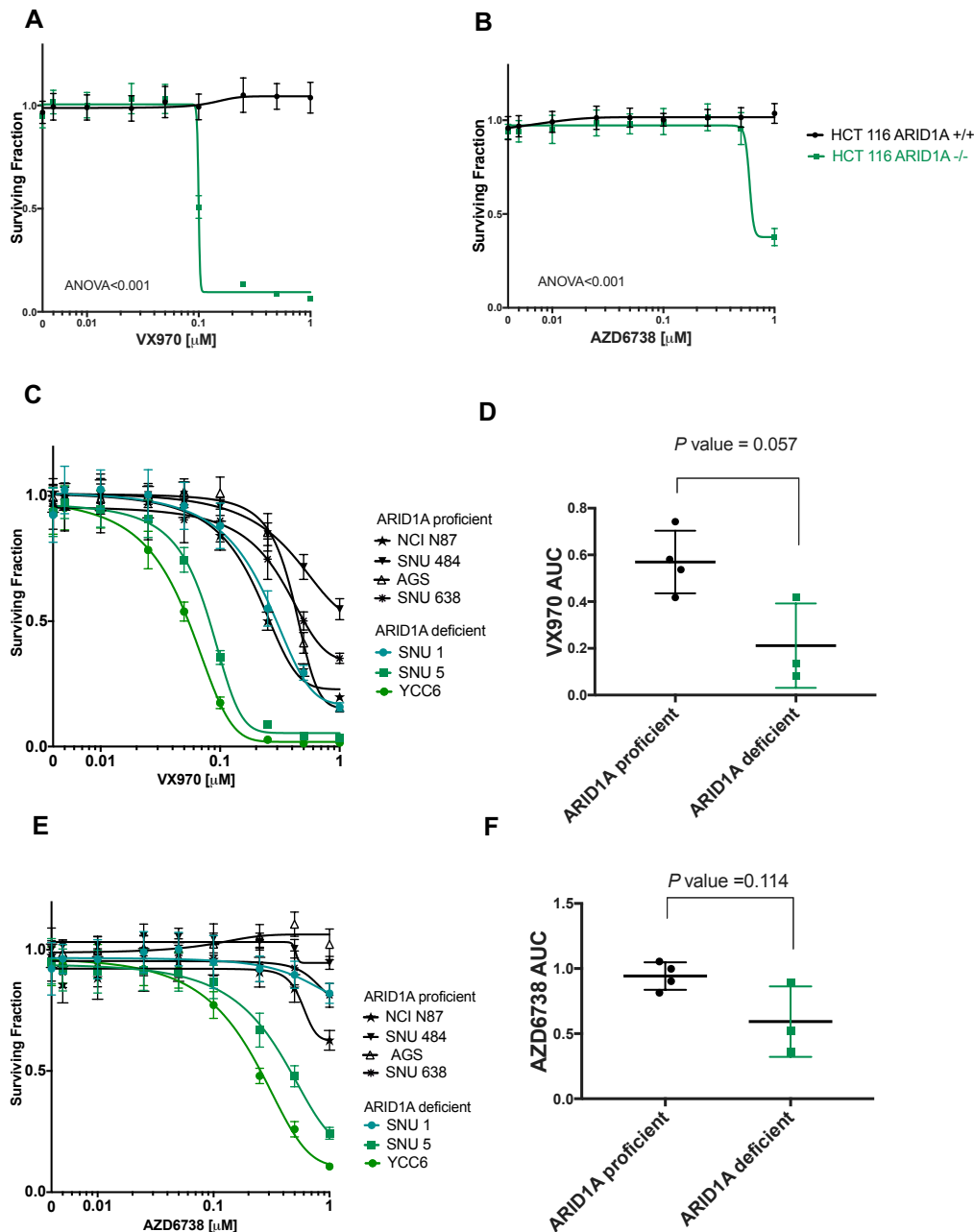


Figure 2. Sensitivity to ATR inhibition in ARID1A deficient GC tumour cell lines. **A.** Drug sensitivity curves showing increased sensitivity to ATR inhibition (VX970) in ARID1A deficient compared with ARID1A proficient HCT 116 isogenic colorectal tumour cell line (two-way ANOVA, $p < 0.001$) **B.** Drug sensitivity curves showing increased sensitivity to ATR inhibition (AZD6738) in ARID1A deficient compared with ARID1A proficient HCT 116 isogenic colorectal tumour cell line (two-way ANOVA, $p < 0.001$). **C.** Drug sensitivity curves for VX970 across the panel of gastric tumour cell lines. **D.** Box and whiskers plot showing no statistical difference in sensitivity to VX970 (AUC) in ARID1A deficient compared with ARID1A proficient GC tumour cell lines (Mann-Whitney U, $p = 0.057$) **E.** Drug sensitivity curves for AZD6738 across the panel of gastric tumour cell lines. **F.** Box and whiskers plot showing no statistical difference in sensitivity to AZD6738 (AUC) in ARID1A deficient GC tumour cell lines compared with ARID1A proficient GC tumour cell lines (Mann-Whitney U, $p = 0.1143$). Cells were seeded in 384-well plates and exposed to a 5-days treatment across 8 different concentrations of drug, ranging between $0.0001 \mu\text{M}$ to $1 \mu\text{M}$. Error bars represent standard deviation between reps ($n = 14$).

PARP inhibitor sensitivity in gastric tumour cell lines.

ARID1A deficiency has been shown to sensitise tumour cells to PARP inhibitors (PARPi) *in vitro* and *in vivo*, through the impairment of the checkpoint activation and repair of DNA DSBs, which could also provide a potential therapeutic strategy for patients with *ARID1A*-mutant tumours (Shen, Peng et al. 2015).

In relation to this, I wanted to explore whether the ARID1A deficient GC tumour cell lines were also sensitive to the clinical PARPi, olaparib and talazoparib (BMN673). I generated PARPi sensitivity curves in a 5-day 384-well plates format and I found that there was a difference in the sensitivity to talazoparib in the HCT 116 ARID1A deficient cell line compared with HCT 116 WT (two-way ANOVA p-value <0.001) (**Figure 3A**), but no difference in sensitivity for olaparib (two-way ANOVA ns) (**Figure 3B**). This could be explained by the fact that talazoparib has a higher capacity to trap PARP into the DNA than olaparib (Murai, Huang et al. 2014), and this ability has been shown to be directly associated with the capacity of the PARPi to kill tumour cells (Shen, Aoyagi-Scharber et al. 2015).

In contrast, no difference in PARPi sensitivity relating to *ARID1A* status was seen when I tested these same inhibitors in the panel of GC tumour GC (AUC values comparison between the ARID1A proficient cell lines with the deficient ones for olaparib, Mann Whitney p-value = 0.999; talazoparib, Mann Whitney p-value = 0.628) (**Figure 3C-3F**), suggesting an independent or, at least non-exclusive ARID1A-mediated response to PARPi in these GC models.

Small molecule inhibition to PI3K, HDAC6 and EZH2 in GC tumour cell lines

As mentioned earlier, *ARID1A* mutations often correlate with PI3K pathway upregulation in patient samples (Samartzis, Noske et al. 2013, Cancer Genome Atlas Research 2014, Huang, Lin et al. 2014, Cristescu, Lee et al. 2015). This phenomenon has been described in various histologies, including GC (Cancer Genome Atlas Research 2014, Cristescu, Lee et al. 2015, Zhang, Yan et al. 2016). It is therefore unsurprising that PI3K inhibitors (PI3Ki) have been reported to be especially potent in ARID1A deficient cells (Zhang, Yan et al. 2016, Lee, Yu et al. 2017, Yang, Yang et al. 2018). Considering the published literature, I exposed the HCT 116 isogenic cell lines as well as the panel of GC tumour cell lines with the pan-PI3Ki BKM120 and AKT inhibitor MZ2206, in a 384-well plate format over 5 days, to assess whether the

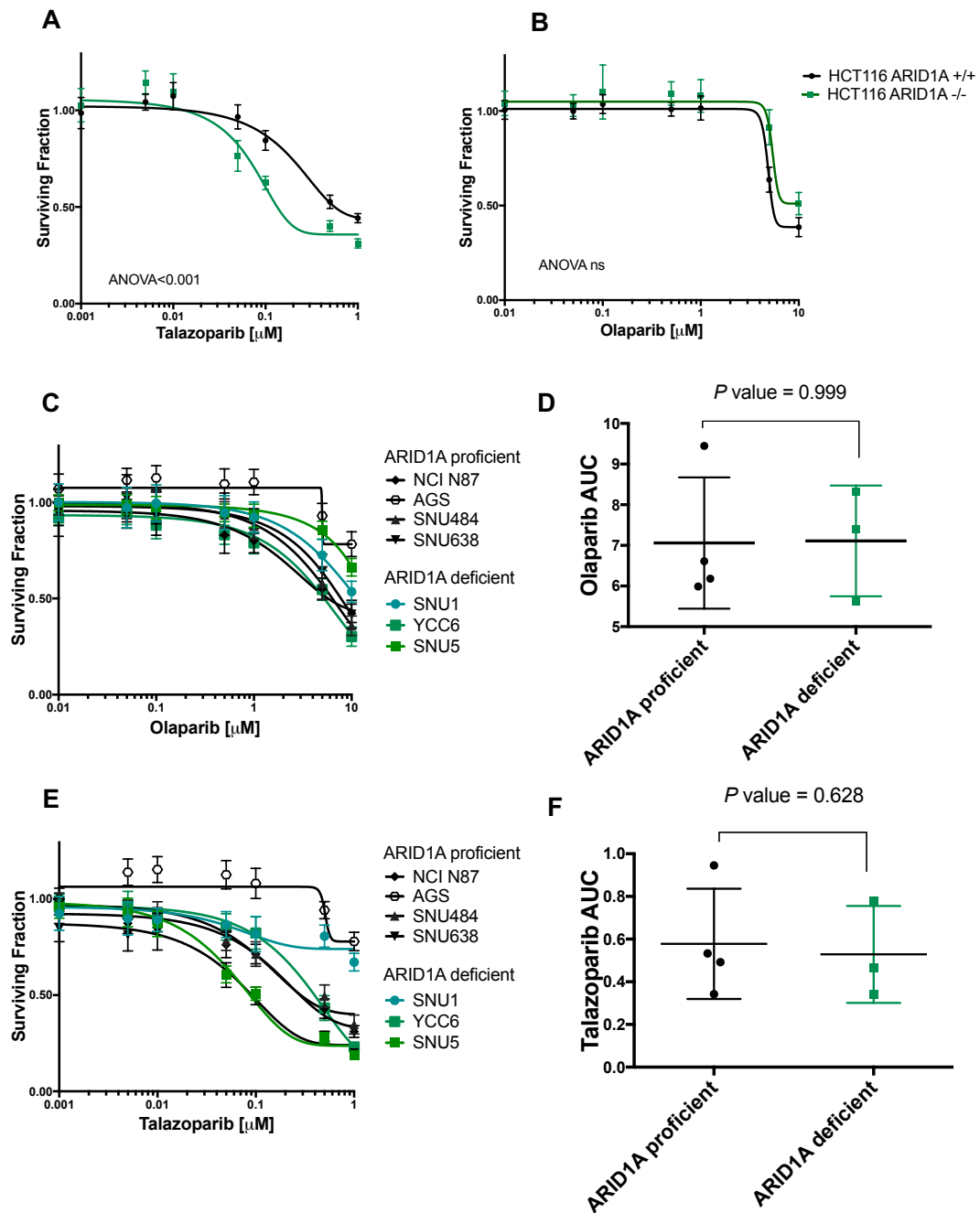


Figure 3. PARP inhibition in GC tumour cell lines. **A.** Drug sensitivity curves showing increased sensitivity to PARPi (talazoparib) in ARID1A deficient HCT 116 compared with ARID1A proficient isogenic HCT 116 colorectal tumour cell line (two-way ANOVA p -value <math>< 0.001</math>). **B.** Drug sensitivity curves showing no difference in sensitivity to PARPi (olaparib) in ARID1A deficient HCT 116 compared with ARID1A proficient isogenic HCT 116 colorectal tumour cell line. **C.** Drug sensitivity curves to olaparib in the panel of GC tumour cell lines. **D.** Box and whiskers plot showing no difference in sensitivity to olaparib in ARID1A deficient compared with ARID1A proficient GC tumour cell lines (Mann-Whitney U, $p=0.999$). **E.** Drug sensitivity curves to talazoparib in the panel of GC tumour cell lines. **F.** Box and whiskers plot showing no difference in sensitivity to talazoparib in ARID1A deficient compared with ARID1A proficient GC tumour cell lines (Mann-Whitney U, $p=0.628$). Cells were seeded in 384-well plates and exposed to a 5-days treatment across 8 different concentrations of drug, ranging between $0.0001\mu\text{M}$ to $1\mu\text{M}$ for talazoparib or from $0.001\mu\text{M}$ to $10\mu\text{M}$ for olaparib. Error bars represent standard deviation between reps ($n=14$).

ARID1A deficient genotype also conferred sensitivity to these inhibitors in our models. I found that the HCT 116 ARID1A deficient cells showed enhanced sensitivity to BKM120 compared with the HCT 116 ARID1A proficient (two-way ANOVA <0.001) (**Figure 4A**). However, I did not find any difference in sensitivity when I compared the both isogenic cells after exposing them to MK2206 (two-way ANOVA p-value = ns) (**Figure 4B**). Furthermore, ARID1A expression did not account for any differences in sensitivity to BKM120 or MK2206 in the panel of GC tumour cell lines (**Figure 4C-4F**).

Due to the fact that PIK3IP1 is a negative regulator of PI3K/AKT pathway which has been identified as a direct ARID1A/EZH2 target, that seems to contribute to the EZH2 inhibition synthetic lethal effect in ARID1A deficient cell lines (Bitler, Aird et al. 2015), I decided to test whether the ARID1A deficient cell lines were also sensitive to the GSK126 EZH2 inhibitor (EZH2i). I also undertook experiments using the HDAC6 inhibitors, as *ARID1A* mutations have been shown to inactivate the apoptosis-promoting function of p53 by upregulating HDAC6, indicating that pharmacological inhibition of HDAC6 could be a therapeutic strategy for *ARID1A*-mutated cancers (Bitler, Wu et al. 2017).

Following these reports, I assessed HDAC6 (ACY1215) and EZH2i (GSK 126) sensitivity across the panel of GC tumour cell lines. Although these compounds have shown promising activity in ovarian ARID1A deficient models (Bitler, Aird et al. 2015, Bitler, Aird et al. 2016, Bitler, Wu et al. 2017, Fukumoto, Park et al. 2018), I did not detect any significant differences in sensitivity to ACY1215 inhibitor or GSK 126 inhibitor associated with ARID1A expression in the HCT 116 ARID1A isogenic cell lines, nor across the panel of GC tumour cell lines (**Figure 5A-5F**), in a 5-day-38 well plate format. Taken together, this data suggested that the previously reported SL relationships between ARID1A and small molecule inhibitors of PI3K, EZH2 or HDAC6 did not appear to be applicable in GC tumour cell line models when used as monotherapy.

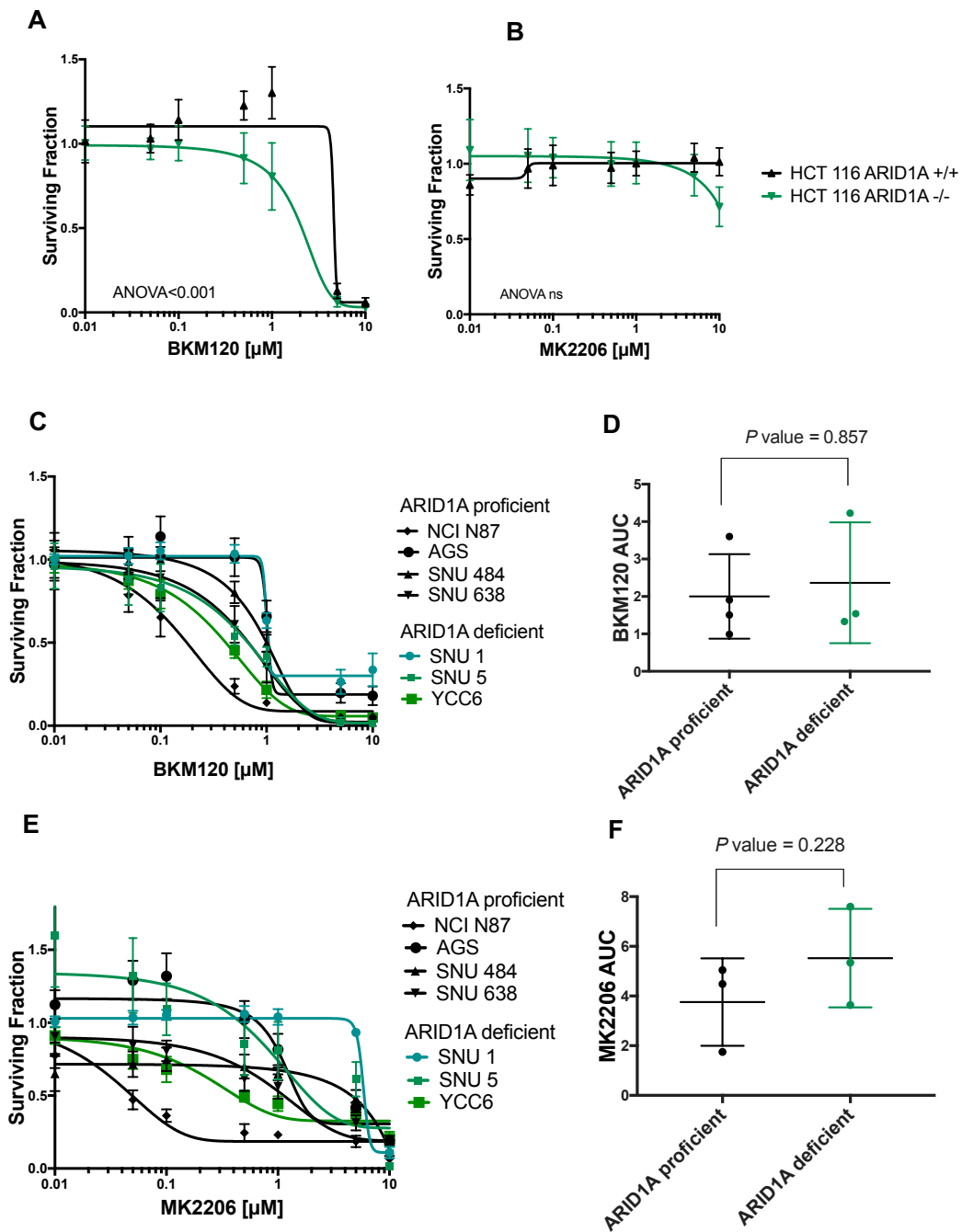


Figure 4. PI3K inhibition in GC tumour cell lines. **A.** Drug sensitivity curves showing increased sensitivity to BKM120 (pan-PI3K inhibitor) in ARID1A deficient HCT 116 compared with ARID1A proficient isogenic HCT 116 colorectal tumour cell line (two-way ANOVA p -value <math>< 0.001</math>). **B.** Drug sensitivity curves showing no difference in sensitivity to MK2206 (AKT inhibitor) in ARID1A deficient HCT 116 compared with ARID1A proficient isogenic HCT 116 colorectal tumour cell line. **C.** Drug sensitivity curves to BKM120 in the panel of GC tumour cell lines. **D.** Box and whiskers plot showing no difference in sensitivity to BKM120 in ARID1A deficient compared with ARID1A proficient GC tumour cell lines (Mann-Whitney U, $p=0.857$). **E.** Drug sensitivity curves to MK2206 in the panel of GC tumour cell lines. **F.** Box and whiskers plot showing no difference in sensitivity to MK2206 in ARID1A deficient compared with ARID1A proficient GC tumour cell lines (Mann-Whitney U, $p=0.228$). Cells were seeded in 384-well plates and exposed to a 5-days treatment across 8 different concentrations of drug, ranging between $0.001\mu\text{M}$ to $10\mu\text{M}$ for both inhibitors. Error bars represent standard deviation between reps ($n=14$).

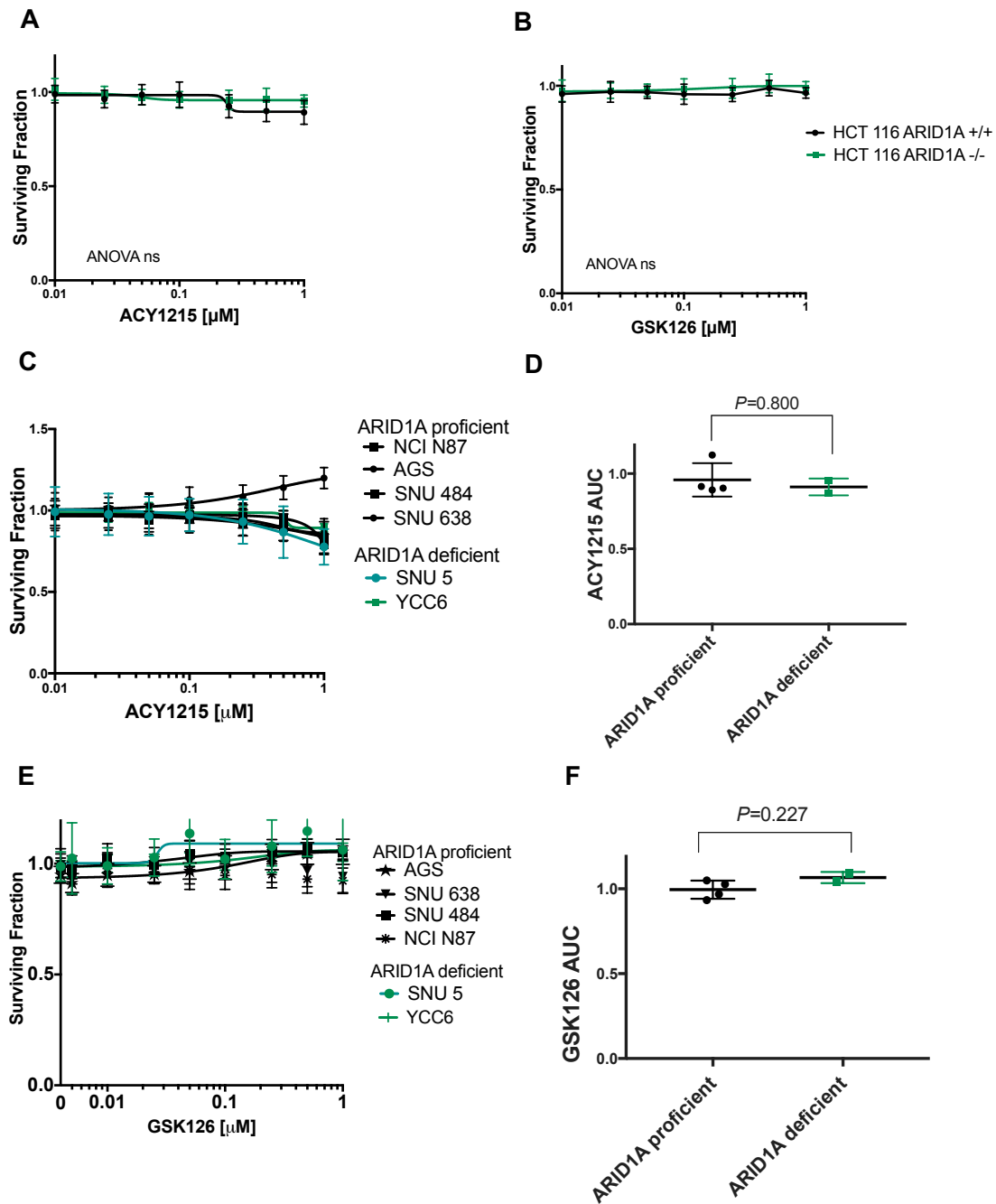


Figure 5. HDAC6 and EZH2 inhibition in GC tumour cell lines. **A.** Drug sensitivity curves showing no difference in sensitivity to ACY1215 (HDAC6 inhibitor) in ARID1A deficient HCT 116 compared with ARID1A proficient isogenic HCT 116 colorectal tumour cell line. **B.** Drug sensitivity curves showing no difference in sensitivity to GSK126 (EZH2 inhibitor) in ARID1A deficient HCT 116 compared with ARID1A proficient isogenic HCT 116 colorectal tumour cell line. **C.** Drug sensitivity curves to ACY1215 in the panel of GC tumour cell lines. **D.** Box and whiskers plot showing no difference in sensitivity to ACY1215 in ARID1A deficient compared with ARID1A proficient GC tumour cell lines (Mann-Whitney U, $p=0.800$) **E.** Drug sensitivity curves to GSK126 in the panel of GC tumour cell lines. **F.** Box and whiskers plot showing no difference in sensitivity to GSK126 in ARID1A deficient compared with ARID1A proficient GC tumour cell lines (Mann-Whitney U, $p=0.227$). Cells were seeded in 384-well plates and exposed to a 5-days treatment across 8 different concentrations of drug, ranging between $0.0001\mu\text{M}$ to $1\mu\text{M}$ for both inhibitors. Error bars represent standard deviation between reps ($n=14$).

ATRi and PARPi combination screens

Because ATRi and PARPi combination could represent a promising strategy for cancer patients with defects in DNA repair genes (Jones, Fleuren et al. 2017), and this strategy is currently being evaluated in the context of clinical trials (e.g. NCT03462342 or NCT02264678), I wanted to see if the addition of PARPi to ATRi exposure could enhance the sensitivity in our models. The 5-day dose-response assays showed enhanced sensitivity to the ATRi + PARPi combination in all cases (VX970/AZD6738 + olaparib/talazoparib) in the ARID1A deficient cells, both in the gastric panel (**Figure 6A and 6B**) and the HCT 116 isogenics (**Figure 6C and 6D**). Although the ARID1A proficient models were generally less sensitive to the combination treatment, some of them presented a good response, as in the case of NCI N87 (**Figure 6A and 6B**). Area under the curve (AUC) analysis of dose-response curves was performed for the HCT 116 isogenic pair, confirming a decrease in the surviving fraction of cells in the ARID1A deficient cells, compared with ARID1A WT cells, especially when I combined VX970 with both PARPi (**Figure 6E**).

ATR and PI3K inhibitors combination screens

Despite the modest described effect of PI3Ki in our panel of gastric cell lines, I decided to determine if the addition PI3Ki to ATRi increased the sensitivity of tumour cells in those cell lines that were deficient for ARID1A, as they might not operate together in the same pathway or not be effective in monotherapy, but could still have an impact in combination, through the impairment of a compensatory mechanism to ATR inhibition in ARID1A deficient models by the upregulation of PI3K pathway.

Differences between ARID1A deficient group of cells and ARID1A WT cells, were less evident in the case of ATRi plus PI3Ki combinations, although significant cell kill was observed in the case of YCC6, SNU 5 and SNU 1 ARID1A deficient cell lines when I combined both ATRi with both PI3Ki (**Figure 7A and 7B**). A modest effect was also observed in the HCT 116 isogenics, both for the surviving fraction analysis (**Figure 7C and 7D**) and for the AUC analysis (**Figure 7E**). Generally, BKM120 seemed to have a high impact on cell survival, compared with MK2206 AKT inhibitor.

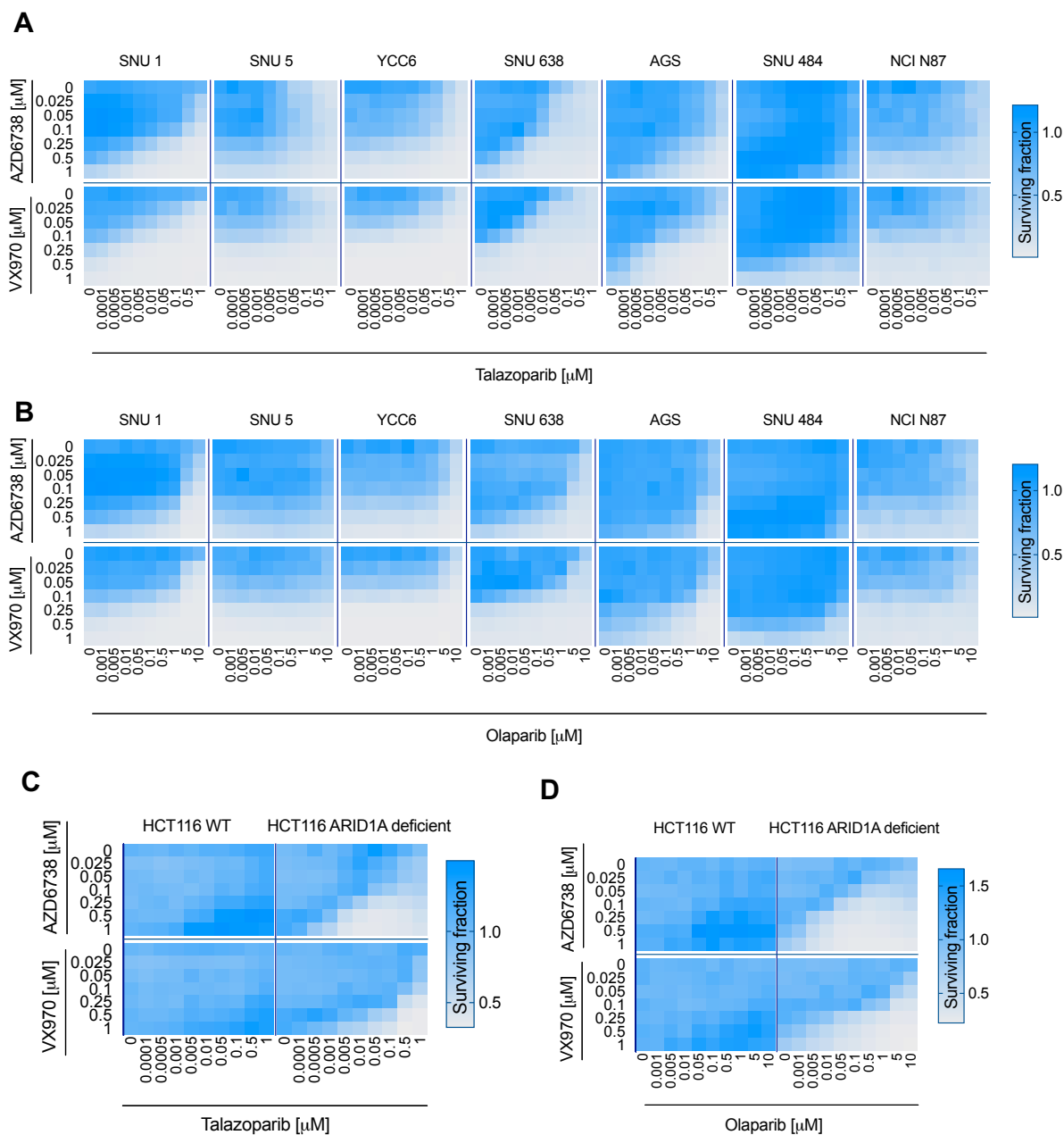


Figure 6. ATR and PARP inhibitor combination in GC tumour cell lines. A. Surviving fraction heatmap showing sensitivity to ATRi in combination with talazoparib in all GC tumour cell lines. Blue shading represents a high surviving cellular fraction and white represents a low surviving cellular fraction. The Y axis shows ATRi concentrations (μM) and the X axis shows concentrations of PARPi (μM). **B.** Surviving fraction heatmap showing sensitivity to ATRi in combination with olaparib in all GC tumour cell lines. **C.** Surviving fraction heatmap showing HCT 116 isogenic cells sensitivity to ATRi in combination with increasing doses of talazoparib. **D.** Surviving fraction heatmap showing HCT 116 isogenic cells sensitivity to ATRi in combination with increasing doses of olaparib.

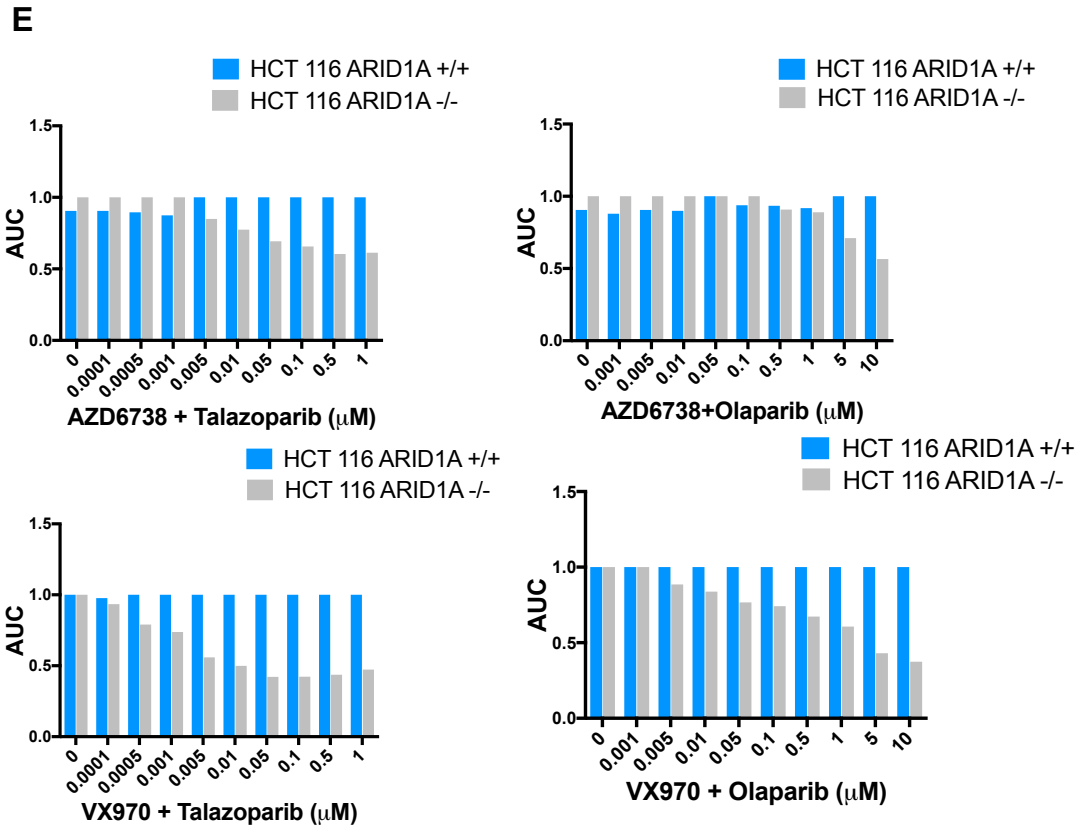


Figure 6 (continuation). E. Histograms showing differences in AUC between HCT 116 WT and HCT 116 ARID1A deficient cell line among all ATRi and PARPi combinations. Cells were seeded in 384-well plates and exposed to a 5-days treatment across 8 different concentrations ranging between $0.0001\mu\text{M}$ to $1\mu\text{M}$ for VX970, AZD6738 and BMN673 or $0.001\mu\text{M}$ to $10\mu\text{M}$ for olaparib. Error bars represent standard deviation between reps ($n=4$).

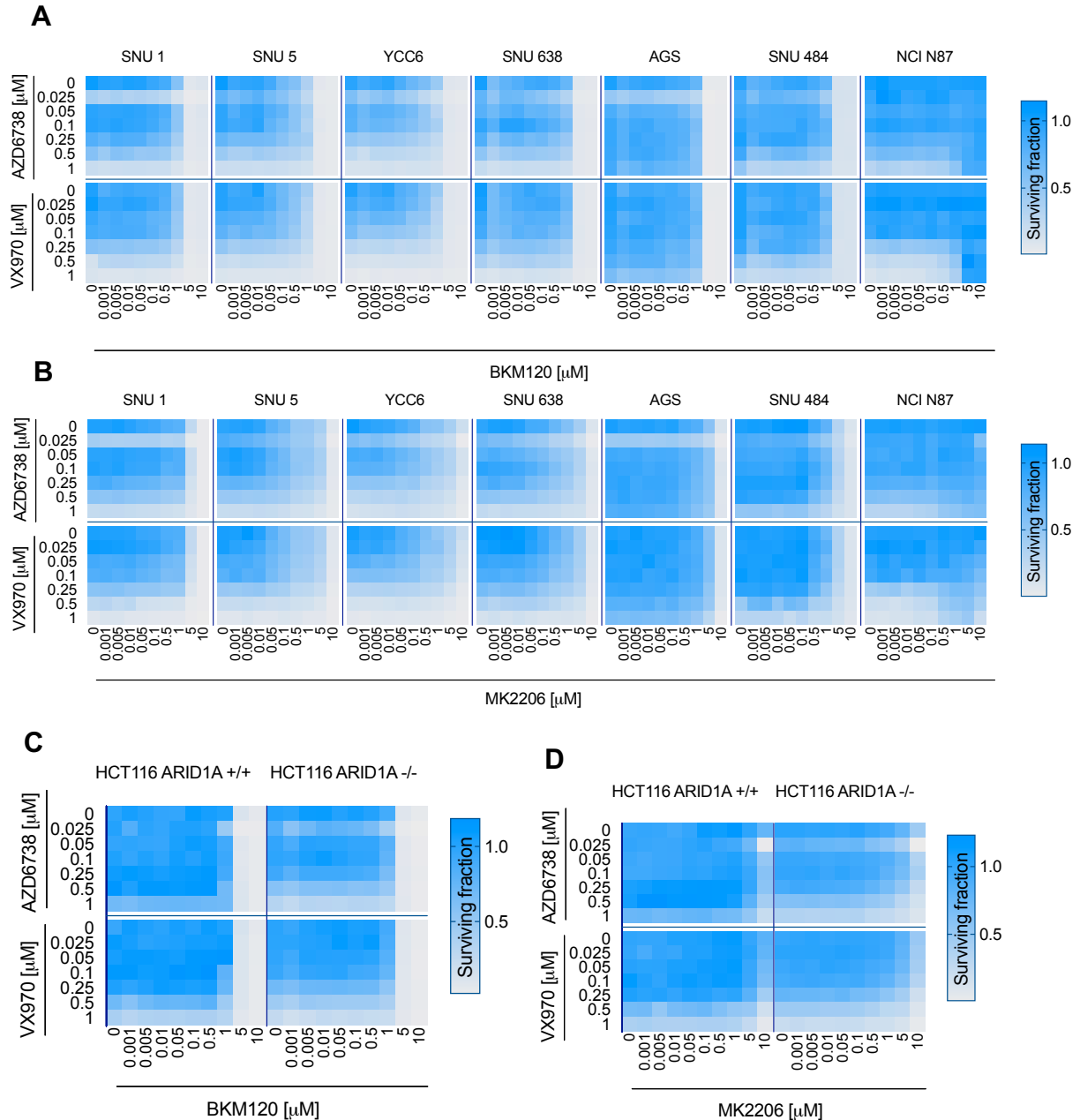


Figure 7. ATR and PI3K inhibitors combination in GC tumour cell lines. A. Surviving fraction heatmap showing sensitivity to ATRi in combination with BKM120 in all GC tumour cell lines. Blue shading represents a high surviving cellular fraction and white represents a low surviving cellular fraction, The Y axis shows ATRi concentrations (μM) and the X axis shows concentrations of PARPi (μM). **B.** Surviving fraction heatmap showing sensitivity to ATRi in combination with MK2206 in all GC tumour cell lines. **C.** Surviving fraction heatmap showing HCT 116 isogenic cells sensitivity to ATRi in combination with increasing doses of BKM120. **D.** Surviving fraction heatmap showing HCT 116 isogenic cells sensitivity to ATRi in combination with increasing doses of MK2206.

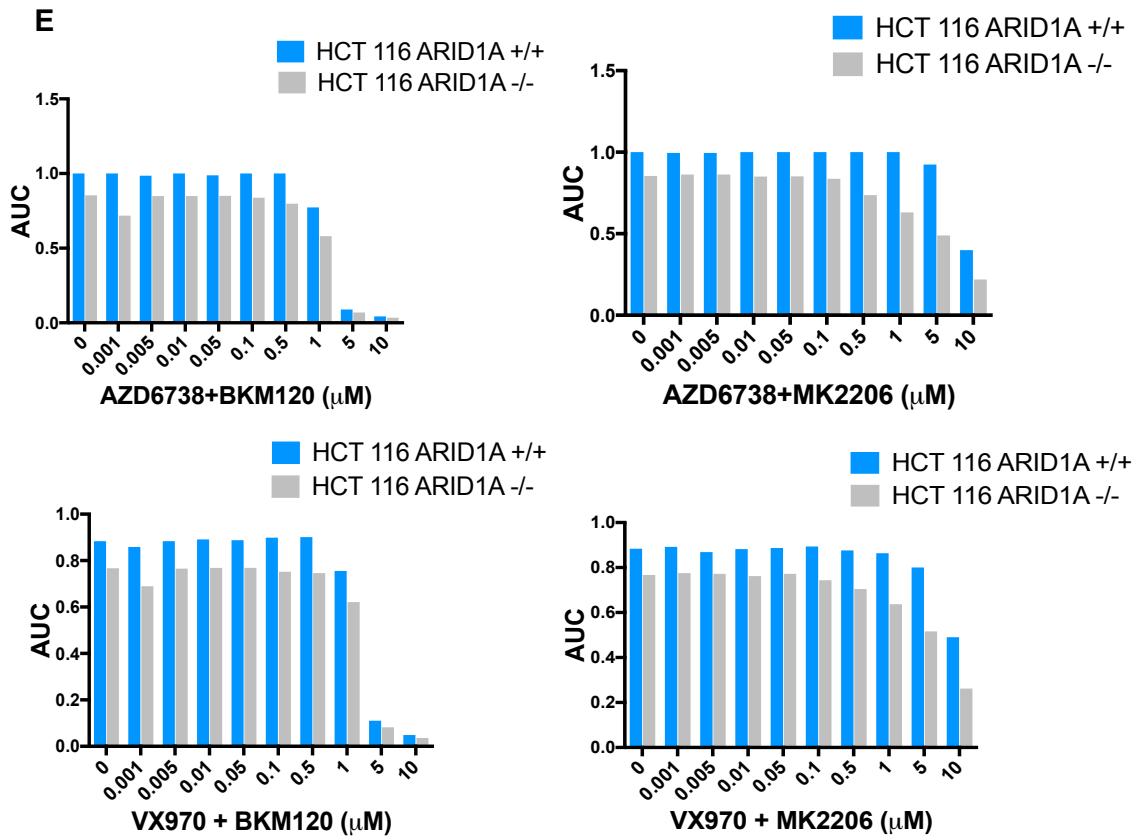


Figure 7 (continuation). E. Histograms showing differences in AUC between HCT 116 WT and HCT 116 ARID1A deficient cell line among all ATR and PI3K inhibitor combinations. Cells were seeded in 384-well plates and exposed to a 5-days treatment across 8 different concentrations ranging between 0.0001 μ M to 1 μ M for VX970 and AZD6738 or 0.0001 μ M to 10 μ M for BKM120 and MK2206. Error bars represent standard deviation between reps (n=4).

Creation of ARID1A isogenic models to assess ARID1A-driven ATR inhibition sensitivity

Given the limited number of cell lines in the GC cell line panel used in the experiments described above, I thought I might be underpowered to detect differences in drug sensitivity associated with ARID1A expression. Furthermore, every tumour cell line has a different mutational background (specially in the case of the MSI models), which can influence the outcome of the treatment sensitivity. Additionally, the isogenic model I used as a control, the HCT 116 cell line is a MSI colorectal cell line, which does not represent the gastric tumour genetic background. Consequently, I decided to create a new gastric isogenic model, using the CRISPR/Cas9 technique, selecting the MSS, ARID1A WT, and most ATRi resistant cell line of our panel, SNU 484, in order to evaluate the specific effect of ARID1A loss on ATR inhibition sensitivity.

After two consecutive rounds of CRISPR/Cas9 mutagenesis, using three different gRNAs, and following an extensive clone-screening, I came to the conclusion that SNU 484 cells were addicted to at least a basal ARID1A expression, as any of the surviving clones harboured a homozygous *ARID1A* mutation, and thus complete ARID1A loss. I then selected a clone with an 8-nucleotide heterozygous deletion (DNA change: g.687_694delAACGCGGG: protein change: N106Pfs*2) according to the Sanger sequencing results (**Figure 8A**). This clone, showed a significantly lower mRNA expression when compared with the ARID1A WT cells (CRISPR negative control) (**Figure 8B**), and undetectable ARID1A protein expression (**Figure 8C**), despite its heterozygosity (**Figure 8A**). Regardless of the remaining of the WT allele, I thought it was a valuable isogenic model, as haploinsufficiency phenomenon (phenotype is present even with a partial loss of the functional alleles with gene dosage effect) seems to operate within the ARID1A deficiency context (Wiegand, Shah et al. 2010, Wu, Wang et al. 2014, Kartha, Shen et al. 2016). I thought this could be relevant in our model, and thus it could mimic what happens in patients (Wu and Roberts 2013, Wu, Wang et al. 2014). When I tested for ATRi sensitivity response over five days, I saw that ARID1A deficient cells were significantly more sensitive to ATR inhibition compared with the wild type cells, both in the case of VX970 (Two-way ANOVA p-Value < 0.001) (**Figure 8D**) and in the case of AZD6738 (Two-way ANOVA < 0.001) (**Figure 8E**). Moreover, I found that *ARID1A* mutated cells had a higher proliferative rate, compared with the WT cells, which is consistent with a tumour suppressor gene role (Wu, Wang et al. 2014), although ARID1A appears to not be a pure tumour suppressor gene, being involved in gene expression regulation, genome maintenance and repair (Wu, Wang et al. 2014, Sun, Wang et al. 2018). I then validated these results using an orthogonal method, silencing *ARID1A* using siRNAs in SNU 484 and AGS cell lines. *ARID1A* silenced cells showed increased sensitive to both VX970 and AZD6738 inhibitors (SNU 484 and AGS two-way ANOVA p-value <0.001 for both inhibitors), although the effect was less profound than in the case of the CRISPR/Cas9 mutated isogenic cells (**Figure 8H-8L**).

I finally tested for the ATRi and PARPi combination in the SNU 484 isogenic cell line, not finding a profound difference in the survival fraction nor in the AUC values of cells to any combination when I compared ARID1A deficient and proficient cells (**Figure 9A and B**), suggesting that *ARID1A* is not the only driver of the response to the combination.

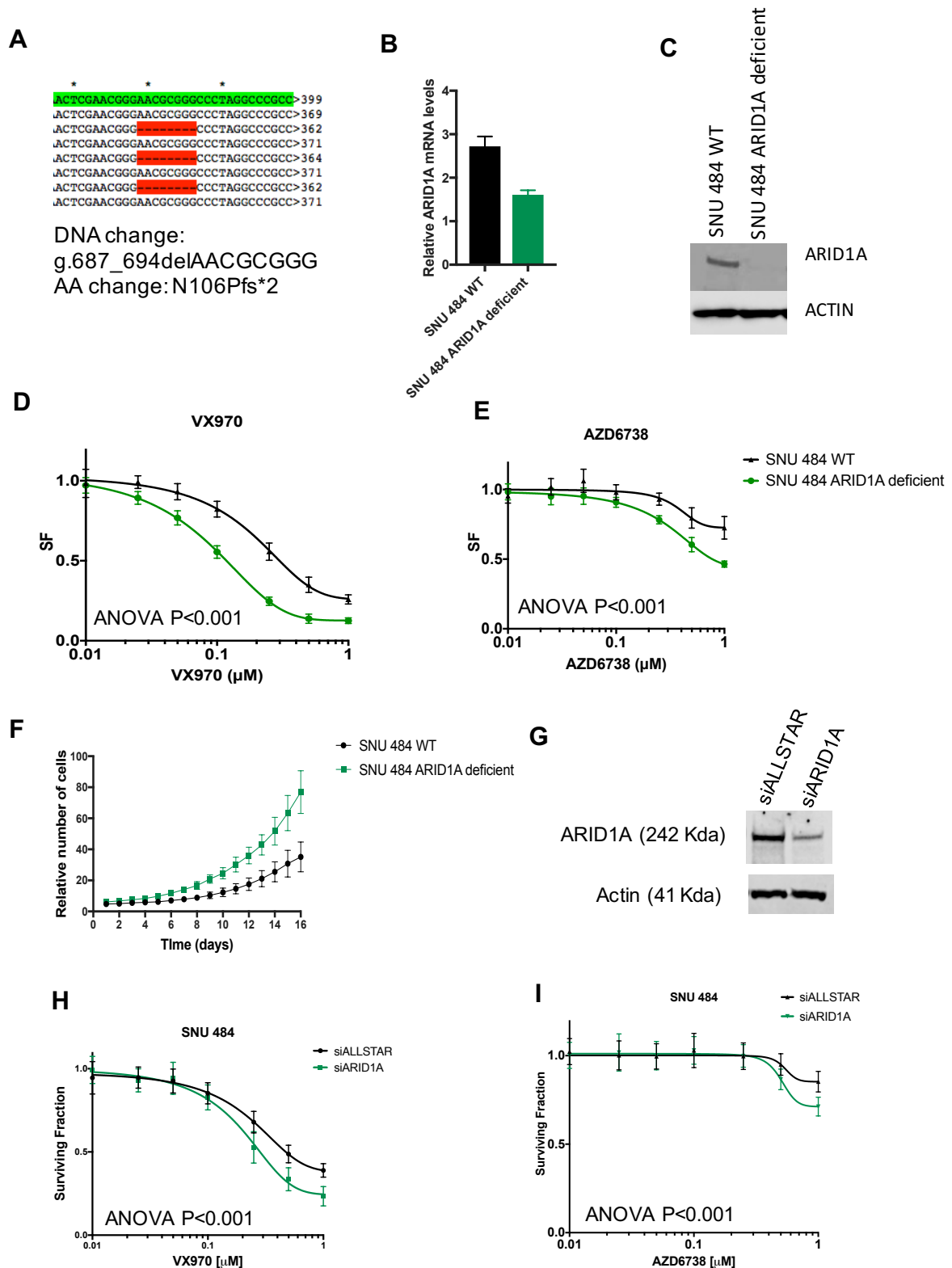


Figure 8. Enhanced ATRi sensitivity in SNU 484 ARID1A deficient isogenic GC tumour cell lines. **A.** *ARID1A* sequence alignment by ApE software in 6 TOPO cloned colonies from SNU 484 *ARID1A* CRISPR/Cas9 mutated cell line, shows an 8-nucleotide deletion (DNA change: g.687_694delAACGCGGG: aminoacid change: N106Pfs*2) in 50% of the sequences (red), when compared with the consensus sequence (green). SNU 484 ARID1A isogenic tumour cells created using the CRISPR/Cas9 technique, using a gRNA towards *ARID1A* sequence or a gRNA no homology to any known mammalian gene as a negative control. All

cell lines were plated in 384-well plates and exposed to a 5-days treatment across 8 different concentrations ranging between 0.0001 μ M to 1 μ M of both drugs. Error bars represent standard deviation between reps (n=14). **B. and C** *ARID1A* relative quantitative PCR mRNA levels and western blot protein expression in SNU 484 isogenic cell line, respectively. **D.** VX970 dose response cell survival curves for the gastric SNU 484 *ARID1A* **E.** AZD6738 dose response cell survival curves for the gastric SNU 484 *ARID1A* isogenic tumour cells **F.** 16-days proliferation curves generated using the IncuCyte Zoom Live Cell Analysis System (essenbio) comparing SNU 484 GC *ARID1A* isogenic cells **G.** WB showing a reduction in *ARID1A* protein in SNU 484 using lysates corresponding to siRNA Knockdown experiments **H and I.** **H.** Drug sensitivity curve to VX970 for SNU 484 GC cell line, after reverse transfection with siRNA targeting *ARID1A* (green) or with a siRNA control that has no homology to any known mammalian gene (siAllstar, black). **I.** Drug sensitivity curve to AZD6738 for SNU 484 GC cell line, after reverse transfection with siRNA targeting *ARID1A* (green) or with a siRNA control that has no homology to any known mammalian gene (siAllstar, black). **J.** WB showing a reduction in *ARID1A* protein in AGS GC cell line using lysates corresponding to siRNA knockdown experiments

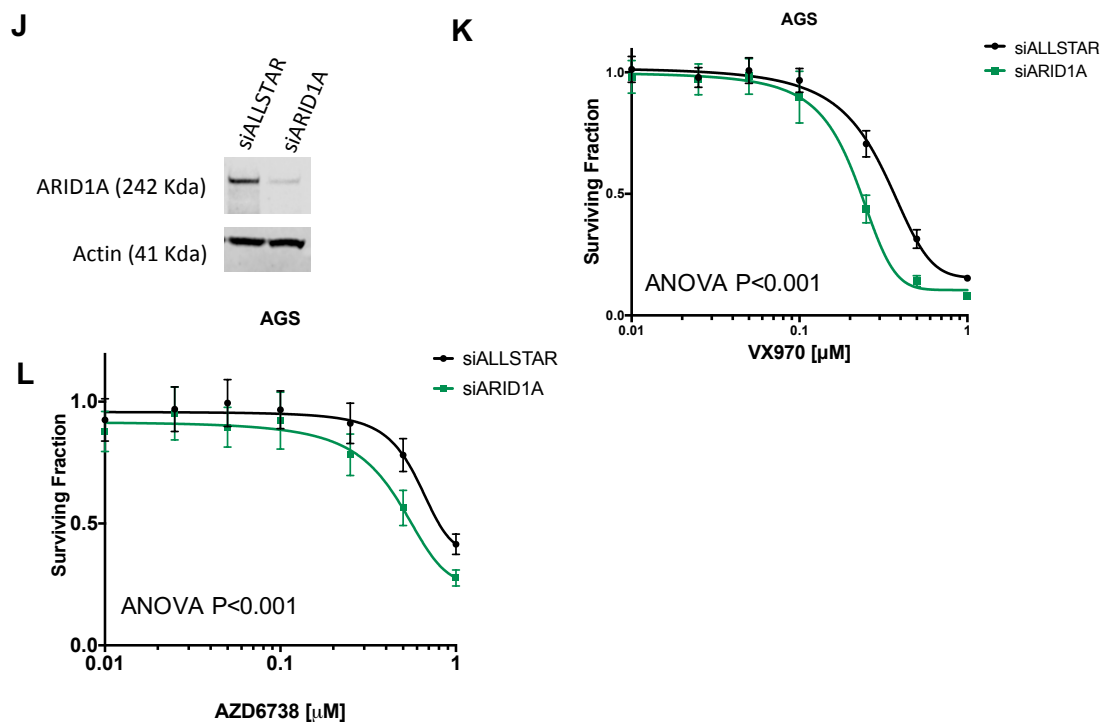


Figure 8 (cont.) K and L. **K.** Drug sensitivity curve to VX970 for AGS GC cell line, after reverse transfection with siRNA targeting *ARID1A* (green) or with a siRNA control that has no homology to any known mammalian gene (siAllstar, black). **L.** Drug sensitivity curve to AZD6738 for AGS GC cell line, after reverse transfection with siRNA targeting *ARID1A* (green) or with a siRNA control that has no homology to any known mammalian gene (siAllstar, black). 48h after transfection, cells were exposed to the ATRi across 8 different concentrations ranging between 0.0001 μ M to 1 μ M of drug for 4 days. Error bars represent standard deviation between reps (n=14). Survival curve siARID1A vs negative control p-value <0.0001, 2-way ANOVA.

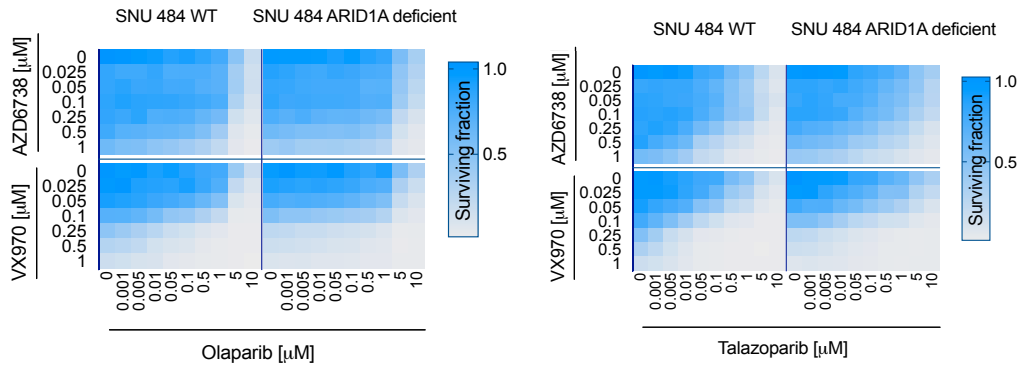
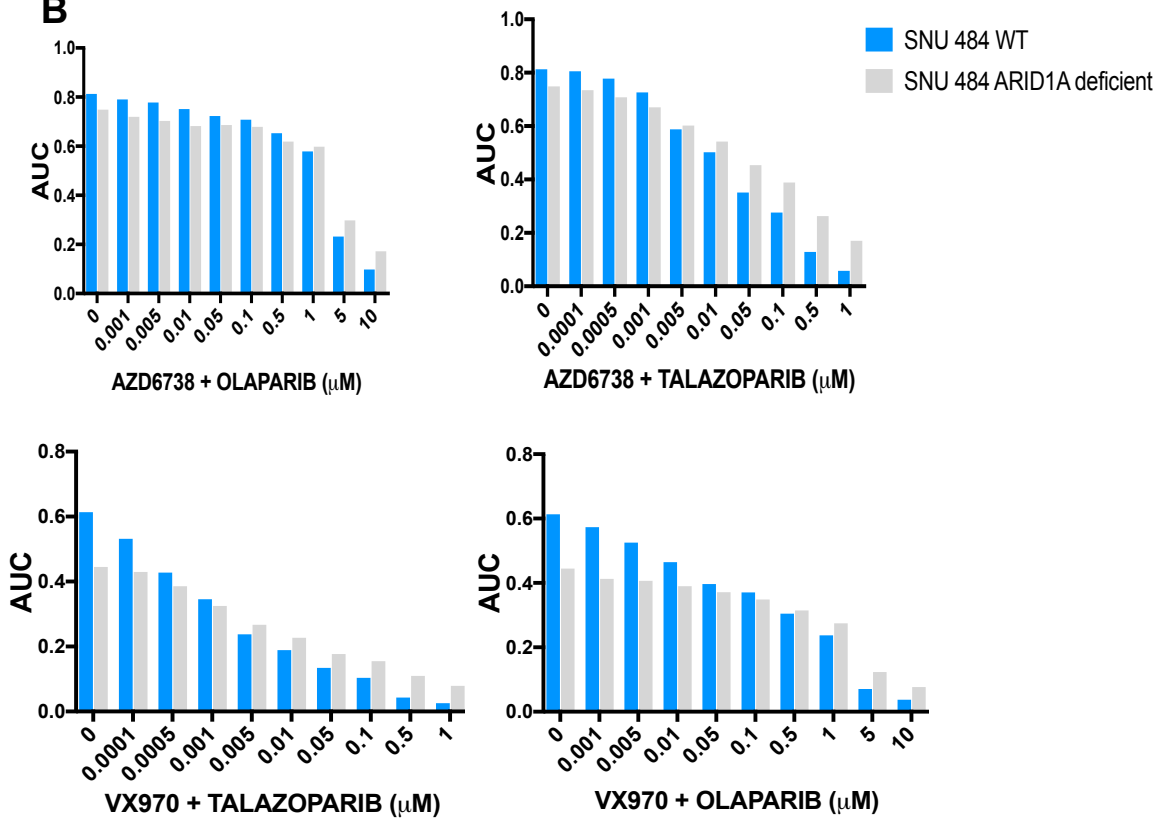
A**B**

Figure 9. Sensitivity to ATRi in combination with PARP inhibition in ARID1A deficient isogenic GC tumour cell lines. A. Surviving fraction heatmap showing SNU 484 ARID1A isogenic cell lines sensitivity to ATRi in combination with PARPi. Cells were seeded in 384-well plates by triplicate and exposed to a 5-days treatment of VX970 or AZD6738, in combination with talazoparib or olaparib. Y axis shows ATRi concentrations in an μM scale, while X axis shows PARPi concentrations in μM . **B.** Histograms showing differences in AUC between SNU 484 isogenic cell line among all ATRi and PARPi combinations.

2. *In vivo* assessment of ATRi Efficacy in Gastric Cancer Patient-Derived Xenografts

Patient-derived xenografts (PDX) consist of tumour fragments originated in patients, that are directly implanted and cultured in immunodeficient mice. PDXs have become an important tool for translational cancer research, as they conserve the cellular and histological structure of the tumour originated in the patient, as well as the genetic profile present in the original tumour (Reyal, Guyader et al. 2012, Tentler, Tan et al. 2012), which makes them optimal for the evaluation of therapeutic responses (Pompili, Porru et al. 2016). PDXs represent valuable models to predict the effect that a drug is going to have in a particular genetic context or an individual patient from which it has been derived, and their use has become common in translational cancer medicine, where the aim is to deliver treatments that are tailored according to the individual (Pompili, Porru et al. 2016).

I selected several GC PDX from CROWNbio database, with the aim of validating the ARID1A and ATR SL found in the GC cell lines.

Following statistical power calculations, assuming normal distribution, and considering an effect larger than 75%, an α lower than 0.05, and a β higher than 0.95 as significant, I determined the number of animals were needed on each arm, to have the statistical power to detect true differences. Thus, the experiments were carried out in a total of 7 mice per arm, in 6 arms.

M4344, rather than VX970 was used, as M4344 is an oral compound that has previously been observed in other tumour models to have superior *in vivo* efficacy, and it is currently being assessed in phase I clinical trials in monotherapy or in combination with PARPi.

I annotated *ARID1A* mutations detected by whole exome sequencing within the PDXs reported by CROWNbio, and validated these mutations using the Ion Torrent sequencing platform and a pre-designed panel of genes that included *ARID1A*. Furthermore, tumours were characterised for microsatellite instability status by sequencing a panel of five markers. Only one PDX presented MSI and it was the GC2 ARID1A deficient model. Information about the PDX models is listed in **Table 7**.

Table 7. Information about the PDX models

Model ID (gastric adenocarcinoma)	Cachexia	Ulceration	Tumour growth characteristics	ARID1A mutation (%)	ARID1A protein expression	Microsatellite instability
GC1	Yes	Yes	Very slow	982del (41), P1349Lfs*132 (64)	No	No
GC2	No	Yes	Slow	K1072Nfs*21 (48)	No	Yes
GC3	Yes	No	Slow	982_982del (52), P2139fs (40)	No	No
GC4	Yes	Yes	Slow	K1072Nfs*21 (50)	No	No
GC5	Yes	No	Fast	-	Yes	No
GC6	Slight body weight loss	Yes	Moderate	-	Yes	No
GC7	Yes	No	Slow	-	Yes	No

The design of the PDX experiment is shown in **Figure 10**. Briefly, four ARID1A deficient PDX models and 3 ARID1A proficient models were selected. Interestingly, some of the models with *ARID1A* mutations seemed to be heterozygous for the mutations (according to the frequency of sequencing reads), but they showed a complete loss of protein. This is consistent to what has previously been reported in the ARID1A SNU 484, where a heterozygous mutation of ARID1A showed a complete loss of protein expression. This has also been described in patients by IHC of tumours with mutations in *ARID1A* (Wiegand, Shah et al. 2010, Wu, Wang et al. 2014, Kartha, Shen et al. 2016). Tumours were then processed and implanted into mice and randomised into different arms, at a final number of 7 mice per arm, and treated with either vehicle; M4344 20mg/kg, M4344 10mg/kg, M4344 3mg/kg, talazoparib 0.1 mg/kg and ATRi M4344 3mg/kg + talazoparib 0.1 mg/kg, all treatments given by oral gavage. Mice were treated for several weeks and tumour volume and body weight was monitored twice a week. In the event of resistant tumour growth, tumours reaching 1000mm³ were collected to be molecular characterised for further ATRi resistance prospective studies (**Figure 10**). Model GC1, the first PDX model to undergo drugging with M4344, was used to optimise the dose and scheduling for the remaining experiments. The subsequent experiments were treated with 10mg/kg twice a week or 5 mg/kg M3433 daily, as severe body weight loss was noted in mice receiving the highest doses of ATRi. Although the reduced dose and modified scheduling of M4344 was better tolerated, the treatment duration required early cessation due to weight loss.

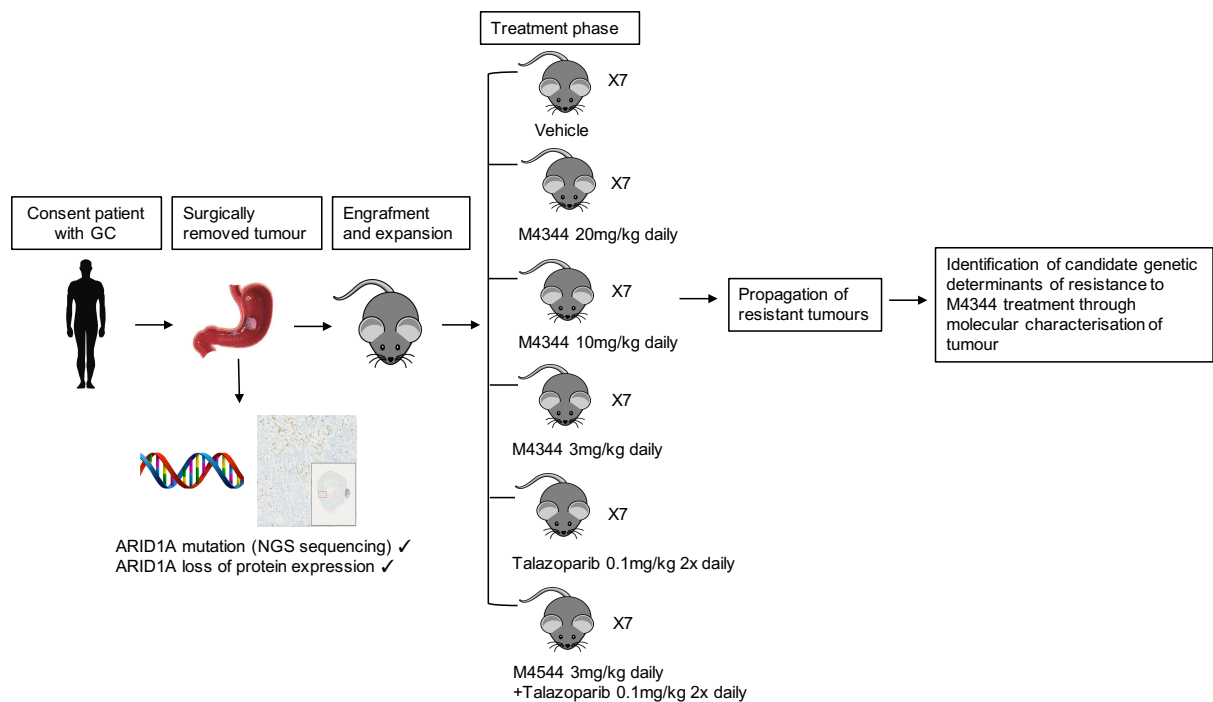


Figure 10. PDX experimental design. Four ARID1A deficient PDX models and 3 ARID1A proficient models were selected from CROWNbio database and validated for *ARID1A* mutations (Ion Torrent NGS) and protein expression by Next-Generation Sequencing (NGS) and IHC, respectively. Tumours were then processed and implanted into Balb/c nude mice with a body weight of approximately 20g. When tumours reached an approximate volume of 100-200mm³, mice were randomised to different arms, at a final number of 7 mice per arm, and treated with either vehicle, M4344 20mg/kg daily, M4344 10mg/kg daily, ATRi M4344 3mg/kg daily, talazoparib 0.1 mg/kg 2x daily and ATRi M4344 3mg/kg daily + talazoparib 0.1 mg/kg 2x daily, all treatments given by oral gavage. Mice were treated for several weeks while tumour volume and body weight was monitored twice a week. In the event of resistant tumour growth, tumours reaching 1000mm³ were collected to be molecularly characterised for further ATRi resistance mechanism studies. All *in vivo* experiments were performed by CrownBio company.

Despite this, all PDX models with an ARID1A deficiency (GC1-GC4) showed a significant growth inhibition to ATRi treatment when compared with the vehicle, in a dose-dependent way (**Figures 11C-14C**, two-way ANOVA p-values <0.0001). In the case of the ARID1A proficient models, two of them did not show a profound sensitivity to the ATRi monotherapy (GC5 and GC6) (**Figures 15C-16C**), although mild differences could be detected. However, model GC7, also ARID1A proficient, showed a profound effect in terms of tumour inhibition in response to M4344, that was dose dependent (**Figure 17C**). Next, I wanted to see if the addition of PARPi could show an enhancement to the sensitivity to ATRi, as I had seen in the cell lines. Previous studies report a sensitisation to PARPi in ARID1A deficient models (Shen, Peng et al. 2015, Jones, Fleuren et al. 2017). Consistent to this, I observed that when the mice

belonging to the ARID1A deficient models were treated with the ATRi + PARPi combination, I could see a clear enhancement of the response for the combination arm, compared with the monotherapies or vehicle, suggesting a synergy between the two drugs (**Figures 11D-14D**, two-way ANOVA p-values < 0.0001). The effect seen in the GC5 and GC6 ARID1A proficient models was much less evident, showing a very modest separation in between the different treatments (**Figures 15D-16D**). Again, the GC7 model proved to be exquisitely sensitive to ATRi, although being ARID1A proficient (**Figure 17D**).

Taken together, it is evident that a dose-dependent tumour inhibition to M4344 was elicited in ARID1A deficient PDX models. However, sensitivity is not restricted to the ARID1A deficient context, as marked tumour inhibition was also observed in the ARID1A proficient model GC7. Comparison of data from whole exome sequencing, RNA sequencing and proteomics between the vehicle and ATRi treated tumours will allow us to identify potential biomarkers of sensitivity to ATRi in an ARID1A deficient context.

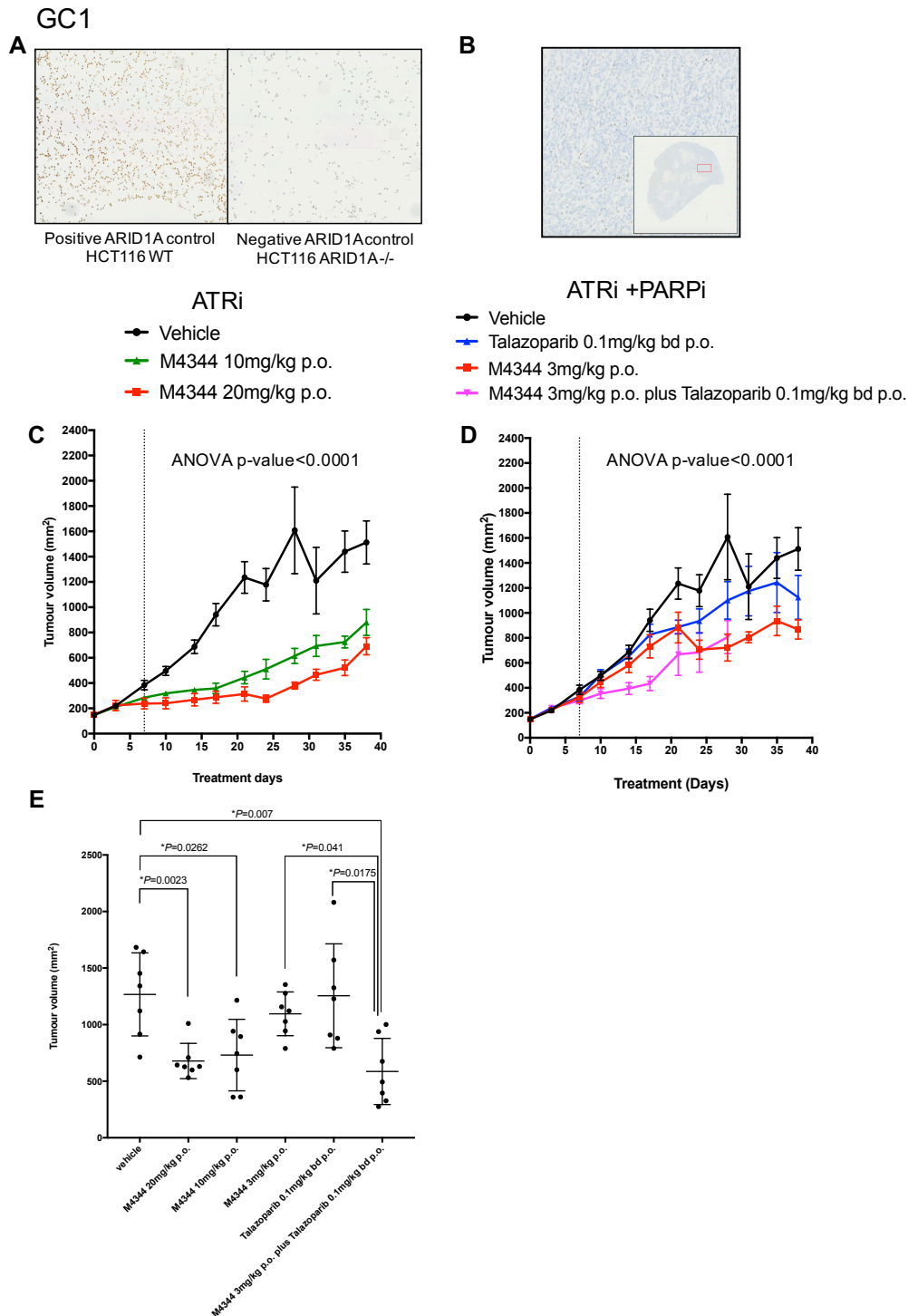


Figure 11. GC1 ARID1A deficient PDX is highly sensitive to ATR inhibition. **A.** HCT 116 colorectal isogenic cell line was used as a positive control for the ARID1A expression testing by IHC, using the D2A8U ARID1A antibody (CST) at a 1:250 dilution. **B.** FFPE sections from the tumour was stained for ARID1A expression showing complete protein loss, according to the controls. **C and D.** Average of tumour volume measurements of all mice in each group along time and ATRi treatment (**C**) or ATR + talazoparib treatment (**D**). Error bars represent Standard error of the mean (n=7). Two-way ANOVA p-values of groups M4344 20mg/kg, 10mg/kg, 3mg/kg and 3mg/kg + talazoparib were lower than 0.0001. Dotted line represents the end of the treatment due to body weight loss >25% in some of the groups. **D.** Box and whiskers representation showing the differences between the final tumour volume in between treatment arms (Mann-Whitney p-values).

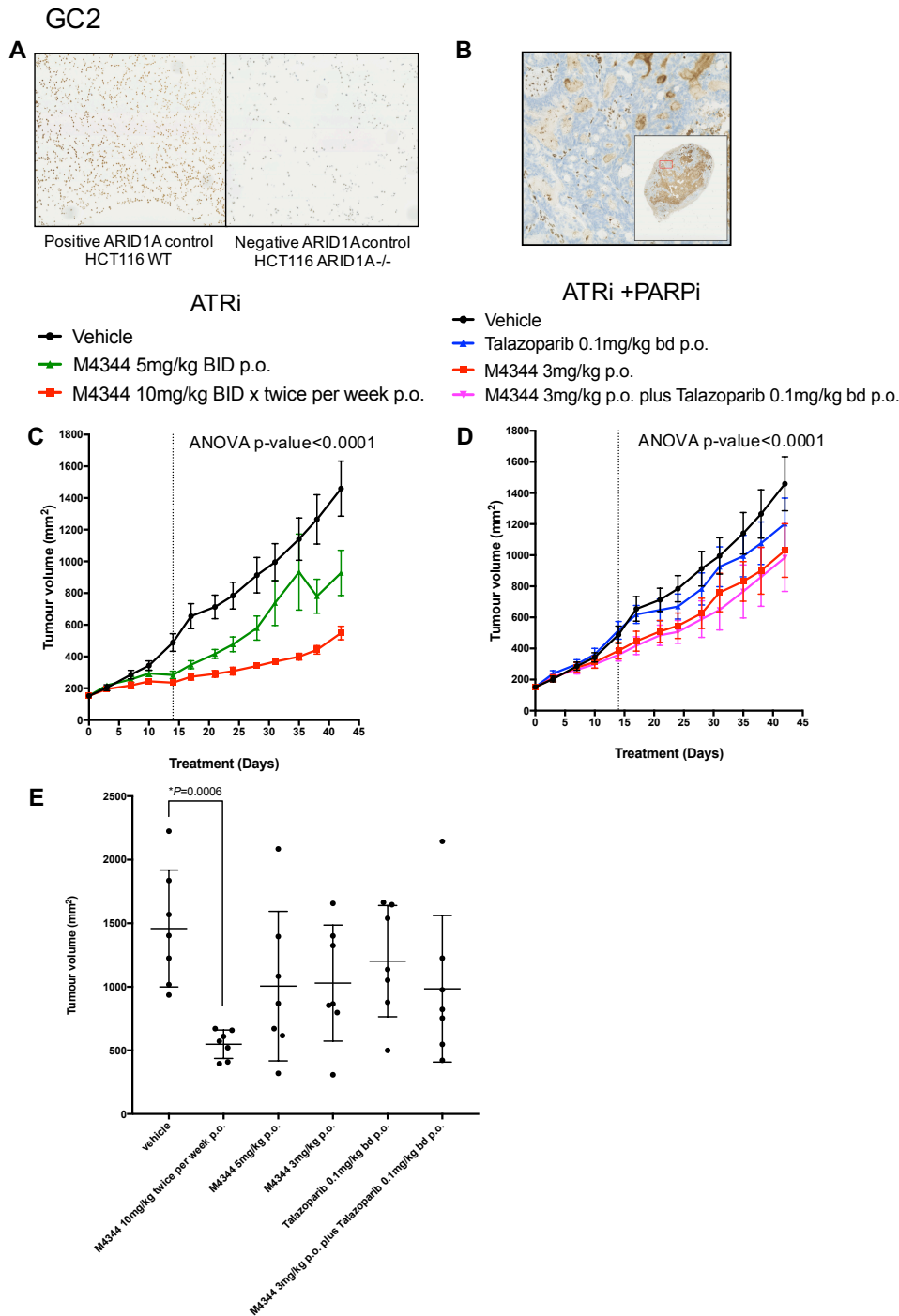


Figure 12. GC2 ARID1A deficient PDX is highly sensitive to ATR inhibition. **A.** HCT 116 colorectal isogenic cell line was used as a positive control for the ARID1A expression testing by IHC, using the D2A8U ARID1A antibody (CST) at a 1:250 dilution. **B.** FFPE sections from the tumour was stained for ARID1A expression showing complete protein loss, according to the controls. **C and D.** Average of tumour volume measurements of all mice in each group along time and ATRi treatment (**C**) or ATR + talazoparib treatment (**D**). Error bars represent Standard error of the mean (n=7). Two-way ANOVA p-values of groups M4344 10mg/kg, 5mg/kg, 3mg/kg and 3mg/kg + talazoparib were lower than 0.0001. Dotted line represents the end of the treatment due to body weight loss >25% in some of the groups. **D.** Box and whiskers representation showing the differences between the final tumour volume in between treatment arms (Mann-Whitney p-values).

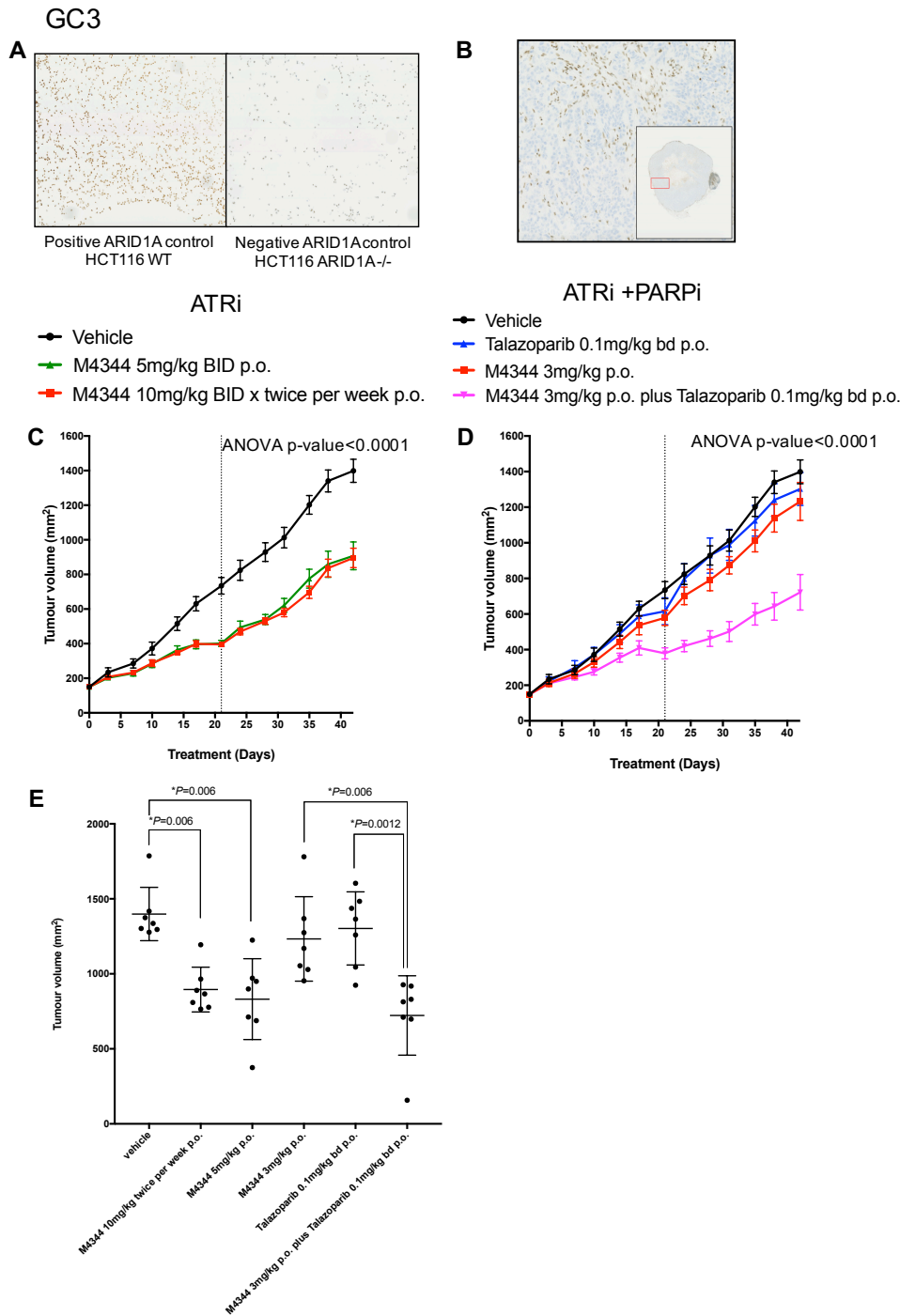


Figure 13. GC3 ARID1A deficient PDX is highly sensitive to ATR inhibition. **A.** HCT 116 colorectal isogenic cell line was used as a positive control for the ARID1A expression testing by IHC, using the D2A8U ARID1A antibody (CST) at a 1:250 dilution. **B.** FFPE sections from the tumour was stained for ARID1A expression showing complete protein loss, according to the controls. **C and D.** Average of tumour volume measurements of all mice in each group along time and ATRi treatment (**C**) or ATR + talazoparib treatment (**D**). Error bars represent Standard error of the mean (n=7). Two-way ANOVA p-values of groups M4344 10mg/kg, 5mg/kg and 3mg/kg + talazoparib were lower than 0.0001. Dotted line represents the end of the treatment due to body weight loss >25% in some of the groups. **D.** Box and whiskers representation showing the differences between the final tumour volume in between treatment arms (Mann-Whitney p-values).

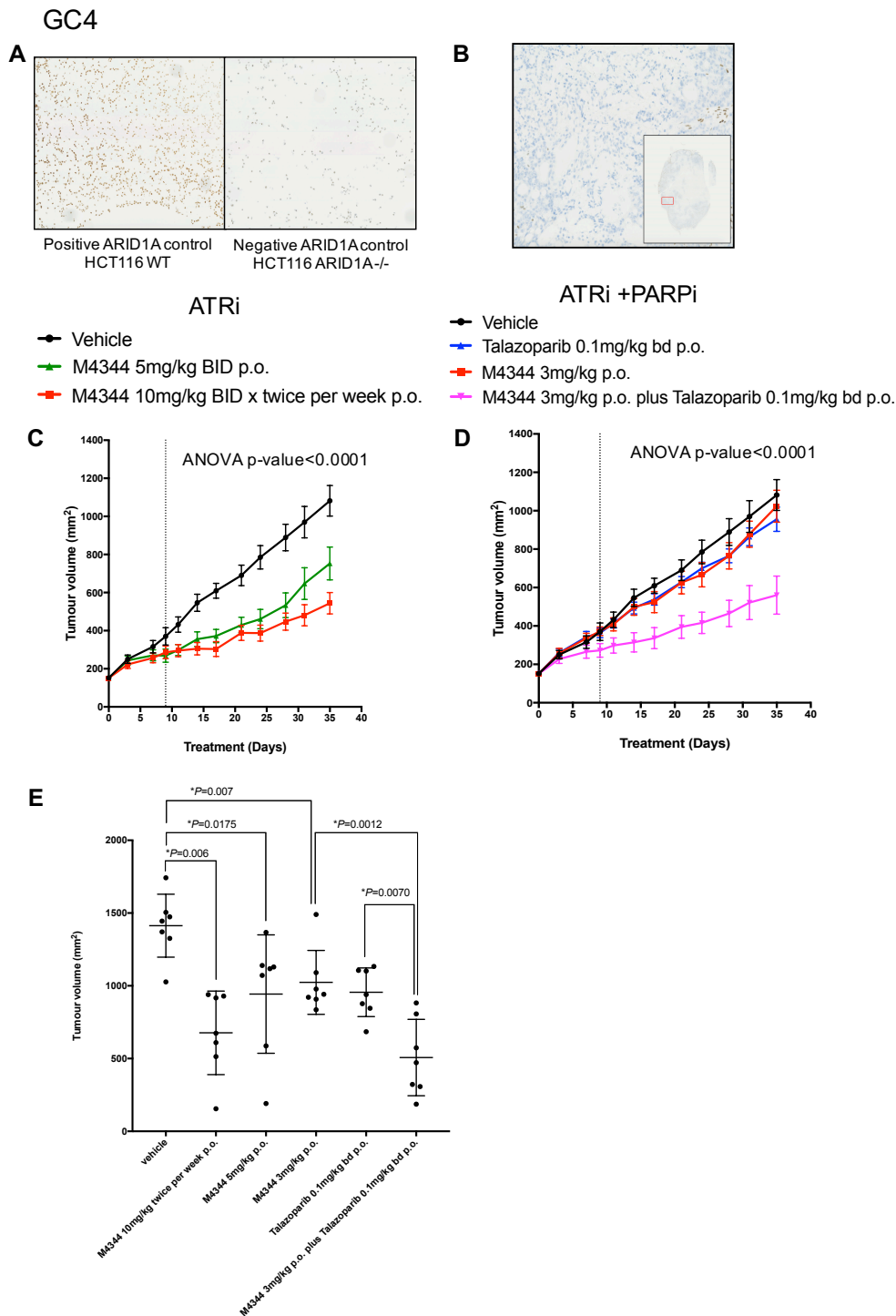


Figure 14. GC4 ARID1A deficient PDX is highly sensitive to ATR inhibition. **A.** HCT 116 colorectal isogenic cell line was used as a positive control for the ARID1A expression testing by IHC, using the D2A8U ARID1A antibody (CST) at a 1:250 dilution. **B.** FFPE sections from the tumour was stained for ARID1A expression showing complete protein loss, according to the controls. **C and D.** Average of tumour volume measurements of all mice in each group along time and ATRi treatment (**C**) or ATR + talazoparib treatment (**D**). Error bars represent Standard error of the mean (n=7). Two-way ANOVA p-values of groups M4344 10mg/kg, 5mg/kg and 3mg/kg + talazoparib were lower than 0.0001. Dotted line represents the end of the treatment due to body weight loss >25% in some of the groups. **D.** Box and whiskers representation showing the differences between the final tumour volume in between treatment arms (Mann-Whitney p-values).

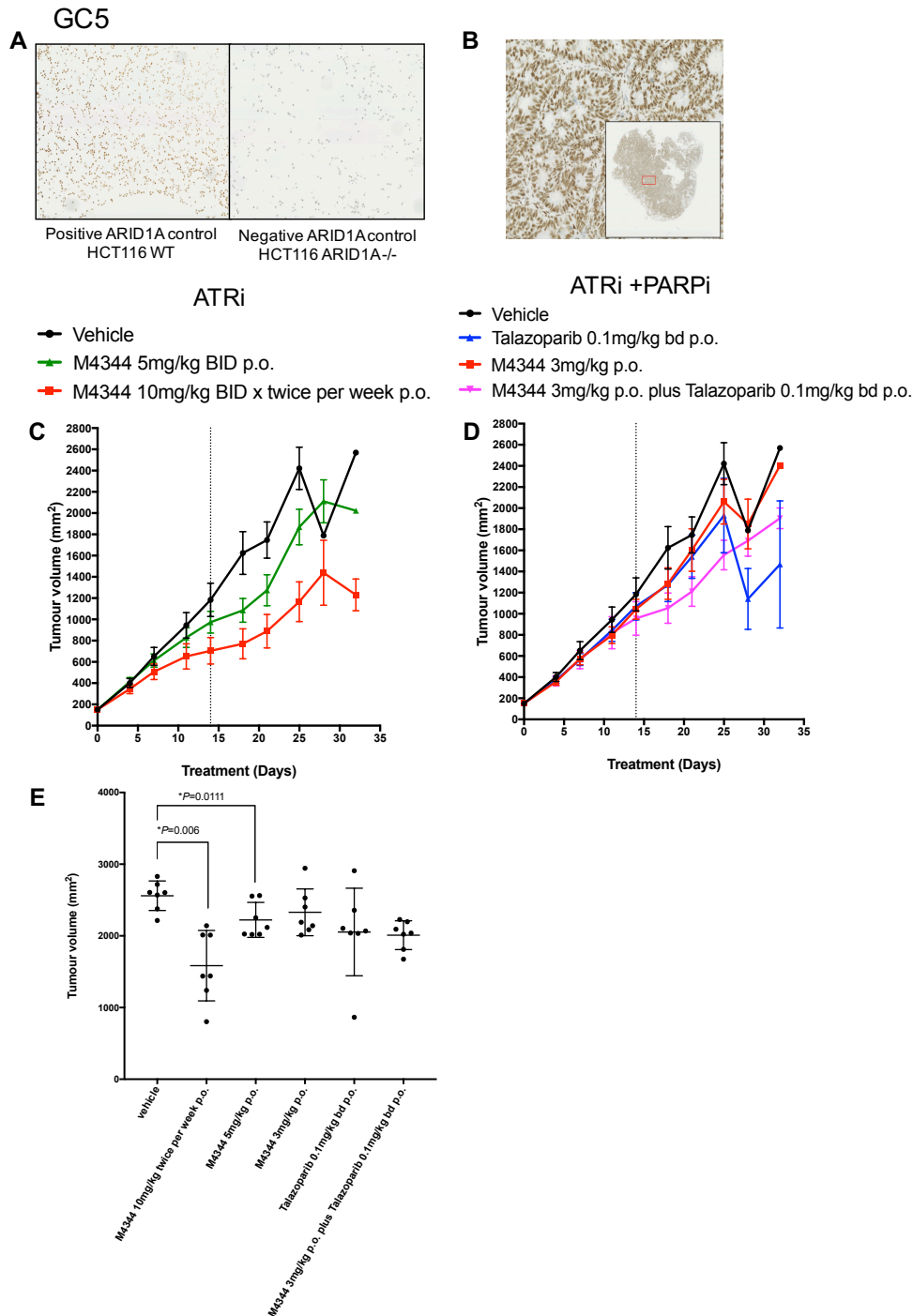


Figure 15. GC5 ARID1A proficient PDX is mildly sensitive to ATR inhibition. **A.** HCT 116 colorectal isogenic cell line was used as a positive control for the ARID1A expression testing by IHC, using the D2A8U ARID1A antibody (CST) at a 1:250 dilution. **B.** FFPE sections from the tumour was stained for ARID1A expression showing complete protein loss, according to the controls. **C and D.** Average of tumour volume measurements of all mice in each group along time and ATRi treatment (**C**) or ATR + talazoparib treatment (**D**). Error bars represent Standard error of the mean (n=7). Only two-way ANOVA p-values of the M4344 10mg/kg group, were lower than 0.0001. Dotted line represents the end of the treatment due to body weight loss >25% in some of the groups. **D.** Box and whiskers representation showing the differences between the final tumour volume in between treatment arms (Mann-Whitney p-values).

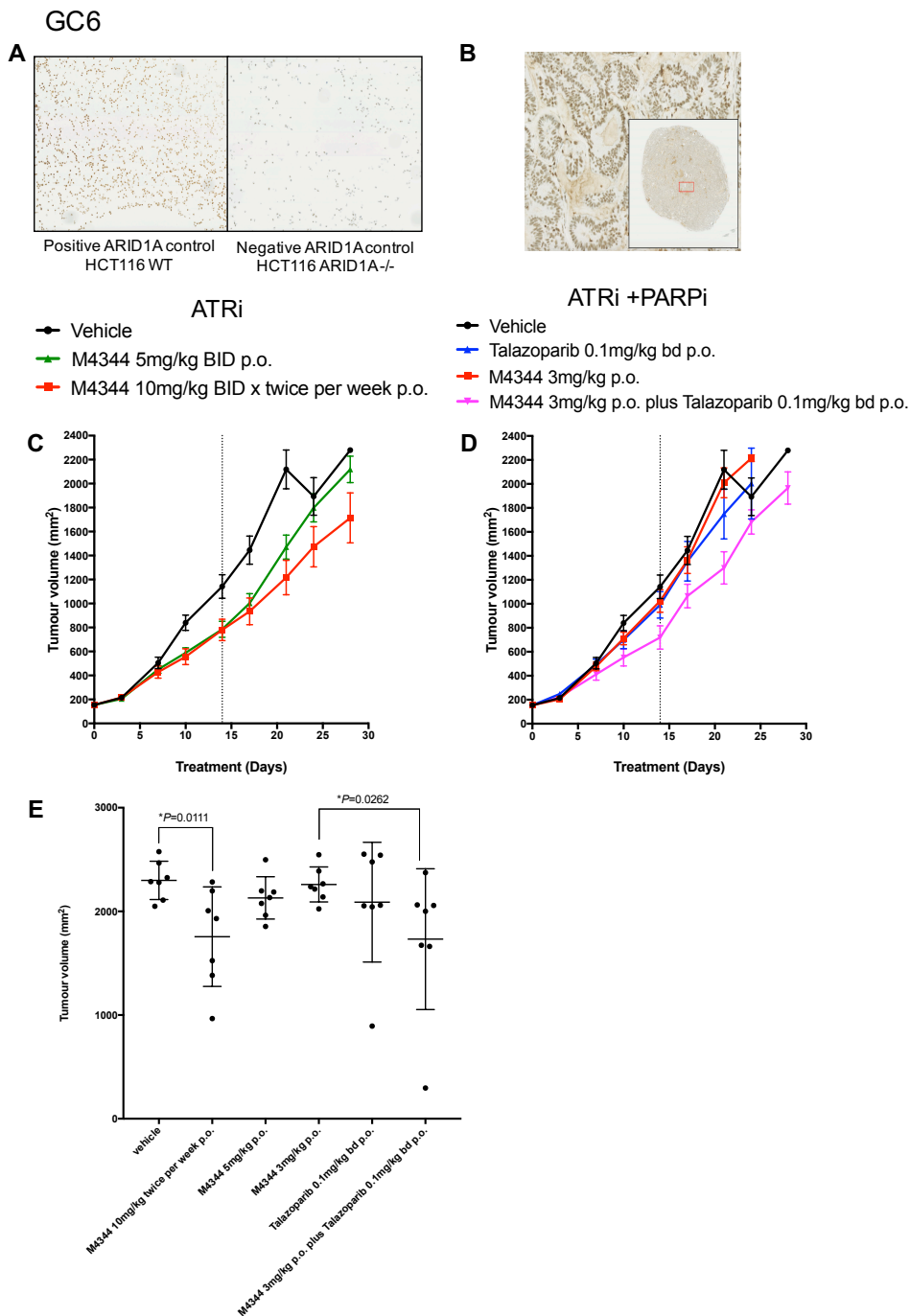


Figure 16. GC6 ARID1A proficient PDX is mildly sensitive to ATR inhibition. **A.** HCT 116 colorectal isogenic cell line was used as a positive control for the ARID1A expression testing by IHC, using the D2A8U ARID1A antibody (CST) at a 1:250 dilution. **B.** FFPE sections from the tumour was stained for ARID1A expression showing complete protein loss, according to the controls. **C and D.** Average of tumour volume measurements of all mice in each group along time and ATRi treatment (**C**) or ATR + talazoparib treatment (**D**). Error bars represent Standard error of the mean (n=7). Only two-way ANOVA p-values of the M4344 10mg/kg group, were lower than 0.0001. Dotted line represents the end of the treatment due to body weight loss >25% in some of the groups. **D.** Box and whiskers representation showing the differences between the final tumour volume in between treatment arms (Mann-Whitney p-values).

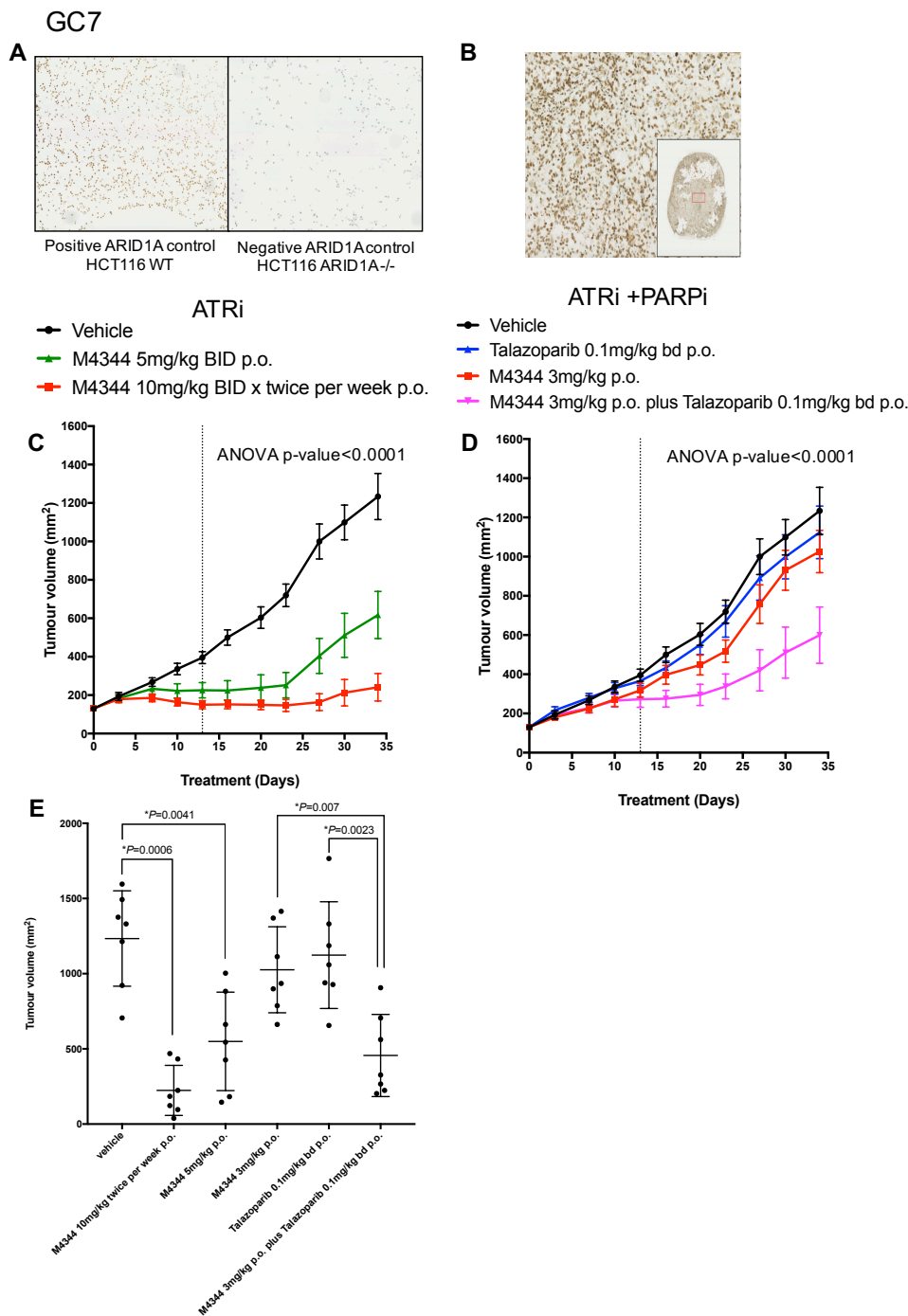


Figure 17. GC7 ARID1A proficient PDX is highly sensitive to ATR inhibition. **A.** HCT 116 colorectal isogenic cell line was used as a positive control for the ARID1A expression testing by IHC, using the D2A8U ARID1A antibody (CST) at a 1:250 dilution. **B.** FFPE sections from the tumour was stained for ARID1A expression showing complete protein loss, according to the controls. **C and D.** Average of tumour volume measurements of all mice in each group along time and ATRi treatment (**C**) or ATR + talazoparib treatment (**D**). Error bars represent Standard error of the mean (n=7). Two-way ANOVA p-values of groups M4344 10mg/kg, 5mg/kg and 3mg/kg + talazoparib were lower than 0.0001. Dotted line represents the end of the treatment due to body weight loss >25% in some of the groups. **D.** Box and whiskers representation showing the differences between the final tumour volume in between treatment arms (Mann-Whitney p-values).

3. VX970 positive selection Genome-Wide CRISPR/Cas9 mutagenesis screen

Although ATRi seem to be a promising therapy for DDR defective cancers, resistance mechanisms are likely to arise from monotherapy treatments. This can be illustrated with the example of *Cell Division Cycle 25A gene (CDC25A)*, which has been demonstrated to cause ATRi resistance due to its failure to induce premature mitosis when CDC25A protein expression is lost (Ruiz, Mayor-Ruiz et al. 2016). Another relevant example of DDR inhibition resistance is the case of the appearance resistance-causing reverting mutations in BRCA1/2 deficient cancers in the context of PARPi-BRCA1/2 SL (Edwards, Brough et al. 2008, Barber, Sandhu et al. 2013, Weigelt, Comino-Mendez et al. 2017).

To try to understand the mechanisms of resistance most likely to cause disease-recurrence in GC patients, I carried out a positive selection GW CRISPR-Cas9 mutagenesis screen (CRISPR screen) using the Kosuke Yusa, Human GW CRISPR guide RNA library, encompassing 87,897 single guide (sg)RNAs targeting more than 17,000 genes) (Koike-Yusa, Li et al. 2014). Using this high-throughput technology, I was able to perform multiple pooled reactions of Cas9-mediated and sgRNA-targeted mutagenesis, aiming to cause independent protein loss of function (LOF) events. After mutagenesis, some of the cells can become resistant to the drug due to a specific protein loss, mediated by a particular sgRNA, that can be tracked and detected using NGS techniques (Wang, Wei et al. 2014, Aguirre, Meyers et al. 2016, Tzelepis, Koike-Yusa et al. 2016, Pettitt, Krastev et al. 2018).

Following this principal, I aimed to identify the genes that are responsible for ATRi resistance in YCC6 gastric tumour cell line, to identify novel mechanisms of resistance that could, potentially be translated into the clinical practice. A workflow including screen optimisation tests, experimental phase and computational analysis required to complete the GW CRISPR screen is illustrated in **Figure 18**.

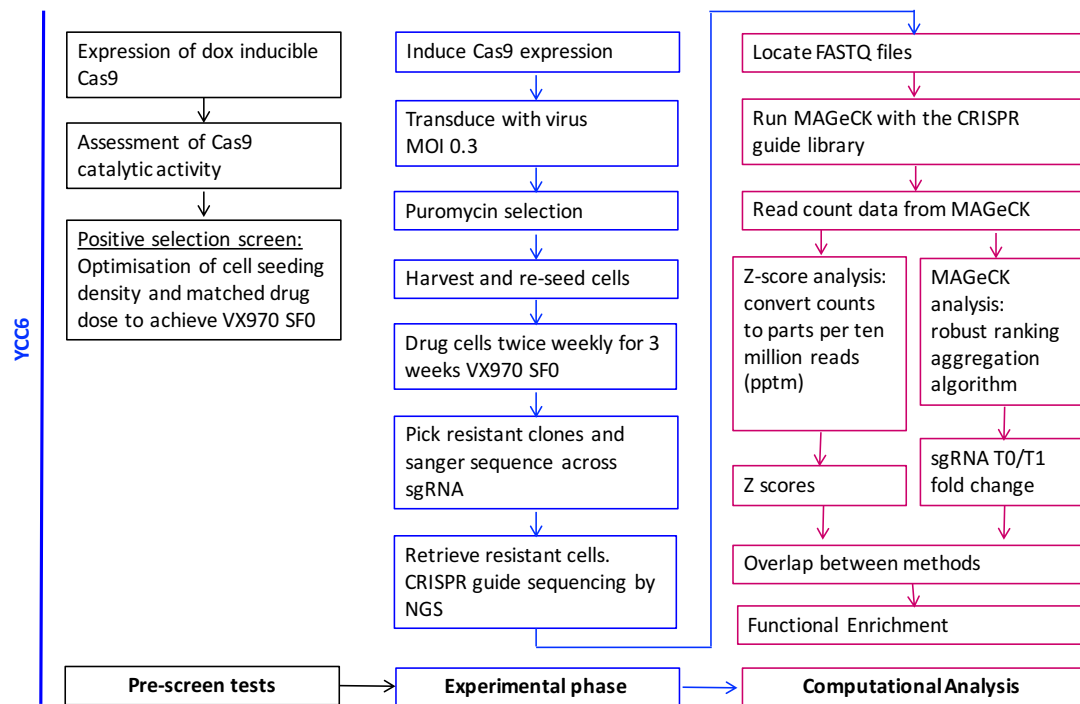


Figure 18. Genome-wide SF₀ positive selection CRISPR/Cas9 screen workflow. First, Dox inducible Cas9 YCC6 cells were created, sorted into individual clones and tested for Cas9 expression. One of the clones was selected (clone 9) and Cas9 catalytic activity was assessed by the two-fluorescence allele method. Cell seeding density and drug dose was optimised in the same format used in the screen. For the screening experiment, Cas9 was induced 24 hours before the cells were transduced with the lentiviral vectors containing the library of GW sgRNA at a low multiplicity of infection, to ensure no more than one sgRNA integration per cell. After 5 days of stringent puromycin selection, sample T=0 was taken and cells were harvested and re-seeded, 24 h before 100nM VX970 was added to the culture media. Cells were drugged twice a week for three weeks. They were then left in drug-free medium for two weeks, prior to the harvesting of the resistant cells for sgRNA sequencing (sample T=1). Additionally, some resistant colonies were picked and sgRNA inserted in them were sanger sequenced. For the computational analysis, FASTQ files were generated from the HiSeq sequencing and sgRNA read count data was calculated using MAGeCK algorithm. After normalisation of sgRNA counts and quality control check, Z-score and MAGeCK analysis was undertaken, comparing T1 to T0 counts, and results were consolidated using MAGeCK and Z-score ranking system. Top hits were taken in account for further validation and functional enrichment analysis.

First, I transduced YCC6 gastric tumour cells with a Dox-inducible Cas9 expressing construct (YCC6^{iCas9}), using the Edit-R Inducible Lentiviral hEF1a-Blast-Cas9 Nuclease (Dharmacon). One of the Cas9 expressing clones was selected, after a 24h of Dox treatment (Clone 9) for further experiments (Western blot showing loss of protein expression in clone 9, compared with YCC6 parental cell line is shown in **Figure 19.A**). To determine the efficiency of the CRISPR-Cas9 editing (Cas9 catalytic activity) in this clone of cells, I co-infected the cells with lentiviral particles carrying

constructs for the green fluorescent protein (GFP) and red fluorescent protein (Cherry, RFP) (GFP/RFP/empty), or with lentiviruses carrying GFP, and a Gfp-targeting gRNA (GFP/RFP/Gfp-sgRNA). I then exposed the cells to Dox for 72 hours and changes in green and red fluorescence were quantified using flow cytometry. I detected a profound decrease in green fluorescence in the GFP/RFP/Gfp-sgRNA cells, demonstrating the ability of Cas9 to generate homozygous mutations in our YCC6^{iCas9} cells, when induced by the Dox treatment (**Figure 19B**).

Cell density and drug concentration was optimised before the actual experiment, using the same format plates and testing a range of VX970 concentrations in a variety of cell densities. A dose of 100nm VX970 in 1 million cells per 15cm plates was selected as the surviving fraction = 0 (SF₀, or 100% lethal dose).

Following optimisation experiments, I transduced YCC6^{iCas9} and non-Dox treated cells (negative control) with the GW sgRNA library at a low multiplicity of infection (MOI), to achieve no more than one sgRNA infection per cell (**Figure 19C**). After puromycin selection, I retrieved T=0 sample and harvested the cells, seeding one million cells per 15 cm plate, following a final x1000 representation per sgRNA in the library, and exposed the cells to 100nM of VX970, a lethal dose for a non-mutated population (SF₀), twice a week for a total of three weeks, until the negative control cells were dead. I left the surviving colonies for two weeks in drug-free media, then picked 24 resistant colonies, that were expanded and retrieved for further analysis. The remaining resistant cells were harvested (T=1 sample) and DNA was extracted and prepared for sgRNA counts NGS.

Following DNA sequencing, the resulting data have been analysed both, through determination of a Z-score statistic (where Z=0 represents no effect on viability and positive Z-scores represent gain of viability), as well as the Model-based Analysis of GW CRISPR/Cas9 Knockout (MAGeCK), method for prioritising sgRNAs, genes and pathways in genome-scale CRISPR/Cas9 knockout screens (Li, Xu et al. 2014), to provide robust normalisation of the sequenced reads (**figure 20A**). I observed that there was an excellent correlation of the data from our screen when the sgRNA log-fold change determined by the MAGeCK method was compared with the median Z-score for each gene (correlation=0.936, p-value<2.2 x 10⁻³⁰⁸) (**Figure 20B**).

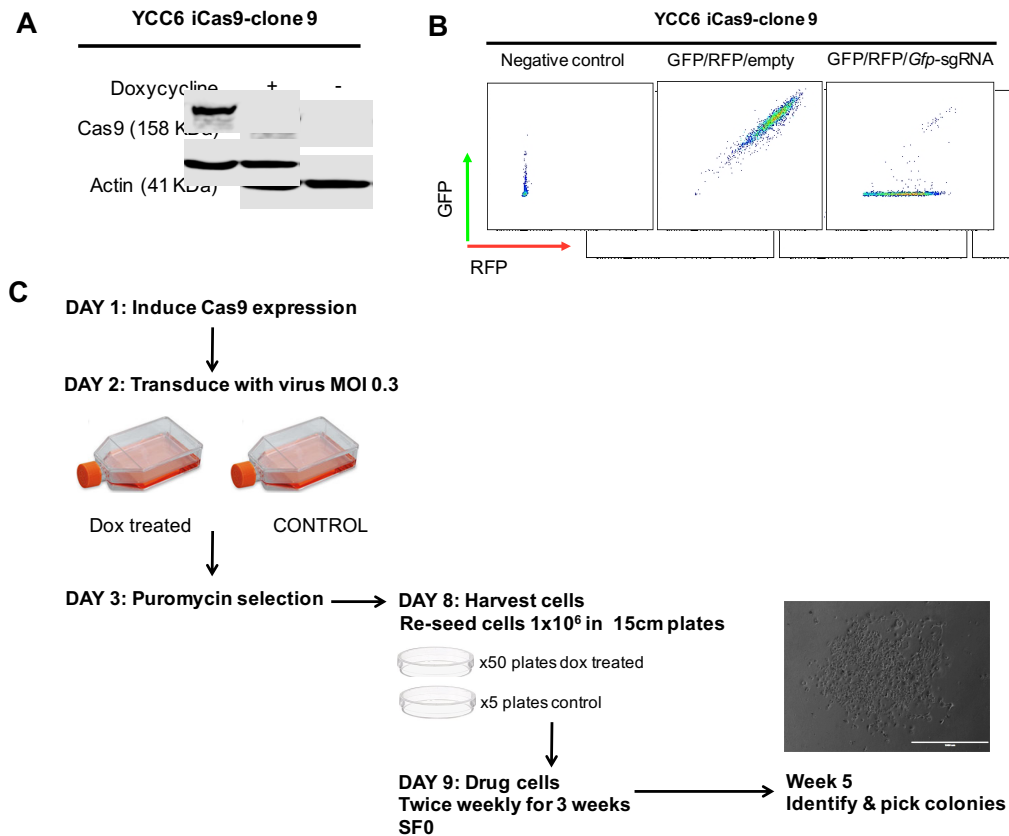


Figure 19. Preparation of the models, dose optimisation and genome-wide CRISPR/Cas9 screen workflow. **A.** YCC6 cells transduced with Edit-R Inducible Lentiviral hEF1a-Blast-Cas9 Nuclease vector (Dharmacon) express Cas9 protein, shown by Western blot after 24h of 1 μ g/ml Dox treatment (clone 9). **B.** iCas9 cells have a catalytic active Cas9. Scheme illustrating the two-allele system used to generate inducible-Cas9 YCC6 cells. GFP/RFP/Empty cells where transduced with GFP and cherry lentiviral constructs, while GFP/RFP/gfp-sgRNA cells where additionally transduced with a sgRNA towards GFP, able to cleave GFP protein and thus decreasing green fluorescence when Cas9 active, detected by flow cytometry. **C.** CRISPR screen workflow. On day one, all cells except the Dox – (negative control) were treated with 1 μ g/ml of Dox. On day two, cells were transduced with the GW sgRNA library at a MOI of 0.3. The following day, successfully transduced cells were selected in puromycin for 5 days, when they were harvested and seeded in 15 cm plates at a determined concentration. On day 9, 100nM VX970 was added to the media and cells were left in drug for three weeks, being fed with fresh drug, twice a week. Resistant colonies were then left to grow in drug-free media for two more weeks, when resistant colonies or cells where retrieved for sequencing.

These analyses have allowed us to identify the genes that display the greatest sgRNA enrichment in ATRi resistant cells retrieved at T1 (after treatment), compared with cells retrieved at T0 (before treatment) (sgRNA fold change). These include, *HECT-UBA* and *WWE domain containing 1-E3 ubiquitin protein ligase (HUWE1)*, *SMG8*, *nonsense mediated mRNA decay factor (SMG8)*, *heterogeneous nuclear ribonucleoprotein F (HNRNPF)*, *interferon regulatory factor 9 (IRF9)*, *cell division cycle*

25B (CDC25B), signal transducer and activator of transcription 2 (STAT2), SMG9, nonsense mediated mRNA decay factor (SMG9), caspase recruitment domain family member 10 (CARD10), cleavage stimulation factor subunit 2 tau variant (CSTF2T), Rho GTPase activating protein 22 (ARHGAP22), coiled-coil domain containing 7 (CCDC7), WDFY family member 4 (WDFY4), FXFD domain containing ion transport regulator 4 (FXFD4), tyrosine kinase 2 (TYK2), RIC8 guanine nucleotide exchange factor A (RIC8A), myopalladin (MYPN), neuropeptide Y receptor Y4 (NPY4R), chromosome 11 open reading frame 86 (C11orf86), CCHC-type zinc finger nucleic acid binding protein (CNBP) and TRAF-type zinc finger domain containing 1 (TRAFD1) (Figure 20C).

The workflow that I used to further validate the hits I found in the NGS results is represented in **Figure 21**. The top 20 candidate genetic determinants of resistance to ATR inhibition in the YCC6 gastric tumour cell line were selected from the hits that had the highest rank product score (combination of MAGeCK and Z-Score value fold-change between sample T=1 and sample T=0), and that had positive results for more than 2 independent sgRNAs for the targeted gene.

Additionally, I sanger sequenced the DNA extracted from the picked colonies, to identify genes targeted by sgRNA in resistant clones (**Table 8**).

To avoid any potential off-target effects of the sgRNA identified in the screen, I carried out a CRISPR/Cas9 mini-screen arrayed validation experiment. Drug dose was optimised by doing a two-weeks exposure drug curve in a 96 well-plate, testing different cell concentrations, and selecting the dose-cell concentration where all cells died after that time (SF_0). Additionally, transfection conditions (reagents and method) was optimised previous to the experiment commencement.

First, infected YCC6^{iCas9} cells with all sgRNA targeting genes identified as candidate genetic determinants of ATR resistance (average of 5 sgRNA per gene), either in the picked colonies, or the sequenced resistant population, in a 96-well format, using the IncuCyte Zoom Live Cell Analysis System, that monitored cell growth in every well after CRISPR/Cas9 mutagenesis. Furthermore, I undertook CTG analysis (Promega) at the end of the screen, which is a luminescent cell viability assay where quantitation of the ATP present in metabolically active cells is used to determine the number of

viable cells in culture. Information regarding the sgRNA used for the validation experiment is present in **Supplementary Table 2**.

CTG reads showed cell proliferation and hence, VX970 resistance for several wells, and this correlated with the growth graphs from the incucyte image analysis. All 5 sgRNAs towards SMG8 and HNRNPF caused resistance to VX970. 4 out of 5 sgRNAs for CDC25B and for CARD10; 3 out of 5 for HUWE1, 2 of 5 for FOXM1 and one sgRNA out of 5 for SMG9, STAT2, ZNF592, FXD4 and JAK1 caused resistance to the ATRi (**Figure 22**), while no proliferative living cells were found in the negative control wells. The sgRNA arrayed validation experiment was carried out three times, and an extra plate was used to further expand the mutated clones to have them as models for future experiments.

Following the results from the arrayed CRISPR/Cas9 screen validation, GW clone 9 and 10 picked colonies were used to validate IRF9 and HUWE1 hits as ATRi resistance-causing genes. Colony GW9 (IRF9 -/-), carried a sgRNA towards exon 1 of IRF9 (AAGAGTTCTGAATTTAAGG) and presented IRF9 protein loss (**Figure 23A**), and ATRi resistance to both, VX970 (**Figure 23B**) and AZD6738 (**figure 23C**) when compared with the parental YCC6^{iCas9} (both VX970 AND AZD6738 two-way ANOVA p-values <0.001).

After TOPO cloning, sanger sequencing of the IRF9 region confirmed the presence of the c.266_284delACAAGAGTTCTGAATTTAA deletion (protein change in approximately half of the copies, and the deletion c.271_285delAGTTCTGAATTTAAG in the other half (**Figure 23D**), consistent with the absolute protein loss found in the western blot (**Figure 23A**). Both deletions were predicted to cause early truncated proteins, according to the online software MutationTaster (<http://www.mutationtaster.org>). Moreover, cell cycle analysis of EdU and PI double stained cells showed decrease in the percentage of cells stalled in inactive S phase in the IRF9 deficient cells, compared with the WT YCC6 (t-test p-value<0.001) (**Figure 23E and F**), consistent with the arising of resistance to ATRi.

Colony GW10 (HUWE1-/-) carried a HUWE1 targeting sgRNA (GCTCTGACGCGTAAGTGAC), and showed complete protein expression loss (**Figure 24A**) and resistance to both ATRi (two-way ANOVA p-value <0.001 for VX970 and AZD6738) (**figures 24B and C**). After TOPO cloning, sanger sequencing revealed a deletion in approximately half of the reads (c.5976_5986delGTCACTTACGC), and an insertion (c.5979_5980insA) in the rest of them (**Figure 24D**).

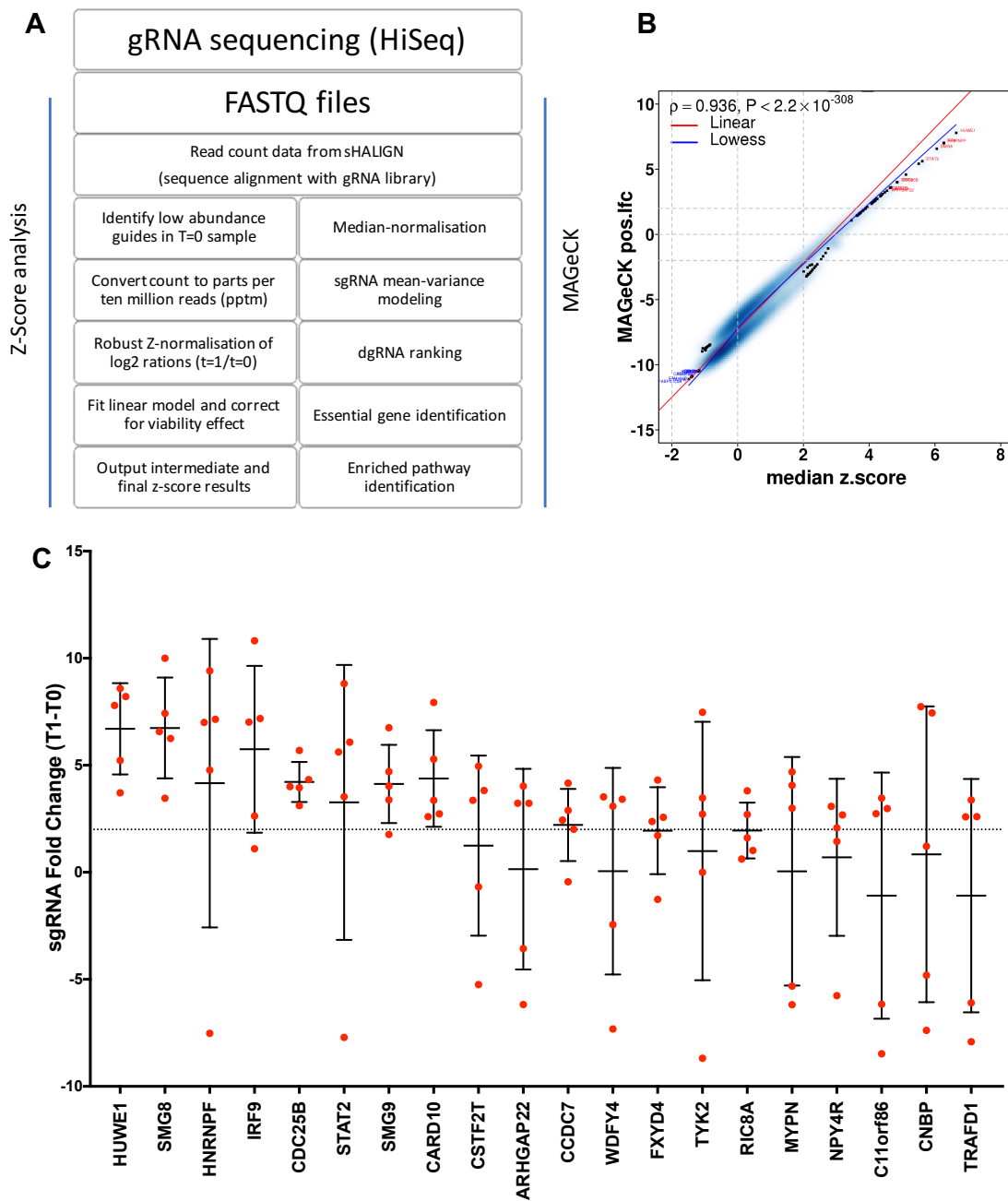


Figure 20. Genome-wide CRISPR/Cas9 screen computational Analysis. A. Z-score and MAGECK analysis workflow. **B.** Concordance of MAGECK sgRNA mean log fold change (T1-T0) with median Z-score. **C.** Box and whiskers plot showing the top 20 candidate genetic determinants of ATRi resistance (red) for the GW CRISPR/Cas9 screen in YCC6 cell line. Each red point represents the fold change (T1 compared with T0 sample) for an individual sgRNA, targeting a potential resistance gene. All top 20 show a p-value <0.00035 according to MAGECK analysis (RRA score – modified robust ranking aggregation algorithm).

GW CRISPR/Cas9 screen validation experiment

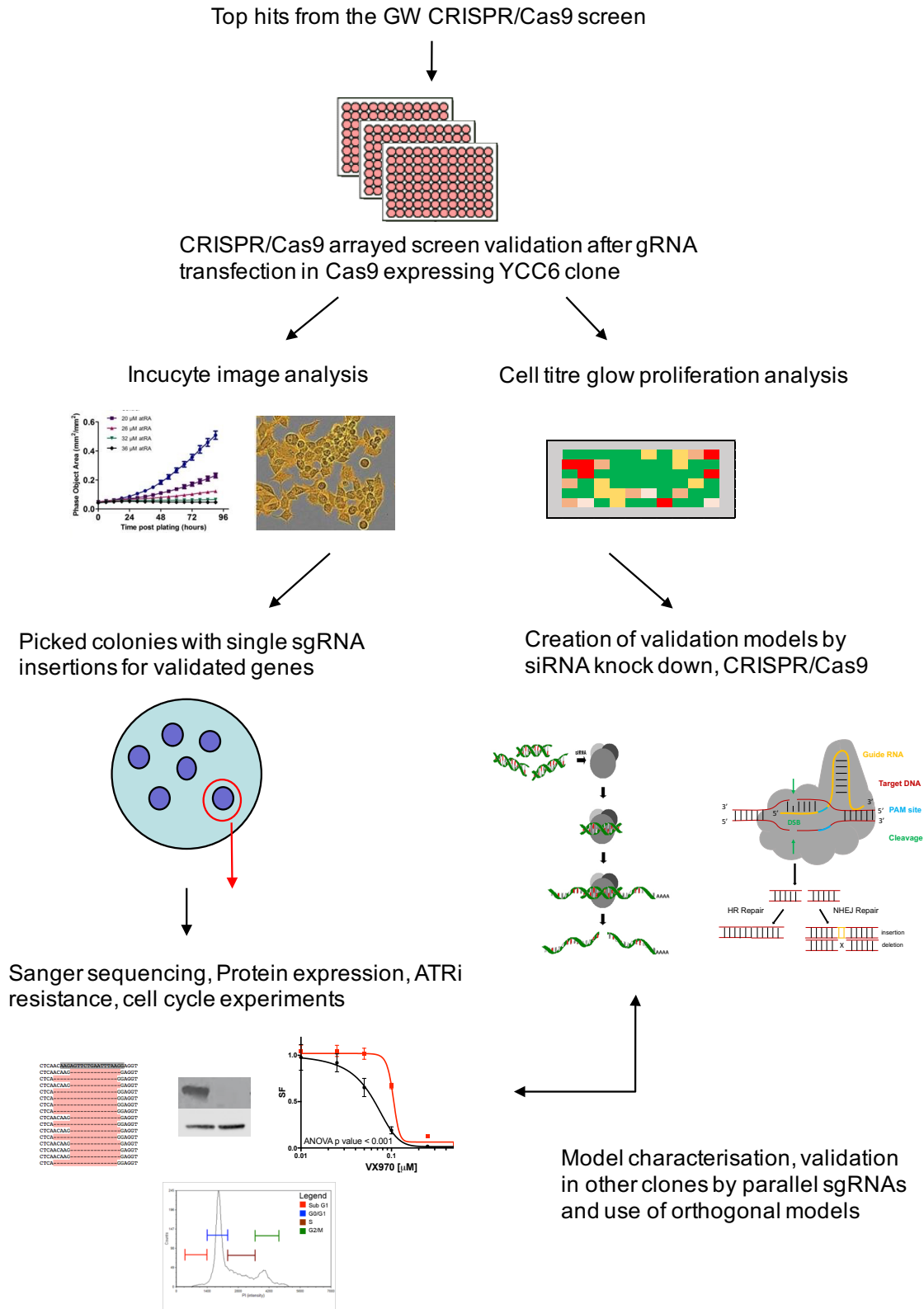


Figure 21. Genome-wide CRISPR/Cas9 YCC6 screen validation pipeline. Top hits from the screen, including 20 top hits from the NGS results, genes listed in the gene cancer census

list present in the top 50 hits, plus gRNA inserted in the picked colonies were selected and transfected to the Cas9 expressing YCC6 cells in a arrayed 96-well plate format. Cells were analysed by the incucyte image analysis system over time, and by cell titre-glo proliferation analysis at a final time. Selected validated hits which had associated resistant picked colonies with no more than one sgRNA insertion, were further validated by sanger sequencing of DNA, protein expression testing (western blot), ATRi resistance checking and cell cycle analysis (FACS) (HUWE1 and IRF). For the validated genes that were not represented in the picked colonies, further validation models were created by siRNA transfection and knockdown or by single CRIPR/Cas9 mutagenesis and those models were then characterised and used for validation experiments. Future testing in parallel clones or orthogonal models will be performed for the strong candidate genes found.

Table 8. sgRNA detected in the picked resistant colonies from the genome-wide CRISPR-Cas9 mutagenesis screen in YCC6 gastric tumour cell line. Highlighted in green the genes amongst the top-50 hits from the NGS-sgRNA count from the remaining resistant population.

Colony number	Gene targeted	sgRNA sequence	Position in rank on hit list
GW1	ZNF592	TCTCCCAAAGCACCTGCGC	160
GW2	GIMAP1 ZNF599	AGCTGCTGGGGATGGTCGA TCTCCCAAAGCACCTGCGC	624 328
GW3	KLLN	CGGAAAGTAGTTCCGACTG	157
GW4	KLLN	CGGAAAGTAGTTCCGACTG	157
GW5	CECR6	AAGAACAGCCGGGGCCGTC	1009
GW6	AMACR STAT2	ACGTGAGCCGCTTGGGCCG TGCTTCCGATATAAGATCC	569 6
GW7	CWF19L1	GCCACCCGGTTTATAGCTC	317
GW8	FDFT1	TCTCCATGAACCGCCAGTC	82
GW9	IRF9	AAGAGTTCTGAATTTAAGG	4
GW10	HUWE1	GCTCTGACGCGTAAGTGAC	1
GW11	LAMTOR2 PTCHD3 USP43	CCATACCATGCAGTCCATG CGTCCAGCATCGACGGCCG CGTACCTCGTCTGGCGCAA	169 2347 56
GW12	THUMPD1	GTCGCCGTATTCGTTGAGG	298
GW13	JAK1	CGGAAGTAGCCATCTACCA	48
GW14	DUSP6 POLDIP3	GCGCTCTTCACGCGCGGCG ATGCCCGATTTCGAATCAA	10990 825
GW15	TYK2	GTGCTGCCGATATGCCGG	14

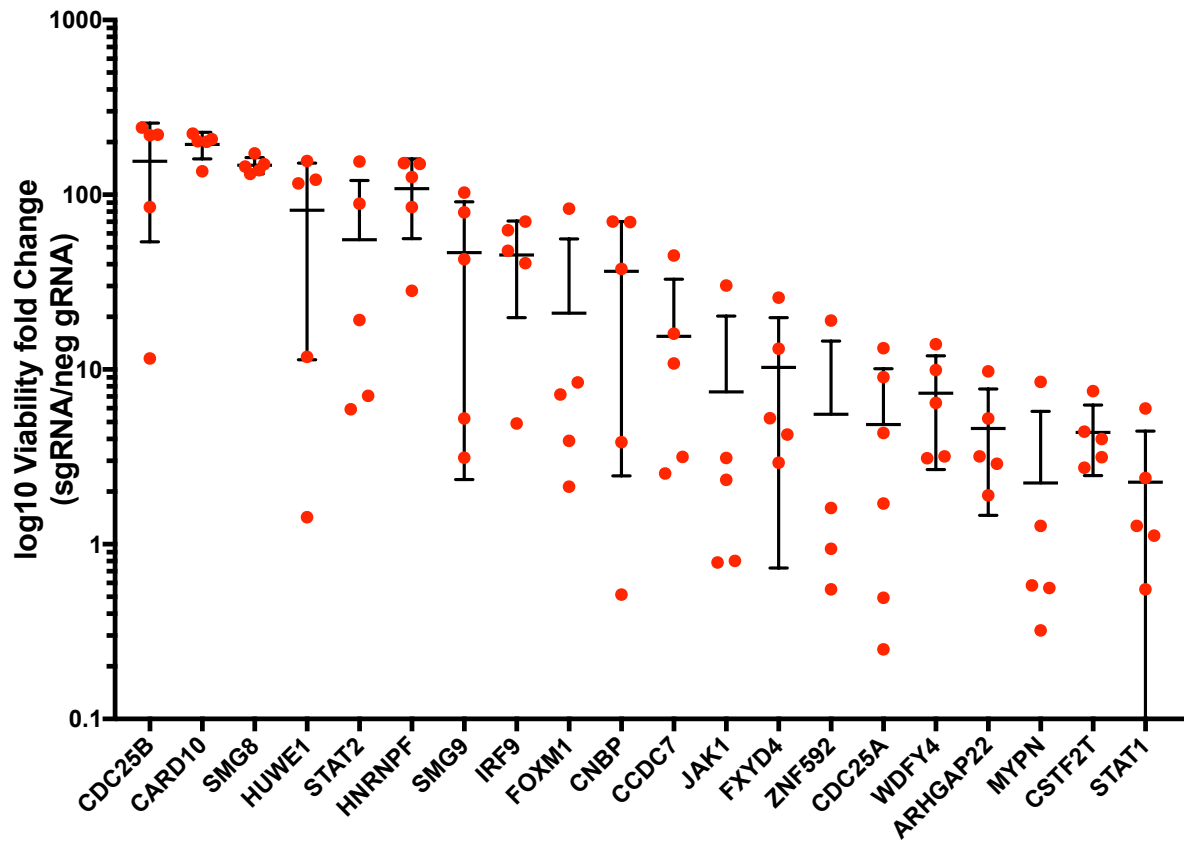


Figure 22. Validation CRISPR/Cas9 mini-screen. Results from the validation CRISPR/Cas9 mini-screen according to the luminescence reads (cell titre-glo) per well, normalised to negative control wells (sgRNA- negative C sgRNA). 31 genes were studied, testing for a total of 159 sgRNAs. Two different negative control sgRNAs were additionally used. 1500 YCC6^{iCas9} cells per well were seeded and reversely transfected with specific sgRNA before they were exposed to 80nM VX970 for two weeks, being fed twice week. Plates were then left to recover for one week with drug-free media. Log10 values of viability per well (sgRNA) are plotted (red dots) in the Y-axis for the top 20 validated genes (X-axis). Complete death is assumed from values equal or lower than log10 of 1 (=0).

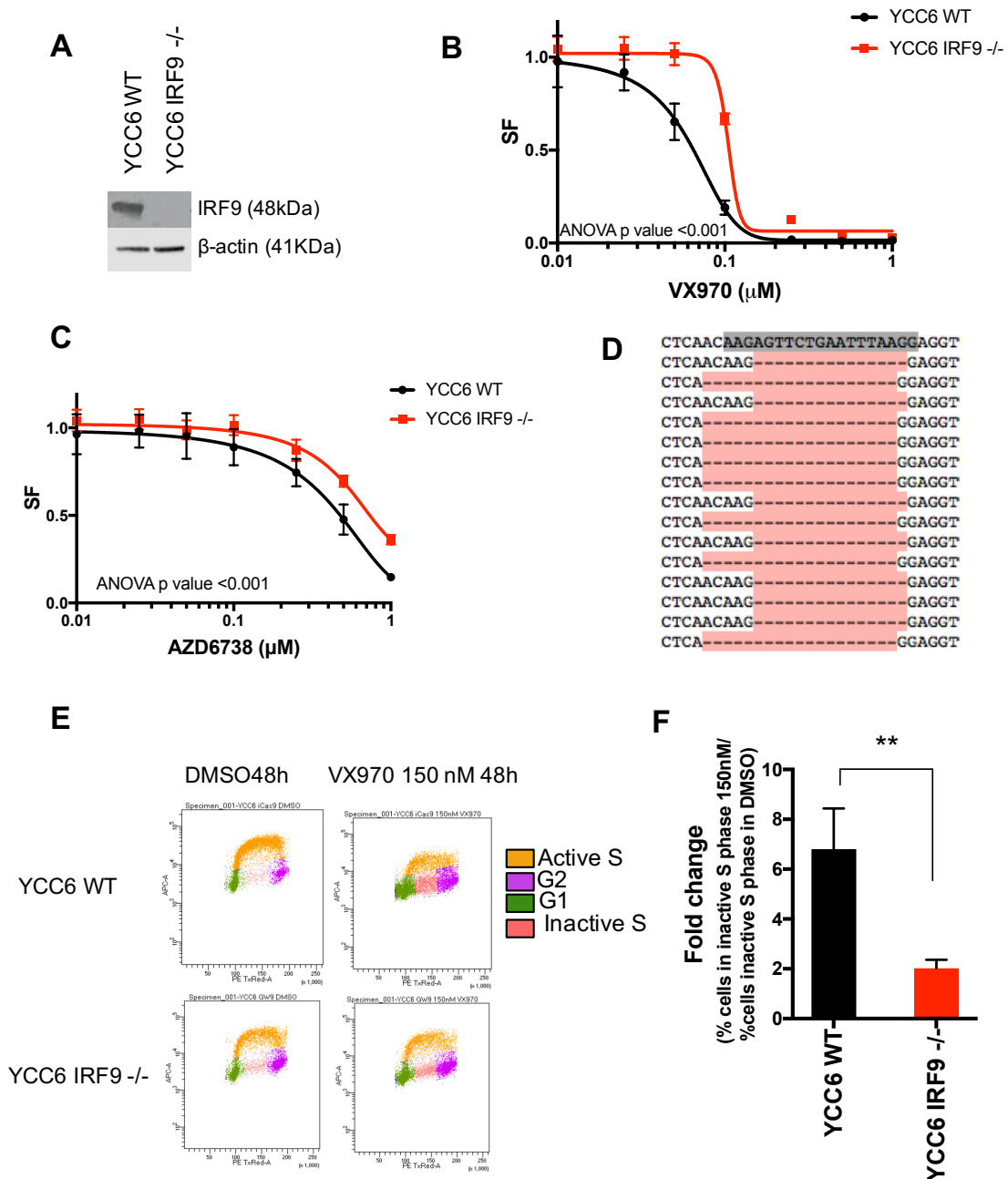


Figure 23. Validation of *IRF9* as a candidate for ATRi resistance mediator in *IRF9* isogenic cells. **A.** WB showing a loss in *IRF9* protein in the resistant clone harbouring a gRNA towards *IRF9*, compared with the parental YCC6 cell line. **B.** Drug sensitivity curves showing decreased sensitivity to VX970 in *IRF9* $-/-$ cells compared with YCC6 *IRF9* WT cells (two-way ANOVA, $p < 0.001$) **C.** Drug sensitivity curves showing decreased sensitivity to AZD6738 in *IRF9* $-/-$ cells compared with YCC6 *IRF9* WT cells (two-way ANOVA, $p < 0.001$). Cells were seeded in 384-well plates and exposed to a 5-days treatment across 8 different concentrations of drug, ranging between $0.0001\mu\text{M}$ to $1\mu\text{M}$. Error bars represent standard deviation between reps ($n=14$). **D** *IRF9* sequence alignment by ApE software in 15 TOPO cloned colonies from YCC6 *IRF9* $-/-$ resistant clone shows two different mutations present in all copies (c.266_284del ACAAGAGTTCTGAATTTAA and c.271_285del AGTTCTGAATTTAAG). **E.** Cell cycle analysis done by FACS with a double EdU (Y-axis, APC-A) and PI (X-axis, TX-Red) staining revealed a decrease of the number of cells stalled in inactive S phase in the *IRF9* $-/-$ cells, compared with the YCC6 WT ones. **F.** Calculation of the fold chance of the percentage of cells in inactive S phase after 48h of 150nM VX970 treatment divided by the percentage of

cells in inactive S phase in the DMSO control as a quantitative measurement of figure E (difference between YCC6 WT and IRF9 -/- t-test p-value <0.001).

Both alterations were predicted to cause early truncated proteins, according to MutationTaster. Similarly, to what I saw in the IRF9 -/- clone, EdU/PI cell cycle analysis showed a decrease of the cells in inactive S phase in the HUWE1-/- deficient clone, compared with the WT after 48h of VX970 treatment (**Figure 24E**). These differences are quantified in **Figure 24F** (t-test p-value >0.001).

Due to the large list of potential ATRi resistance causing candidate genes I have described in this section, and with the aim of shortlisting the ones that are more relevant in cancer, I cross-referenced our data regarding to the YCC6 gastric tumour cell line to other available data from other screens. I had previously carried out a CRISPR screen in the ovarian clear cancer cell (OCCC) tumour cell line TOV21G, following the same format than the one carried out in the YCC6 screen (data not shown). Additionally, a recent publication carried out a SF₅₀ CRISPR screen where they have described both, ATRi sensitivity and resistance causing genes in three cell lines, including the 239A (Kidney), HCT 116 (Colorectal) and MCF10A (Breast) tumour cell lines, using the AZD6738 ATRi. Selecting only the genes that had a Z-score >2 from the resistance causing genes list, I was able to observe a surprisingly high overlap of genes in between the four cell lines and our YCC6 screen (**Figure 25A, Supplementary Table 3**). I found two genes that were currently represented in all five cell lines which were *CDC25B* and *TRIT1*. 24 of the genes found to be significant in YCC6, were also ATRi resistance-causing mediators in three of the four additional cell lines, and 249 genes were found in two out of four cell lines (**Supplementary Table 3**).

This analysis has allowed me to select the genes for further study, in order to define its implication in ATRi resistance from a mechanistic perspective. Therefore, I cross-referenced the top 50 hits from our YCC6 screen and determined their effect in the other cell lines, defining a list of genes illustrated in **Figure 25B**. I observed that *CDC25B* is present in all five analysed cell lines; *SMG8* in four cell lines; *HUWE1*, *HNRNPF*, *SMG9*, *STAT2*, *KIF5B*, *IFNAR1* and *RET* in three out of five cell lines. As I have already been able to validate the implications of many of these genes in our 96 well-plate arrayed screen, I had a strong rationale to generate isogenic models that

can represent these potential main drivers of ATRi resistance and will guarantee the generation of valuable information that can potentially be used in the clinical practice.

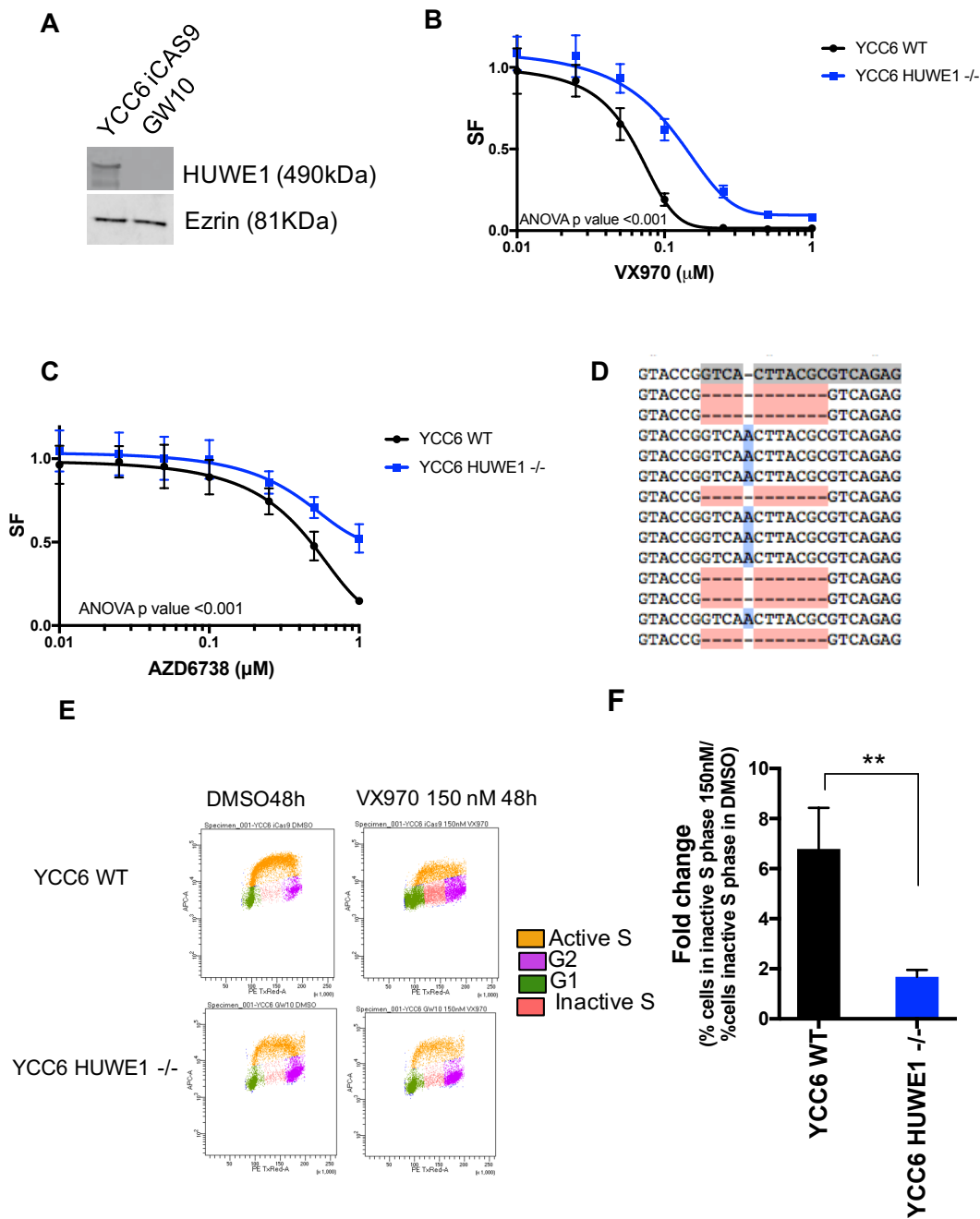


Figure 24. Validation of *HUWE1* as a candidate for ATRi resistance mediator in *HUWE1* isogenic cells. **A. WB showing a loss in *HUWE1* protein in the resistant clone harbouring a gRNA towards *HUWE1*, compared with the parental YCC6 cell line. **B.** Drug sensitivity curves showing decreased sensitivity to VX970 in *HUWE1* $-/-$ cells compared with YCC6 WT cells (two-way ANOVA, $p < 0.001$). **C.** Drug sensitivity curves showing decreased sensitivity to AZD6738 in *HUWE1* $-/-$ cells compared with YCC6 WT cells (two-way ANOVA, $p < 0.001$). Cells were seeded in 384-well plates and exposed to a 5-days treatment across 8 different concentrations of drug, ranging between $0.0001 \mu\text{M}$ to $1 \mu\text{M}$. Error bars represent standard deviation between reps ($n = 14$). **D** *HUWE1* sequence alignment by ApE software in 15 TOPO**

cloned colonies from YCC6 *HUWE1* *-/-* resistant clone, shows two different mutations present in all copies (c.5976_5986del GTCACCTACGC and c.5979_5980ins A). **E.** Cell cycle analysis done by FACS with a double EdU (Y-axis, APC-A) and PI (X-axis, TX-Red) staining revealed a decrease of the number of cells stalled in inactive S phase in the *HUWE1* *-/-* cells, compared with the YCC6 WT ones. **F.** Calculation of the fold change of the percentage of cells in inactive S phase after 48h of 150nM VX970 treatment divided by the percentage of cells in inactive S phase in the DMSO control as a quantitative measurement of figure **E** (difference between YCC6 WT and *HUWE1* *-/-* t-test p-value <0.001).

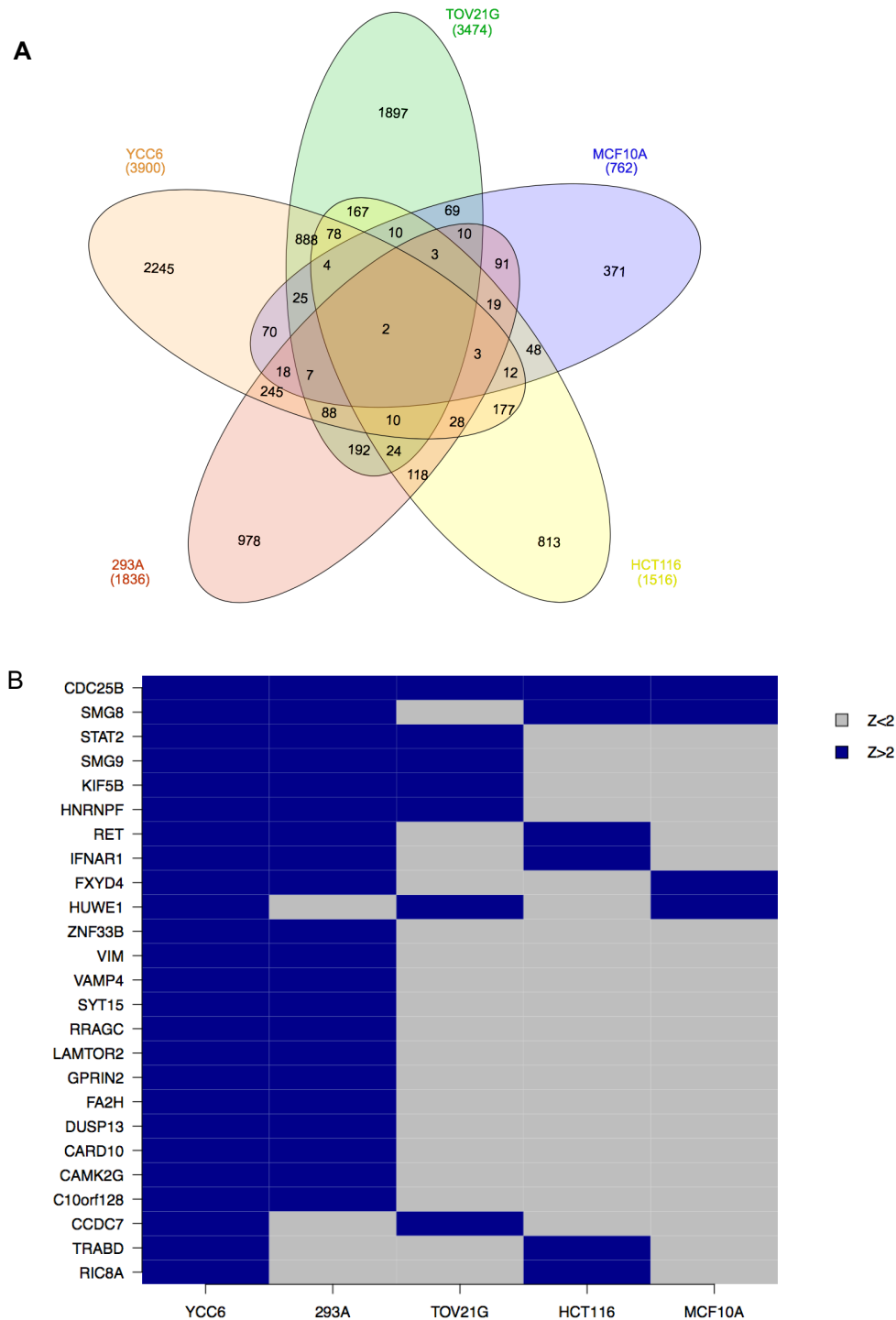


Figure 25. Candidate ATRi resistance causing genes identified from GW CRISPR screens of 5 cell lines (including data from Wang et al., 2018). A. Venn diagram created

with <http://www.interactivenn.net> showing the overlapping candidate ATRi resistance causing genes with Z-score >2 identified from our GW CRISPR screens performed in YCC6 and TOV21G cell lines, and the 293A, HCT 116 and MFC10A available data extracted from Wang *et al*, 2018. **B.** Heatmap of overlapping candidate genes from figure A present in the top 50 hits described the YCC6 GC tumour cell line.

4. Creation and characterisation of YCC6 ATR inhibitor resistant clones

In order to discover genetic determinants to ATRi resistance in GC, I generated YCC6 VX970 resistant cells by seeding them at a low density and exposing them to increasing doses of VX970 for approximately six months, in two parallel experiments (see **Figure 26A**). Cells from the first experiment reached a high level of resistance to VX970 (H), approximately 8-fold higher than the initial SF_{50} (54 nM), after being exposed to VX970 at a concentration of 430nM. Cells from the second experiment reached a medium resistance level (M) of approximately 5-fold increase, compared with the initial SF_{50} of VX970, proliferating at a concentration of 260nM VX970. Both Highly resistant (H) and Medium resistant (M) YCC6 populations proved to be resistant to ATR inhibition when exposed to a range of VX970 concentrations in a five-days exposure drugging experiment (**Figure 26B**) compared with the parental population in a dose-dependent fashion (two-way ANOVA p-values <0.001). These findings were validated by using another ATRi, AZD6738, which showed the same effect as VX970 (all two-way ANOVA p-values <0.001) (**Figure 26C**), suggesting that these findings were not private to VX970, but to ATR inhibition, as a class effect.

I then generated resistant clones by single cell sorting the resistant population by FACS. Pellets were retrieved from the 8-surviving independent clones (6 H clones and 2 M clones) that demonstrated profound resistance to both, VX970 and AZD6738 ATRi, compared with the parental cell line (all two-way ANOVA p-values <0.001) (**Figures 26D and E**). Next, I expanded the clones during exposure to VX970 to extract the protein fraction, for purposes of the proteomic mass spectrometry analysis (MS). Finally, clone M2 was discarded from the analysis due to its very slow growth rate.

Interestingly, I visualised a change in the morphology of the clones as they became resistant to ATRi (**Figure 27**). Originally, YCC6 is an epithelial cell line, which is mainly constituted by small semi-rounded epithelial cells, although some larger and amoeboid cells can be observed. Conversely, clones H2, H3, H4 and H6 presented a pattern mesenchymal-like cells with a more elongated morphology. In the case of H1 clone, I

could see large cells with an amoeboid structure, which might be a result of the selection of these cells from the parental population. In contrast, I did not see a change in morphology of the H5 and M1 clones compared with the parental population (**Figure 27**).

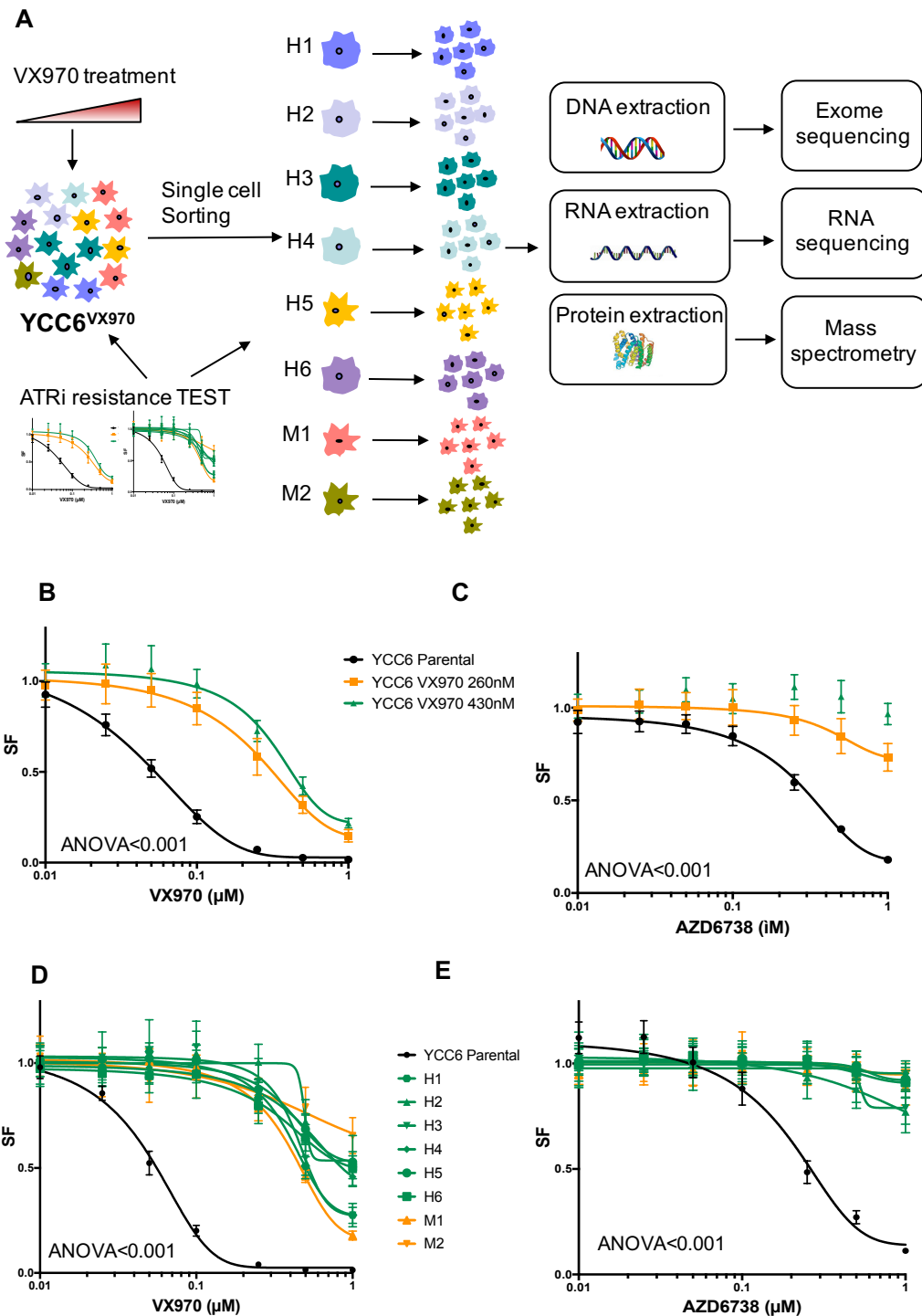


Figure 26. YCC6 ATRi resistant cell experiment design. YCC6 cells were exposed to increasing concentration of VX970 until they became resistant to ATR inhibition. After sorting single clones by FACS from the parental population, surviving colonies were tested for ATRi

resistance (VX970 and AZD6738) in comparison with the parental cell line. Colonies were expanded and pellets were retrieved to extract DNA, RNA and protein in order to perform exome sequencing, RNA sequencing and Mass Spectrometry, respectively. **B and C** Drug sensitivity curve for AZD6738 and VX970 in the generated ATRi resistant pool, compared with the parental population. Green curve shows dose-response to ATRi for cells resistant to 430nM (H). Orange curve shows dose-response to ATRi for cells resistant to 260nM (M). All two-way ANOVA p-values for both groups were lower than 0.001. **D and E**. Drug sensitivity curve for AZD6738 and VX970 in the FACS sorted clones (H clones come from H resistant parental population while M clones come from M parental population). All two-way ANOVA p-values for both groups were lower than 0.001. Cells were seeded in 384-well plates and exposed to a 5-days treatment across 8 different concentrations of drug, ranging between 0.0001 μ M to 1 μ M. Error bars represent standard deviation between reps (n=14).

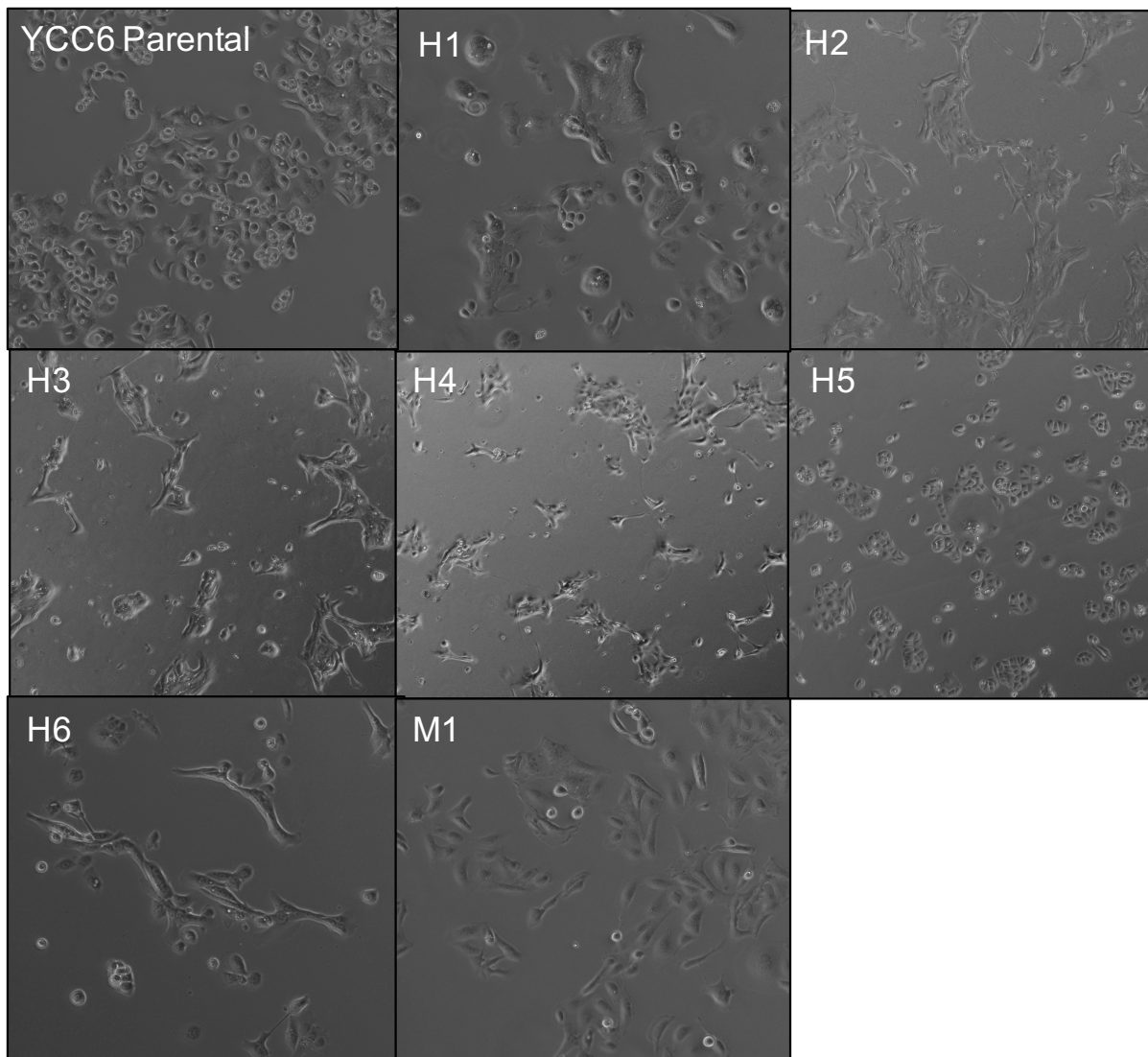


Figure 27. Detection of morphological changes in YCC6 ATRi resistant clones. Pictures taken from the ATRi resistant clones (highly resistant H1, H2, H3, H4, H5 and H6 and medium resistant M1) using the EVOS imaging system (20x Objective, Invitrogen) show changes in cell shape, compared with the parental cells.

Principal components analysis (PCA) analysis was carried out with the proteomic data, comparing the expression profiles between the clones and the parental cell line, to check for the quality of the biological replicates in both experiments. PCA plots demonstrated a very high reproducibility of the results in between replicates (**Figure 28**). Additionally, these analyses showed that clones H5 and M1 clustered separately to an H1, H2, H3, H4 and H6 cluster, and to the parental cell lines, which showed a completely different proteomic profile. This is consistent with the change to a mesenchymal cell morphology that was observed in the H1, H2, H3, H4 and H6 cluster but not in the H5 and M1 clones. According to these observations, I decided to do all the further statistical evaluations comparing the parental cells to i) all resistant clones grouped together; ii) H5 and M1 cluster; iii) H1, H2, H3, H4 and H6 cluster (**Figure 28**).

Proteomic mass spectrometry analysis was undertaken in seven ATRi resistant clones, compared with the parental YCC6 cell line, by measuring the expression of 9,410 proteins in a mass spectrometry multiplexed reaction. After applying the Welch t-test analysis, comparing the protein expression levels in all the resistant clones with the parental cells, 204 proteins showed a consistent statistically significant differential expression in between the two groups, establishing a cut-off of FDR (multiple comparisons corrected p-value) lower than 0.05, plus an absolute log₂ fold-change higher than 0.5 or lower than -0.5. Thus, I detected a significant under or over expression of a large list of proteins in the resistant clones represented in a volcano plot (**Figure 29A**). LGALS2 (*Beta-Galactoside-Binding Lectin L-14-II*), MUC13 (*Mucin 13, Cell Surface Associated*), TSPAN8 (*Tetraspanin 8*), VIL1 (*Vilin 1*), ECM1 (*Extracellular matrix protein 1*), KRT7 (*Keratin 7*) and RIC8 (*RIC8 Guanine Nucleotide Exchange Factor A*) were amongst the most significantly overexpressed in the resistant clones, compared with the parental cells (all p-values <0.05). MAP1B (*Microtubule Associated Protein 1B*), NCAM1 (*Neural Cell Adhesion Molecule 1*), CD44 (*Extracellular Matrix Receptor III*), CD70 (*Tumour Necrosis Factor Ligand Superfamily Member 7*), MT2A (*Metallothionein 2A*) and MTF1 (*Transcription Factor MTF-1*) were amongst the proteins that were downregulated. Protein-protein interaction networks using STRING online software and Cytoscape software revealed a large network of protein interactions in our hits (**Figure 29B**).

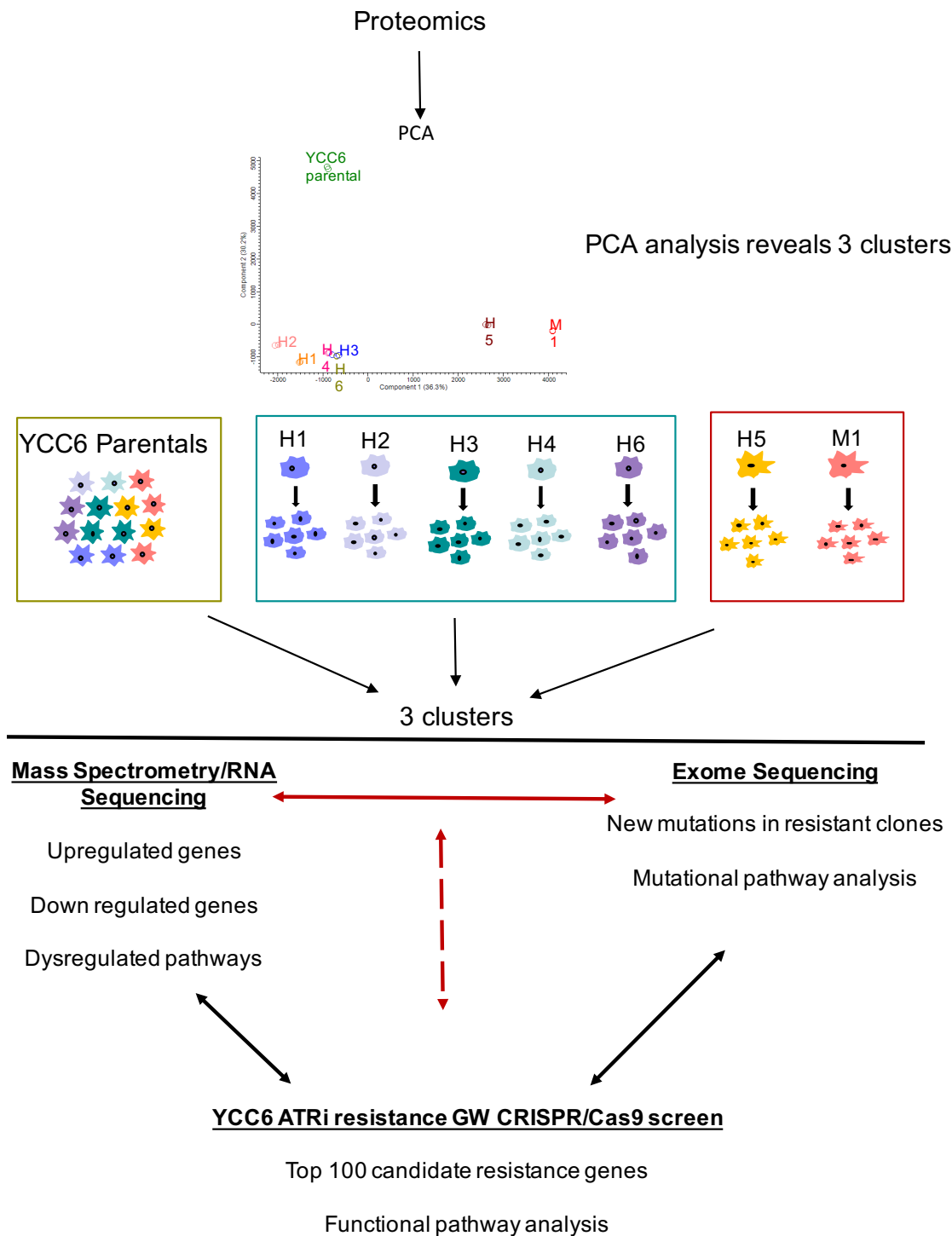


Figure 28. ATRi resistant clones' data analysis workflow. Principal component analysis of proteomics data revealed 3 independent clusters of clones, dividing the parental cells from a M1/H5 group and a H1/H2/H3/H4/H6 group. Therefore, further analyses were done in comparison of the three clusters. First, upregulated and downregulated genes or pathways were determined and compared from the mass spectrometry and RNA sequencing data. Then, a description of new acquired mutations in the resistant clones, compared with the parental cell lines was determined using the exome sequencing data. After cross-referencing results from DNA and RNA/Protein results, I looked for common resistance-causing genes, comparing the results to the candidate resistance-causing genes from the GW CRISPR/Cas9 screen data. For purposes of this thesis, I have only presented the proteomics data.

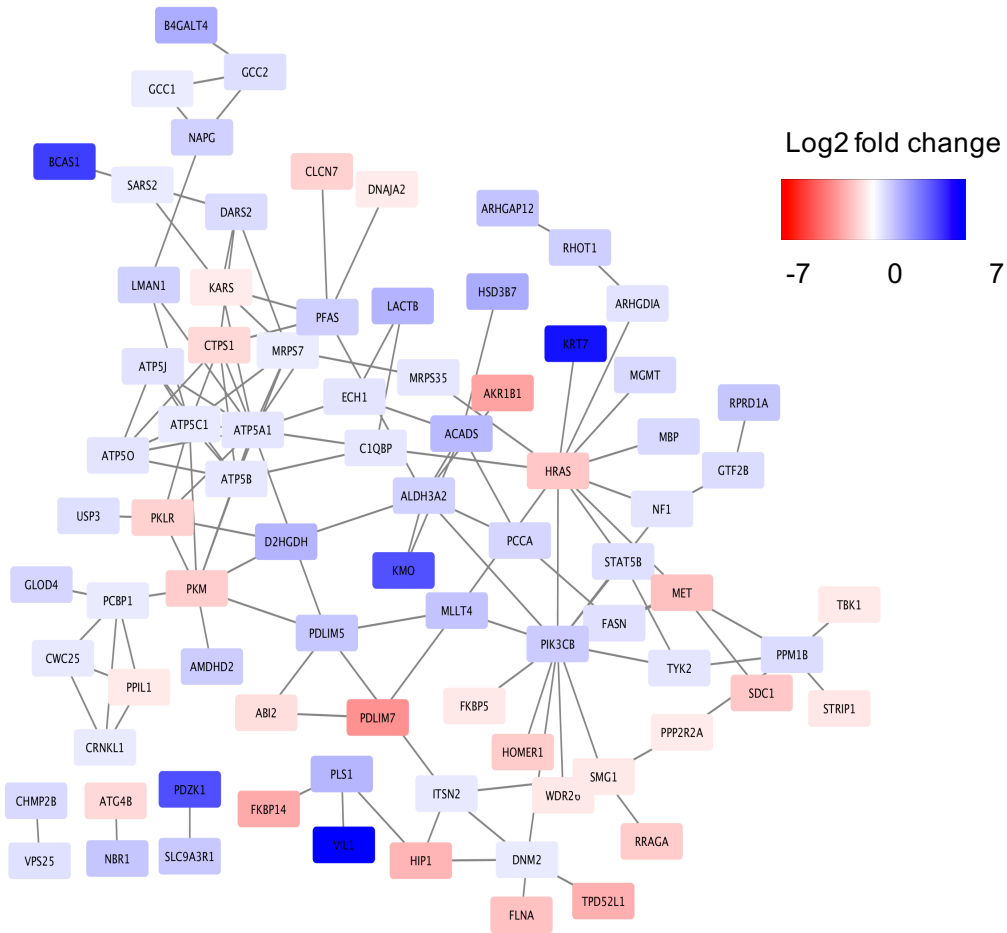
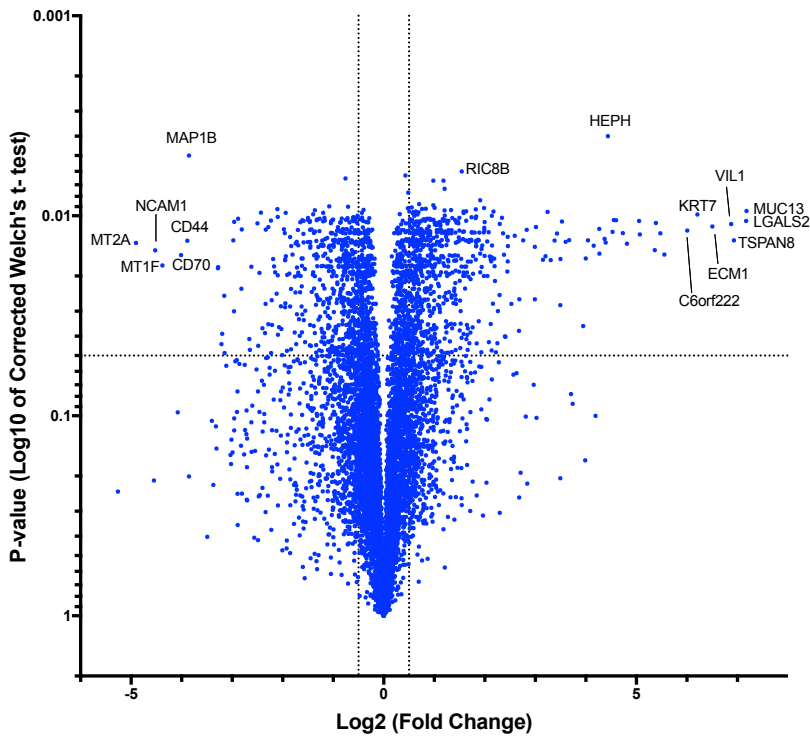


Figure 29. Mass spectrometry transcriptomic data reveals common differentially expressed proteins in all YCC6 ATRi resistant clones. A. Volcano plot representing Log10

multiple comparisons corrected Welch's test p-values against the Log₂ fold-change of the differences between all resistant clones and the parental YCC6 cell line **B**. Protein interaction map generated by STRING online software showing protein interactions from the differentially up (Red) and downregulated (Blue) genes showed in figures A and B. Only proteins showing at least one interaction are included in the network. Statistical significance means differences in protein expression levels with a FDR corrected Welch's test p-value <0.01 and Log₂ fold change differences lower than -0.5 or larger than 0.5. All experiments were performed in two biological replicates.

Interestingly, several protein complexes were found to be represented by several of its components, where typically all units in a complex followed the same trend. Proteins that form part of the ATP complex (ATP11A, ATP5J, ATP5O, ATP5A1, ATP5I, ATP5B, MT-ATP6, ATP5C1), were found to be downregulated in the resistant cells, compared with the parentals. Also, conserved oligomeric Golgi (COG) complex, in charge of protein glycosylation (COG2 COG3 and COG6) were downregulated in the resistant cells. Proteins ALDH9A1, ALDH1A3, ALDH3A2, part of the Aldehyde Dehydrogenase (ALDH) complex, which plays a role in aldehyde metabolism, were found to be downregulated in the resistant clones, compared with the parentals. Of note, ALDH complex has been previously associated to cellular detoxification, DNA damage protection and cancer (Jelski, Zalewski et al. 2008, Orywal and Szmitkowski 2017). Additionally, several potential mediators to ATRi resistance found were listed in the cancer genome census and thus related to carcinogenesis (present in the cancer genome census list) (Sondka, Bamford et al. 2018), including MLLT4 (*Afadin*, *Adherens Junction Formation Factor*), PIK3CB (*Phosphatidylinositol-4,5-Bisphosphate 3-Kinase Catalytic Subunit Beta*), MGMT (*O-6-Methylguanine-DNA Methyltransferase*), STAT3 (*Signal Transducer And Activator Of Transcription 3*), STAT5B (*Signal Transducer And Activator Of Transcription 5B*) NF1 (*Neurofibromin 1*), PCBP1 (*Poly(RC) Binding Protein 1*), DNM2 (*Dynamain 2*), PARP4 (*Poly(ADP-Ribose) Polymerase Family Member 4*) and CRNKL1 (*Crooked Neck Pre-mRNA Splicing Factor 1*). I then cross-referenced the proteins that were expressed at a lower level in the resistant clones, compared with the parental cell line with the candidate ATRi resistance hits from the GW CRISPR screen data and found that ARHGAP21 (*Rho GTPase Activating Protein 21*) and TYK2 (*Tyrosine Kinase 2*) were present in both datasets.

When I compared the cluster containing clones H1, H2, H3, H4 and H6 to the parental cells (**Figure 30**), CDH1 (*E-Cadherin*), GNA (*Guanine nucleotide-binding protein alpha-1 subunit*), JAK1 (*Janus Kinase 1*), NOTCH1 and 2 (*Notch 1 and 2*), SMAD2

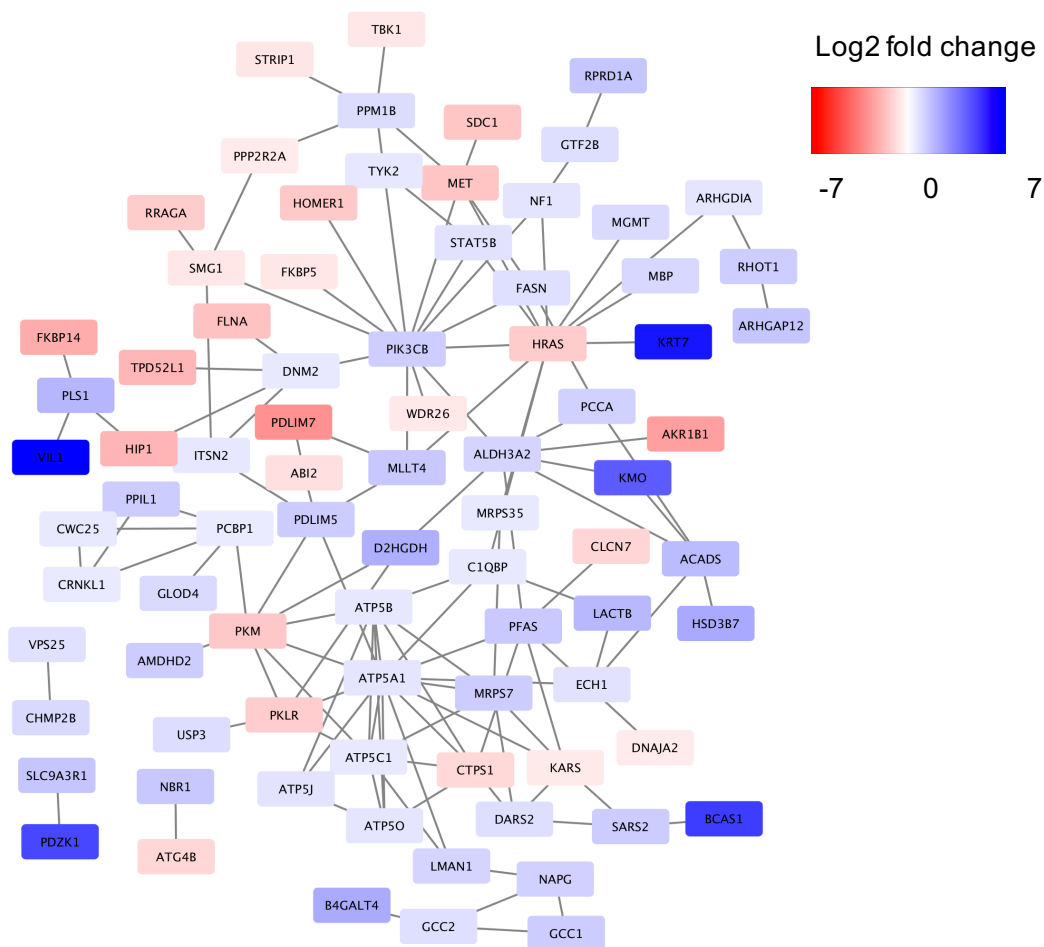
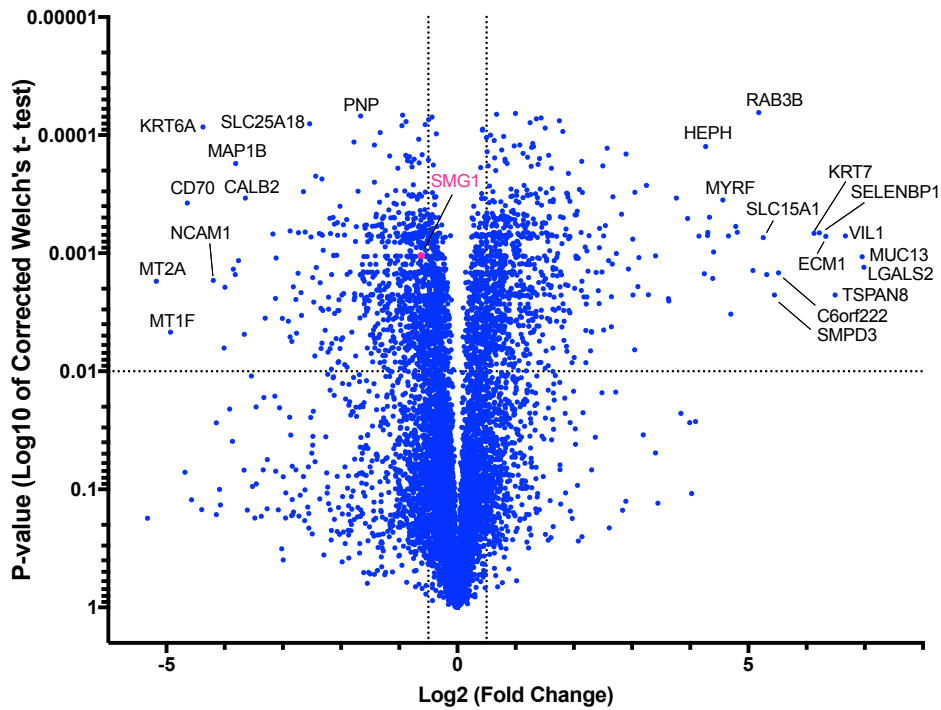


Figure 30. Mass spectrometry transcriptomic data reveals common differentially expressed proteins in H1/H2/H3/H4/H6 YCC6 ATRi resistant clones. A. Volcano plot representing Log₁₀ multiple comparisons corrected Welch's test p-values against the Log₂

fold-change of the differences between the H1/H2/H3/H4/H6 resistant cluster, compared with the parental YCC6 cell line. **B.** Protein interaction map generated by STRING online software showing protein interactions from the differentially up (Red) and downregulated (Blue) genes showed in figures A and B. Only proteins showing at least one interaction are included in the network. Statistical significance means differences in protein expression levels with a FDR corrected Welch's test p-value <0.01 and Log2 fold change differences lower than -0.5 or larger than 0.5. All experiments were performed in two biological replicates.

and 4 (*SMAD Family Member 2 and 4*), KIAA1598 (*Shootin 1*) and MSI2 (*Musashi RNA Binding Protein 2*) were identified as candidates to ATRi resistance-causing proteins. Importantly, SMG1 (*Nonsense Mediated mRNA Decay Associated PI3K Related Kinase*), pivotal in regulating the nonsense-mediated mRNA decay pathway, that controls the degradation of mRNA transcript carrying premature stop codons (Azzalin and Lingner 2006, Azzalin and Lingner 2006, Fernandez, Yamashita et al. 2011, Lee, Pratt et al. 2015), was found to be downregulated in the resistant cell lines when compared with the parental cell line (Welch t-test FDR = 0.0098). Upregulation of SMG1 as a mechanism of ATRi resistance is consistent with the GW CRISPR/Cas9 screen results, where I found SMG8 and SMG9, negative regulators of SMG1 to cause resistance to ATRi when lost (positive selection GW CRISPR-Cas9 mutagenesis screen section, **Figures 20C, 22 and 25**).

Finally, when I compared the H5-M1 cluster with the parental cell line, 40 differentially expressed proteins were identified, including VHL (*Von Hippel-Lindau Tumor Suppressor*), STAT5B (*Signal Transducer And Activator Of Transcription 5B*) and YAP1 (*Yes Associated Protein 1*), previously being related to cancer. Additionally, VIL (*Villin 1*), ANO1 (*Anoctamin 1*), MRAS (*Muscle RAS Oncogene Homolog*), ZADH2 (*Zinc Binding Alcohol Dehydrogenase Domain Containing 2*), RBP7 (*Retinol Binding Protein 7*) and TSFM (*Ts Translation Elongation Factor, Mitochondrial*) were amongst the top deregulated proteins in the resistant clones, compared with the parental cell line (**Figure 31**). No interactions were detected amongst this list of proteins.

The top one-hundred most upregulated and downregulated genes found in the resistant clones, comparing all clones and the two different clusters to the parental cell lines are represented in **Supplementary Figures 1-3**.

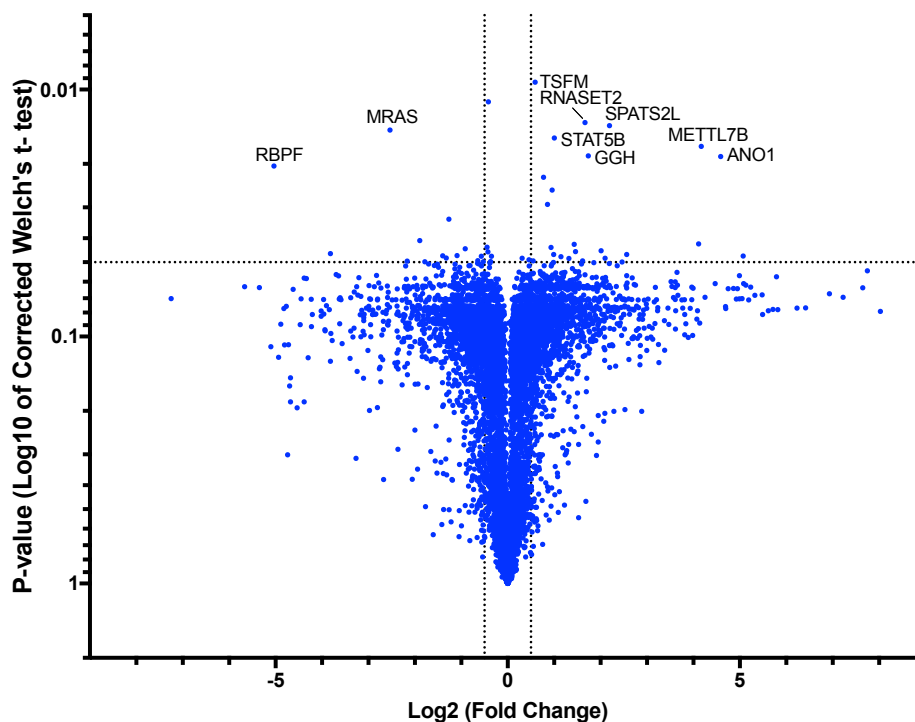


Figure 31. Mass spectrometry transcriptomic data reveals common differentially expressed proteins in H5/M1 YCC6 ATRi resistant clones. A. Volcano plot representing Log₁₀ multiple comparisons corrected Welch's test p-values against the Log₂ fold-change of the differences between the H5/M1 resistant cluster, compared with the parental YCC6 cell line. Statistical significance means differences in protein expression levels with a FDR corrected Welch's test p-value <0.05 and Log₂ fold change differences lower than -0.5 or larger than 0.5. All experiments were performed in two biological replicates. No protein interactions were seen.

Following the fact that SMG1 was one of the proteins found to be upregulated in the ATRi resistant clones, and because this finding correlates with our results from the GW CRISPR screen and the cross-referencing data with Wang *et al.* study, I decided to validate the overexpression of SMG1 and its downstream protein UPF1 in the resistant clones, compared with the parental YCC6 cells. The H2, H3, H4 and M1 resistant clones but not the H2, H5 and H6 showed an increase of both proteins parental cell line (**Figure 32A**). I then wondered if the silencing of SMG1 would be enough to rescue the resistance to ATRi and thus performed a siRNA knockdown experiment in one of the clones expressing higher levels of SMG1 protein, H3. Although SMG1 was not completely silenced (**Figure 32B**), the moderate reduced levels of protein were enough to re-sensitise H3 cells to both, VX970 and AZD6738 ATRi (Two-way ANOVA p-values <0.001), demonstrating that the overexpression of SMG1 mediates ATRi resistance in GC (**Figure 32C and D**).

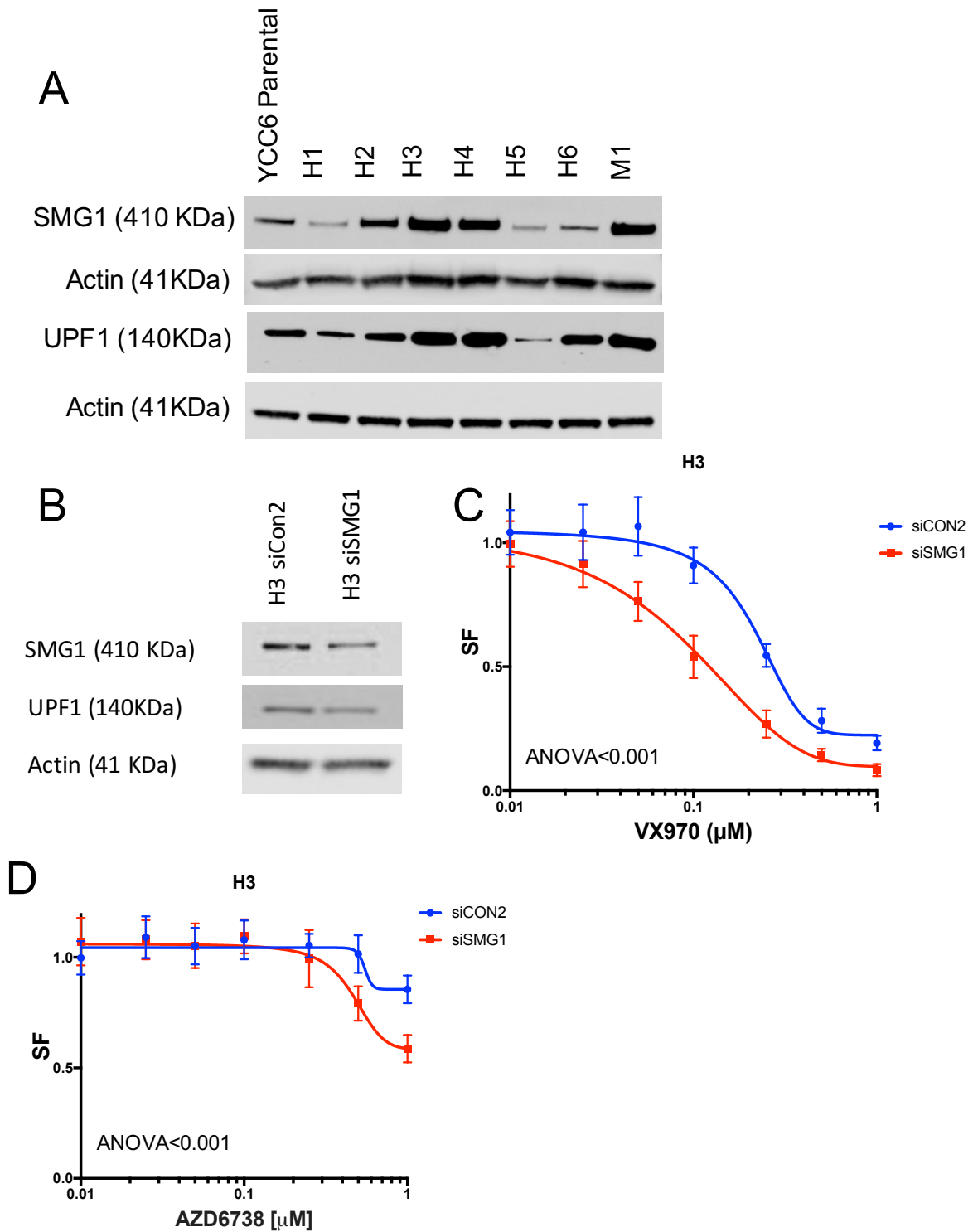


Figure 32. Silencing of SMG1 re-sensitises the resistant clones H3 to VX970. **A.** Western blot showing that colonies H2, H3, H4 and M1 overexpress SMG1 and UPF1, compared with the YCC6 parental cell line. **B.** Western blot showing SMG1 and UPF1 expression in the H3 siRNA knockdown cells, compared the the parental H3 cells. **C and D.** Drug sensitivity curves for VX970 and AZD6738 in the silenced cells from **B**, compared with the parental H3 cells. All two-way ANOVA p-values for both groups were lower than 0.001.

5. Dense Tiling ATR CRISPRx Screen

ATR is a member of the phospho-inositide 3-kinase related kinases family (PIKK), in charge of monitoring the progression of replication forks in S phase, maintaining genomic stability and promoting a complete and accurate replication of the genome by mediating the phosphorylation of a large number of substrates (Casper, Nghiem et al. 2002, Cimprich and Cortez 2008, McNees, Tejera et al. 2010, Flynn and Zou 2011). Structurally, it contains several HEAT (*Huntington, Elongation factor 3, Protein phosphatase 2A, and PI3K TOR1*) repeats in the N-terminal part, that are thought to be involved in protein-protein interactions (like the interaction with its partner ATRIP), as well as in DNA-Protein interactions (Ball, Myers et al. 2005, Chen, Zhao et al. 2007, Rubinson, Gowda et al. 2010), and a C-terminal catalytic kinase domain (PI3K/PI4K), flanked by a FAT (*FRAP, ATM, TRRAP*) and FATC (*FAT-C*) domains, that are known to mediate protein-protein interactions and ATR activation through autophosphorylation and TopBP1 stimulation (Mordes and Cortez 2008, Mordes, Glick et al. 2008).

Traditionally, the genome editing techniques comprising the introduction of DSB at a determined genomic locus, selecting for the cells where the NHEJ error-prone DNA damage repair pathway had allowed the appearance of indels and disruption of the targeted gene (Komor, Badran et al. 2017). Techniques that facilitate targeted gene editing through the use of base editors without causing DSB in the genome have been developed, thanks to the use of base editors. Base editors consist of a hybrid of a cytidine deaminase enzyme and a catalytically inactive Cas9 protein, which binds to a determined locus of interest through its union to a specific guide RNA. When the base editor binds the DNA, a loop structure is formed, that exposes a region of around 5 nucleotides of DNA where the deaminase carries out its function, resulting in the appearance of point mutations (Komor, Kim et al. 2016, Gaudelli, Komor et al. 2017, Kim, Komor et al. 2017).

Following this principal, and to identify regions in the ATR protein that may be important for the development of ATRi resistance, due to either the impairment of ATR function or its role in modulating other DDR downstream effectors, I used a tiling CRISPR library comprising 552 guides designed to result in a dense coverage of

mutations across the entire ATR gene. Thus, I carried out a tiling CRISPRx screen in YCC6 cells that enabled us to mutagenize, select the ATRi resistant cells and sequence them to identify ATRi resistance-conferring mutations. In this experiment, I have used the fourth generation *Staphylococcus aureus* Cas9-derived BE4 (SaBE4-Gam, BE4) cytidine deaminase (Komor, Zhao et al. 2017), and the newly described adenine deaminase ABE7.10 (ABE) in comparison with a regular nCas9, to cause missense mutations in YCC6 cells all along the ATR region, using the pKLV5-U6gRNA5-PGKPuroBFP shRNA library. The YCC6 cells were also modified to constitutively express deadCas9 (dCas9) protein and then transfected with a modified cytidine deaminase, pGH156_MS2-AID-Hygro (AID), combined with the pGH224_sgRNA_2xMS2_Puro library of sgRNA bearing two MS2 hairpin-binding sites allowing specific mutagenesis with limited off-target damage (Hess, Fresard et al. 2016) permitting comparison of orthogonal methods (**Figure 33**). Finally, I used a catalytically inactive MS2-AID Δ Dead as a negative control. After drugging the cells for two weeks with 100nM of VX970, resistant cells were harvested and RNA was extracted and converted to cDNA and prepared for sequencing (**Figure 34**). Briefly, the ATR sequence was amplified and purified in two sequential PCR reactions, were Ion Torrent adaptors were added for further sequencing of a panel of 36 amplicons, representing the whole ATR coding sequence, using the PGM 318 Chip (Ion Torrent).

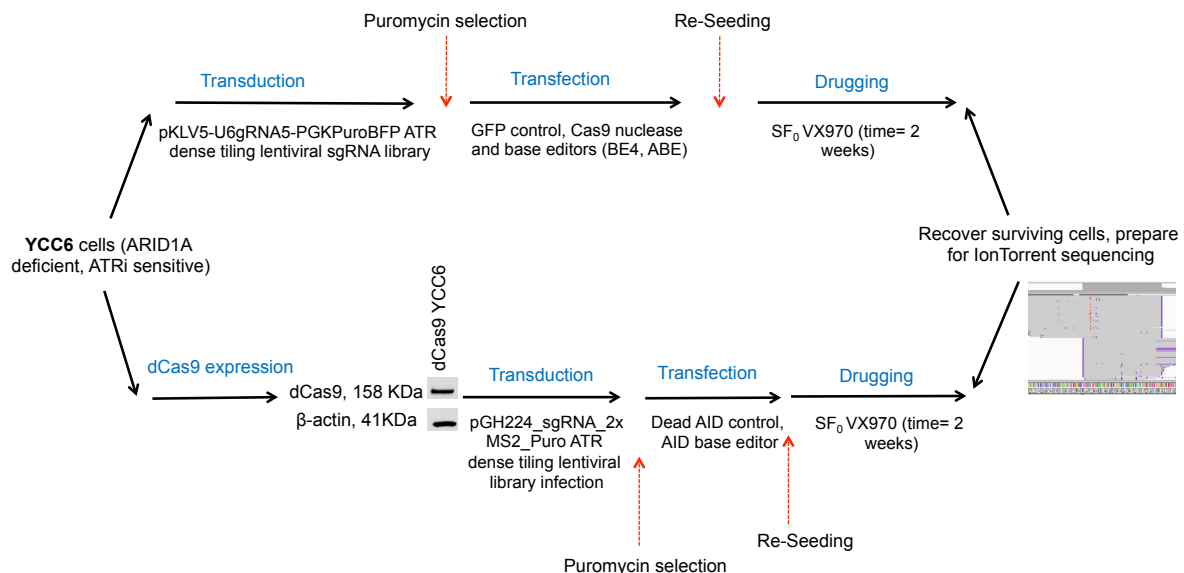


Figure 33. CRISPRx screen workflow. CRISPRx screens were carried out in two parallel arms. First (upper panel), YCC6 cells were transduced with the pKLV5-U6gRNA5-PGKPuroBFP ATR dense tiling lentiviral sgRNA library and selected in puromycin for 5 days. Cells were then transfected with GFP control, Cas9 nuclease or constructs carrying BE4 or ABE base editor sequences. Cells were incubated for 2-3 days before being re-seeded in

10cm plates, at a 50,000 cells/ml concentration, 24 hours' prior VX970 treatment started, at a dose of 100nM. Cells were drugged for two weeks, being fed with fresh drug twice a week. Resistant cells were left to expand for an extra week, and harvested to send for NGS. For the second approach (lower panel), YCC6 cells were transduced with a dCas9 expressing construct and selected in blasticidin. Once selected, they were transduced with the pGH224_sgRNA_2xMS2_Puro sgRNA library, and selected in puromycin. Cells were then transfected with dead AID, as a negative control, or the AID base editor construct, and left incubating for 2-3 days. Drugging and the following steps were the same than in the other arm.

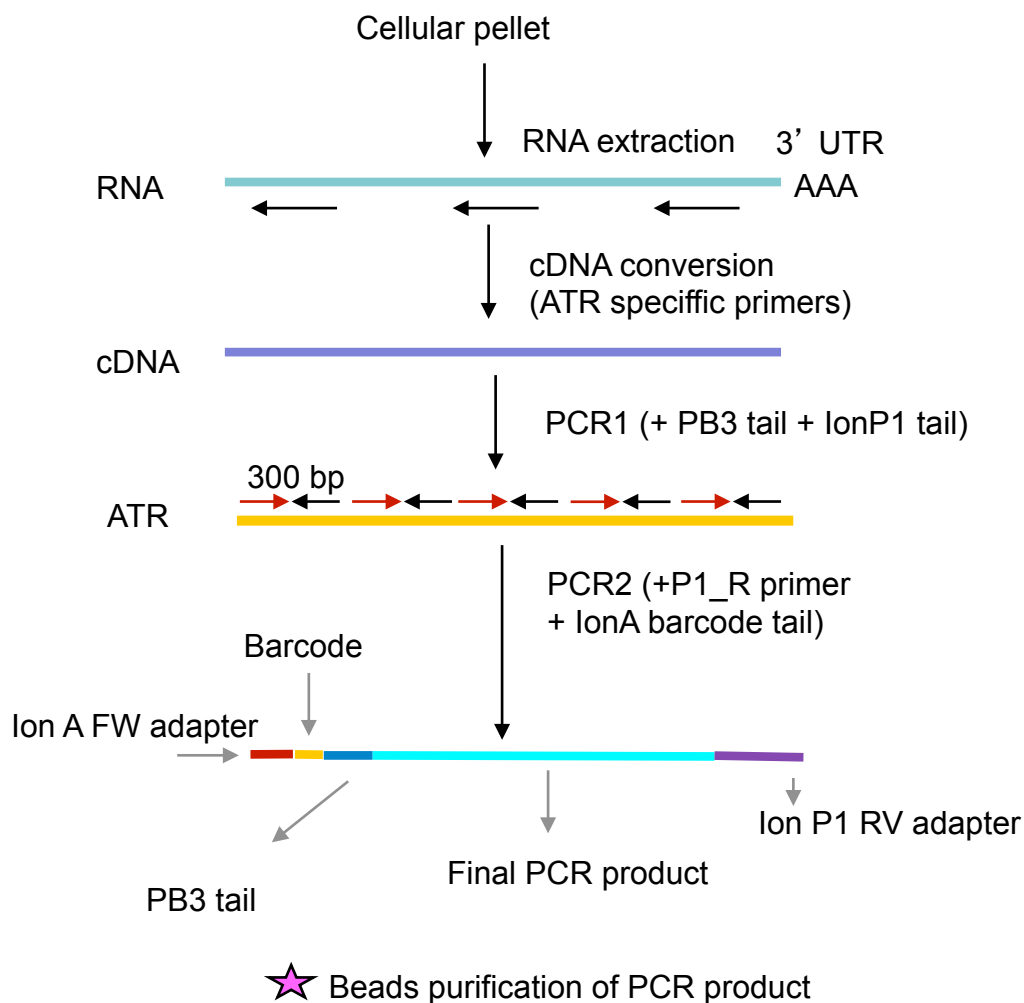


Figure 34. Ion Torrent CRISPRx Sample preparation. RNA was extracted from the resistant cells and was converted to cDNA in three independent reactions, using ATR specific primers, each of them complementary to one third of the protein sequence. The resulting cDNA was used to amplify all ATR sequence in 36 independent reactions, using 36 tiling primer pairs, to generate 250-300 bp amplicons. Primers used for PCR 1 included a PB3 sequence, used as a bridge to add a barcoded IonA sequence in the second PCR, and an Ion Torrent P1 sequence used as reverse primer. All PCR1 reactions were checked on a 2% agarose gel

and mixed to purify DNA. DNA for PCR1 was mixed in one reaction per sample and amplified by PCR2, adding the 5' barcoded tail. Final product was purified and sent for sequencing.

Sequencing coverage was generated with a maximum depth of 50,000, and only sequences that perfectly matched to the barcodes, and with an average quality score greater than Q20 were selected for further analysis. After the alignment of sequencing reads to the version 19 of the human consensus sequence, the sequenced sequences were visualized with IGV tool to direct inspection of mutations. Only mutations that were present in any of the base editor samples, but not present in the negative control arm were selected and localised to the protein structure (**Figure 35A and 35B**). Although I have sequenced the whole resistant population of cells in one reaction, and therefore expect a low frequency of a determined mutation, only mutations that were detected in more than one read were considered for further analysis.

A summary of all mutations detected by NGS is listed in **Table 9**. All base editors proved to be functional and caused point mutations in the targeted sequence. I did not see an association between the type of substitutions and the library or base editor used, although nCas9, BE4 and ABE were responsible for most of the mutations, compared with the more modest role of AID. 54% of the mutations localised in ATR coding sequence were found to cluster in the FAT domain. Two mutations, G2635G and E2419K were found in the catalytic (CAT) or FATC domains, respectively (**Figure 35A and 3B5**), and the remaining mutations affected residues located in the area in between the HEAT repeats (residues 974-977) (32%). Additionally, I detected a cluster of mutations beyond the C-terminal part of ATR coding sequence, which do not directly affect the protein but could have an impact in the mRNA stability and protein expression (not included in the general count, data not shown). T974T, K2025N and D977V mutations were found in more than one sample, caused by both MS2 structure-based AID and the cytidine and adenine deaminases BE4 and ABE, suggesting that these are less likely to be off-target effects specific to one base editor or method and adding robustness to these data.

Table 9. Mutations found in the CRISPRx screen VX970 resistant YCC6 cells.

Base editor	DNA change	Coverage	Number of reads	Protein change
ABE	8027G>A	210	2	G2635G
AID	7377G>A	165	3	E2419K
nCas9	6609A>T	7452	85	I2163L
nCas9	6598T>G	7094	146	V2159G
nCas9	6597G>T	8490	204	V2159F
ABE	6545A>T	77	2	A2141A
ABE	6532A>C	103	2	Q2137P
ABE	6531C>T	102	2	Q2137*
ABE	6522G>A	105	2	A2134T
AID	6404G>C	27	2	W2094C
BE4	6194A>T	1064	10	K2025N
AID	6194A>T	1783	9	K2025N
nCas9	6193A>T	9	8	K2025I
ABE	5603A>G	427	3	R1827S
AID	3071C>T	175	2	D984D
BE4	3052A>T	2113	28	D977V
AID	3052A>T	225	2	D977V
ABE	3052A>T	4223	34	D977V
BE4	3044G>A	2712	29	T974T
AID	3044G>A	278	5	T974T
ABE	3044G>A	5103	37	T974T
nCas9	290A>G	36	3	V56V

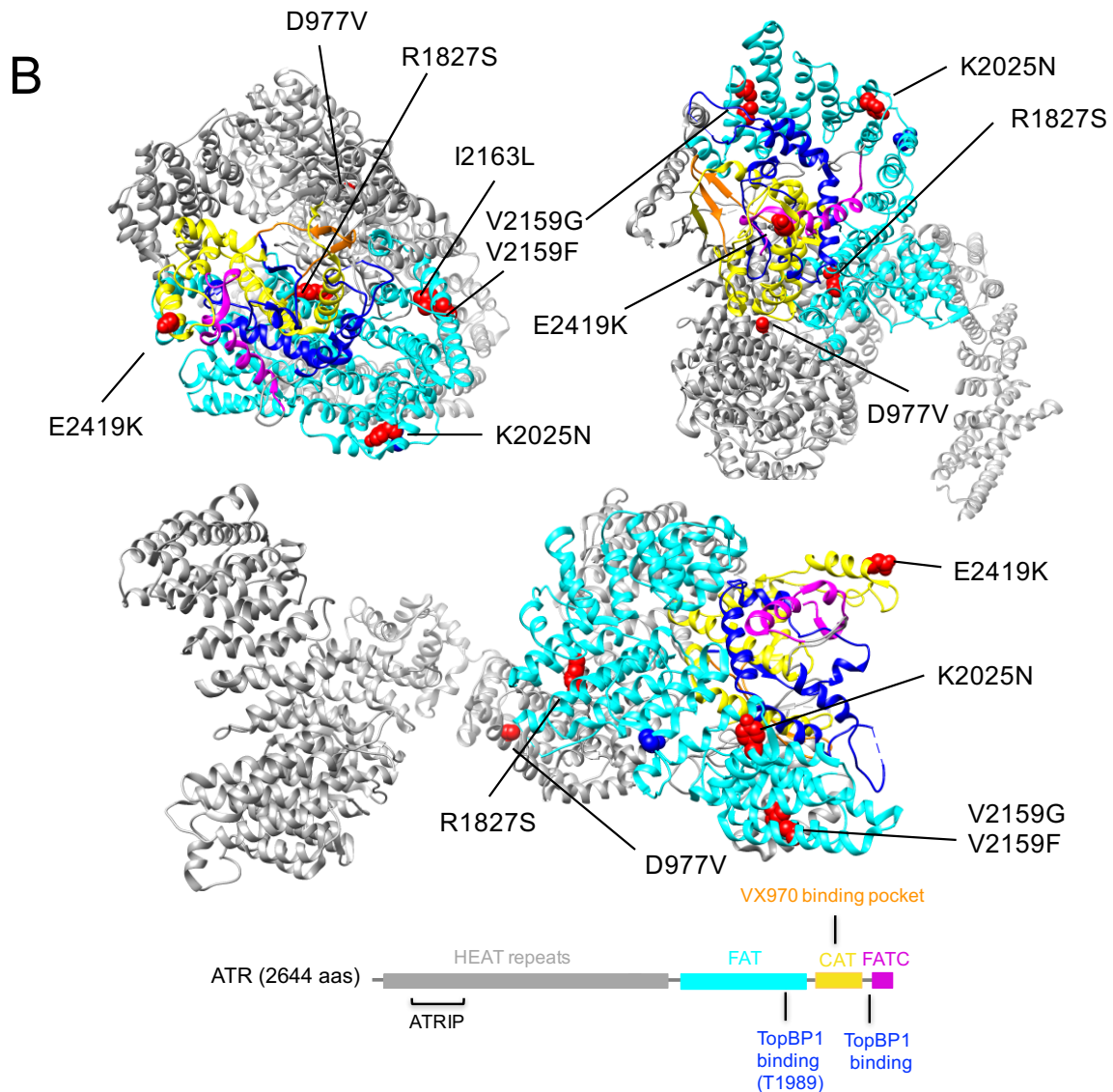
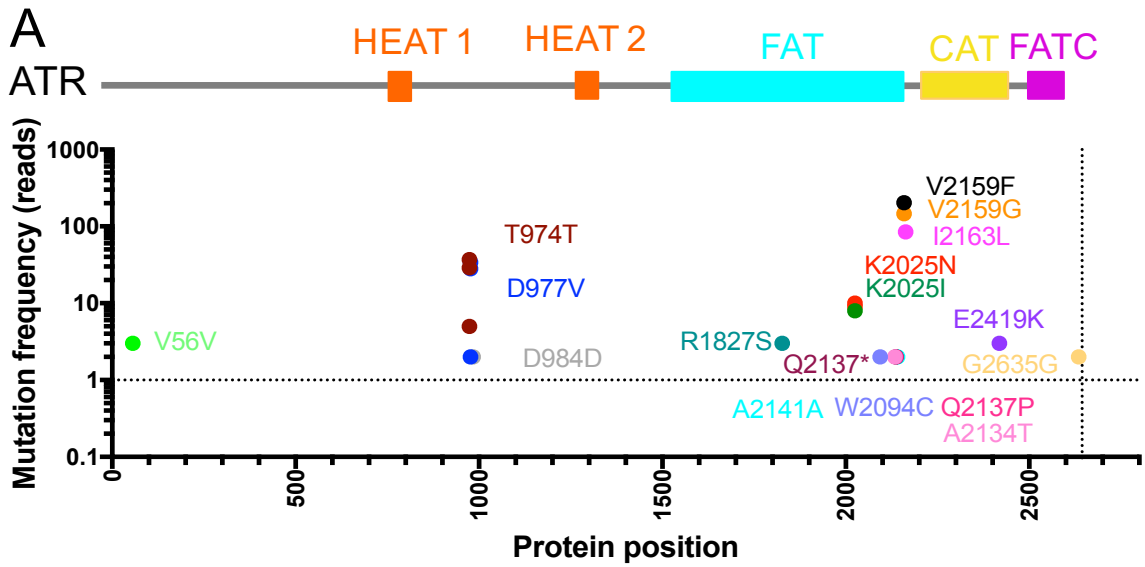


Figure 35. The majority of the ATRi-resistance causing mutations locate in the FAT or catalytic domains. A. Mutational information obtained from Ion Torrent sequencing of ATRi-

resistant cells cDNA revealed a cluster of mutations in the FAT, CAT (PI3K, PI4K catalytic) and FATC domains of ATR, and in a region located in between the two HEAT repeats. **B.** Location of the mutations from figure A associated with ATRi resistance on a model of the ATR protein structure. Mutations are represented in red. TopBP1 binding domain represented in blue, according to Mordes *et al.* (Mordes, Glick *et al.* 2008) and Liu *et al.* (Liu, Shiotani *et al.* 2011). VX970 binding pocket in the catalytic domain is represented in orange, according to Rao *et al.* (Rao, Liu *et al.* 2018).

Discussion

Rationale of this thesis

One of the current strategies in the understanding of cancer consists in the identification of driver DNA mutations or molecular mechanisms that contribute to the carcinogenic process. The main aim of this approach is to improve clinical practice, moving towards personalised medicine where a deeper understanding of the molecular profile of each patient leads to the appropriate selection of targeted therapies, that exploit the genetic vulnerabilities found within each tumour.

Despite the recent advances in this field, including a comprehensive knowledge of the genome, only a small number of genetic targets are validated as predictive biomarkers to select for therapy, or to stratify patients into different treatment arms within the context of clinical trials. This is well illustrated in GC, where there is a lack of robust molecular biomarkers and limited treatment options, making it the third leading cause of cancer-related deaths worldwide. Therefore, the identification of robust synthetic lethal (SL) targets in GC, which can be exploited therapeutically, represents an urgent need.

Summary of the work presented in this thesis

1. *ARID1A* and *ATR* are synthetically lethal *in vitro*

Alterations in the SWI/SNF complex are very common in cancer (Reisman, Glaros et al. 2009, Kadoch and Crabtree 2015), with more than 20% of human cancers bearing mutations in at least one subunit of the complex (Kadoch, Hargreaves et al. 2013, Shain and Pollack 2013). From all subunits in the SWI/SNF complex, *ARID1A* is the SWI/SNF subunit gene that is most frequently mutated in cancer, maintaining the 20% rate of mutations in the general cancer population (Jones, Wang et al. 2010, Jones, Li et al. 2012, Wu, Wang et al. 2014) including GC, where it results in a loss of protein expression in most cases (Wang, Kan et al. 2011, Jones, Li et al. 2012, Zang, Cutcutache et al. 2012). Despite the frequency and possible functional implications of *ARID1A* loss in GC, it is currently not being used as a biomarker, nor as a therapeutic target, and a deep understanding of the role of *ARID1A* in carcinogenesis and its

potentially SL with other genes, that can be therapeutically targeted, is required for maximal clinical benefit.

In the first part of my thesis, I describe the characterisation of a panel of seven gastric tumour cell lines, plus the *ARID1A* isogenic HCT 116 colorectal tumour cell line, in terms of exome sequencing and *ARID1A* status determination (at a DNA, RNA and protein level). I have additionally tested their response to a collection of small molecule inhibitors, that had previously been reported to be preferentially sensitive in *ARID1A* deficient cell lines of other histologies (Bitler, Aird et al. 2015, Shen, Peng et al. 2015, Williamson, Miller et al. 2016, Bitler, Wu et al. 2017, Jones, Fleuren et al. 2017). These included ATRi (AZD6738 and VX970), PARPi (olaparib and talazoparib), PI3K pathway inhibitors (BKM120 and MK2206), HDAC6 inhibitors (ACY1215) and EZH2 inhibitors (GSK126), and drug combinations including ATRi plus PARPi; and ATRi plus PI3Ki. I have shown how *ARID1A* deficient cell lines, especially those carrying large deletions or that predict for early protein frameshift mutations with complete loss of protein function (YCC6, SNU 5 and HCT 116 *ARID1A* -/-), show exquisite sensitivity to ATRi, compared with those with the models expressing *ARID1A* (SNU 638, AGS, NCI N87 and HCT 116 WT). In the case of the SNU 1 cell line, which has shown to have complete *ARID1A* loss of expression due to two frameshift mutations detected by exome sequencing, I only saw a moderate ATRi response. This could be explained by a residual expression of *ARID1A* protein, undetectable by WB. Alternatively, it is possible that *ARID1A* is not the only ATRi sensitising factor in these *ARID1A* deficient cell lines, thus not being a completely penetrant SL in GC. Further research using larger panels of GC cell lines and those of other histologies, that express different levels of *ARID1A* will be necessary to better describe the implications of *ARID1A* status in ATRi response.

When I tested PARPi in our cell lines, I could only see a differential sensitivity in the HCT 116 isogenic cells, where the *ARID1A* -/- cell line was more sensitive compared with the *ARID1A* WT cell line. This difference was not detected in the panel of GC cell lines, showing that the *ARID1A*-PARP SL described by Shen and colleagues is not extensive to our GC models (Shen, Peng et al. 2015).

Despite the promising results that ATRi have shown as monotherapy, they will more likely be used in combination treatment with other drugs that exploit its mechanism of action inducing replication stress and genomic instability. Combinations with other

drugs that can synergise in the induction of DNA damage, are more likely to increase the effect, thereby avoiding the development of resistance. This approach has already been used in several cancers combining ATRi with other DNA damaging agents, including a number of intra strand cross-linking inducing agents like cisplatin, carboplatin or mitomycin C (Reaper, Griffiths et al. 2011, Huntoon, Flatten et al. 2013, Hall, Newsome et al. 2014, Mohni, Thompson et al. 2015, Vendetti, Lau et al. 2015, Li, Yang et al. 2016, Liu, Ge et al. 2017, Min, Im et al. 2017), nucleoside analogues like gemcitabine (Hall, Newsome et al. 2014, Ma, Li et al. 2017) and PARPi (Peasland, Wang et al. 2011, Huehls, Wagner et al. 2012, Ogiwara, Ui et al. 2013, Abu-Sanad, Wang et al. 2015, Mohni, Thompson et al. 2015, Kim, George et al. 2017), amongst others. Taking this into consideration, I set out to test the combination of ATRi with PARPi. Apart from the potential synergy of this drug combination in the treatment of DDR deficient cancers, ATR inhibition has been shown to overcome resistance to PARPi in patient-derived cell lines (Yazinski, Comaills et al. 2017), a promising therapeutic strategy that is being investigated in several clinical trials (NCT03330847, NCT03682289, NCT03462342, NCT03428607, NCT02264678, NCT02576444 and NCT02723864). In our GC models, cell growth inhibition was observed in both, ARID1A deficient and proficient cell lines when exposed to the combination of ATRi and PARPi, although a greater effect was seen in the ARID1A deficient ones.

Since loss of ARID1A expression has been suggested to be predictive for the overactivation of PI3K pathway as a compensatory effect, and this could result in the sensitisation of tumour cells to PI3Ki (Samartzis, Gutsche et al. 2014, Zhang, Yan et al. 2016, Lee, Yu et al. 2017), I hypothesised that the combination with PI3Ki could be synergistic in our ARID1A deficient and proficient models.

My data from PI3Ki monotherapy only showed ARID1A-associated vulnerability in the HCT 116 isogenic model and not in our GC panel of cell lines. However, the sensitivity to ATRi and PI3Ki combinations was more evident in selected ARID1A deficient cell lines such as YCC6, SNU 5 and SNU 1 than in the ARID1A WT cell lines, supporting the rationale for testing ATRi and PI3Ki combinations in an ARID1A deficient context

In contrast to what Bitler and colleagues have published in several studies using ovarian cancer models (Bitler, Aird et al. 2015, Bitler, Wu et al. 2017), HDAC6 and EZH2 inhibitors did not show any ARID1A-associated sensitivity in our panel of cell

lines. This could be due to a histology specific effect of those inhibitors, or could also be related to experimental conditions as Bitler *et al.* prove these effects using 3D long-term culture experiments, whilst my experiments have been performed in a 2D short-term exposure format (Bitler, Aird *et al.* 2015, Bitler, Wu *et al.* 2017).

From all the inhibitors I tested in these thesis, I observed that ATRi presented the largest ARID1A associated effect. In order to validate this effect, and to avoid the potential confounding factors of comparing cell lines with different genetic backgrounds, I generated a GC isogenic model using the CRISPR/Cas9 technology. Despite the extensive screening and the several CRISPR/Cas9 mutational rounds undertaken in the SNU 484 cell line, and in AGS cell line (results not shown for AGS), I was not able to generate *ARID1A* homozygously mutated clones, as the cells seem to be addicted to ARID1A expression and died when ARID1A expression was completely abrogated. However, because ARID1A levels are regulated post-transcriptionally (Wiegand, Shah *et al.* 2010, Wu, Wang *et al.* 2014, Kartha, Shen *et al.* 2016, Roumeliotis, Williams *et al.* 2017), and a haploinsufficiency phenomenon (the loss of function phenotype is present even with a partial loss of the functional alleles) seems to operate in oncologic patients within the ARID1A deficiency context (Wiegand, Shah *et al.* 2010, Wu, Wang *et al.* 2014, Kartha, Shen *et al.* 2016), I think the SNU 484 ARID1A isogenic cell line is still a valid model to represent ARID1A deficiency and proficiency in GC (Wu and Roberts 2013, Wu, Wang *et al.* 2014). Finally, orthogonal validations carried out through the performance of an ARID1A-siRNA transient silencing transfection experiment confirmed our observations, showing that the silencing of *ARID1A* sensitises the cells to ATRi.

In conclusion, sensitivity to ATR inhibition has been observed in ARID1A deficient GC tumour cells and *ARID1A* isogenic models, which supports the previously identified hypothesis of ATR as a synthetically lethal partner to ARID1A deficiency. It is likely that this represents a partial penetrant effect where other proteins are involved in the sensitisation of the tumour cells to the inhibition of a pivotal protein in DDR cascade, such as ATR. However, this will need to be clarified by increasing the number of models of study and undertaking new mechanistic approaches which will inform us about the role of ARID1A in ATRi response.

2. *In vivo* assessment of ATR inhibitor efficacy in gastric cancer Patient-Derived Xenografts.

For the *in vivo* experiments, a different ATRi has been used for this experiment (M4344). Despite this, our data is consistent in between experiments, as we are looking for an ATRi class effect, that is not private to any specific inhibitor. This was the rationale of performing all *in vitro* experiments using two parallel ATRi, VX970 and AZD6738. In addition, M4344 is an oral compound that has previously been observed in other tumour models to have superior *in vivo* efficacy than VX970 (now called M6620, which is not available in oral gavage), and it is currently being assessed in phase I clinical trials in monotherapy and in combination with PARPi, what makes it more likely to be used for the new starting clinical trials.

The results presented through the use of *in vitro* gastric tumour cell lines showed a preferential effect for ARID1A in sensitising the cells to VX970 and AZD6738 ATRi. With the aim of testing this SL *in vivo*, I selected seven PDX models, which represent ARID1A deficiency and proficiency within the context of GC. Taking into consideration that the animals were only treated over a short time due to weight loss, I observed significant tumour inhibition in all four ARID1A deficient PDX models (GC1-4), that were administered with M4344, compared with vehicle controls in a dose-dependent manner. Moreover, the addition of the PARPi, talazoparib, enhanced this effect in two of the four ARID1A deficient PDX models, compared with the vehicle treated controls (all p-values <0.0001). In two out of the three ARID1A proficient tumours (GC5 and GC6), the effect seen with ATRi monotherapy or combination treatment was small. However, the remaining ARID1A proficient model, GC7, was highly sensitive to ATR inhibition, despite also being treated for a short time, strongly suggesting that *ARID1A* is not the only determinant of ATRi sensitivity. In order to identify candidate biomarkers of sensitivity, I will focus on molecularly characterising the PDX tumours derived from the GC7 model. Additionally, I will also molecularly characterise the remaining resistant tumours propagated, and compare to vehicle controls from the other PDX models, to identify determinants to ATRi resistance in GC.

Considering our *in vitro* and *in vivo* data together, I have demonstrated a sensitisation of ARID1A deficient GC models to small molecule ATR inhibition. This has been previously reported in ovarian models, where defects in ARID1A sensitised tumour

cells to ATRi, both *in vivo* and *in vitro*, by triggering premature mitotic entry, genomic instability and apoptosis (Williamson, Miller et al. 2016). Although the effects described in our gastric tumour models were less profound than what described by Williamson *et. al*, which might be due to the involvement of other genetic factors such as MSI, that could contribute to the observed sensitivity, both studies suggest that *ATR* is a synthetically lethal partner to *ARID1A*. Thus, I believe it should be considered as a biomarker in an ATRi context, and could represent a promising therapeutic strategy, given that there is a high frequency of *ARID1A* mutations across all cancers and the promising results seen in clinical trials utilising DDR inhibitors. Further study of the collected resistant PDX tumours, along with additional mechanistic approaches is required to determine the exact role of *ARIDA* in the ATRi response and its implication in DDR.

3. ATR inhibitor resistance mechanisms in gastric cancer

Genomic instability constitutes one of the hallmarks of cancer. Genomic instability is characteristic of most of the tumours, and this seems to be related with the high proliferative rate of cancer cells, together with the inability of the DDR machinery to efficiently repair DNA damage (Lindahl and Barnes 2000, Hoeijmakers 2009, Lord and Ashworth 2012). Although genomic instability remains one of the main causes of cancer, it can also be exploited as a vulnerability in cancer cells that can be therapeutically targeted. Traditionally, this strategy has been exploited by the use of chemotherapeutical agents, or radiotherapy, which still remain the standard of care in many cancers, where no targeted therapies are available. In the last few decades, several drugs targeting DDR proteins have been developed. One of the most successful examples of this approach is the use of PARPi for the treatment of *BRCA1/BRCA2*-deficient tumours, which is currently being exploited for the treatment of several types of cancer (Farmer, McCabe et al. 2005, Lord and Ashworth 2012, Lord and Ashworth 2017, Ashworth and Lord 2018, Ferrara, Simionato et al. 2018). Following the example of PARPi, ATRi have also been tested in several clinical trials, and they seem to be a promising therapy for cancers with DDR defects due to the central role of ATR in regulating DDR processes and the development of specific and potent ATRi (Sundar, Brown et al. 2017).

As in other monotherapies, clinical resistance to DDR inhibitors is inevitable. An

example of this is the appearance of resistance-causing reversion mutations in BRCA1/2 deficient cancers in the context of PARPi-BRCA1/2 SL (Edwards, Brough et al. 2008, Barber, Sandhu et al. 2013, Weigelt, Comino-Mendez et al. 2017). To the date, only two published studies have informed about ATRi resistance-causing genes. The first study demonstrated how CDC25A deficient mouse embryonic stem cells were able to resist high doses of ATRi due to their failure to prematurely enter mitosis in response to the drug-induced DNA damage (Ruiz, Mayor-Ruiz et al. 2016). The other manuscript published data validating the hypothesis of *CDC25A* as an ATRi-resistance causing gene in a CRISPR/Cas9 screen undertaken in three different tumour cell lines, along with *CDC25B*, *cyclin-dependant kinase 2* (*CDK2*), *Kelch Like ECH Associated Protein 1* (*KEAP1*) and several genes involved in the cyclin C complex (Chen, Alexe et al. 2018).

3.1. Positive selection genome-wide CRISPR/Cas9 mutagenesis screen reveals ATR inhibitor resistance-mediating genes

In order to pinpoint the potential mechanisms of ATRi resistance, I have undertaken a positive selection GW CRISPR/Cas9 mutagenesis screen that has revealed a list of candidate genes causing ATRi resistance when gene function is lost. I have validated many of the top hits found to be relevant in the initial GW screen by undertaking an arrayed mini-CRISPR/Cas9 screen. This included the cell cycle regulators *CDC25B* and *FOXM1*, the apoptosis-related gene *CARD10*, the E3 ubiquitin ligase *HUWE1*, the nuclear ribonucleoprotein *HNRNPF*, the nonsense mediated decay pathway regulators *SMG8* and *SMG9*, and genes coding for proteins involved in the Interferon/JAK/STAT pathway, such as *STAT1*, *STAT2* and *IRF9*, amongst others. Given that *HUWE1* and *IRF9* were validated from my screen, I decided to study the role of these genes in ATRi resistance, through the use of these Isogenic *HUWE1*^{-/-}/*+/+* and *IRF9*^{-/-}/*+/+* models, picked from the GW screen.

I subsequently demonstrated that loss of function mutations in *HUWE1* induced resistance to ATR inhibition (VX970 and AZD6738) in YCC6 gastric tumour cells. Cell cycle experiments, using these isogenic models have revealed a decrease of the number of cells in inactive S phase, an indicator of S phase arrest, after inducing DNA damage by ATRi treatment in *HUWE1*^{-/-} cells, in comparison to the WT parental cells. Which seems to indicate an enhancer ability of *HUWE1*^{-/-} cells to repair DNA damage

in a more efficient way in response to ATRi. *HUWE1* is an E3 ubiquitin ligase part of the HECT (*homologous to E6-associated protein C-terminus*) family in charge of the ubiquitination and degradation of a high number of substrates, including p53 (Chen, Kon et al. 2005), MCL-1 (Zhong, Gao et al. 2005), c-MYC/n-MYC (Zhao, Heng et al. 2008, Myant, Cammareri et al. 2017), CDC6 (Hall, Kow et al. 2007), TOPBP1 (Herold, Hock et al. 2008), POL β /Y (Parsons, Tait et al. 2009, Markkanen, van Loon et al. 2012) and BRCA1 (Wang, Lu et al. 2014). Apart from its interaction with BRCA1 and its known role in base excision repair (Parsons, Tait et al. 2009, Markkanen, van Loon et al. 2012), *HUWE1* has also been described to participate in DNA damage response, by its direct association with replication forks, mediated by PCNA, and the activation of H2AX, a key recruiter of DDR proteins (Choe, Nicolae et al. 2016). Conversely, both oncogenic and tumour suppressor roles have been attributed to *HUWE1*, and both activating and silencing mutations have been found in different cancer types (Adhikary, Marinoni et al. 2005, Hall, Kow et al. 2007, Bernassola, Karin et al. 2008, Zhao, Heng et al. 2008, Zhao, D'Arca et al. 2009, Wang, Lu et al. 2014, Wang, Lu et al. 2014, Choe, Nicolae et al. 2016, Myant, Cammareri et al. 2017, Yang, Sun et al. 2017, Yang, Cheng et al. 2018), demonstrating that *HUWE1* plays a wide number of roles through the modulation of a large number of substrates. Loss of *HUWE1*, has been shown to lead to accelerated proliferation, repression of apoptosis and tumourigenesis through the increase of levels of MYC (Myant, Cammareri et al. 2017), and MCL-1 (Zhong, Gao et al. 2005), which results in increased proliferation, a failure of cells to enter apoptosis and thus, the ability to resist death after the ATRi treatment. Data published by other groups have shown that *HUWE1* depleted cells demonstrate increased resistance to several DNA damaging agents, mediated by an increase of BRCA1 levels, and a decrease of p53 and MCL-1 roles in DDR, cell cycle regulation and apoptosis, leading to genomic instability and tumourigenesis in tumour cells (Wang, Lu et al. 2014).

Contrary to what our data suggests, and to the previously described studies, Choe *et al.* reported a model where loss of *HUWE1* expression was able to confer sensitivity to replication fork stalling agents such as hydroxyurea (HU) and UV light. They showed a reduction in the progression of replication forks by DNA fibre assays and an increase in the inactive S phase population when *HUWE1* was lost in BrdU/PI stained cell cycle experiments. Considering this data, I hypothesise this conflicting results might be due

the ability HUWE1 to modulate different DDR proteins in a context-dependent manner, influencing the pathway of choice in the DDR (Wang, Lu et al. 2014). Furthermore, the effect of ATR inhibition in cancer cells could have different consequences than HU treatment of UV light induced mutagenesis. Going forward, I will test if the HUWE1 deficient models are also resistant to other DNA damaging agents, including DSB causing agents such as carboplatin. In addition, I will also assess whether HUWE1 depletion increases genomic instability in the YCC6 cells through DNA fibre assay experiments and the determination of γ -H2AX levels, to better understand the effect of losing HUWE1 function in terms of DNA repair dynamics. Due to the wide range of *HUWE1* substrates, further evaluation of protein levels modulation by western blot or mass spectrometry will be useful to determine which pathways are involved in the ATRi induced resistance in our models. Finally, given that YCC6 cell line is an ARID1A deficient cell line, and ARID1A has also been related to DNA damage processes (Shen, Peng et al. 2015, Williamson, Miller et al. 2016), it would be important to test this effect in other GC ARID1A deficient and proficient models, to further determine the role of *ARID1A* in this process.

Similar to what I saw in the HUWE1 deficient cells, IRF9 deficient YCC6 cells followed the same trend in the cell cycle experiments, although the effect was less profound. IRF9 is the DNA binding domain of the IFN-stimulated gene factor 3 (ISGF3) complex, which is also constituted by the STAT1/2 heterodimer, downstream of the type I interferon pathway (IFN), in charge of mediating major innate immune responses to infectious agents through the modulation of the interferon stimulated genes (ISGs) (Platanias 2005). Although interferon regulatory factors (IRFs) have been associated with other signalling pathways, different from its well-known role in the immune response processes, the implications of *IRF9* in tumorigenesis remain unclear, and its possible association to DDR has not been studied yet. Nevertheless, some other IRF family members have previously been related to the tumorigenic processes. Studies carried out in human breast cancer tissues, revealed a downregulation of IRF5, which was associated with an increased metastatic potential of the cancer cells (Bi, Hameed et al. 2011, Pimenta and Barnes 2013). In addition, some other authors have defined a role of loss of IRF1 in the development of human leukaemia, oesophageal and GC, being considered as a tumour suppressor gene (Boultonwood, Fidler et al. 1993, Willman, Sever et al. 1993, Ogasawara, Tamura et al. 1996,

Tamura, Ogasawara et al. 1996, Nozawa, Oda et al. 1998). Likewise, the other partners of IRF9 in the ISGF3 complex, STAT1 and STAT2 seem to have tumour suppressive functions and have been found to show reduced expression in melanoma and chronic myeloid leukaemia (Wong, Krauer et al. 1997, Landolfo, Guarini et al. 2000). What is interesting is that I have found all three genes (*IRF9*, *STAT1* and *STAT2*) as top ATR resistance candidates in our screen, which suggests a tumour suppressor role that can be extended to the whole ISGF3 complex. Nevertheless, the fact that our experiments have been done *in vitro*, in a model lacking an immune microenvironment, makes the interpretation of this data more complex, as there is a possibility for these results to be triggered by the lentiviral infection of the cells, part of the protocol of the CRISPR/Cas9 screen. Although we cannot entirely exclude the possibility of off target effects caused by the lentiviral infectious process, this is not likely to be the case as I have found dysregulation of this pathway in the YCC6 ATRi resistant clones which have not been infected with lentivirus, suggesting that the proposed resistance mechanism is real. Moreover, other studies have demonstrated IRF9 to be implicated in resistance to antimicrotubule agents' and in the regulation of IL6 and PD-L1, both related with the carcinogenic process, using cell lines as a model (Luker, Pica et al. 2001, Morimoto, Kishida et al. 2018, Nan, Wang et al. 2018). Despite of this, it would be interesting to validate these results using *in vivo* models with a competent immune system, as well as undertaking further experiments that can inform us about the role of IRF9, STAT1/2 in the DDR response, through the modulation of its target genes (ISGs). Finally, an abstract presented in ESMO 2018 (*Annals of Oncology*, Volume 29, Issue suppl_8, 1 October 2018, mdy303.019), Dillon et al. reported an IFN-mediated response in *in vivo* cancer models when treated with a combination of the ATRi, AZD6738 and radiotherapy, that caused an increase in the number of several immune cell types. Considering this, it is possible that within the context of ATR inhibition, the loss of IRF9 or other factors involved in the IFN pathway could impair the recruitment of immune cells, favouring resistance. Further *in vivo* experiments will be necessary to evaluate this hypothesis in GC.

The use of high-throughput genetic CRISPR/Cas9 screens has allowed us to identify potential candidate genes that are relevant to the acquired resistance to ATRi. Because this screen has been performed on a GW scale, I have defined a long list of genes that are potential candidates implicated in this process. One challenge of

working with big data is how to prioritise the results, as well as the discrimination of the positives from the false positives. This makes, the use of validation experiments in several orthogonal methodologies and models absolutely necessary to select the true candidates and validate their implication in the genetic pathway. At the same time that I performed the CRISPR screen in the YCC6 GC cell line, I also carried out a parallel screen in the OCCC TOV21G. In this thesis, I have focused on the YCC6 screen, as I am principally interested in mechanisms of resistance arising in GC. Nevertheless, I have also used the results from the TOV21G screen to cross-reference the data from both screens, to give robustness to the data, to help us narrow the list of top candidate genes for further following up, and to identify mechanisms that are common to other models and not private to the GC models used in this thesis. Additionally, a recent study published data from three other cancer cell line models revealing genetic determinants of response to ATRi in the kidney cancer cell line 293A, the colorectal cancer cell line HCT 116 and the breast epithelial cell line MCF10A (Wang, Wang et al. 2018). Despite of the fact the authors used a different ATRi in their study (AZD6738), I considered that it would be informative to annotate the genes that remain significant independently of the ATRi used or the histology of the models. Analysing this combined set of data has allowed me to 1) generate a list of ATRi resistant-causing relevant genes across cancer and ATRi 2) narrow down the list of genes I want to focus my attention in the next steps of the project. This analysis has shown that *CDC25B* is the gene with a largest effect in causing ATRi resistance as, it is a candidate resistance gene present in all 5 cell lines analysed. *CDC25B* is a member of the *CDC25* family of phosphatases that can also be found in the *CDC25C* and *CDC25A* isoforms in humans, and catalyses the dephosphorylation and activation of the cyclin dependent kinases (CDKs) required for mitotic entry and cell cycle progression in cells (Sohn, Kristjansdottir et al. 2004). While *CDC25A* has been linked to the G1/S checkpoint, the three isoforms are known to have a pivotal role in G2/M transition and control mitosis by the modulation of cell cycle regulatory proteins as CDK1/2 and CDC2 (Boutros, Lobjois et al. 2007, Aressy and Ducommun 2008). *CDC25A* has been identified as a determinant of resistance to ATR inhibition in murine embryonic stem cell based CRISPR/Cas9 positive selection mutagenesis screen. This is described to occur through the cell's failure to enter mitosis prematurely in response to the drug, as *CDC25A* is a key mediator of apoptosis, after DNA damage (Ruiz, Mayor-Ruiz et al. 2016). In the latter study, Ruiz *et al.* investigated the possibility for

CDC25B to play similar roles to *CDC25A* in ATRi resistance, finding no clear effect of ATRi resistance in *CDC25B* deficient cells. Moreover, ATR inhibition did not increase *CDC25B* expression, suggesting a different function to *CDC25A* in mediating the DNA damage cascade in those models. In our initial screen as well as in the validation data, I detected *CDC25A* to be a determinant of ATRi resistance, although the effect seems to be much less profound than the one observed for *CDC25B*. It is possible that these differences are due to a model-specific features and that the activation of either *CDC25A* or B depends on the genetic context of each cell line. Furthermore, our model is ARID1A deficient, which is a protein implicated in the DDR, and described be recruited to DSBs through its interaction with ATR, facilitating DSB end processing to generate RPA-coated ssDNA, and sustaining ATR activity in response to DNA damage (Shen, Peng et al. 2015). As all the components of the CDC25 family are directly regulated by ATR and its downstream effectors, it is possible that ATR influences the expression CDC25s to regulate mitosis. As discussed above, a recent study has described some ATRi resistance-conferring genes including both *CDC25A* and *CDC25B* in three different cell lines (HCT 116, MCF10A and 293A). Although none of these cell lines are from GC histology, nor ARID1A deficient, this data strongly supports a model where both isoforms are implicated in ATRi response and resistance. The role *CDC25C* is less clear; and there is no available data that associates its loss to ATRi resistance mechanisms.

Going forward, it would be informative to evaluate whether the levels of YH2AX, a marker of genomic instability, or the decrease of premature mitotic entry occurs in the absence of *CDC25B* in our models, and, if the use of WEE1 inhibitors (WEE1i), can re-sensitise our cells to ATRi through the induction of the pro-mitotic factor CDK1, as described in *CDC25A* null models. This would be the rational for combining ATRi and WEE1i in the clinic, with the aim of avoiding drug-resistance. Related to this, I also found FOXM1 loss to cause ATRi resistance from the YCC6 GW CRISPR screen. Recent publications have defined FOXM1 as a direct regulator of mitosis, controlled by the ATR-CHK1-CDC25 axis (Saldivar, Hamperl et al. 2018). In the model Saldivar *et al.* propose, an ETAA1-DNA damage mediated activation of ATR causes the phosphorylation of CHK1, which inhibits CDC25 proteins, which are then not able to activate CDK1 and subsequently FOXM1, controlling S/G2 transition and mitosis, to ensure the correct replication of DNA before the cell divides. In the context of ATRi, cells undergo accelerated mitosis and this is associated with high levels of

phosphorylated FOXM1 in S phase (Saldivar, Hamperl et al. 2018). Because of the direct implications of FOXM1 downstream the ATR/CHK1/CDC25s pathway, it makes sense to think that loss of FOXM1 could mimic what happens when CDC25A or CDC25B are not present. If CDC25A deficient cells fail to enter mitosis in response to drug, due to an impairment of CDK1 activation after DNA damage, causing resistance to ATR inhibition (Ruiz, Mayor-Ruiz et al. 2016), it seems logical to expect that FOXM1 loss would have similar consequences in the cells. Thus, FOXM1 could be another mediator of ATRi resistance, as CDC25 proteins loss causes a reduction in CDK1 and FOXM1 activity after DNA damage. With this in mind, I am developing both, CDC25B and FOXM1 deficient models, which would be useful to test whether they are both involved in mediating ATRi resistance through the impairment of premature mitosis (Ruiz, Mayor-Ruiz et al. 2016).

Apart from *CDC25B/A* and *FOXM1*, I have validated other interesting ATRi determinants of resistance in the arrayed CRISPR/Cas9 screen experiment that have been found to be important in the other cell lines analysed (**Figure 25B**). As an example, *CARD10*, encodes for a structural protein, member of the CARMA (membrane associated guanylate kinase-like domain) family of proteins, that participates in apoptosis mediation, and plays a role in the activation of the NF-kappa-B (NF-κB) signalling pathway, forming a complex with BCL10 and MALT1 (CBM) (Grabiner, Blonska et al. 2007, Jiang, Grabiner et al. 2011). Interestingly, NF-κB is a cancer-related pathway that has been described to be activated through ATM phosphorylation in response to DNA damage to induce the expression of anti-apoptotic genes, which is a process that has also been related to the development of resistance to chemotherapy (Zhang, Pan et al. 2017), making *CARD10* an interesting ATRi resistance gene to study further.

Finally, I also validated *SMG8* and *SMG9* as ATRi resistance genes. *SMG8* and *SMG9* are both members of the non-sense mediated decay (NMD) pathway, in charge of the post-transcriptional modulation mRNAs expression and degradation of defective mRNAs that contain premature stop codons, preventing aberrant protein truncation (Popp and Maquat 2013, Lykke-Andersen and Bennett 2014, Lykke-Andersen and Jensen 2015, Karousis, Nasif et al. 2016). *SMG8* and *SMG9* form a heterodimer that acts as a negative regulator of the PIKK *SMG1* (Arias-Palomo, Yamashita et al. 2011,

Fernandez, Yamashita et al. 2011), pivotal in the NMD pathway. In addition to its role in the NMD pathway, SMG1 it is known to play a role in the maintenance of the genomic instability, similar to other PIKKs like ATR and ATM (Brumbaugh, Otterness et al. 2004). Moreover, the three PIKKs converge in the phosphorylation of UPF1, which is an 5'-3' DNA and RNA helicase in charge of facilitating several RNA degradation pathways (including NMD), as well of a mediator of DNA replication in S phase of cell cycle (Azzalin and Lingner 2006). Depletion of UPF1, leads to the impairment of the NMD pathway, as well as to the accumulation of genomic instability and an S phase cell cycle arrest (Azzalin and Lingner 2006, Azzalin and Lingner 2006). Depletion of ATR has been shown to lead to the impairment of UPF1 chromatin loading and accumulation of DNA damage (Azzalin and Lingner 2006) which suggests a central role of ATR in UPF1 regulation. Being a helicase, it has been hypothesised that UPF1 it might be in charge of unwinding the DNA in front of the replication fork, physically interacting with DNA polymerase delta, a main polymerase in DNA replication (Azzalin and Lingner 2006). This could be an explanation for the S phase arrest observed in UPF1 knockdown cells, and would suggest multiple roles for this protein. As SMG1 is known to have the ability to phosphorylate UPF1, especially in the context of the NMD pathway, it is reasonable to think that it might be implicated in UPF1 regulation upon other conditions, like ATR depletion. SMG1 depletion in the cells, leads to the accumulation of DNA damage, which could be explained by the aberrant regulation of UPF1 (Azzalin and Lingner 2006). Thus, in an ATR depleted situation, the impairment of SMG8 and SMG9 (as negative regulators of SMG1), could potentially lead to the upregulation of SMG1, activating UPF1 at the DNA fork, and thus facilitating the DNA repair in the cells before mitosis, causing resistance to ATRi. Interestingly, one of the proteins found upregulated in our ATRi resistant clones was SMG1, supporting its implication in mediating ATRi resistance. Consistent with my hypothesis, siRNA knockdown experiments have demonstrated that SMG1 downregulation is able to re-sensitise the cancer cells to ATRi, underlying the role of SMG1 as a mediator of ATRi resistance. Further experiments will be carried out to determine if this resistance is mediated through the modulation of UPF1 and the facilitation of DDR in condition of ATR depletion. These observations open the possibility to develop and test SMG1 inhibitors in combination with ATRi, to avoid resistance in the cancer cells, which can be widely relevant in the clinical practice, now that ATRi are starting to be used in clinical trials.

Therefore, in this section I have discovered and validated a number of novel determinants to ATRi resistance in GC, providing with a rationale to study their role in carcinogenesis and drug resistance and that can potentially be considered as biomarkers or therapy-guiding genes in the clinical practice.

3.2. ATR inhibitor resistant isogenic cells

With the aim of identifying genetic determinants to ATRi resistance in GC, I created eight ATRi resistant isogenic clones from YCC6 tumour cell line and performed proteomic analyses to detect significant deregulated proteins that can cause ATRi resistance. I observed that five of the clones, all part of the same cluster, according to the principal components analysis of the proteome presented a change in the micromorphology of the cell (H1, H2, H3, H4 and H6), exhibiting mesenchymal attributes, different from the epithelial parental cell line. Epithelial-mesenchymal morphology changes have been widely described in tumour cells that undergo genetic changes, as mesenchymal morphology has been related to an enhanced capacity of cancer cells to invade and metastasise, which can be related to the development of drug resistance mechanisms (Lyons, Alizadeh et al. 2016). Metastasis of tumour cells requires the following sequence of events: the ability of detachment from the primary tumour, migrating to the vascular supply, trespassing of the vessel wall (intravasation), transiting in the blood or lymphatics, exiting from the vascular supply (extravasation), and finally with the attachment and proliferation at the new site (Chambers, Groom et al. 2002). Usually, metastatic cells are associated with deformable shape and a low expression of proteins related to cell-cell adhesion or cell-extracellular matrix adhesion, which confers to the cell a larger size, mesenchymal-like elongated spindle morphology, and changes in the cytoskeleton structure (Cavallaro and Christofori 2004, Cross, Jin et al. 2007, Cross, Jin et al. 2008, Bex and van Roy 2009). Using the REACTOME 2016 pathway database to carry out a pathway analysis in relation to the differences in proteome found in the resistant clones in comparison to the parental cell line, one of the highest deregulated group of proteins in our resistant clones were the cell-cell adhesion proteins (data not shown). These included proteins expressed from the following genes: *CDH1* (*E-Cadherin*), *n-CAM* (*Neural Cell Adhesion Molecule 1*), *KRT7* (*Keratin 7*), *KRT19* (*Keratin 19*), *SMAD4* (*SMAD Family Member 4*), *PIK3CB* (*Phosphatidylinositol-4,5-Bisphosphate 3-Kinase Catalytic Subunit Beta*), *SPTBN1*

(Spectrin Beta, Non-Erythrocytic 1), ITGB4 (Integrin Subunit Beta 4), PARD6B (Par-6 Family Cell Polarity Regulator Beta), ROCK2 (Rho Associated Coiled-Coil Containing Protein Kinase 2), RHOB (Ras Homolog Family Member B), PAK1(P21 (RAC1) Activated Kinase 1), ECM1 (Extracellular matrix protein 1), MLLT4 (Afadin, Adherens Junction Formation Factor), EZR (Ezrin), VIM (Vimentin), ARHGAP21(Rho GTPase Activating Protein 21) and CD2AP (CD2 Associated Protein), which are known to be involved in cell-cell adhesion, cell-extracellular matrix adhesion and the cytoskeletal structure in the cell. These changes were seen in the YCC6 ATRi resistant clones that had acquired a mesenchymal morphology but were absent in the clones that did not undergo morphological changes. This indicates that the changes in the morphology of the tumour cells play an important role in the ATRi-resistance mechanism. In contrast, some of the resistant clones did not undergo morphological changes, and other proteins, not related to cell morphology were detected as significantly deregulated proteins, suggesting that this is not the only mechanism mediating resistance.

Apart from the changes in the cell-morphology associated proteins, I detected other deregulated proteins in the ATRi resistant clones, compared with the parental cell line. This list varied widely when I compared all the clones together to the parental cell lines and also when I divided them in two clusters, determined by similarities in the proteome (PCA). Several proteins previously related with the carcinogenic process were detected. Amongst them, MET/HRAS/PIK3CB have been related to drug resistance in cancer (Hah, Zhao et al. 2014, Leiser, Medova et al. 2015, Pietrantonio, Fuca et al. 2018). Moreover, NF1 was found to be downregulated in the resistant clones. *NF1*, or *Neurofibromatosis type 1* is a tumour suppressor gene that has previously been identified as an Cetuximab-resistance conferring factor in EGFR-amplified colorectal tumours (Mei, Shao et al. 2018). When I cross-referenced the results from the proteomic analysis with the GW CRISPR screen data, only ARHGAP21 and TYK2 were downregulated in the resistant clones, as well as displaying enrichment of sgRNA in the resistant cells. Notably, TYK2 was found in in the Top 20 candidates from the screen, and also found to be downregulated in one of the resistant colonies (See VX970 positive selection GW CRISPR-Cas9 mutagenesis screen section, **Figure 20C** and **Table 8**). Additionally, STAT5B was found deregulated, also a component of the JAK/STAT pathway, which supports an important role of this pathway in the ATRi resistance process. I was especially

interested in SMG1, as it validates our hypothesis regarding the role of SMG8/SMG9 as ATRi resistance mediators. As discussed before, SMG8 and SMG9 form a heterodimer in charge of negatively regulating SMG1 (Arias-Palomo, Yamashita et al. 2011, Fernandez, Yamashita et al. 2011). Therefore, it is reasonable to expect that SMG8/SMG9 downregulation could cause an increase in SMG1 expression, which could be the mediator of ATRi resistance I have seen in our cells. SMG1 is also upregulated in the ATRi resistant clones, which supports our working hypothesis.

In this thesis, I have presented data regarding the proteomic analysis undertaken in the resistant clones, although additional mRNA sequencing and exome sequencing of the resistant colonies are currently being performed, to achieve a comprehensive view of the mechanisms involved in the ATRi resistance process. Integration of sequencing results extracted from the different high-throughput techniques, as well as with the GW CRISPR screen data will be useful to give us a deeper understanding of the main ATRi resistance-causing mechanisms in GC.

Moreover, for the purposes of this thesis, and due to its interest in relation with the GW CRISPR screen data, only SMG1 validation is presented, although more proteins will be tested for its part in ATRi resistance mechanisms in the near future.

3.3. Dense Tiling ATR CRISPRx Screen

With the aim of identifying regions in the ATR protein that are relevant for the development of ATRi resistance, I have carried out a dense tiling CRISPRx screen, following the principals and methodology described previously (Komor, Kim et al. 2016, Gaudelli, Komor et al. 2017, Komor, Badran et al. 2017, Komor, Zhao et al. 2017, Pettitt, Krastev et al. 2018). This approach has allowed me to describe candidate mutations in the ATR sequence that cause resistance to the ATRi VX970 in the GC tumour cell line YCC6.

I have detected a cluster of ATRi resistance-conferring mutations affecting residues located in the FAT domain (**Figure 35A and 35B**). The FAT domain has been previously described to be crucial for ATR activation through the autophosphorylation and stimulation of TopBP1 function, which is crucial for ATR substrate recognition and the transmission of the DDR signal (Liu, Shiotani et al. 2011). Apart from its role in ATR activation, it has been hypothesised that, due to the fact that FAT and FATC domains only occur in combination in the PIKKs, they must structurally interact with

each other in a way that ensures the ATR kinase domain function, that is located between the two domains (Bosotti, Isacchi et al. 2000, Lempiainen and Halazonetis 2009). This has also been described to be the case in other PIKKs as ATM, DNA-PKcs, SMG1 and mTOR, where structural changes in the FAT or the FATC domains impair their kinase activity (Stan, McLaughlin et al. 1994, Choi, Chen et al. 1996, Bosotti, Isacchi et al. 2000, Peterson, Beal et al. 2000, Takahashi, Hara et al. 2000, You, Chahwan et al. 2005, Cavalieri, Funaro et al. 2006, Spagnolo, Rivera-Calzada et al. 2006, Morita, Yamashita et al. 2007, Lempiainen and Halazonetis 2009). Lastly, mutations in ATR's FAT domain have been reported to impair ATR-dependent responses to DNA damage through the impairment of CHK1 and p53 activation, as well as the abrogation of cell cycle arrest (Fang, Tsao et al. 2004, Lewis, Mullany et al. 2005, Tanaka, Weinell et al. 2012), which could potentially explain the emergence of ATRi resistance mechanisms in our model (**Figure 35B**). Therefore, I hypothesise that mutations in the ATR's FAT domain are likely to cause ATRi resistance due to the impairment of the proper protein folding and kinase function, not allowing ATR to ensure the correct repair of DNA damage before cells undergo mitosis.

The 3D ATR structure has not yet been constructed (due to the technical challenges of the large protein size). However, the cryo-electron microscopy structure of the ATR-ATRIP complex was partially described recently, providing valuable information about the complex assembly, and where the ATRi VX970 binds (Rao, Liu et al. 2018). VX970 is predicted to bind to the catalytic domain of ATR through a deep pocket that is thought to accommodate ATP for substrate phosphorylation, preventing the transfer of the group phosphate to the substrates (Rao, Liu et al. 2018). Hence, another explanation for the observed resistance could be that the aberrant folding of the protein impairs the binding of the inhibitor VX970 to bind the ATR catalytic domain, and therefore, causing a physical resistance to the drug. The use of other ATRi inhibitors, known to bind to other parts of the protein, will reveal if this is the case.

Following the acquisition of my data, I have designed validation experiments to identify the exact effect of a determined mutation in ATR protein activity with respect to ATRi response. With this aim, I picked and expanded several resistant clones from the initial CRISPRx experiment at the time I retrieved the resistant population for sequencing. This will allow us to characterise the clones in terms of ATR mutations and ATRi

resistance (to VX970 and other ATRi), and therefore to have a collection of isogenic models with mutations located in several areas of the protein. When these models will be generated I will create additional isogenic models to represent other areas of the protein in this and other cell lines, using the CRISPR/Cas9 technique. This will be important to discard model-specific conclusions, thereby removing false positive results from our screen. Due to the role of ATR in mediating the DDR cascade through its interaction with downstream proteins, it would also be interesting to determine the effect of the mutations in a specific region of the protein in other relevant protein-protein interaction. This could be tested through immunoprecipitation experiments, where ATR and its interacting proteins are studied to see changes in the protein populations in the ATR mutated cells. At the same time, it would be noteworthy to describe the ability of mutated ATR to orchestrate the DDR cascade by carrying out a study of the state of phosphorylation of downstream proteins, such as CHK1, TopBP1 and CDK2. These isogenic models would help to determine whether they are resistant to other ATRi that bind to other residues, and whether the resistance I see is due to the physical impairment of VX970 accession to ATR catalytic domain.

4. Biological implications of the results and future perspectives

In this thesis, I have demonstrated that ARID1A deficiency plays an important role in ATRi sensitivity, in both, *in vitro* and *in vivo* GC models. Although this effect is clear in our GC models, the penetrance of this SL (the percentage of models with ARID1A deficiency where ATRi enhanced sensitivity is observed) does not seem to be complete. To date, only a few highly penetrant SLs have been described, and low penetrance SL remains a clinical barrier to exploit genetic dependencies from a therapeutic perspective (Ryan, Bajrami et al. 2018). In this study, I have demonstrated the ARID1A and ATR SL in GC *in vitro* and *in vivo*. More studies, incorporating a larger number of models will be necessary to determine the penetrance of this SL in GC or across all histologies and thereby, identify robust determinants to ATRi response, in the presence or absence of ARID1A deficiency. Therefore, I currently sequencing the retrieved resistant tumours from the PDX models to identify other predictive biomarkers of ATRi, by comparing them with tumours harvested from the vehicle control arm. *ARID1A* is a gene that is highly mutated across cancer (20%). As a result of the data described in this thesis, we are currently negotiating a clinical study evaluating response to VX970 in four cohorts of GC: MSI and ARID1A null, MSI and

ARID1A WT, MSS and ARID1A null and MSS and ARID1A WT. This will allow us to compare responses to ATRi within each genotypic group in a prospective study.

Additionally, I have described and validated several genes involved in the ATRi resistance process in GC through undertaking a GW CRISPR screen and the creation of ATRi resistant models. Several candidate resistance genes including HUWE1, SMG8, SMG9, SMG1, HNRNPF, IRF9, CARD10, CDC25B and STAT2 have been robustly validated in orthogonal formats and models. Of note, I have demonstrated that SMG1 overexpression mediates ATRi resistance in GC. I am currently creating new isogenic models using the CRISPR/Cas9 technique, to generate YCC6 clones representing SMG8, SMG9 and SMG1 deficiency in the YCC6 cell line, as well as in other mutant gastric cell lines to validate the effect I have described in the YCC6 cells. In parallel, I am undertaking knockdown experiments to try to clarify whether this resistance is mediated by the regulation of UPF1. The use of orthogonal models will allow us to detect ATRi response determinants that are not influenced by the genetic/epigenetic profile of a specific model. Additionally, siRNA knockdown and cell cycle experiments will be performed to better define the mechanisms by which this resistance is occurring.

Furthermore, I have created ATRi resistant models that will allow me to validate previous hypotheses generated from the GW CRISPR screen experiment that will be useful to further characterise mechanisms of ATRi resistance through DNA whole exome sequencing and RNA sequencing.

Finally, I have shown how mutations in the FAT domain of ATR cause resistance to ATRi. Going forward, I will create isogenic models that harbour mutations in this stretch of the ATR protein, to enable functional validation and to determine whether ATRi resistance is caused by an impairment of the inhibitor binding or by the structural inability of ATR to carry out its normal function. I will utilise the CRISPRx technique for model generation. Mass spectrometry and immunoprecipitation experiments will help me to define the changes of ATR-protein interactions in the mutant clones, compared with an ATR WT control.

Conclusions

In this thesis, I have:

1. Shown that ATR inhibition constitutes an ARID1A synthetically lethal interaction in gastric cancer that can be elicited with small molecule inhibitors such as VX970, AZD6738 and M4344. These effects have been observed in a panel of gastric tumour cell lines, ARID1A isogenic models and gastric cancer human-derived xenografts. These results provide with a rationale to test these compounds in clinical trials recruiting patients with gastric cancer, within the context of ARID1A deficiency.
2. Identified and validated HUWE1, HNRNPF, IRF9, SMG8, SMG9, CARD10, CDC25B and STAT2 as genetic determinants to ATRi resistance in gastric cancer.
3. Described that the overexpression of SMG1 causes resistance to ATRi in gastric cancer.
4. Identified potential ATR inhibitors-resistance mediators through the creation of ATR inhibition resistance gastric cancer models.
5. Pinpointed how mutations in the FAT domain of ATR cause resistance to ATRi.

References

- (1994). "IARC working group on the evaluation of carcinogenic risks to humans: some industrial chemicals. Lyon, 15-22 February 1994." *IARC Monogr Eval Carcinog Risks Hum* **60**: 1-560.
- Abdel-Fatah, T. M. A., F. K. Middleton, A. Arora, D. Agarwal, T. Chen, P. M. Moseley, C. Perry, R. Doherty, S. Chan, A. R. Green, E. Rakha, G. Ball, I. O. Ellis, N. J. Curtin and S. Madhusudan (2015). "Untangling the ATR-CHEK1 network for prognostication, prediction and therapeutic target validation in breast cancer." *Molecular Oncology* **9**(3): 569-585.
- Abu-Sanad, A., Y. Z. Wang, F. Hasheminasab, J. Panasci, A. Noe, L. Rosca, D. Davidson, L. Amrein, B. Sharif-Askari, R. Aloyz and L. Panasci (2015). "Simultaneous inhibition of ATR and PARP sensitizes colon cancer cell lines to irinotecan." *Frontiers in Pharmacology* **6**.
- Adhikary, S., F. Marinoni, A. Hock, E. Hulleman, N. Popov, R. Beier, S. Bernard, M. Quarto, M. Capra, S. Goettig, U. Kogel, M. Scheffner, K. Helin and M. Eilers (2005). "The ubiquitin ligase HectH9 regulates transcriptional activation by myc and is essential for tumor cell proliferation." *Cell* **123**(3): 409-421.
- Aguirre, A. J., R. M. Meyers, B. A. Weir, F. Vazquez, C. Z. Zhang, U. Ben-David, A. Cook, G. Ha, W. F. Harrington, M. B. Doshi, M. Kost-Alimova, S. Gill, H. Xu, L. D. Ali, G. Jiang, S. Pantel, Y. Lee, A. Goodale, A. D. Cherniack, C. Oh, G. Kryukov, G. S. Cowley, L. A. Garraway, K. Stegmaier, C. W. Roberts, T. R. Golub, M. Meyerson, D. E. Root, A. Tsherniak and W. C. Hahn (2016). "Genomic Copy Number Dictates a Gene-Independent Cell Response to CRISPR/Cas9 Targeting." *Cancer Discov* **6**(8): 914-929.
- Al-Batran, S. E., R. D. Hofheinz, C. Pauligk, H. G. Kopp, G. M. Haag, K. B. Luley, J. Meiler, N. Homann, S. Lorenzen, H. Schmalenberg, S. Probst, M. Koenigsmann, M. Egger, N. Prasnika, K. Caca, J. Trojan, U. M. Martens, A. Block, W. Fischbach, R. Mahlberg, M. Clemens, G. Illerhaus, K. Zirlik, D. M. Behringer, W. Schmiegel, M. Pohl, M. Heike, U. Ronellenfitsch, M. Schuler, W. O. Bechstein, A. Konigsrainer, T. Gaiser, P. Schirmacher, W. Hozaeel, A. Reichart, T. O. Goetze, M. Sievert, E. Jager, S. Monig and A. Tannapfel (2016). "Histopathological regression after neoadjuvant docetaxel, oxaliplatin, fluorouracil, and leucovorin versus epirubicin, cisplatin, and fluorouracil or capecitabine in patients with resectable gastric or gastro-oesophageal junction adenocarcinoma (FLOT4-AIO): results from the phase 2 part of a multicentre, open-label, randomised phase 2/3 trial." *Lancet Oncol* **17**(12): 1697-1708.
- Allo, G., M. Q. Bernardini, R. C. Wu, M. Shih le, S. Kalloger, A. Pollett, C. B. Gilks and B. A. Clarke (2014). "ARID1A loss correlates with mismatch repair deficiency and intact p53 expression in high-grade endometrial carcinomas." *Mod Pathol* **27**(2): 255-261.
- Aressy, B. and B. Ducommun (2008). "Cell cycle control by the CDC25 phosphatases." *Anticancer Agents Med Chem* **8**(8): 818-824.
- Arias-Palomo, E., A. Yamashita, I. S. Fernandez, R. Nunez-Ramirez, Y. Bamba, N. Izumi, S. Ohno and O. Llorca (2011). "The nonsense-mediated mRNA decay SMG-1 kinase is regulated by large-scale conformational changes controlled by SMG-8." *Genes Dev* **25**(2): 153-164.
- Ashworth, A. and C. J. Lord (2018). "Synthetic lethal therapies for cancer: what's next after PARP inhibitors?" *Nat Rev Clin Oncol* **15**(9): 564-576.
- Azzalin, C. M. and J. Lingner (2006). "The double life of UPF1 in RNA and DNA stability pathways." *Cell Cycle* **5**(14): 1496-1498.
- Azzalin, C. M. and J. Lingner (2006). "The human RNA surveillance factor UPF1 is required for S phase progression and genome stability." *Curr Biol* **16**(4): 433-439.
- Bak, S. T., D. Sakellariou and J. Pena-Diaz (2014). "The dual nature of mismatch repair as antimutator and mutator: for better or for worse." *Front Genet* **5**: 287.
- Ball, H. L., J. S. Myers and D. Cortez (2005). "ATRIP binding to replication protein A-single-stranded DNA promotes ATR-ATRIP localization but is dispensable for Chk1 phosphorylation." *Molecular Biology of the Cell* **16**(5): 2372-2381.
- Bang, Y. J., E. Van Cutsem, A. Feyereislova, H. C. Chung, L. Shen, A. Sawaki, F. Lordick, A. Ohtsu, Y. Omuro, T. Satoh, G. Aprile, E. Kulikov, J. Hill, M. Lehle, J. Ruschoff, Y. K. Kang and G. A. T. I. To (2010). "Trastuzumab in combination with chemotherapy versus chemotherapy alone for treatment of HER2-positive advanced gastric or gastro-oesophageal junction cancer (ToGA): a phase 3, open-label, randomised controlled trial." *Lancet* **376**(9742): 687-697.
- Barber, L. J., S. Sandhu, L. N. Chen, J. Campbell, I. Kozarewa, K. Fenwick, I. Assiotis, D. N. Rodrigues, J. S. Reis, V. Moreno, J. Mateo, L. R. Molife, J. De Bono, S. Kaye, C. J. Lord and A. Ashworth (2013). "Secondary mutations in BRCA2 associated with clinical resistance to a PARP inhibitor." *Journal of Pathology* **229**(3): 422-429.

Bass, T. E., J. W. Luzwick, G. Kavanaugh, C. Carroll, H. Dungrawala, G. G. Glick, M. D. Feldkamp, R. Putney, W. J. Chazin and D. Cortez (2016). "ETAA1 acts at stalled replication forks to maintain genome integrity." *Nature Cell Biology* **18**(11): 1185-+.

Bernassola, F., M. Karin, A. Ciechanover and G. Melino (2008). "The HECT family of E3 ubiquitin ligases: Multiple players in cancer development." *Cancer Cell* **14**(1): 10-21.

Bertuccio, P., L. Chatenoud, F. Levi, D. Praud, J. Ferlay, E. Negri, M. Malvezzi and C. La Vecchia (2009). "Recent patterns in gastric cancer: a global overview." *Int J Cancer* **125**(3): 666-673.

Berx, G. and F. van Roy (2009). "Involvement of Members of the Cadherin Superfamily in Cancer." *Cold Spring Harbor Perspectives in Biology* **1**(6).

Bhaya, D., M. Davison and R. Barrangou (2011). "CRISPR-Cas systems in bacteria and archaea: versatile small RNAs for adaptive defense and regulation." *Annu Rev Genet* **45**: 273-297.

Bi, X. H., M. Hameed, N. Mirani, E. M. Pimenta, J. Anari and B. J. Barnes (2011). "Loss of interferon regulatory factor 5 (IRF5) expression in human ductal carcinoma correlates with disease stage and contributes to metastasis." *Breast Cancer Research* **13**(6).

Bitler, B. G., K. M. Aird, A. Garipov, H. Li, M. Amatangelo, A. V. Kossenkov, D. C. Schultz, Q. Liu, M. Shih le, J. R. Conejo-Garcia, D. W. Speicher and R. Zhang (2015). "Synthetic lethality by targeting EZH2 methyltransferase activity in ARID1A-mutated cancers." *Nat Med* **21**(3): 231-238.

Bitler, B. G., K. M. Aird and R. Zhang (2016). "Epigenetic synthetic lethality in ovarian clear cell carcinoma: EZH2 and ARID1A mutations." *Mol Cell Oncol* **3**(1): e1032476.

Bitler, B. G., N. Fatkhutdinov and R. Zhang (2015). "Potential therapeutic targets in ARID1A-mutated cancers." *Expert Opin Ther Targets* **19**(11): 1419-1422.

Bitler, B. G., S. Wu, P. H. Park, Y. Hai, K. M. Aird, Y. Wang, Y. Zhai, A. V. Kossenkov, A. Vara-Ailor, F. J. Rauscher, III, W. Zou, D. W. Speicher, D. G. Huntsman, J. R. Conejo-Garcia, K. R. Cho, D. W. Christianson and R. Zhang (2017). "ARID1A-mutated ovarian cancers depend on HDAC6 activity." *Nat Cell Biol* **19**(8): 962-973.

Bosotti, R., A. Isacchi and E. L. Sonnhammer (2000). "FAT: a novel domain in PIK-related kinases." *Trends Biochem Sci* **25**(5): 225-227.

Bosse, T., N. T. ter Haar, L. M. Seeber, P. J. v Diest, F. J. Hes, H. F. Vasen, R. A. Nout, C. L. Creutzberg, H. Morreau and V. T. Smit (2013). "Loss of ARID1A expression and its relationship with PI3K-Akt pathway alterations, TP53 and microsatellite instability in endometrial cancer." *Mod Pathol* **26**(11): 1525-1535.

Boultonwood, J., C. Fidler, S. Lewis, A. Maccarthy, H. Sheridan, S. Kelly, D. Oscier, V. J. Buckle and J. S. Wainscoat (1993). "Allelic Loss of Irf1 in Myelodysplasia and Acute Myeloid-Leukemia - Retention of Irf1 on the 5q-Chromosome in Some Patients with the 5q-Syndrome." *Blood* **82**(9): 2611-2616.

Boutros, R., V. Lobjois and B. Ducommun (2007). "CDC25 phosphatases in cancer cells: key players? Good targets?" *Nat Rev Cancer* **7**(7): 495-507.

Brandsma, I., E. D. G. Fleuren, C. T. Williamson and C. J. Lord (2017). "Directing the use of DDR kinase inhibitors in cancer treatment." *Expert Opinion on Investigational Drugs* **26**(12): 1341-1355.

Brandsma, I. and D. C. Gent (2012). "Pathway choice in DNA double strand break repair: observations of a balancing act." *Genome Integr* **3**(1): 9.

Brough, R., J. R. Frankum, S. Costa-Cabral, C. J. Lord and A. Ashworth (2011). "Searching for synthetic lethality in cancer." *Curr Opin Genet Dev* **21**(1): 34-41.

Brown, E. J. and D. Baltimore (2000). "ATR disruption leads to chromosomal fragmentation and early embryonic lethality." *Genes & Development* **14**(4): 397-402.

Brumbaugh, K. M., D. M. Otterness, C. Geisen, V. Oliveira, J. Brognard, X. Li, F. Lejeune, R. S. Tibbetts, L. E. Maquat and R. T. Abraham (2004). "The mRNA surveillance protein hSMG-1 functions in genotoxic stress response pathways in mammalian cells." *Mol Cell* **14**(5): 585-598.

Bryant, H. E., E. Petermann, N. Schultz, A. S. Jemth, O. Loseva, N. Issaeva, F. Johansson, S. Fernandez, P. McGlynn and T. Helleday (2009). "PARP is activated at stalled forks to mediate Mre11-dependent replication restart and recombination." *EMBO J* **28**(17): 2601-2615.

Buhard, O., F. Cattaneo, Y. F. Wong, S. F. Yim, E. Friedman, J. F. Flejou, A. Duval and R. Hamelin (2006). "Multipopulation analysis of polymorphisms in five mononucleotide repeats used to determine the microsatellite instability status of human tumors." *J Clin Oncol* **24**(2): 241-251.

Cancer Genome Atlas Research, N. (2014). "Comprehensive molecular characterization of gastric adenocarcinoma." *Nature* **513**(7517): 202-209.

Cancer Genome Atlas Research, N., C. Kandoth, N. Schultz, A. D. Cherniack, R. Akbani, Y. Liu, H. Shen, A. G. Robertson, I. Pashtan, R. Shen, C. C. Benz, C. Yau, P. W. Laird, L. Ding, W. Zhang, G. B. Mills, R. Kucherlapati, E. R. Mardis and D. A. Levine (2013). "Integrated genomic characterization of endometrial carcinoma." *Nature* **497**(7447): 67-73.

Casper, A. M., P. Nghiem, M. F. Arlt and T. W. Glover (2002). "ATR regulates fragile site stability." *Cell* **111**(6): 779-789.

Cavaliere, S., A. Funaro, P. Porcedda, V. Turinetti, N. Migone, R. A. Gatti and A. Brusco (2006). "ATM mutations in Italian families with ataxia telangiectasia include two distinct large genomic deletions." *Hum Mutat* **27**(10): 1061.

Cavallaro, U. and G. Christofori (2004). "Cell adhesion and signalling by cadherins and Ig-CAMs in cancer." *Nature Reviews Cancer* **4**(2): 118-132.

Cervantes, A., D. Roda, N. Tarazona, S. Rosello and J. A. Perez-Fidalgo (2013). "Current questions for the treatment of advanced gastric cancer." *Cancer Treat Rev* **39**(1): 60-67.

Chambers, A. F., A. C. Groom and I. C. MacDonald (2002). "Dissemination and growth of cancer cells in metastatic sites." *Nature Reviews Cancer* **2**(8): 563-572.

Chang, D. J. and K. A. Cimprich (2009). "DNA damage tolerance: when it's OK to make mistakes." *Nat Chem Biol* **5**(2): 82-90.

Chen, D. L., N. Kon, M. Y. Li, W. Z. Zhang, J. Qin and W. Gu (2005). "ARF-BP1/mule is a critical mediator of the ARF tumor suppressor." *Cell* **121**(7): 1071-1083.

Chen, L. Y., G. Alexe, N. V. Dharia, L. Ross, A. B. Iniguez, A. S. Conway, E. J. Wang, V. Veschi, N. Lam, J. Qi, W. C. Gustafson, N. Nasholm, F. Vazquez, B. A. Weir, G. S. Cowley, L. D. Ali, S. Pantel, G. Z. Jiang, W. F. Harrington, Y. Lee, A. Goodale, R. Lubonja, J. M. Krill-Burger, R. M. Meyers, A. Tsherniak, D. E. Root, J. E. Bradner, T. R. Golub, C. W. M. Roberts, W. C. Hahn, W. A. Weiss, C. J. Thiele and K. Stegmaier (2018). "CRISPR-Cas9 screen reveals a MYCN-amplified neuroblastoma dependency on EZH2." *Journal of Clinical Investigation* **128**(1): 446-462.

Chen, X. P., R. X. Zhao, G. G. Glick and D. Cortez (2007). "Function of the ATR N-terminal domain revealed by an ATM/ATR chimera." *Experimental Cell Research* **313**(8): 1667-1674.

Cheung, H. W., G. S. Cowley, B. A. Weir, J. S. Boehm, S. Rusin, J. A. Scott, A. East, L. D. Ali, P. H. Lizotte, T. C. Wong, G. Z. Jiang, J. Hsiao, C. H. Mermel, G. Getz, J. Barretina, S. Gopal, P. Tamayo, J. Gould, A. Tsherniak, N. Stransky, B. A. Luo, Y. Ren, R. Drapkin, S. N. Bhatia, J. P. Mesirov, L. A. Garraway, M. Meyerson, E. S. Lander, D. E. Root and W. C. Hahn (2011). "Systematic investigation of genetic vulnerabilities across cancer cell lines reveals lineage-specific dependencies in ovarian cancer." *Proceedings of the National Academy of Sciences of the United States of America* **108**(30): 12372-12377.

Choe, K. N., C. M. Nicolae, D. Constantin, Y. I. Kawasawa, M. R. Delgado-Diaz, S. De, R. Freire, V. A. J. Smits and G. L. Moldovan (2016). "HUWE1 interacts with PCNA to alleviate replication stress." *Embo Reports* **17**(6): 874-886.

Choi, J. W., J. Chen, S. L. Schreiber and J. Clardy (1996). "Structure of the FKBP12-rapamycin complex interacting with the binding domain of human FRAP." *Science* **273**(5272): 239-242.

Chong, I. Y., D. Cunningham, L. J. Barber, J. Campbell, L. Chen, I. Kozarewa, K. Fenwick, I. Assiotis, S. Guettler, I. Garcia-Murillas, S. Awan, M. Lambros, N. Starling, A. Wotherspoon, G. Stamp, D. Gonzalez-de-Castro, M. Benson, I. Chau, S. H. Hultki, M. Nohadani, Z. Eltahir, A. Lemnrau, N. Orr, S. Rao, C. J. Lord and A. Ashworth (2013). "The genomic landscape of oesophagogastric junctional adenocarcinoma." *J Pathol* **231**(3): 301-310.

Chou, A., C. W. Toon, A. Clarkson, L. Sioson, M. Houang, N. Watson, K. DeSilva and A. J. Gill (2014). "Loss of ARID1A expression in colorectal carcinoma is strongly associated with mismatch repair deficiency." *Hum Pathol* **45**(8): 1697-1703.

Ciccio, A. and S. J. Elledge (2010). "The DNA damage response: making it safe to play with knives." *Mol Cell* **40**(2): 179-204.

Cimprich, K. A. and D. Cortez (2008). "ATR: an essential regulator of genome integrity." *Nat Rev Mol Cell Biol* **9**(8): 616-627.

Cimprich, K. A. and D. Cortez (2008). "ATR: an essential regulator of genome integrity." *Nature Reviews Molecular Cell Biology* **9**(8): 616-627.

Clauson, C., O. D. Scharer and L. Niedernhofer (2013). "Advances in understanding the complex mechanisms of DNA interstrand cross-link repair." *Cold Spring Harb Perspect Biol* **5**(10): a012732.

Cortez, D., S. Guntuku, J. Qin and S. J. Elledge (2001). "ATR and ATRIP: Partners in checkpoint signaling." *Science* **294**(5547): 1713-1716.

Cristescu, R., J. Lee, M. Nebozhyn, K. M. Kim, J. C. Ting, S. S. Wong, J. Liu, Y. G. Yue, J. Wang, K. Yu, X. S. Ye, I. G. Do, S. Liu, L. Gong, J. Fu, J. G. Jin, M. G. Choi, T. S. Sohn, J. H. Lee, J. M. Bae, S. T. Kim, S. H. Park, I. Sohn, S. H. Jung, P. Tan, R. Chen, J. Hardwick, W. K. Kang, M. Ayers, D. Hongyue, C. Reinhard, A. Loboda, S. Kim and A. Aggarwal (2015). "Molecular analysis of gastric cancer identifies subtypes associated with distinct clinical outcomes." *Nat Med* **21**(5): 449-456.

Cross, S. E., Y. S. Jin, J. Rao and J. K. Gimzewski (2007). "Nanomechanical analysis of cells from cancer patients." *Nature Nanotechnology* **2**(12): 780-783.

Cross, S. E., Y. S. Jin, J. Tondre, R. Wong, J. Rao and J. K. Gimzewski (2008). "AFM-based analysis of human metastatic cancer cells." *Nanotechnology* **19**(38).

Croxtall, J. D. and K. McKeage (2010). "Trastuzumab: in HER2-positive metastatic gastric cancer." *Drugs* **70**(17): 2259-2267.

Cunningham, D., W. H. Allum, S. P. Stenning, J. N. Thompson, C. J. Van de Velde, M. Nicolson, J. H. Scarffe, F. J. Lofts, S. J. Falk, T. J. Iveson, D. B. Smith, R. E. Langley, M. Verma, S. Weeden, Y. J. Chua and M. T. Participants (2006). "Perioperative chemotherapy versus surgery alone for resectable gastroesophageal cancer." *N Engl J Med* **355**(1): 11-20.

Cunningham, D., J. Oliveira and E. G. W. Group (2008). "Gastric cancer: ESMO clinical recommendations for diagnosis, treatment and follow-up." *Ann Oncol* **19** Suppl 2: ii23-24.

Cunningham, D., N. Starling, S. Rao, T. Iveson, M. Nicolson, F. Coxon, G. Middleton, F. Daniel, J. Oates, A. R. Norman and K. Upper Gastrointestinal Clinical Studies Group of the National Cancer Research Institute of the United (2008). "Capecitabine and oxaliplatin for advanced esophagogastric cancer." *N Engl J Med* **358**(1): 36-46.

Deveau, H., J. E. Garneau and S. Moineau (2010). "CRISPR/Cas system and its role in phage-bacteria interactions." *Annu Rev Microbiol* **64**: 475-493.

Dykhuisen, E. C., D. C. Hargreaves, E. L. Miller, K. Cui, A. Korshunov, M. Kool, S. Pfister, Y. J. Cho, K. Zhao and G. R. Crabtree (2013). "BAF complexes facilitate decatenation of DNA by topoisomerase IIalpha." *Nature* **497**(7451): 624-627.

Edwards, S. L., R. Brough, C. J. Lord, R. Natrajan, R. Vatcheva, D. A. Levine, J. Boyd, J. S. Reis and A. Ashworth (2008). "Resistance to therapy caused by intragenic deletion in BRCA2." *Nature* **451**(7182): 1111-U1118.

Fang, Y., C. C. Tsao, B. K. Goodman, R. Furumai, C. A. Tirado, R. T. Abraham and X. F. Wang (2004). "ATR functions as a gene dosage-dependent tumor suppressor on a mismatch repair-deficient background." *Embo Journal* **23**(15): 3164-3174.

Farmer, H., N. McCabe, C. J. Lord, A. N. Tutt, D. A. Johnson, T. B. Richardson, M. Santarosa, K. J. Dillon, I. Hickson, C. Knights, N. M. Martin, S. P. Jackson, G. C. Smith and A. Ashworth (2005). "Targeting the DNA repair defect in BRCA mutant cells as a therapeutic strategy." *Nature* **434**(7035): 917-921.

Fernandez, I. S., A. Yamashita, E. Arias-Palomo, Y. Bamba, R. A. Bartolome, M. A. Canales, J. Teixido, S. Ohno and O. Llorca (2011). "Characterization of SMG-9, an essential component of the nonsense-mediated mRNA decay SMG1C complex." *Nucleic Acids Res* **39**(1): 347-358.

Ferrara, R., F. Simionato, C. Ciccarese, E. Grego, S. Cingarlini, R. Iacovelli, E. Bria, G. Tortora and D. Melisi (2018). "The development of PARP as a successful target for cancer therapy." *Expert Rev Anticancer Ther* **18**(2): 161-175.

Fishel, R., M. K. Lescoe, M. R. Rao, N. G. Copeland, N. A. Jenkins, J. Garber, M. Kane and R. Kolodner (1993). "The human mutator gene homolog MSH2 and its association with hereditary nonpolyposis colon cancer." *Cell* **75**(5): 1027-1038.

Fisher, A. E., H. Hohegger, S. Takeda and K. W. Caldecott (2007). "Poly(ADP-ribose) polymerase 1 accelerates single-strand break repair in concert with poly(ADP-ribose) glycohydrolase." *Mol Cell Biol* **27**(15): 5597-5605.

Flynn, R. L. and L. Zou (2011). "ATR: a master conductor of cellular responses to DNA replication stress." *Trends in Biochemical Sciences* **36**(3): 133-140.

Foote, K. M., K. Blades, A. Cronin, S. Fillery, S. S. Guichard, L. Hassall, I. Hickson, X. Jacq, P. J. Jewsbury, T. M. McGuire, J. W. M. Nissink, R. Odedra, K. Page, P. Perkins, A. Suleman, K. Tam, P. Thommes, R. Broadhurst and C. Wood (2013). "Discovery of 4-{4-[(3R)-3-Methylmorpholin-4-yl]-6[1-(methylsulfonyl)cyclopropyl]pyrimidin-2-yl}-1H-indole (AZ20): A Potent and Selective Inhibitor of ATR Protein Kinase with Monotherapy in Vivo Antitumor Activity." *Journal of Medicinal Chemistry* **56**(5): 2125-2138.

Fuchs, C. S., T. Doi, R. W. Jang, K. Muro, T. Satoh, M. Machado, W. Sun, S. I. Jalal, M. A. Shah, J. P. Metges, M. Garrido, T. Golan, M. Mandala, Z. A. Wainberg, D. V. Catenacci, A. Ohtsu, K. Shitara, R. Geva, J. Bleeker, A. H. Ko, G. Ku, P. Philip, P. C. Enzinger, Y. J. Bang, D. Levitan, J. Wang, M. Rosales, R. P. Dalal and H. H. Yoon (2018). "Safety and Efficacy of Pembrolizumab Monotherapy in Patients With Previously Treated Advanced Gastric and Gastroesophageal Junction Cancer: Phase 2 Clinical KEYNOTE-059 Trial." *JAMA Oncol* **4**(5): e180013.

Fuchs, C. S., J. Tomasek, C. J. Yong, F. Dumitru, R. Passalacqua, C. Goswami, H. Safran, L. V. Dos Santos, G. Aprile, D. R. Ferry, B. Melichar, M. Tehfe, E. Topuzov, J. R. Zalcborg, I. Chau, W. Campbell, C. Sivanandan, J. Pikiel, M. Koshiji, Y. Hsu, A. M. Liepa, L. Gao, J. D. Schwartz, J. Taberero and R. T. Investigators (2014). "Ramucirumab monotherapy for previously treated

advanced gastric or gastro-oesophageal junction adenocarcinoma (REGARD): an international, randomised, multicentre, placebo-controlled, phase 3 trial." Lancet **383**(9911): 31-39.

Fukumoto, T., P. H. Park, S. Wu, N. Fatkhutdinov, S. Karakashev, T. Nacarelli, A. V. Kossenkov, D. W. Speicher, S. Jean, L. Zhang, T. L. Wang, I. M. Shih, J. R. Conejo-García, B. G. Bitler and R. Zhang (2018). "Repurposing Pan-HDAC Inhibitors for ARID1A-Mutated Ovarian Cancer." Cell Rep **22**(13): 3393-3400.

Garneau, J. E., M. E. Dupuis, M. Villion, D. A. Romero, R. Barrangou, P. Boyaval, C. Fremaux, P. Horvath, A. H. Magadan and S. Moineau (2010). "The CRISPR/Cas bacterial immune system cleaves bacteriophage and plasmid DNA." Nature **468**(7320): 67-71.

Gaudelli, N. M., A. C. Komor, H. A. Rees, M. S. Packer, A. H. Badran, D. I. Bryson and D. R. Liu (2017). "Programmable base editing of A.T to G.C in genomic DNA without DNA cleavage." Nature **551**(7681): 464-+.

Grabiner, B. C., M. Blonska, P. C. Lin, Y. You, D. H. Wang, J. Y. Sun, B. G. Darnay, C. Dong and X. Lin (2007). "CARMA3 deficiency abrogates G protein-coupled receptor-induced NF-kappa B activation." Genes & Development **21**(8): 984-996.

Guan, B., T. L. Mao, P. K. Panuganti, E. Kuhn, R. J. Kurman, D. Maeda, E. Chen, Y. M. Jeng, T. L. Wang and M. Shih le (2011). "Mutation and loss of expression of ARID1A in uterine low-grade endometrioid carcinoma." Am J Surg Pathol **35**(5): 625-632.

Guichard, S. M., E. Brown, R. Odedra, A. Hughes, D. Heathcote, J. Barnes, A. Lau, S. Powell, C. D. Jones, W. Nissink, K. M. Foote, P. J. Jewsbury and M. Pass (2013). "The pre-clinical in vitro and in vivo activity of AZD6738: A potent and selective inhibitor of ATR kinase." Cancer Research **73**(8).

Haahr, P., S. Hoffmann, M. A. X. Tollenaere, T. Ho, L. I. Toledo, M. Mann, S. Bekker-Jensen, M. Raschle and N. Mailand (2016). "Activation of the ATR kinase by the RPA-binding protein ETAA1." Nature Cell Biology **18**(11): 1196-+.

Hah, J. H., M. Zhao, C. R. Pickering, M. J. Frederick, G. A. Andrews, S. A. Jasser, D. R. Fooshee, Z. L. Milas, C. Galer, D. Sano, W. N. William, E. Kim, J. Heymach, L. A. Byers, V. Papadimitrakopoulou and J. N. Myers (2014). "HRAS mutations and resistance to the epidermal growth factor receptor tyrosine kinase inhibitor erlotinib in head and neck squamous cell carcinoma cells." Head and Neck- Journal for the Sciences and Specialties of the Head and Neck **36**(11): 1547-1554.

Hall, A. B., D. Newsome, Y. X. Wang, D. M. Boucher, B. Eustace, Y. Gu, B. Hare, M. A. Johnson, H. Li, S. Milton, C. E. Murphy, D. Takemoto, C. Tolman, M. Wood, P. Charlton, J. D. Charrier, B. Furey, J. Golec, P. M. Reaper and J. R. Pollard (2014). "Potentiation of tumor responses to DNA damaging therapy by the selective ATR inhibitor VX-970." Oncotarget **5**(14): 5674-5685.

Hall, J. R., E. Kow, K. R. Nevis, C. K. Lu, K. S. Luce, Q. Zhong and J. G. Cook (2007). "Cdc6 stability is regulated by the Huwe1 ubiquitin ligase after DNA damage." Molecular Biology of the Cell **18**(9): 3340-3350.

Han, N., M. A. Kim, H. S. Lee and W. H. Kim (2016). "Loss of ARID1A Expression is Related to Gastric Cancer Progression, Epstein-Barr Virus Infection, and Mismatch Repair Deficiency." Appl Immunohistochem Mol Morphol **24**(5): 320-325.

Hartgrink, H. H., E. P. Jansen, N. C. van Grieken and C. J. van de Velde (2009). "Gastric cancer." Lancet **374**(9688): 477-490.

Hartlerode, A. J. and R. Scully (2009). "Mechanisms of double-strand break repair in somatic mammalian cells." Biochem J **423**(2): 157-168.

Heberle, H., G. V. Meirelles, F. R. da Silva, G. P. Telles and R. Minghim (2015). "InteractiVenn: a web-based tool for the analysis of sets through Venn diagrams." Bmc Bioinformatics **16**.

Helming, K., X. F. Wang, B. Wilson, F. Vazquez, J. Haswell, H. Manchester, Y. Kim, G. V. Kryukov, M. Ghandi, A. J. Aguirre, Z. Jagani, Z. Wang, L. Garraway, W. Hahn and C. Roberts (2014). "ARID1B is a specific vulnerability in ARID1A-mutant cancers." Cancer Research **74**(19).

Herold, S., A. Hock, B. Herkert, K. Berns, J. Mullenders, R. Beijersbergen, R. Bernards and M. Eilers (2008). "Miz1 and HectH9 regulate the stability of the checkpoint protein, TopBP1." Embo Journal **27**(21): 2851-2861.

Hess, G. T., L. Fresard, K. Han, C. H. Lee, A. Li, K. A. Cimprich, S. B. Montgomery and M. C. Bassik (2016). "Directed evolution using dCas9-targeted somatic hypermutation in mammalian cells." Nature Methods **13**(12): 1036-+.

Heyer, W. D., K. T. Ehmsen and J. Liu (2010). "Regulation of homologous recombination in eukaryotes." Annu Rev Genet **44**: 113-139.

Hochegger, H., D. Dejsuphong, T. Fukushima, C. Morrison, E. Sonoda, V. Schreiber, G. Y. Zhao, A. Saberi, M. Masutani, N. Adachi, H. Koyama, G. de Murcia and S. Takeda (2006). "Parp-1 protects homologous recombination from interference by Ku and Ligase IV in vertebrate cells." EMBO J **25**(6): 1305-1314.

Hoeijmakers, J. H. (2009). "DNA damage, aging, and cancer." *N Engl J Med* **361**(15): 1475-1485.

Horvath, P. and R. Barrangou (2010). "CRISPR/Cas, the immune system of bacteria and archaea." *Science* **327**(5962): 167-170.

Howson, C. P., T. Hiyama and E. L. Wynder (1986). "The decline in gastric cancer: epidemiology of an unplanned triumph." *Epidemiol Rev* **8**: 1-27.

Huang, H. N., M. C. Lin, W. C. Huang, Y. C. Chiang and K. T. Kuo (2014). "Loss of ARID1A expression and its relationship with PI3K-Akt pathway alterations and ZNF217 amplification in ovarian clear cell carcinoma." *Mod Pathol* **27**(7): 983-990.

Huehls, A. M., J. M. Wagner, C. J. Huntoon and L. M. Karnitz (2012). "Identification of DNA Repair Pathways That Affect the Survival of Ovarian Cancer Cells Treated with a Poly(ADP-Ribose) Polymerase Inhibitor in a Novel Drug Combination." *Molecular Pharmacology* **82**(4): 767-776.

Humans, I. W. G. o. t. E. o. C. R. t. (2012). "Personal habits and indoor combustions. Volume 100 E. A review of human carcinogens." *IARC Monogr Eval Carcinog Risks Hum* **100**(Pt E): 1-538.

Huntoon, C. J., K. S. Flatten, A. E. W. Hendrickson, A. M. Huehls, S. L. Sutor, S. H. Kaufmann and L. M. Karnitz (2013). "ATR Inhibition Broadly Sensitizes Ovarian Cancer Cells to Chemotherapy Independent of BRCA Status." *Cancer Research* **73**(12): 3683-3691.

Imbalzano, A. N., H. Kwon, M. R. Green and R. E. Kingston (1994). "Facilitated binding of TATA-binding protein to nucleosomal DNA." *Nature* **370**(6489): 481-485.

Janjigian, Y. Y., J. Bendell, E. Calvo, J. W. Kim, P. A. Ascierto, P. Sharma, P. A. Ott, K. Peltola, D. Jaeger, J. Evans, F. de Braud, I. Chau, C. T. Harbison, C. Dorange, M. Tschaika and D. T. Le (2018). "CheckMate-032 Study: Efficacy and Safety of Nivolumab and Nivolumab Plus Ipilimumab in Patients With Metastatic Esophagogastric Cancer." *J Clin Oncol* **36**(28): 2836-2844.

Jelski, W., B. Zalewski and M. Szmitkowski (2008). "Alcohol dehydrogenase (ADH) isoenzymes and aldehyde dehydrogenase (ALDH) activity in the sera of patients with pancreatic cancer." *Dig Dis Sci* **53**(8): 2276-2280.

Jiang, T., B. Grabiner, Y. F. Zhu, C. Y. Jiang, H. X. Li, Y. You, J. Y. Lang, M. C. Hung and X. Lin (2011). "CARMA3 is Crucial for EGFR-Induced Activation of NF-kappa B and Tumor Progression." *Cancer Research* **71**(6): 2183-2192.

Jones, S., M. Li, D. W. Parsons, X. Zhang, J. Wesseling, P. Kristel, M. K. Schmidt, S. Markowitz, H. Yan, D. Bigner, R. H. Hruban, J. R. Eshleman, C. A. Iacobuzio-Donahue, M. Goggins, A. Maitra, S. N. Malek, S. Powell, B. Vogelstein, K. W. Kinzler, V. E. Velculescu and N. Papadopoulos (2012). "Somatic mutations in the chromatin remodeling gene ARID1A occur in several tumor types." *Hum Mutat* **33**(1): 100-103.

Jones, S., M. Li, D. W. Parsons, X. S. Zhang, J. Wesseling, P. Kristel, M. K. Schmidt, S. Markowitz, H. Yan, D. Bigner, R. H. Hruban, J. R. Eshleman, C. A. Iacobuzio-Donahue, M. Goggins, A. Maitra, S. N. Malek, S. Powell, B. Vogelstein, K. W. Kinzler, V. E. Velculescu and N. Papadopoulos (2012). "Somatic Mutations in the Chromatin Remodeling Gene ARID1A Occur in Several Tumor Types." *Human Mutation* **33**(1): 100-103.

Jones, S., T. L. Wang, M. Shih le, T. L. Mao, K. Nakayama, R. Roden, R. Glas, D. Slamon, L. A. Diaz, Jr., B. Vogelstein, K. W. Kinzler, V. E. Velculescu and N. Papadopoulos (2010). "Frequent mutations of chromatin remodeling gene ARID1A in ovarian clear cell carcinoma." *Science* **330**(6001): 228-231.

Jones, S. E., E. D. G. Fleuren, J. Frankum, A. Konde, C. T. Williamson, D. B. Krastev, H. N. Pemberton, J. Campbell, A. Gulati, R. Elliott, M. Menon, J. L. Selfe, R. Brough, S. J. Pettitt, W. Niedzwiedz, W. T. A. van der Graaf, J. Shipley, A. Ashworth and C. J. Lord (2017). "ATR Is a Therapeutic Target in Synovial Sarcoma." *Cancer Res* **77**(24): 7014-7026.

Josse, R., S. E. Martin, R. Guha, P. Ormanoglu, T. D. Pfister, P. M. Reaper, C. S. Barnes, J. Jones, P. Charlton, J. R. Pollard, J. Morris, J. H. Doroshow and Y. Pommier (2014). "ATR Inhibitors VE-821 and VX-970 Sensitize Cancer Cells to Topoisomerase I Inhibitors by Disabling DNA Replication Initiation and Fork Elongation Responses." *Cancer Research* **74**(23): 6968-6979.

Kadoch, C. and G. R. Crabtree (2015). "Mammalian SWI/SNF chromatin remodeling complexes and cancer: Mechanistic insights gained from human genomics." *Science Advances* **1**(5).

Kadoch, C., D. C. Hargreaves, C. Hodges, L. Elias, L. Ho, J. Ranish and G. R. Crabtree (2013). "Proteomic and bioinformatic analysis of mammalian SWI/SNF complexes identifies extensive roles in human malignancy." *Nature Genetics* **45**(6): 592-+.

Kang, Y. K., N. Boku, T. Satoh, M. H. Ryu, Y. Chao, K. Kato, H. C. Chung, J. S. Chen, K. Muro, W. K. Kang, K. H. Yeh, T. Yoshikawa, S. C. Oh, L. Y. Bai, T. Tamura, K. W. Lee, Y. Hamamoto, J. G. Kim, K. Chin, D. Y. Oh, K. Minashi, J. Y. Cho, M. Tsuda and L. T. Chen (2017). "Nivolumab in patients with advanced gastric or gastro-oesophageal junction cancer refractory to, or intolerant of, at least two previous chemotherapy regimens (ONO-4538-12, ATTRACTION-2): a randomised, double-blind, placebo-controlled, phase 3 trial." *Lancet* **390**(10111): 2461-2471.

Karousis, E. D., S. Nasif and O. Muhlemann (2016). "Nonsense-mediated mRNA decay: novel mechanistic insights and biological impact." *Wiley Interdiscip Rev RNA* **7**(5): 661-682.

Kartha, N., L. Shen, C. Maskin, M. Wallace and J. C. Schimenti (2016). "The Chromatin Remodeling Component Arid1a Is a Suppressor of Spontaneous Mammary Tumors in Mice." *Genetics* **203**(4): 1601-1611.

Katagiri, A., K. Nakayama, M. T. Rahman, M. Rahman, H. Katagiri, M. Ishikawa, T. Ishibashi, K. Iida, Y. Otsuki, S. Nakayama and K. Miyazaki (2012). "Frequent loss of tumor suppressor ARID1A protein expression in adenocarcinomas/adenosquamous carcinomas of the uterine cervix." *Int J Gynecol Cancer* **22**(2): 208-212.

Khalique, S., K. Naidoo, A. D. Attygalle, D. Kriplani, F. Daley, A. Lowe, J. Campbell, T. Jones, M. Hubank, K. Fenwick, N. Matthews, A. G. Rust, C. J. Lord, S. Banerjee and R. Natrajan (2018). "Optimised ARID1A immunohistochemistry is an accurate predictor of ARID1A mutational status in gynaecological cancers." *J Pathol Clin Res* **4**(3): 154-166.

Kim, H., E. George, R. L. Ragland, S. Rafail, R. G. Zhang, C. Krepler, M. A. Morgan, M. Herlyn, E. J. Brown and F. Simpkins (2017). "Targeting the ATR/CHK1 Axis with PARP Inhibition Results in Tumor Regression in BRCA-Mutant Ovarian Cancer Models." *Clinical Cancer Research* **23**(12): 3097-3108.

Kim, K. J., H. Y. Jung, M. H. Oh, H. Cho, J. H. Lee, H. J. Lee, S. H. Jang and M. S. Lee (2015). "Loss of ARID1A Expression in Gastric Cancer: Correlation with Mismatch Repair Deficiency and Clinicopathologic Features." *J Gastric Cancer* **15**(3): 201-208.

Kim, M. S., E. M. Je, N. J. Yoo and S. H. Lee (2012). "Loss of ARID1A expression is uncommon in gastric, colorectal, and prostate cancers." *APMIS* **120**(12): 1020-1022.

Kim, S., A. Barzi and L. Rajdev (2018). "Biomarker-driven targeted therapies for gastric/gastro-esophageal junction malignancies." *Semin Oncol*.

Kim, Y. B., A. C. Komor, J. M. Levy, M. S. Packer, K. T. Zhao and D. R. Liu (2017). "Increasing the genome-targeting scope and precision of base editing with engineered Cas9-cytidine deaminase fusions." *Nature Biotechnology* **35**(4): 371-+.

Koike-Yusa, H., Y. Li, E. P. Tan, C. Velasco-Herrera Mdel and K. Yusa (2014). "Genome-wide recessive genetic screening in mammalian cells with a lentiviral CRISPR-guide RNA library." *Nat Biotechnol* **32**(3): 267-273.

Kolonel, L. N., J. H. Hankin and A. M. Nomura (1985). "Multiethnic studies of diet, nutrition, and cancer in Hawaii." *Princess Takamatsu Symp* **16**: 29-40.

Komor, A. C., A. H. Badran and D. R. Liu (2017). "CRISPR-Based Technologies for the Manipulation of Eukaryotic Genomes." *Cell* **168**(1-2): 20-36.

Komor, A. C., A. H. Badran and D. R. Liu (2017). "CRISPR-Based Technologies for the Manipulation of Eukaryotic Genomes (vol 168, pg 20, 2017)." *Cell* **169**(3): 559-559.

Komor, A. C., Y. B. Kim, M. S. Packer, J. A. Zuris and D. R. Liu (2016). "Programmable editing of a target base in genomic DNA without double-stranded DNA cleavage." *Nature* **533**(7603): 420-424.

Komor, A. C., K. T. Zhao, M. S. Packer, N. M. Gaudelli, A. L. Waterbury, L. W. Koblan, Y. B. Kim, A. H. Badran and D. R. Liu (2017). "Improved base excision repair inhibition and bacteriophage Mu Gam protein yields C:G-to-T:A base editors with higher efficiency and product purity." *Sci Adv* **3**(8): eaao4774.

Kwon, H., A. N. Imbalzano, P. A. Khavari, R. E. Kingston and M. R. Green (1994). "Nucleosome disruption and enhancement of activator binding by a human SW1/SNF complex." *Nature* **370**(6489): 477-481.

Landolfo, S., A. Guarini, L. Riera, M. Gariglio, G. Gribaudo, A. Cignetti, I. Cordone, E. Montefusco, F. Mandelli and R. Foa (2000). "Chronic myeloid leukemia cells resistant to interferon-alpha lack STAT1 expression." *Hematol J* **1**(1): 7-14.

Langelier, M. F., J. L. Planck, S. Roy and J. M. Pascal (2012). "Structural basis for DNA damage-dependent poly(ADP-ribosylation) by human PARP-1." *Science* **336**(6082): 728-732.

Lauren, P. (1965). "The Two Histological Main Types of Gastric Carcinoma: Diffuse and So-Called Intestinal-Type Carcinoma. An Attempt at a Histo-Clinical Classification." *Acta Pathol Microbiol Scand* **64**: 31-49.

Leach, F. S., N. C. Nicolaides, N. Papadopoulos, B. Liu, J. Jen, R. Parsons, P. Peltomaki, P. Sistonen, L. A. Aaltonen, M. Nystrom-Lahti and et al. (1993). "Mutations of a mutS homolog in hereditary nonpolyposis colorectal cancer." *Cell* **75**(6): 1215-1225.

Lee, D., E. J. Yu, I. H. Ham, H. Hur and Y. S. Kim (2017). "AKT inhibition is an effective treatment strategy in ARID1A-deficient gastric cancer cells." *Onco Targets Ther* **10**: 4153-4159.

Lee, S. R., G. A. Pratt, F. J. Martinez, G. W. Yeo and J. Lykke-Andersen (2015). "Target Discrimination in Nonsense-Mediated mRNA Decay Requires Upf1 ATPase Activity." *Mol Cell* **59**(3): 413-425.

Leiser, D., M. Medova, K. Mikami, L. Nisa, D. Stroka, A. Blaukat, F. Blatt, D. M. Aebersold and Y. Zimmer (2015). "KRAS and HRAS mutations confer resistance to MET targeting in preclinical models of MET-expressing tumor cells." *Molecular Oncology* **9**(7): 1434-1446.

Lempiainen, H. and T. D. Halazonetis (2009). "Emerging common themes in regulation of PIKKs and PI3Ks." *EMBO J* **28**(20): 3067-3073.

Lewis, K. A., S. Mullany, B. Thomas, J. Chien, R. Loewen, V. Shridhar and W. A. Cliby (2005). "Heterozygous ATR mutations in mismatch repair-deficient cancer cells have functional significance." *Cancer Research* **65**(16): 7091-7095.

Li, C. C., J. C. Yang, M. C. Lu, C. L. Lee, C. Y. Peng, W. Y. Hsu, Y. H. Dai, F. R. Chang, D. Y. Zhang, W. J. Wu and Y. C. Wu (2016). "ATR-Chk1 signaling inhibition as a therapeutic strategy to enhance cisplatin chemosensitivity in urothelial bladder cancer." *Oncotarget* **7**(2): 1947-1959.

Li, W., H. Xu, T. Xiao, L. Cong, M. I. Love, F. Zhang, R. A. Irizarry, J. S. Liu, M. Brown and X. S. Liu (2014). "MAGeCK enables robust identification of essential genes from genome-scale CRISPR/Cas9 knockout screens." *Genome Biol* **15**(12): 554.

Liang, H., L. W. Cheung, J. Li, Z. Ju, S. Yu, K. Stemke-Hale, T. Dogruluk, Y. Lu, X. Liu, C. Gu, W. Guo, S. E. Scherer, H. Carter, S. N. Westin, M. D. Dyer, R. G. Verhaak, F. Zhang, R. Karchin, C. G. Liu, K. H. Lu, R. R. Broaddus, K. L. Scott, B. T. Hennessy and G. B. Mills (2012). "Whole-exome sequencing combined with functional genomics reveals novel candidate driver cancer genes in endometrial cancer." *Genome Res* **22**(11): 2120-2129.

Lieber, M. R. (2010). "The mechanism of double-strand DNA break repair by the nonhomologous DNA end-joining pathway." *Annu Rev Biochem* **79**: 181-211.

Lindahl, T. and D. E. Barnes (2000). "Repair of endogenous DNA damage." *Cold Spring Harb Symp Quant Biol* **65**: 127-133.

Liu, N., A. Balliano and J. J. Hayes (2011). "Mechanism(s) of SWI/SNF-induced nucleosome mobilization." *Chembiochem* **12**(2): 196-204.

Liu, Q. H., S. Guntuku, X. S. Cui, S. Matsuoka, D. Cortez, K. Tamai, G. B. Luo, S. Carattini-Rivera, F. DeMayo, A. Bradley, L. A. Donehower and S. J. Elledge (2000). "Chk1 is an essential kinase that is regulated by Atr and required for the G(2)/M DNA damage checkpoint." *Genes & Development* **14**(12): 1448-1459.

Liu, S., Y. B. Ge, T. T. Wang, H. Edwards, Q. H. Ren, Y. Q. Jiang, C. S. Quan and G. Wang (2017). "Inhibition of ATR potentiates the cytotoxic effect of gemcitabine on pancreatic cancer cells through enhancement of DNA damage and abrogation of ribonucleotide reductase induction by gemcitabine." *Oncology Reports* **37**(6): 3377-3386.

Liu, S. Z., B. Shiotani, M. Lahiri, A. Marechal, A. Tse, C. C. Y. Leung, J. N. M. Glover, X. H. H. Yang and L. Zou (2011). "ATR Autophosphorylation as a Molecular Switch for Checkpoint Activation." *Molecular Cell* **43**(2): 192-202.

Lord, C. J. and A. Ashworth (2012). "The DNA damage response and cancer therapy." *Nature* **481**(7381): 287-294.

Lord, C. J. and A. Ashworth (2017). "PARP inhibitors: Synthetic lethality in the clinic." *Science* **355**(6330): 1152-1158.

Lordick, F., C. Mariette, K. Haustermans, R. Obermannova, D. Arnold and E. G. Committee (2016). "Oesophageal cancer: ESMO Clinical Practice Guidelines for diagnosis, treatment and follow-up." *Ann Oncol* **27**(suppl 5): v50-v57.

Lordick, F. and M. Terashima (2016). "Gastric cancer adjuvant therapy." *Best Pract Res Clin Gastroenterol* **30**(4): 581-591.

Lou, Z., K. Minter-Dykhouse and J. Chen (2005). "BRCA1 participates in DNA decatenation." *Nat Struct Mol Biol* **12**(7): 589-593.

Lowery, W. J., J. M. Schildkraut, L. Akushevich, R. Bentley, J. R. Marks, D. Huntsman and A. Berchuck (2012). "Loss of ARID1A-associated protein expression is a frequent event in clear cell and endometrioid ovarian cancers." *Int J Gynecol Cancer* **22**(1): 9-14.

Luker, K. E., C. M. Pica, R. D. Schreiber and D. Piwnica-Worms (2001). "Overexpression of IRF9 confers resistance to antimicrotubule agents in breast cancer cells." *Cancer Res* **61**(17): 6540-6547.

Lykke-Andersen, J. and E. J. Bennett (2014). "Protecting the proteome: Eukaryotic cotranslational quality control pathways." *J Cell Biol* **204**(4): 467-476.

Lykke-Andersen, S. and T. H. Jensen (2015). "Nonsense-mediated mRNA decay: an intricate machinery that shapes transcriptomes." *Nat Rev Mol Cell Biol* **16**(11): 665-677.

Lyons, S. M., E. Alizadeh, J. Mannheimer, K. Schuamberg, J. Castle, B. Schroder, P. Turk, D. Thamm and A. Prasad (2016). "Changes in cell shape are correlated with metastatic potential in murine and human osteosarcomas." *Biol Open* **5**(3): 289-299.

Ma, J., X. Y. Li, Y. W. Su, J. Y. Zhao, D. A. Luedtke, V. Epshteyn, H. Edwards, G. Wang, Z. H. Wang, R. Chu, J. W. Taub, H. Lin, Y. Wang and Y. B. Ge (2017). "Mechanisms responsible for the synergistic antileukemic interactions between ATR inhibition and cytarabine in acute myeloid leukemia cells." Scientific Reports **7**.

Mahaney, B. L., K. Meek and S. P. Lees-Miller (2009). "Repair of ionizing radiation-induced DNA double-strand breaks by non-homologous end-joining." Biochem J **417**(3): 639-650.

Mali, P., L. Yang, K. M. Esvelt, J. Aach, M. Guell, J. E. DiCarlo, J. E. Norville and G. M. Church (2013). "RNA-guided human genome engineering via Cas9." Science **339**(6121): 823-826.

Marechal, A. and L. Zou (2013). "DNA damage sensing by the ATM and ATR kinases." Cold Spring Harb Perspect Biol **5**(9).

Markkanen, E., B. van Loon, E. Ferrari, J. L. Parsons, G. L. Dianov and U. Hubscher (2012). "Regulation of oxidative DNA damage repair by DNA polymerase lambda and MutYH by cross-talk of phosphorylation and ubiquitination." Proceedings of the National Academy of Sciences of the United States of America **109**(2): 437-442.

Marteijn, J. A., H. Lans, W. Vermeulen and J. H. Hoeijmakers (2014). "Understanding nucleotide excision repair and its roles in cancer and ageing." Nat Rev Mol Cell Biol **15**(7): 465-481.

Masutani, C., K. Sugawara, J. Yanagisawa, T. Sonoyama, M. Ui, T. Enomoto, K. Takio, K. Tanaka, P. J. van der Spek, D. Bootsma and et al. (1994). "Purification and cloning of a nucleotide excision repair complex involving the xeroderma pigmentosum group C protein and a human homologue of yeast RAD23." EMBO J **13**(8): 1831-1843.

Mayne, S. T., M. C. Playdon and C. L. Rock (2016). "Diet, nutrition, and cancer: past, present and future." Nat Rev Clin Oncol **13**(8): 504-515.

McNees, C. J., A. M. Tejera, P. Martinez, M. Murga, F. Mulero, O. Fernandez-Capetillo and M. A. Blasco (2010). "ATR suppresses telomere fragility and recombination but is dispensable for elongation of short telomeres by telomerase." Journal of Cell Biology **188**(5): 639-652.

Mei, Z., Y. W. Shao, P. Lin, X. Cai, B. Wang, Y. Ding, X. Ma, X. Wu, Y. Xia, D. Zhu, Y. Shu, Z. Fu and Y. Gu (2018). "SMAD4 and NF1 mutations as potential biomarkers for poor prognosis to cetuximab-based therapy in Chinese metastatic colorectal cancer patients." BMC Cancer **18**(1): 479.

Miles, L. A., R. J. Garippa and J. T. Poirier (2016). "Design, execution, and analysis of pooled in vitro CRISPR/Cas9 screens." Febs Journal **283**(17): 3170-3180.

Miller, R. E., R. Brough, I. Bajrami, C. T. Williamson, S. McDade, J. Campbell, A. Kigozi, R. Rafiq, H. Pemberton, R. Natrajan, J. Joel, H. Astley, C. Mahoney, J. D. Moore, C. Torrance, J. D. Gordan, J. T. Webber, R. S. Levin, K. M. Shokat, S. Bandyopadhyay, C. J. Lord and A. Ashworth (2016). "Synthetic Lethal Targeting of ARID1A-Mutant Ovarian Clear Cell Tumors with Dasatinib." Mol Cancer Ther **15**(7): 1472-1484.

Min, A., S. A. Im, H. Jang, S. Kim, M. Lee, D. K. Kim, Y. Yang, H. J. Kim, K. H. Lee, J. W. Kim, T. Y. Kim, D. Y. Oh, J. Brown, A. Lau, M. J. O'Connor and Y. J. Bang (2017). "AZD6738, A Novel Oral Inhibitor of ATR, Induces Synthetic Lethality with ATM Deficiency in Gastric Cancer Cells." Molecular Cancer Therapeutics **16**(4): 566-577.

Mohni, K. N., P. S. Thompson, J. W. Luzwick, G. G. Glick, C. S. Pendleton, B. D. Lehmann, J. A. Pietenpol and D. Cortez (2015). "A Synthetic Lethal Screen Identifies DNA Repair Pathways that Sensitize Cancer Cells to Combined ATR Inhibition and Cisplatin Treatments." Plos One **10**(5).

Mordes, D. A. and D. Cortez (2008). "Activation of ATR and related PIKKs." Cell Cycle **7**(18): 2809-2812.

Mordes, D. A., G. G. Glick, R. X. Zhao and D. Cortez (2008). "TopBP1 activates ATR through ATRIP and a PIKK regulatory domain." Genes & Development **22**(11): 1478-1489.

Morimoto, Y., T. Kishida, S. Kotani, K. Takayama and O. Mazda (2018). "Interferon-beta signal may up-regulate PD-L1 expression through IRF9-dependent and independent pathways in lung cancer cells." Biochemical and Biophysical Research Communications **507**(1-4): 330-336.

Morita, T., A. Yamashita, I. Kashima, K. Ogata, S. Ishiura and S. Ohno (2007). "Distant N- and C-terminal domains are required for intrinsic kinase activity of SMG-1, a critical component of nonsense-mediated mRNA decay." Journal of Biological Chemistry **282**(11): 7799-7808.

Murai, J., S. Y. Huang, A. Renaud, Y. Zhang, J. Ji, S. Takeda, J. Morris, B. Teicher, J. H. Doroshov and Y. Pommier (2014). "Stereospecific PARP trapping by BMN 673 and comparison with olaparib and rucaparib." Mol Cancer Ther **13**(2): 433-443.

Myant, K. B., P. Cammareri, M. C. Hodder, J. Wills, A. Von Kriegsheim, B. Gyorffy, M. Rashid, S. Polo, E. Maspero, L. Vaughan, B. Gurung, E. Barry, A. Malliri, F. Camargo, D. J. Adams, A. Iavarone, A. Lasorella and O. J. Sansom (2017). "HUWE1 is a critical colonic tumour suppressor gene that prevents MYC signalling, DNA damage accumulation and tumour initiation." Embo Molecular Medicine **9**(2): 181-197.

Nan, J., Y. Wang, J. Yang and G. R. Stark (2018). "IRF9 and unphosphorylated STAT2 cooperate with NF-kappaB to drive IL6 expression." *Proc Natl Acad Sci U S A* **115**(15): 3906-3911.

Ngoan, L. T., T. Mizoue, Y. Fujino, N. Tokui and T. Yoshimura (2002). "Dietary factors and stomach cancer mortality." *Br J Cancer* **87**(1): 37-42.

Nishida, K., T. Arazoe, N. Yachie, S. Banno, M. Kakimoto, M. Tabata, M. Mochizuki, A. Miyabe, M. Araki, K. Y. Hara, Z. Shimatani and A. Kondo (2016). "Targeted nucleotide editing using hybrid prokaryotic and vertebrate adaptive immune systems." *Science* **353**(6305).

Nozawa, H., E. Oda, S. Ueda, G. Tamura, C. Maesawa, T. Muto, T. Taniguchi and N. Tanaka (1998). "Functionally inactivating point mutation in the tumor-suppressor IRF-1 gene identified in human gastric cancer." *International Journal of Cancer* **77**(4): 522-527.

O'Carrigan, B., M. J. D. M. Luken, D. Papadatos-Pastos, J. Brown, N. Tunariu, R. P. Lopez, M. Ganegoda, R. Riisnaes, I. Figueiredo, S. Carreira, B. Hare, F. Yang, K. McDermott, M. S. Penney, J. Pollard, J. S. Lopez, U. Banerji, J. S. De Bono, S. Z. Fields and T. A. Yap (2016). "Phase I trial of a first-in-class ATR inhibitor VX-970 as monotherapy (mono) or in combination (combo) with carboplatin (CP) incorporating pharmacodynamics (PD) studies." *Journal of Clinical Oncology* **34**(15).

O'Driscoll, M., V. L. Ruiz-Perez, C. G. Woods, P. A. Jeggo and J. A. Goodship (2003). "A splicing mutation affecting expression of ataxia-telangiectasia and Rad3-related protein (ATR) results in Seckel syndrome." *Nature Genetics* **33**(4): 497-501.

Ogasawara, S., G. Tamura, C. Maesawa, Y. Suzuki, K. Ishida, N. Satoh, N. Uesugi, K. Saito and R. Satodate (1996). "Common deleted region on the long arm of chromosome 5 in esophageal carcinoma." *Gastroenterology* **110**(1): 52-57.

Ogiwara, H., A. Ui, B. Shiotani, L. Zou, A. Yasui and T. Kohno (2013). "Curcumin suppresses multiple DNA damage response pathways and has potency as a sensitizer to PARP inhibitor." *Carcinogenesis* **34**(11): 2486-2497.

Okines, A., I. Chau and D. Cunningham (2008). "Capecitabine in gastric cancer." *Drugs Today (Barc)* **44**(8): 629-640.

Orywal, K. and M. Szmikowski (2017). "Alcohol dehydrogenase and aldehyde dehydrogenase in malignant neoplasms." *Clin Exp Med* **17**(2): 131-139.

Pagin, A., F. Zerimech, J. Leclerc, A. Wacrenier, S. Lejeune, C. Descarpentries, F. Escande, N. Porchet and M. P. Buisine (2013). "Evaluation of a new panel of six mononucleotide repeat markers for the detection of DNA mismatch repair-deficient tumours." *Br J Cancer* **108**(10): 2079-2087.

Pardo, B., B. Gomez-Gonzalez and A. Aguilera (2009). "DNA repair in mammalian cells: DNA double-strand break repair: how to fix a broken relationship." *Cell Mol Life Sci* **66**(6): 1039-1056.

Parsons, J. L., P. S. Tait, D. Finch, I. I. Dianova, M. J. Edelmann, S. V. Khoronenkova, B. M. Kessler, R. A. Sharma, W. G. McKenna and G. L. Dianov (2009). "Ubiquitin ligase ARF-BP1/Mule modulates base excision repair." *Embo Journal* **28**(20): 3207-3215.

Patil, D. T., M. P. Bronner, B. P. Portier, C. R. Fraser, T. P. Plesec and X. Liu (2012). "A five-marker panel in a multiplex PCR accurately detects microsatellite instability-high colorectal tumors without control DNA." *Diagn Mol Pathol* **21**(3): 127-133.

Peasland, A., L. Z. Wang, E. Rowling, S. Kyle, T. Chen, A. Hopkins, W. A. Cliby, J. Sarkaria, G. Beale, R. J. Edmondson and N. J. Curtin (2011). "Identification and evaluation of a potent novel ATR inhibitor, NU6027, in breast and ovarian cancer cell lines." *British Journal of Cancer* **105**(3): 372-381.

Peterson, R. T., P. A. Beal, M. J. Comb and S. L. Schreiber (2000). "FKBP12-rapamycin-associated protein (FRAP) autophosphorylates at serine 2481 under translationally repressive conditions." *J Biol Chem* **275**(10): 7416-7423.

Pettitt, S. J., D. B. Krastev, I. Brandsma, A. Drean, F. Song, R. Aleksandrov, M. I. Harrell, M. Menon, R. Brough, J. Campbell, J. Frankum, M. Raney, H. N. Pemberton, R. Rafiq, K. Fenwick, A. Swain, S. Guettler, J. M. Lee, E. M. Swisher, S. Stoyanov, K. Yusa, A. Ashworth and C. J. Lord (2018). "Genome-wide and high-density CRISPR-Cas9 screens identify point mutations in PARP1 causing PARP inhibitor resistance." *Nat Commun* **9**(1): 1849.

Pietrantonio, F., G. Fuca, F. Morano, A. Gloghini, S. Corso, G. Aprile, F. Perrone, F. De Vita, E. Tamborini, G. Tomasello, A. V. Gualeni, E. Ongaro, A. Busico, E. Giommoni, C. C. Volpi, M. M. Laterza, S. Corallo, M. Prisciandaro, M. Antista, A. Pellegrinelli, L. Castagnoli, S. M. Pupa, G. Pruneri, F. de Braud, S. Giordano, C. Cremolini and M. Di Bartolomeo (2018). "Biomarkers of Primary Resistance to Trastuzumab in HER2-Positive Metastatic Gastric Cancer Patients: the AMNESIA Case-Control Study." *Clin Cancer Res* **24**(5): 1082-1089.

Pimenta, E. M. and B. J. Barnes (2013). "Loss of interferon regulatory factor 5 expression in breast cancer alters the tumor microenvironment to promote metastasis." *Cancer Research* **73**.

Platanias, L. C. (2005). "Mechanisms of type-I- and type-II-interferon-mediated signalling." *Nature Reviews Immunology* **5**(5): 375-386.

Plummer, M., S. Franceschi, J. Vignat, D. Forman and C. de Martel (2015). "Global burden of gastric cancer attributable to *Helicobacter pylori*." *Int J Cancer* **136**(2): 487-490.

Pompili, L., M. Porru, C. Caruso, A. Biroccio and C. Leonetti (2016). "Patient-derived xenografts: a relevant preclinical model for drug development." *J Exp Clin Cancer Res* **35**(1): 189.

Popp, M. W. and L. E. Maquat (2013). "Organizing principles of mammalian nonsense-mediated mRNA decay." *Annu Rev Genet* **47**: 139-165.

Prevo, R., E. Fokas, P. M. Reaper, P. A. Charlton, J. R. Pollard, W. G. McKenna, R. J. Muschel and T. B. Brunner (2012). "The novel ATR inhibitor VE-821 increases sensitivity of pancreatic cancer cells to radiation and chemotherapy." *Cancer Biology & Therapy* **13**(11): 1072-1081.

Ran, F. A., P. D. Hsu, J. Wright, V. Agarwala, D. A. Scott and F. Zhang (2013). "Genome engineering using the CRISPR-Cas9 system." *Nat Protoc* **8**(11): 2281-2308.

Rao, Q., M. Liu, Y. Tian, Z. Wu, Y. Hao, L. Song, Z. Qin, C. Ding, H. W. Wang, J. Wang and Y. Xu (2018). "Cryo-EM structure of human ATR-ATRIP complex." *Cell Res* **28**(2): 143-156.

Rao, S., N. Starling, D. Cunningham, M. Benson, A. Wotherspoon, C. Lupfert, R. Kurek, J. Oates, J. Baselga and A. Hill (2008). "Phase I study of epirubicin, cisplatin and capecitabine plus matuzumab in previously untreated patients with advanced oesophagogastric cancer." *Br J Cancer* **99**(6): 868-874.

Reaper, P. M., M. R. Griffiths, J. M. Long, J. D. Charrier, S. MacCormick, P. A. Charlton, J. M. C. Golec and J. R. Pollard (2011). "Selective killing of ATM- or p53-deficient cancer cells through inhibition of ATR." *Nature Chemical Biology* **7**(7): 428-430.

Reisman, D., S. Glaros and E. A. Thompson (2009). "The SWI/SNF complex and cancer." *Oncogene* **28**(14): 1653-1668.

Reyal, F., C. Guyader, C. Decraene, C. Lucchesi, N. Auger, F. Assayag, L. De Plater, D. Gentien, M. F. Poupon, P. Cottu, P. De Cremoux, P. Gestraud, A. Vincent-Salomon, J. J. Fontaine, S. Roman-Roman, O. Delattre, D. Decaudin and E. Marangoni (2012). "Molecular profiling of patient-derived breast cancer xenografts." *Breast Cancer Res* **14**(1): R11.

Robertson, A. B., A. Klungland, T. Rognes and I. Leiros (2009). "DNA repair in mammalian cells: Base excision repair: the long and short of it." *Cell Mol Life Sci* **66**(6): 981-993.

Roumeliotis, T. I., S. P. Williams, E. Goncalves, C. Alsinet, M. Del Castillo Velasco-Herrera, N. Aben, F. Z. Ghavidel, M. Michaut, M. Schubert, S. Price, J. C. Wright, L. Yu, M. Yang, R. Dienstmann, J. Guinney, P. Beltrao, A. Brazma, M. Pardo, O. Stegle, D. J. Adams, L. Wessels, J. Saez-Rodriguez, U. McDermott and J. S. Choudhary (2017). "Genomic Determinants of Protein Abundance Variation in Colorectal Cancer Cells." *Cell Rep* **20**(9): 2201-2214.

Rubinson, E. H., A. S. Gowda, T. E. Spratt, B. Gold and B. F. Eichman (2010). "An unprecedented nucleic acid capture mechanism for excision of DNA damage." *Nature* **468**(7322): 406-411.

Ruiz, S., C. Mayor-Ruiz, V. Lafarga, M. Murga, M. Vega-Sendino, S. Ortega and O. Fernandez-Capetillo (2016). "A Genome-wide CRISPR Screen Identifies CDC25A as a Determinant of Sensitivity to ATR Inhibitors." *Mol Cell* **62**(2): 307-313.

Ryan, C. J., I. Bajrami and C. J. Lord (2018). "Synthetic Lethality and Cancer - Penetrance as the Major Barrier." *Trends Cancer* **4**(10): 671-683.

Saldivar, J. C., S. Hamperl, M. J. Bocek, M. Chung, T. E. Bass, F. Cisneros-Soberanis, K. Samejima, L. Xie, J. R. Paulson, W. C. Earnshaw, D. Cortez, T. Meyer and K. A. Cimprich (2018). "An intrinsic S/G2 checkpoint enforced by ATR." *Science* **361**(6404): 806-810.

Sale, J. E., A. R. Lehmann and R. Woodgate (2012). "Y-family DNA polymerases and their role in tolerance of cellular DNA damage." *Nat Rev Mol Cell Biol* **13**(3): 141-152.

Samartzis, E. P., K. Gutsche, K. J. Dedes, D. Fink, M. Stucki and P. Imesch (2014). "Loss of ARID1A expression sensitizes cancer cells to PI3K- and AKT-inhibition." *Oncotarget* **5**(14): 5295-5303.

Samartzis, E. P., A. Noske, K. J. Dedes, D. Fink and P. Imesch (2013). "ARID1A mutations and PI3K/AKT pathway alterations in endometriosis and endometriosis-associated ovarian carcinomas." *Int J Mol Sci* **14**(9): 18824-18849.

Sarris, P. F., E. A. Trantas, D. A. Baltrus, C. T. Bull, W. P. Wechter, S. C. Yan, F. Ververidis, N. F. Almeida, C. D. Jones, J. L. Dangl, N. J. Panopoulos, B. A. Vinatzer and D. E. Goumas (2013). "Comparative Genomics of Multiple Strains of *Pseudomonas cannabina* pv. *alisalensis*, a Potential Model Pathogen of Both Monocots and Dicots." *Plos One* **8**(3).

Schultz, N., E. Lopez, N. Saleh-Gohari and T. Helleday (2003). "Poly(ADP-ribose) polymerase (PARP-1) has a controlling role in homologous recombination." *Nucleic Acids Res* **31**(17): 4959-4964.

Sclafani, F., G. Brown, D. Cunningham, A. Wotherspoon, D. Tait, C. Peckitt, J. Evans, S. Yu, L. Sena Teixeira Mendes, J. Taberero, B. Glimelius, A. Cervantes, J. Thomas, R. Begum, J. Oates and I. Chau (2016). "PAN-EX: a pooled analysis of two trials of neoadjuvant chemotherapy followed by chemoradiotherapy in MRI-defined, locally advanced rectal cancer." *Ann Oncol* **27**(8): 1557-1565.

Shain, A. H. and J. R. Pollack (2013). "The Spectrum of SWI/SNF Mutations, Ubiquitous in Human Cancers." *Plos One* **8**(1).

Shain, A. H. and J. R. Pollack (2013). "The spectrum of SWI/SNF mutations, ubiquitous in human cancers." *PLoS One* **8**(1): e55119.

Shapiro, G., R. Wesolowski, M. Middleton, C. Devoe, A. Constantinidou, D. Papadatos-Pastos, M. Fricano, Y. Q. Zhang, S. Karan, J. Pollard, M. Penney, M. Asmal, F. G. Renshaw, S. Z. Fields and T. A. Yap (2016). "Phase 1 trial of first-in-class ATR inhibitor VX-970 in combination with cisplatin (Cis) in patients (pts) with advanced solid tumors (NCT02157792)." *Cancer Research* **76**.

Sharma, S., C. M. Helchowski and C. E. Canman (2013). "The roles of DNA polymerase zeta and the Y family DNA polymerases in promoting or preventing genome instability." *Mutat Res* **743-744**: 97-110.

Shen, J., Z. Ju, W. Zhao, L. Wang, Y. Peng, Z. Ge, Z. D. Nagel, J. Zou, C. Wang, P. Kapoor, X. Ma, D. Ma, J. Liang, S. Song, J. Liu, L. D. Samson, J. A. Ajani, G. M. Li, H. Liang, X. Shen, G. B. Mills and G. Peng (2018). "ARID1A deficiency promotes mutability and potentiates therapeutic antitumor immunity unleashed by immune checkpoint blockade." *Nat Med* **24**(5): 556-562.

Shen, J., Y. Peng, L. Wei, W. Zhang, L. Yang, L. Lan, P. Kapoor, Z. Ju, Q. Mo, M. Shih le, I. P. Uray, X. Wu, P. H. Brown, X. Shen, G. B. Mills and G. Peng (2015). "ARID1A Deficiency Impairs the DNA Damage Checkpoint and Sensitizes Cells to PARP Inhibitors." *Cancer Discov* **5**(7): 752-767.

Shen, Y., M. Aoyagi-Scharber and B. Wang (2015). "Trapping Poly(ADP-Ribose) Polymerase." *J Pharmacol Exp Ther* **353**(3): 446-457.

Sohn, J., K. Kristjansdottir, A. Safi, B. Parker, B. Kiburz and J. Rudolph (2004). "Remote hot spots mediate protein substrate recognition for the Cdc25 phosphatase." *Proc Natl Acad Sci U S A* **101**(47): 16437-16441.

Sondka, Z., S. Bamford, C. G. Cole, S. A. Ward, I. Dunham and S. A. Forbes (2018). "The COSMIC Cancer Gene Census: describing genetic dysfunction across all human cancers." *Nat Rev Cancer* **18**(11): 696-705.

Spagnolo, L., A. Rivera-Calzada, L. H. Pearl and O. Llorca (2006). "Three-dimensional structure of the human DNA-PKcs/Ku70/Ku80 complex assembled on DNA and its implications for DNA DSB repair." *Molecular Cell* **22**(4): 511-519.

Stan, R., M. M. McLaughlin, R. Cafferkey, R. K. Johnson, M. Rosenberg and G. P. Livi (1994). "Interaction between FKBP12-rapamycin and TOR involves a conserved serine residue." *J Biol Chem* **269**(51): 32027-32030.

Stracker, T. H. and J. H. Petrini (2011). "The MRE11 complex: starting from the ends." *Nat Rev Mol Cell Biol* **12**(2): 90-103.

Streppel, M. M., S. Lata, M. DelaBastide, E. A. Montgomery, J. S. Wang, M. I. Canto, A. M. Macgregor-Das, S. Pai, F. H. Morsink, G. J. Offerhaus, E. Antoniou, A. Maitra and W. R. McCombie (2014). "Next-generation sequencing of endoscopic biopsies identifies ARID1A as a tumor-suppressor gene in Barrett's esophagus." *Oncogene* **33**(3): 347-357.

Sugiyama, T., E. M. Zaitseva and S. C. Kowalczykowski (1997). "A single-stranded DNA-binding protein is needed for efficient presynaptic complex formation by the *Saccharomyces cerevisiae* Rad51 protein." *J Biol Chem* **272**(12): 7940-7945.

Sun, X., S. C. Wang, Y. Wei, X. Luo, Y. Jia, L. Li, P. Gopal, M. Zhu, I. Nassour, J. C. Chuang, T. Maples, C. Celen, L. H. Nguyen, L. Wu, S. Fu, W. Li, L. Hui, F. Tian, Y. Ji, S. Zhang, M. Sorouri, T. H. Hwang, L. Letzig, L. James, Z. Wang, A. C. Yopp, A. G. Singal and H. Zhu (2018). "Arid1a Has Context-Dependent Oncogenic and Tumor Suppressor Functions in Liver Cancer." *Cancer Cell* **33**(1): 151-152.

Sundar, R., J. Brown, A. I. Russo and T. A. Yap (2017). "Targeting ATR in cancer medicine." *Current Problems in Cancer* **41**(4): 302-315.

Takahashi, T., K. Hara, H. Inoue, Y. Kawa, C. Tokunaga, S. Hidayat, K. Yoshino, Y. Kuroda and K. Yonezawa (2000). "Carboxyl-terminal region conserved among phosphoinositide-kinase-related kinases is indispensable for mTOR function in vivo and in vitro (vol 5, pg 765, 2000)." *Genes to Cells* **5**(11): 949-952.

Tamura, G., S. Ogasawara, S. Nishizuka, K. Sakata, C. Maesawa, Y. Suzuki, M. Terashima, K. Saito and R. Satodate (1996). "Two distinct regions of deletion on the long arm of chromosome 5 in differentiated adenocarcinomas of the stomach." *Cancer Research* **56**(3): 612-615.

Tanaka, A., S. Weinel, N. Nagy, M. O'Driscoll, J. E. Lai-Cheong, C. L. Kulp-Shorten, A. Knable, G. Carpenter, S. A. Fisher, M. Hiragun, Y. Yanase, M. Hide, J. Callen and J. A. McGrath (2012). "Germline mutation in ATR in autosomal-dominant oropharyngeal cancer syndrome." *Am J Hum Genet* **90**(3): 511-517.

Tentler, J. J., A. C. Tan, C. D. Weekes, A. Jimeno, S. Leong, T. M. Pitts, J. J. Arcaroli, W. A. Messersmith and S. G. Eckhardt (2012). "Patient-derived tumour xenografts as models for oncology drug development." *Nat Rev Clin Oncol* **9**(6): 338-350.

Tutt, A. N., C. J. Lord, N. McCabe, H. Farmer, N. Turner, N. M. Martin, S. P. Jackson, G. C. Smith and A. Ashworth (2005). "Exploiting the DNA repair defect in BRCA mutant cells in the design of new therapeutic strategies for cancer." *Cold Spring Harb Symp Quant Biol* **70**: 139-148.

Tzelepis, K., H. Koike-Yusa, E. De Braekeleer, Y. Li, E. Metzakopian, O. M. Dovey, A. Mupo, V. Grinkevich, M. Li, M. Mazan, M. Gozdecka, S. Ohnishi, J. Cooper, M. Patel, T. McKerrell, B. Chen, A. F. Domingues, P. Gallipoli, S. Teichmann, H. Ponstingl, U. McDermott, J. Saez-Rodriguez, B. J. P. Huntly, F. Iorio, C. Pina, G. S. Vassiliou and K. Yusa (2016). "A CRISPR Dropout Screen Identifies Genetic Vulnerabilities and Therapeutic Targets in Acute Myeloid Leukemia." *Cell Rep* **17**(4): 1193-1205.

Van Cutsem, E., Y. J. Bang, F. Feng-Yi, J. M. Xu, K. W. Lee, S. C. Jiao, J. L. Chong, R. I. Lopez-Sanchez, T. Price, O. Gladkov, O. Stoss, J. Hill, V. Ng, M. Lehle, M. Thomas, A. Kiermaier and J. Ruschoff (2015). "HER2 screening data from ToGA: targeting HER2 in gastric and gastroesophageal junction cancer." *Gastric Cancer* **18**(3): 476-484.

Vendetti, F. P., A. Lau, S. Schamus, T. P. Conrads, M. J. O'Connor and C. J. Bakkenist (2015). "The orally active and bioavailable ATR kinase inhibitor AZD6738 potentiates the anti-tumor effects of cisplatin to resolve ATM-deficient non-small cell lung cancer in vivo." *Oncotarget* **6**(42): 44289-44305.

Wakasugi, M., A. Kawashima, H. Morioka, S. Linn, A. Sancar, T. Mori, O. Nikaido and T. Matsunaga (2002). "DDB accumulates at DNA damage sites immediately after UV irradiation and directly stimulates nucleotide excision repair." *J Biol Chem* **277**(3): 1637-1640.

Wang, C., G. Wang, X. Feng, P. Shepherd, J. Zhang, M. Tang, Z. Chen, M. Srivastava, M. E. McLaughlin, N. M. Navone, G. T. Hart and J. Chen (2018). "Genome-wide CRISPR screens reveal synthetic lethality of RNASEH2 deficiency and ATR inhibition." *Oncogene*.

Wang, D., C. Li, Y. Zhang, M. Wang, N. Jiang, L. Xiang, T. Li, T. M. Roberts, J. J. Zhao, H. Cheng and P. Liu (2016). "Combined inhibition of PI3K and PARP is effective in the treatment of ovarian cancer cells with wild-type PIK3CA genes." *Gynecol Oncol* **142**(3): 548-556.

Wang, D., M. Wang, N. Jiang, Y. Zhang, X. Bian, X. Wang, T. M. Roberts, J. J. Zhao, P. Liu and H. Cheng (2016). "Effective use of PI3K inhibitor BKM120 and PARP inhibitor Olaparib to treat PIK3CA mutant ovarian cancer." *Oncotarget* **7**(11): 13153-13166.

Wang, K., J. Kan, S. T. Yuen, S. T. Shi, K. M. Chu, S. Law, T. L. Chan, Z. Kan, A. S. Chan, W. Y. Tsui, S. P. Lee, S. L. Ho, A. K. Chan, G. H. Cheng, P. C. Roberts, P. A. Rejto, N. W. Gibson, D. J. Pocalyko, M. Mao, J. Xu and S. Y. Leung (2011). "Exome sequencing identifies frequent mutation of ARID1A in molecular subtypes of gastric cancer." *Nat Genet* **43**(12): 1219-1223.

Wang, T., J. J. Wei, D. M. Sabatini and E. S. Lander (2014). "Genetic screens in human cells using the CRISPR-Cas9 system." *Science* **343**(6166): 80-84.

Wang, X., N. G. Nagl, Jr., S. Flowers, D. Zweitzig, P. B. Dallas and E. Moran (2004). "Expression of p270 (ARID1A), a component of human SWI/SNF complexes, in human tumors." *Int J Cancer* **112**(4): 636.

Wang, X. Z., G. Lu, L. Li, Y. A. Juan, K. W. Yan, Y. Q. Wang, B. L. Zhu, J. Y. Kuang, M. Lin, S. Zhang and G. Z. Shao (2014). "HUWE1 interacts with BRCA1 and promotes its degradation in the ubiquitin-proteasome pathway." *Biochemical and Biophysical Research Communications* **444**(3): 290-295.

Wang, X. Z., G. Lu, L. Li, J. Yi, K. W. Yan, Y. Q. Wang, B. L. Zhu, J. Y. Kuang, M. Lin, S. Zhang and G. Z. Shao (2014). "HUWE1 interacts with BRCA1 and promotes its degradation in the ubiquitin-proteasome pathway." *Biochemical and Biophysical Research Communications* **444**(4): 549-554.

Weigelt, B., I. Comino-Mendez, I. de Bruijn, L. Tian, J. L. Meisel, I. Garcia-Murillas, C. Fribbens, R. Cutts, L. G. Martelotto, C. K. Y. Ng, R. S. Lim, P. Selenica, S. Piscuoglio, C. Aghajanian, L. Norton, R. Murali, D. M. Hyman, L. Borsu, M. E. Arcila, J. Konner, J. S. Reis, R. A. Greenberg, M. E. Robson and N. C. Turner (2017). "Diverse BRCA1 and BRCA2 Reversion Mutations in Circulating Cell-Free DNA of Therapy-Resistant Breast or Ovarian Cancer." *Clinical Cancer Research* **23**(21): 6708-6720.

Wiegand, K. C., S. P. Shah, O. M. Al-Agha, Y. Zhao, K. Tse, T. Zeng, J. Senz, M. K. McConechy, M. S. Anglesio, S. E. Kalloger, W. Yang, A. Heravi-Moussavi, R. Giuliany, C. Chow, J. Fee, A. Zayed, L. Prentice, N. Melnyk, G. Turashvili, A. D. Delaney, J. Madore, S. Yip, A. W. McPherson, G. Ha, L. Bell, S. Fereday, A. Tam, L. Galletta, P. N. Tonin, D. Provencher, D. Miller, S. J. Jones, R. A. Moore, G. B. Morin, A. Oloumi, N. Boyd, S. A. Aparicio, M. Shih, A. M. Mes-Masson, D. D. Bowtell, M. Hirst, B. Gilks, M. A. Marra and D. G. Huntsman (2010). "ARID1A mutations in endometriosis-associated ovarian carcinomas." *N Engl J Med* **363**(16): 1532-1543.

Wilke, H., K. Muro, E. Van Cutsem, S. C. Oh, G. Bodoky, Y. Shimada, S. Hironaka, N. Sugimoto, O. Lipatov, T. Y. Kim, D. Cunningham, P. Rougier, Y. Komatsu, J. Ajani, M. Emig, R. Carlesi, D. Ferry, K.

Chandrawansa, J. D. Schwartz, A. Ohtsu and R. S. Group (2014). "Ramucirumab plus paclitaxel versus placebo plus paclitaxel in patients with previously treated advanced gastric or gastro-oesophageal junction adenocarcinoma (RAINBOW): a double-blind, randomised phase 3 trial." Lancet Oncol **15**(11): 1224-1235.

Williams, R. S., J. S. Williams and J. A. Tainer (2007). "Mre11-Rad50-Nbs1 is a keystone complex connecting DNA repair machinery, double-strand break signaling, and the chromatin template." Biochem Cell Biol **85**(4): 509-520.

Williamson, C. T., R. Miller, H. N. Pemberton, S. E. Jones, J. Campbell, A. Konde, N. Badham, R. Rafiq, R. Brough, A. Gulati, C. J. Ryan, J. Francis, P. B. Vermulen, A. R. Reynolds, P. M. Reaper, J. R. Pollard, A. Ashworth and C. J. Lord (2016). "ATR inhibitors as a synthetic lethal therapy for tumours deficient in ARID1A." Nat Commun **7**: 13837.

Willman, C. L., C. E. Sever, M. G. Pallavicini, H. Harada, N. Tanaka, M. L. Slovak, H. Yamamoto, K. Harada, T. C. Meeker, A. F. List and T. Taniguchi (1993). "Deletion of Irf-1, Mapping to Chromosome 5q31.1 in Human Leukemia and Preleukemic Myelodysplasia." Science **259**(5097): 968-971.

Wong, L. H., K. G. Krauer, I. Hatzinisiriou, M. J. Estcourt, P. Hersey, N. D. Tam, S. Edmondson, R. J. Devenish and S. J. Ralph (1997). "Interferon-resistant human melanoma cells are deficient in ISGF3 components, STAT1, STAT2, and p48-ISGF3 gamma." Journal of Biological Chemistry **272**(45): 28779-28785.

Wu, J. N. and C. W. Roberts (2013). "ARID1A mutations in cancer: another epigenetic tumor suppressor?" Cancer Discov **3**(1): 35-43.

Wu, R. C., T. L. Wang and M. Shih le (2014). "The emerging roles of ARID1A in tumor suppression." Cancer Biol Ther **15**(6): 655-664.

Wu, S., R. Zhang and B. G. Bitler (2016). "Arid1a controls tissue regeneration." Stem Cell Investig **3**: 35.

Wyman, C. and R. Kanaar (2006). "DNA double-strand break repair: all's well that ends well." Annu Rev Genet **40**: 363-383.

Yamamoto, S., H. Tsuda, M. Takano, S. Tamai and O. Matsubara (2012). "PIK3CA mutations and loss of ARID1A protein expression are early events in the development of cystic ovarian clear cell adenocarcinoma." Virchows Arch **460**(1): 77-87.

Yang, D., D. M. Cheng, Q. Tu, H. H. Yang, B. Sun, L. Z. Yan, H. J. Dai, J. R. Luo, B. Y. Mao, Y. Cao, X. P. Yu, H. Jiang and X. D. Zhao (2018). "HUWE1 controls the development of non-small cell lung cancer through down-regulation of p53." Theranostics **8**(13): 3517-3529.

Yang, D., B. Sun, X. H. Zhang, D. M. Cheng, X. P. Yu, L. Z. Yan, L. Li, S. Q. An, H. Jiang, A. Lasorella, A. Iavarone, S. Zhang, F. D. Zou and X. D. Zhao (2017). "Huwe1 Sustains Normal Ovarian Epithelial Cell Transformation and Tumor Growth through the Histone H1.3-H19 Cascade." Cancer Research **77**(18): 4773-4784.

Yang, L., G. Yang, Y. Ding, Y. Huang, S. Liu, L. Zhou, W. Wei, J. Wang and G. Hu (2018). "Combined treatment with PI3K inhibitor BKM120 and PARP inhibitor olaparib is effective in inhibiting the gastric cancer cells with ARID1A deficiency." Oncol Rep **40**(1): 479-487.

Yap, T. A., M. G. Krebs, S. Postel-Vinay, Y. J. Bang, A. El-Khoueiry, W. Abida, K. Harrington, R. Sundar, L. Carter, E. Castanon-Alvarez, S. A. Im, A. Berges, M. Khan, C. Stephens, G. Ross and J. C. Soria (2016). "Phase I modular study of AZD6738, a novel oral, potent and selective ataxia telangiectasia Rad3-related (ATR) inhibitor in combination (combo) with carboplatin, olaparib or durvalumab in patients (pts) with advanced cancers." European Journal of Cancer **69**: S2-S2.

Yazinski, S. A., V. Comaills, R. Buisson, M. M. Genois, H. D. Nguyen, C. K. Ho, T. T. Kwan, R. Morris, S. Lauffer, A. Nussenzweig, S. Ramaswamy, C. H. Benes, D. A. Haber, S. Maheswaran, M. J. Birrer and L. Zou (2017). "ATR inhibition disrupts rewired homologous recombination and fork protection pathways in PARP inhibitor-resistant BRCA-deficient cancer cells." Genes & Development **31**(3): 318-332.

You, Z. S., C. Chahwan, J. Bailis, T. Hunter and P. Russell (2005). "ATM activation and its recruitment to damaged DNA require binding to the C terminus of Nbs1." Molecular and Cellular Biology **25**(13): 5363-5379.

Zang, Z. J., I. Cutcutache, S. L. Poon, S. L. Zhang, J. R. McPherson, J. Tao, V. Rajasegaran, H. L. Heng, N. Deng, A. Gan, K. H. Lim, C. K. Ong, D. Huang, S. Y. Chin, I. B. Tan, C. C. Ng, W. Yu, Y. Wu, M. Lee, J. Wu, D. Poh, W. K. Wan, S. Y. Rha, J. So, M. Salto-Tellez, K. G. Yeoh, W. K. Wong, Y. J. Zhu, P. A. Futreal, B. Pang, Y. Ruan, A. M. Hillmer, D. Bertrand, N. Nagarajan, S. Rozen, B. T. Teh and P. Tan (2012). "Exome sequencing of gastric adenocarcinoma identifies recurrent somatic mutations in cell adhesion and chromatin remodeling genes." Nat Genet **44**(5): 570-574.

Zhang, Q., H. B. Yan, J. Wang, S. J. Cui, X. Q. Wang, Y. H. Jiang, L. Feng, P. Y. Yang and F. Liu (2016). "Chromatin remodeling gene AT-rich interactive domain-containing protein 1A suppresses gastric cancer cell proliferation by targeting PIK3CA and PDK1." Oncotarget **7**(29): 46127-46141.

Zhang, S. L., D. Pan, X. M. Jia, X. Lin and X. Q. Zhao (2017). "The CARMA3-BCL10-MALT1 (CBM) complex contributes to DNA damage-induced NF-kappa B activation and cell survival." Protein & Cell **8**(11): 856-860.

Zhao, X., D. D'Arca, W. K. Lim, M. Brahmachary, M. S. Carro, T. Ludwig, C. C. Cardo, F. Guillemot, K. Aldape, A. Califano, A. Iavarone and A. Lasorella (2009). "The N-Myc-DLL3 Cascade Is Suppressed by the Ubiquitin Ligase Huwe1 to Inhibit Proliferation and Promote Neurogenesis in the Developing Brain." Developmental Cell **17**(2): 210-221.

Zhao, X. D., J. I. T. Heng, D. Guardavaccaro, R. Jiang, M. Pagano, F. Guillemot, A. Iavarone and A. Lasorella (2008). "The HECT-domain ubiquitin ligase Huwe1 controls neural differentiation and proliferation by destabilizing the N-Myc oncoprotein." Nature Cell Biology **10**(6): 643-653.

Zhong, Q., W. H. Gao, F. H. Du and X. D. Wang (2005). "Mule/ARF-BP1, a BH3-only E3 ubiquitin ligase, catalyzes the polyubiquitination of Mcl-1 and regulates apoptosis." Cell **121**(7): 1085-1095.

Zhou, B. B. and S. J. Elledge (2000). "The DNA damage response: putting checkpoints in perspective." Nature **408**(6811): 433-439.

Appendix

Supplementary Table 1. sgRNA and target genes used in the genome-wide screen validation experiment. Highlighted in red, the sgRNA used in (Mayor-Ruiz et al., 2016)

Gene	sgRNA sequence
HUWE1-1	GCTCTGACGCGTAAGTGAC
HUWE1-2	ATCGGGGAGATCCTGATCC
HUWE1-3	CAAGCGTGCGATTCACTGC
HUWE1-4	TGTAGCCGAGTTAGCAGCG
HUWE1-5	TCCATCGAAGCGGTCCAAC
SMG8-1	AATACGGTGTGCGACCGAC
SMG8-2	CCGGAAGATTCTATAGATC
SMG8-3	GCTTTCGTGTACATAGTAC
SMG8-4	GGTCCAGCAACATACCTAC
SMG8-5	TCATCACCTGGTATCGCCT
HNRNPF-1	TCTAGGGAAACACAAGGAG
HNRNPF-2	TTCCTTTGTGCATCCAAAT
HNRNPF-3	AAGTCCCACAGAACCGAGA
HNRNPF-4	AAAAAGACAGGGAAAGCAT
HNRNPF-5	CTGACTGCACGATTCATGA
IRF9-1	GGCCCTTTCACCTTGAAGA
IRF9-2	AAGAGTTCTGAATTTAAGG
IRF9-3	TGTATCAGTTGCTGCCACC
IRF9-4	TACATTATTGAGGGAGTCC
IRF9-5	TGGTACCTTCCTGTGGCTC
CDC25B-1	AGACCATGCACGACCTCGC
CDC25B-2	TGCCCGTTCGAGACAGGGAT
CDC25B-3	TCACGTCTGCTCCGCCATG
CDC25B-4	TACTTTCGAATGATCCGGC
CDC25B-5	GACACTCACCGGCATAGAC
STAT2-1	AAACTTTGACCCCGAGAA
STAT2-2	TTCACCGTCCGAACAAGGT
STAT2-3	GTGGACCTACGCAACGCCC
STAT2-4	TGCTTCCGATATAAGATCC
STAT2-5	GAGATTGAATCCCGGATCC
SMG9-1	ACTCACGGTCCATGGCTGC
SMG9-2	GAACGATGGGCTTCTCCAG
SMG9-3	AGGGACTACATTGCACCAT
SMG9-4	GCGCTGAAATGAAGGAACG
SMG9-5	GGACCCCTCGGTACCTCGA
CARD10-1	GGCCATCCAGAGCCGTGAC

CARD10-2	GCGGCTGACGGCGTCACTG
CARD10-3	GGTGCGGTTGACGCGGCAC
CARD10-4	TGCCGGGTCATCGACGAGC
CARD10-5	AATCGAGGGCGTCCGGCAT
CSTF2T-1	TCAGCAGAACATTAGGTCC
CSTF2T-2	GATCGATGGGATCCCCATA
CSTF2T-3	AGTCAATAATGGGCGCTGC
CSTF2T-4	ATGCGGAACCTCAATGGGC
CSTF2T-5	CTCTCTATCGTATAACCAGC
ARHGAP22-1	CCTAACATTCTGCGGCCAC
ARHGAP22-2	AGTCCTCGTACCTGGCGAA
ARHGAP22-3	ACAACAGACGTGCACACGG
ARHGAP22-4	CGGAAGTATGGCCCCCGCC
ARHGAP22-5	GCCCAGATGACTCGGCGGA
CCDC7-1	CCATTATCACCTGAGCTAA
CCDC7-2	GGCAAAGCATAACCGTAAAA
CCDC7-3	TTGTCTTACTCGATGGAAT
CCDC7-4	ATGGACATTGCGATCAGAA
CCDC7-5	GACAACATGACTTTCACGG
WDFY4-1	TATTGCTACTCCTCGAGTC
WDFY4-2	TCCGCTACACTGGTGATAG
WDFY4-3	GTCAGTGTACGTGCTCACG
WDFY4-4	GTATGGTCATCTGTCGCTA
WDFY4-5	CCGGTAGCACTCGTCATCC
FXYD4-1	CAGCTCTTACCATAGTAGA
FXYD4-2	GGAAAAACCTGCAGCTGAG
FXYD4-3	GAGCGGACTGATCTGCGGA
FXYD4-4	CTGGCCATTGCTGGGATCG
FXYD4-5	GCATTTGCATTTGCCACCT
TYK2-1	GACGGCTATTTCCGCCTGA
TYK2-2	CCTGCGGAAGACGTTCCGA
TYK2-3	GTGCTGCCGGATATGCCGG
TYK2-4	GGTACACAGCCGGTTCCCG
TYK2-5	GATGCTATATTTCCGCATA
RIC8A-1	ACGTTTGATGATGCCCAAC
RIC8A-2	CTGCTGGCGCACATCGGTG
RIC8A-3	CGCCTGCTAACTGACACAC
RIC8A-4	GGTCCCCAGGTGTCGGTAA
RIC8A-5	GTGTGATGATCGCTACTGC
MYPN-1	AGGACTGCCGAAATGGCAA
MYPN-2	CATTATCCCTGGTATCCGC
MYPN-3	GTAACTTTTGAGTGAACCG
MYPN-4	GCTGGATGGTTGCCACACG

MYPN-5	CTTTTAGAACCTCGATCCA
NPY4R-1	CAGGATTCCGTGGACGTGA
NPY4R-2	AGCATTGAGACTGTCGTGG
NPY4R-3	CTACACCATCATGGACTAC
NPY4R-4	GAAGGCCGACATCTTGACAG
NPY4R-5	GACCGTCACCGACATGCAC
C11orf86-1	GCTTAGCGCCCTGCGGAGT
C11orf86-2	ACAGGGGCAAGAGAAGTCC
C11orf86-3	GTGCCTCTCTCGAGGCCCT
C11orf86-4	AGATGCCACTGCCAGGAG
C11orf86-5	TGATCCAAGCCCAGCGAAG
CNBP-1	CCTGCTATAACTGCGGTAG
CNBP-2	AAGGATTGTGATCTTCAGG
CNBP-3	GAGTCTGGTCATCTTGCCA
CNBP-4	CAGACATTTGTTATCGCTG
CNBP-5	GGTAAAACCACCTCTGCCA
TRAFD1-1	GTTGCCACATAGTTCCGTC
TRAFD1-2	TATGATGAATCTTGGGGTC
TRAFD1-3	CAATAGAACTACCAACCAA
TRAFD1-4	GGTGAAGAGAGTGCAAAC
TRAFD1-5	GACTGGTCGGCCTCACATA
JAK1-1	GATCCGATCGAAACTCAGC
JAK1-2	ATGTTGTGGACGATCAACG
JAK1-3	CGGAAGTAGCCATCTACCA
JAK1-4	CCGGCTCCACTACCGGATG
JAK1-5	GATCTTCTATCTGTCGGAC
USP43-1	ACCACCGCGTTCATGAAAC
USP43-2	CTTGAACTCCGCGGAAAGT
USP43-3	GATCGTGTACATGAGGACC
USP43-4	GACCGACCTTCTCCGACAC
USP43-5	CGTACCTCGTCTGGCGCAA
STAT1-1	TCCGCAACTATAGTGAACC
STAT1-2	TTGGGCGGCCCCCAATAC
STAT1-3	ACTAGTTCATCATTAAATCA
STAT1-4	CCCATTACAGGCTCAGTCG
STAT1-5	GTAAATGATCATAGACATC
FOXM1-1	CCCATACTAACGTGCGCCC
FOXM1-2	TCAAGTAGCGGTTGGCACT
FOXM1-3	CGGACAAACATGTCGTGCA
FOXM1-4	CTCCCGTTTCTGCTCGCAA
FOXM1-5	ATGCCCAACACGCAAGTAG
KLLN-1	CGAGCCCCTGTTTCCGCCG
KLLN-2	TTGCCTCCGGAGCTATCAC

KLLN-3	TTGGAAAGTTCCCCAACTA
KLLN-4	CGGAAAGTAGTTCCGACTG
KLLN-5	GTGGAAAGTACGGAACGGT
ZNF592-1	CTCCGCTTCAAATGACTCC
ZNF592-2	CGAAGAATCGAGTGGCATC
ZNF592-3	TGCTACGAGGGCTGTCCGA
ZNF592-4	AATCAAACGGACTGTCACA
CECR6-1	TAGAGCCAGAGCACCGGCG
CECR6-2	GAAGTAGACGGCGATAAGC
CECR6-3	CTGCTCGACAGCTTCACGC
CECR6-4	CAGGAAGCATCCGGCCGCG
CECR6-5	CAGCCCCAGCGGCACCGCG
CECR6-6	AAGAACAGCCGGGGCCGTC
CECR6-7	CACCAGTACAGGTCCGGTGA
CECR6-8	GACAGCCGCGGACTTCGGC
CECR6-9	GCGCGGCGTTGGGCACCAG
CWF19L1-1	GCCACCCGGTTTATAGCTC
CWF19L1-2	GAAATGCTACTCACCGATA
CWF19L1-3	TATCTTGGTTTCAAGCCCG
CWF19L1-4	CCTTAAATGAGCCAGTACC
CWF19L1-5	TGAAGATACCTTTACGACC
FDFT1-1	ACAGCTGCGAAACTGCGAC
FDFT1-2	TCTCCATGAACCGCCAGTC
FDFT1-3	GCGTAACCCCACTCACCGT
FDFT1-4	CCGACATTTGCCGGAGAAT
FDFT1-5	GTGACCTCTGAACAGGAGT
THUMPD1-1	GGTTTAAAGCTCCAAACAA
THUMPD1-2	TGCTCCACTTTCCACTGAC
THUMPD1-3	GTCGCCGTATTCGTTGAGG
THUMPD1-4	TTGCGCTCGTTCATATTGC
THUMPD1-5	GCCCCGGGCTCTAGCTGACG
CDC25A-1	GCCTCAGAATCGACCGATTC
CDC25A-2	AGTGATTATGAGCAACCAC
CDC25A-3	TATTTGGCGCTTCAGCCGC
CDC25A-4	TTGTAGTTCTCATGACGAG
CDC25A-5	AGAGGCTTGCCATGCACGA
CDC25A-6	GCTTCGTGGACCTTCTCGA

Supplementary Table 2. Table of ATR tiling primers for CRISPRx PCR 1

Primer	Sequence
ATR-F1	GATGCGTCAATTTTACGCAGACTATCTTTCgcggtggcgtggtgactag
ATR-R1	CCTCTCTATGGGCAGTCGGTGATCCTCAGCCATGGCTTCCACTCACATTTAC
ATR-F2	GATGCGTCAATTTTACGCAGACTATCTTTCCTGATGTTGCTTGATTTTCATCC
ATR-R2	CCTCTCTATGGGCAGTCGGTGATCCTCAGCCCCATCACATTTCTTCTATGG
ATR-F3	GATGCGTCAATTTTACGCAGACTATCTTTCGAGTCCTGCTATTTTTGGGG
ATR-R3	CCTCTCTATGGGCAGTCGGTGATCCTCAGCGAACACAACCTATCTGCCAAAG
ATR-F4	GATGCGTCAATTTTACGCAGACTATCTTTCCTTACTCGTATTATTGCAATTGTGT
ATR-R4	CCTCTCTATGGGCAGTCGGTGATCCTCAGCCTTCTGCTTCAAAGGGAAATAG
ATR-F5	GATGCGTCAATTTTACGCAGACTATCTTTCCAATTGAACTCTATGAAGAGCC
ATR-R5	CCTCTCTATGGGCAGTCGGTGATCCTCAGCCCTCAATTCCAAGCACATCC
ATR-F6	GATGCGTCAATTTTACGCAGACTATCTTTCACAAGTCAGGAAGGTCTATGTG
ATR-R6	CCTCTCTATGGGCAGTCGGTGATCCTCAGCCTCCATAATATGCTCTTTTGGTT
ATR-F7	GATGCGTCAATTTTACGCAGACTATCTTTCACCAAACAGACTGAGG
ATR-R7	CCTCTCTATGGGCAGTCGGTGATCCTCAGCGCACTTTTGTGTAATAATCCAATG
ATR-F8	GATGCGTCAATTTTACGCAGACTATCTTTCCTCAAGAAGAAACCTTCTGTAG
ATR-R8	CCTCTCTATGGGCAGTCGGTGATCCTCAGCTAGCGGCAAATGTGGTCAAC
ATR-F9	GATGCGTCAATTTTACGCAGACTATCTTTCCTGGTATGCTCTCACTTCCATG
ATR-R9	CCTCTCTATGGGCAGTCGGTGATCCTCAGCCACTAACACAACACTAGCCCGGATTAC
ATR-F10	GATGCGTCAATTTTACGCAGACTATCTTTCCTTGGAGTGGAGAACAGCAG
ATR-R10	CCTCTCTATGGGCAGTCGGTGATCCTCAGCGTGGCTTTCAAGTTCCTACAG
ATR-F11	GATGCGTCAATTTTACGCAGACTATCTTTCCTCAACCTTCTCTGAACACGG
ATR-R11	CCTCTCTATGGGCAGTCGGTGATCCTCAGCCCACTAAAAGCCACTCTAAC
ATR-F12	GATGCGTCAATTTTACGCAGACTATCTTTCCTCAGATGTAAGCAGTTCTTGG
ATR-R12	CCTCTCTATGGGCAGTCGGTGATCCTCAGCGCTGACTTGGATAACAAACAATG
ATR-F13	GATGCGTCAATTTTACGCAGACTATCTTTCGATATTGGAAGGGCCGCAAA
ATR-R13	CCTCTCTATGGGCAGTCGGTGATCCTCAGCTCTCTCTGGTGAGCCACATCTTG
ATR-F14	GATGCGTCAATTTTACGCAGACTATCTTTCAGCACTTCCGAATACTCCATG
ATR-R14	CCTCTCTATGGGCAGTCGGTGATCCTCAGCCTTTGGAACAAGAACAGACC
ATR-F15	GATGCGTCAATTTTACGCAGACTATCTTTCGTTCTACTACCTGATCTTGCTGC
ATR-R15	CCTCTCTATGGGCAGTCGGTGATCCTCAGCTAATCAGCCATCAGTTCAGGTG
ATR-F16	GATGCGTCAATTTTACGCAGACTATCTTTCGGTTTTGTCAATACTTGCCCTC
ATR-R16	CCTCTCTATGGGCAGTCGGTGATCCTCAGCAAGCTCTGCAACACAATTCAGG
ATR-F17	GATGCGTCAATTTTACGCAGACTATCTTTCCTCTGTGAGGGTGAAGATGATGAC
ATR-R17	CCTCTCTATGGGCAGTCGGTGATCCTCAGCCGGCTTTTATCTTTTTTAATTCTGG
ATR-F18	GATGCGTCAATTTTACGCAGACTATCTTTCAAACAGGGATGCTGTGCAAG
ATR-R18	CCTCTCTATGGGCAGTCGGTGATCCTCAGCCACCAACTGTGAGATAATAGG
ATR-F19	GATGCGTCAATTTTACGCAGACTATCTTTCCTGATAAAGTATGCAACAGACAGT
ATR-R19	CCTCTCTATGGGCAGTCGGTGATCCTCAGCGCTATTATCAGCATACGCAAGG
ATR-F20	GATGCGTCAATTTTACGCAGACTATCTTTCGATTCAAGCTTTGCCTATGG
ATR-R20	CCTCTCTATGGGCAGTCGGTGATCCTCAGCCTTTACTCCAGACCAATCGGTTGAC
ATR-F21	GATGCGTCAATTTTACGCAGACTATCTTTCCTACTAGAACCTCATCTAAATACCAG
ATR-R21	CCTCTCTATGGGCAGTCGGTGATCCTCAGCTGCATAAACCTCCTGCTGATC
ATR-F22	GATGCGTCAATTTTACGCAGACTATCTTTCCTGGTGTATGTCTTACTGGG
ATR-R22	CCTCTCTATGGGCAGTCGGTGATCCTCAGCCACTCTGATAGTCTTATAATCCAC
ATR-F23	GATGCGTCAATTTTACGCAGACTATCTTTCCTCCACACAGCAAATCAAACAG
ATR-R23	CCTCTCTATGGGCAGTCGGTGATCCTCAGCGCCACTCCATCAGGTTTCATGC
ATR-F24	GATGCGTCAATTTTACGCAGACTATCTTTCACACACGAGCTGTAATGCAC
ATR-R24	CCTCTCTATGGGCAGTCGGTGATCCTCAGCTTCATCTGTCCACTCGGACCTG
ATR-F25	GATGCGTCAATTTTACGCAGACTATCTTTCCTGCTACTGTTATCACTCAGGTG
ATR-R25	CCTCTCTATGGGCAGTCGGTGATCCTCAGCCATATCCTCGTTGGTAGGAG
ATR-F26	GATGCGTCAATTTTACGCAGACTATCTTTCGAACAAATTGTACCTCTTTCAGC
ATR-R26	CCTCTCTATGGGCAGTCGGTGATCCTCAGCCTCTGCAGCCAGCATTCT
ATR-F27	GATGCGTCAATTTTACGCAGACTATCTTTCGAAGCCTCAACAAAAGACCAG

ATR-R27	CCTCTCTATGGGCAGTCGGTGATCCTCAGCCCCACTAGTAGCATAGCT
ATR-F28	GATGCGTCAATTTTACGCAGACTATCTTTCCACCTGAGGGTAAGAACATG
ATR-R28	CCTCTCTATGGGCAGTCGGTGATCCTCAGCCGTGGCATTGACTGATATATG
ATR-F29	GATGCGTCAATTTTACGCAGACTATCTTTCATAAGGATGTGACCGCGTGC
ATR-R29	CCTCTCTATGGGCAGTCGGTGATCCTCAGCTGCTTGTTGAGGATAGGCTAG
ATR-F30	GATGCGTCAATTTTACGCAGACTATCTTTCTCGAATTTGTCATTCTCACG
ATR-R30	CCTCTCTATGGGCAGTCGGTGATCCTCAGCTGAGTGCTCATGCTTAATGTGG
ATR-F31	GATGCGTCAATTTTACGCAGACTATCTTTCTAGAATTGTGCAATAAACCGG
ATR-R31	CCTCTCTATGGGCAGTCGGTGATCCTCAGCCCATCTGAGCCTTTTAAAGAAA
ATR-F32	GATGCGTCAATTTTACGCAGACTATCTTTGATGATATGGTGGAATTCTTGC
ATR-R32	CCTCTCTATGGGCAGTCGGTGATCCTCAGCGTCAGAATAGGTCTCAAACCAGCAG
ATR-F33	GATGCGTCAATTTTACGCAGACTATCTTTCCCACTAAATGATGAATGTGGG
ATR-R33	CCTCTCTATGGGCAGTCGGTGATCCTCAGCGCAGTGGAACGGCAGTAAGC
ATR-F34	GATGCGTCAATTTTACGCAGACTATCTTTCTGAGAACATTCCCTGATCC
ATR-R34	CCTCTCTATGGGCAGTCGGTGATCCTCAGCCACATGCTCTTCGAAAAAGAC
ATR-F35	GATGCGTCAATTTTACGCAGACTATCTTTCCGGTTAATGGAATGGGTCCTATGG
ATR-R35	CCTCTCTATGGGCAGTCGGTGATCCTCAGCCCTTCAATAGATAACGGCAGT
ATR-F36	GATGCGTCAATTTTACGCAGACTATCTTTCCGGTGAATCAAGACTCGAAATAGA
ATR-R36	CCTCTCTATGGGCAGTCGGTGATCCTCAGCgtattaagaagcagttatttcta

Supplementary Table 3. List of overlapping resistance hits with Z-Score >2 comparing our YCC6 CRISPR screen results with the TOV21G screen and the 293A, HCT 116 and MCF10A cell lines extracted from Wang *et al.*, 2018. Highlighted in blue are the hits that I have validated for our YCC6 CRISPR screen.

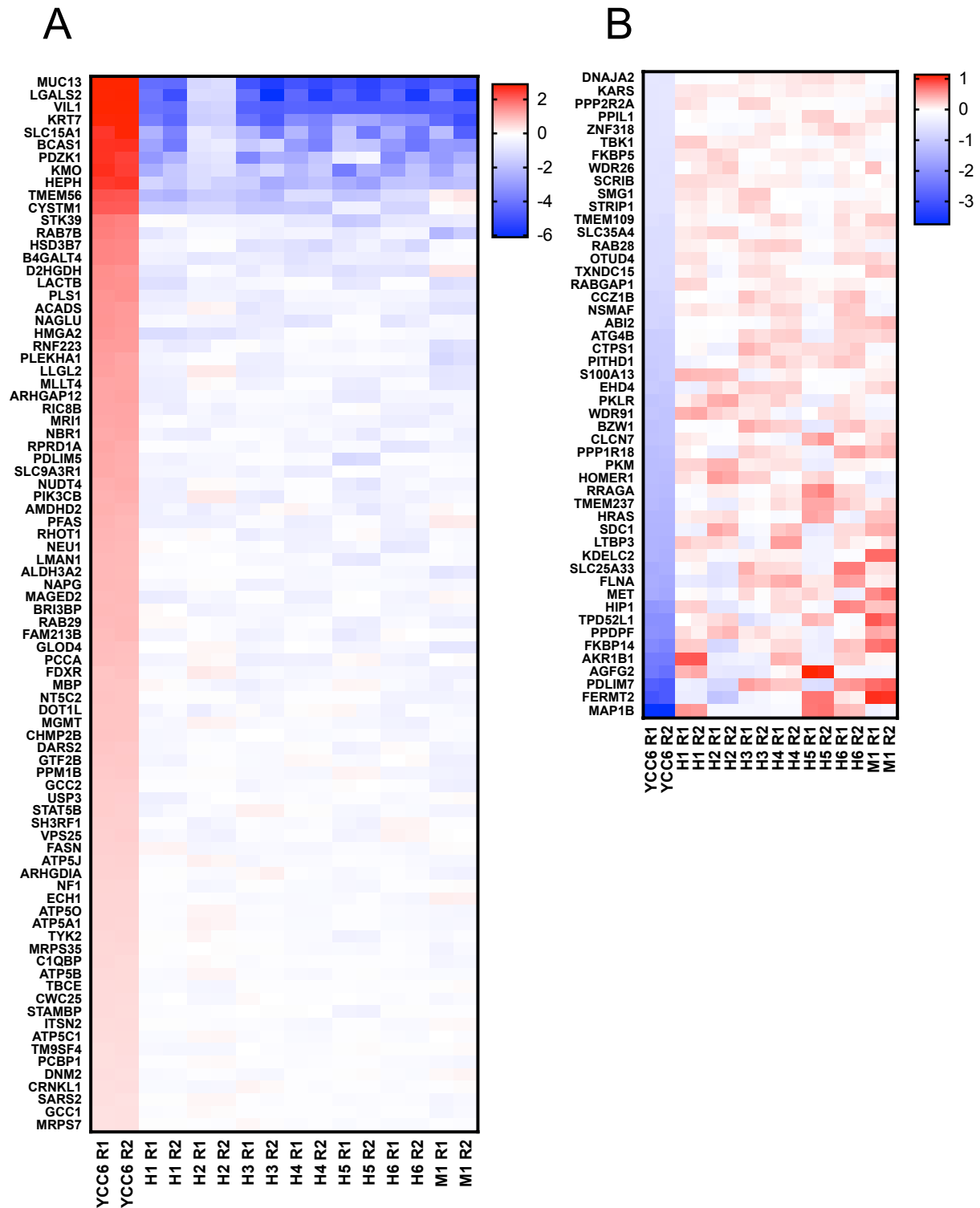
YCC6 + 4 CL	POLL	CDC34	PLBD1	EBLN1	GNB4
CDC25B	SHROOM3	CXCR1	NUDT5	PRR16	GPR161
TRIT1	UNC45A	GALR2	SGMS1	PRKAR1A	ALG9
YCC6 + 3 CL	FBXL22	ZSCAN5B	CCDC97	ANKRD35	GBE1
CHCHD1	ATXN3	PPP1R7	INA	RRAGA	IL22RA1
C10orf32	CDC26	RBAK-RBAKDN	CDH22	SCARF1	PIK3C2B
CPN1	RXFP3	PSMA1	C12orf56	CTU2	LAMTOR3
OSGEPL1	FAM69A	MXI1	STXBP2	ZNF33A	MED7
URM1	IGF1R	GFRA4	NKIRAS2	ADRB1	RGS17
ATAD1	NDUFS5	PADI2	SNTA1	TLN1	TP53TG5
ABI3	MRPS18B	RDH11	NANP	ZNF251	HOXA5
STYX	TFAM	CALCRL	CDKN1A	LAMTOR1	USP31
GATA5	PIK3CA	EDNRA	CYP2U1	MAPKAP1	LIPT1
DARS	TTC14	TMIE	KIF3C	AIP	GPIHBP1
ASIP	CEP44	VILL	LRRC15	ARHGAP32	JPH4
RICTOR	KRT27	ICAM4	KCNH4	SGOL2	TAF13
SYNPR	PAPOLA	LRRC43	SYNGR2	PCTP	INSL5
WFIKKN2	HNRNPF	CCDC160	APEH	OLA1	AP1G1
AVEN	SMG9	S100P	GADD45GIP1	CMIP	YCC6 + 1 CL
SELPLG	STAT2	PKN1	HUWE1	MYLPF	RIC8A
TMPRSS11A	KIF5B	CCRN4L	RBP4	ZDHHC7	TRABD
MRPL50	BLOC1S2	ATP8B1	HNRNPD	MTMR4	MSRB2
CSTA	GAP43	TADA2A	CUEDC2	MRPS16	GAD2
FGD6	MIB1	DESI2	AKT2	SEC63	ARL5B
PLD6	EFCAB11	GABRG1	DERL2	GTPBP10	GNA13
SMG8	ITIH2	SPATA22	HOGA1	CFHR5	TNRC6A
CDC25A	GLUD1	PLA2G7	INCA1	MFSD9	RGCC
AEBP2	BTBD7	RGS13	PRPH2	PFDN4	SEMA3G
YCC6 + 2 CL	ERGIC2	NUDT6	NLRP8	MLNR	RXFP2
SYNPO2L	IVD	FAM96A	PDE6G	PHPT1	SOX13
MTOR	CST9L	SPIN3	KIAA1984	CCDC117	ZNF268
SUV39H2	C17orf80	PPFIA2	POLR3F	CPQ	LTA4H
MOB3A	GPR65	CLIP3	HTR7	COX17	CCSER2
MED12	VWA5A	PHF14	ZFYVE28	ASB6	PTPDC1
CNPY2	CYP46A1	BROX	CALHM2	LOXL2	PML
SCD	USP46	VAT1L	MEPE	CCDC82	RNF5
ALKBH5	MAGEB5	NEO1	SCGB3A1	MBOAT2	PAK4
FAM212A	ZFP64	TEKT1	C10orf95	ALG5	RERE
WDR87	RASSF5	LCN9	OTUD4	ENG	SLC6A13
HNRNPA0	ADCYAP1	CSN2	C4orf17	MITD1	MIEF1
NDUFAF1	SYNPO2	SLC6A14	HSPB6	GTF2E2	DCUN1D5
CHUK	CYP3A43	PRRX2	SUPT6H	TNPO1	CEBPA
FOXM1	HSP90B1	RGS1	KCTD8	VENTX	MGMT
TRAPPC10	RCAN1	GUCY2C	ZNF677	FAF1	VPS37B
ZFP36L1	RRAS	FUT8	IFNAR1	SIGLEC8	COMMD7
CD164	C17orf105	RNF128	RET	RSRC2	BCAT2
TIGD7	SNX13	NEUROD2	LDB1	STK4	MTF1
BCAS3	ODF3B	TBC1D14	DCUN1D1	FCRL2	HSPA8
KLK5	MED12L	INTU	FASTK	WDR59	ZMAT1
NFYB	TM4SF19	ADIRF	USP6NL	RWDD1	LIPJ
TDP1	CA4	CMAS	SEPHS1	SLC6A12	CDR2L
TRIM69	SLBP	TIGD2	BOK	UBQLN1	SSR2

ALDH6A1	KLHDC1	INPP5F	TMEM126B	SLC5A2	MYO1C
CCDC34	C14orf79	NUDT13	TRHR	ELMOD2	C15orf60
CCDC63	CCDC137	VNN2	DGCR2	PSPC1	C17orf58
TEX29	AP3B1	RAD51AP2	CNIH4	ESCO1	DOK3
CYP4Z1	NANOS1	MRPL1	TFDP3	CXorf61	TAOK1
IMPG2	WDR83OS	MS4A7	ZNF107	DCTN1	LAMP5
SKIV2L	GRM3	APPBP2	LRRN3	SERTM1	GPR174
LINGO1	ELOVL2	SNX6	SKA1	DSC3	AIPL1
SPTB	HPS1	ZC2HC1B	TMPRSS7	IFT81	HDAC5
UCK1	AFP	TACR2	GLRA3	GBX2	BLOC1S1
DUS2	CHST8	ARHGEF3	RNF31	RNF138	SEC62
PTBP1	TRDN	VPS13A	RAB1A	HEBP2	ADSSL1
SAMHD1	CDV3	ANGPTL5	C21orf33	TMEM168	CST9
TCERG1	RBM12	CNNM2	LRRC16B	MLXIPL	ORM2
FAM214A	NCAN	RAB21	APBA1	CCDC114	LRRC46
NPAS1	SCN4B	ARRB1	TRAF1	MYH3	AGFG1
MOB3C	GZF1	PDE6C	RWDD4	KPRP	MDM1
C10orf111	ULBP1	CHAT	MAP3K13	PF4V1	DLGAP2
EFCAB4B	TSPAN3	CKLF	PROL1	KPNA4	CTSC
TOR1AIP2	ARSH	COMTD1	RABL2B	AGBL4	AKAP1
KLRG2	SLC45A3	C11orf91	MLC1	RAP1A	OSBPL8
SPTY2D1	SUGP2	GLYATL2	ABCB1	PAX4	FUT11
CYFIP1	STARD10	DCAF10	TMEM26	VPS26A	RPUSD3
BTN3A1	C20orf78	PLXDC2	CCDC152	SAA2	CXCR2
SNX17	C9orf117	ZNF93	VAX1	GJD2	CACNG4
ECH1	WDR31	C11orf58	RNFT2	IFNGR1	EXD3
KLF6	ZNF333	ARFGEF1	DENND2A	FBRSL1	NREP
ZSCAN32	FBXL2	TAS2R40	TCTA	RAB33B	IL23R
TEAD1	FAM173A	AFAP1L2	OXTR	BLOC1S5	RSPH3
ADO	MYOM3	HMOX1	LRRC48	ANKS6	PDE6A
NGLY1	CDC40	CA2	ATP11C	DSN1	PLEKHS1
HMSD	C17orf102	SLC46A3	SPAG11B	SFTPD	CTNNA1
A4GNT	ILDR1	TMEM180	THAP6	BSND	MPHOSPH9
PXN	PCDHA9	LHFPL4	PRR24	KIT	OTUD6B
SERPINB13	STK38L	IL1A	KCNJ11	FAM189B	CAMK2G
TBC1D24	SMYD4	C12orf79	PCGF6	ARHGAP11A	VIM
E2F8	COMP	PRSS1	MTERFD1	TOR2A	SKIDA1
C5orf47	MARK4	NGFRAP1	IKBIP	SLC24A5	UNC5B
LRRC37B	TMEM106A	OPALIN	HSDL2	NKX2-2	STOX1
KHDC1L	HSPB8	TTC18	OMG	RPL21	GJD4
BCL6B	POLR2A	HIST1H4D	ARSK	RALGAPB	MYPN
VSTM2B	GGT7	LRIF1	KIF20B	PKDCC	TCEB3
NEMF	SPACA3	CD300LD	APOL1	MEIS1	WDFY4
NUDCD1	CLDN12	NRP1	SDF4	GIN1	PTPLA
HSD3B2	TLR2	SOCS7	PCSK4	MUC1	RBP3
CCNB2	MAVS	PACSIN3	AMOTL1	NDFIP1	A1CF
MAD1L1	TBCK	LOXL4	ELK4	CD2AP	FAM107B
ZNF75A	SLC25A41	LCOR	ZBTB33	KPNA6	RAP2B
ZMYM3	NCR2	TLX1	FAM177A1	OAZ3	PRSS27
CCNL1	ZNF648	AMN	HGSNAT	PCK1	FAM13C
CD274	LRRC8E	FAM47A	FOXRED2	YAP1	ARHGAP21
TULP4	CADM2	PDS5A	NET1	RDX	MAGEH1
UBQLN4	WEE2	PTER	PIK3IP1	LARP1B	C10orf11
VN1R1	UROC1	TAGLN	ZNF429	CD47	ANKRD30A
MDM4	UCMA	MNDA	ZNF654	PHF19	PPP3CB
PSMB9	ARL13A	SLFN12L	TFPI	37316	DTNA
PPAPDC2	TRPV1	IRF1	STOM	PLEKHA1	LRRC20
HOXA4	ARHGEF26	RASSF7	SMIM19	SLC4A8	APPL1

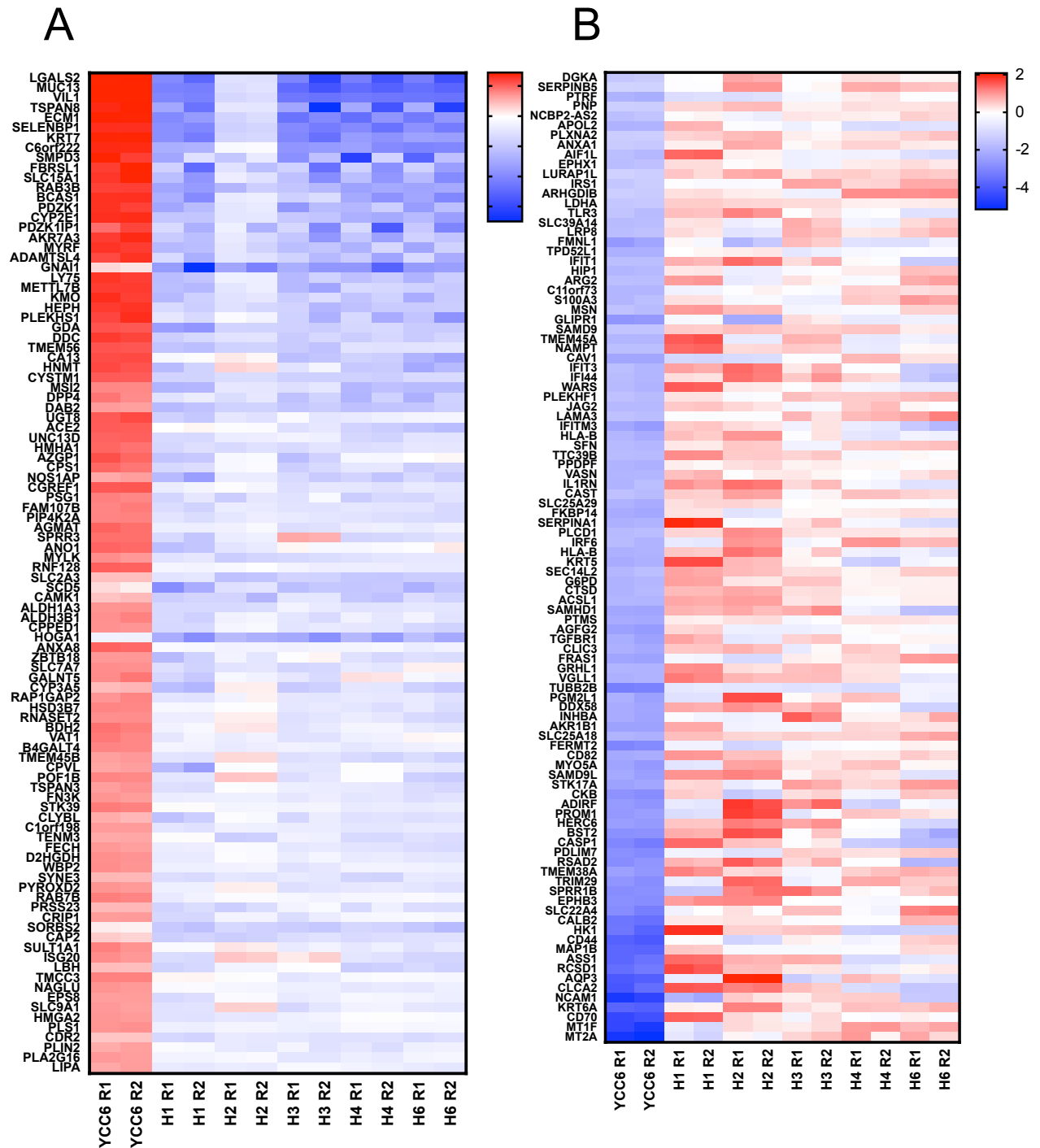
ZZEF1	C20orf197	SCN5A	UHRF2	ERLIN1	CTSD
CHAF1A	UGT2A1	CCNYL1	CPEB1	ZNF90	PHF2
ZNF213	CLDN20	BRAF	DYNC2LI1	PSKH1	NPM3
KLK11	SHISA2	REG1A	DOCK5	KERA	ASB13
CCDC37	CNN1	IRS1	GJB7	BCO2	ANK3
N6AMT1	NAGLU	CCL19	CCDC166	C1QTNF8	TMEM72
DOK4	ERAP2	EVA1B	MCCC2	ASTL	PTF1A
HDAC8	SH3GL2	SEC61B	FLVCR2	NHLRC3	PARD3
NSUN3	BRD9	ZBTB6	CCDC179	JAKMIP3	CENPH
GK5	TMEM40	PSD	CCDC121	SPOCK2	ZNF124
SPIRE2	TJAP1	ZNF732	C6orf211	ZNF639	C12orf75
TLCD2	MANEAL	PAPOLG	IDH3G	PLEC	POLR3G
TOP1MT	KRTDAP	LIPA	TCTN1	P2RY11	PPP1R42
TANK	APBB2	RPRD1A	EPS8L1	APAF1	RLN2
C16orf71	MST1	SNX10	NT5C3A	DTWD1	SRCIN1
ERBB3	UNC5C	P2RY10	ATP5L2	CD302	C11orf30
EBF2	FOXA1	SCD5	AGTR2	PAPSS2	ATXN2
SMAD2	ZNF518B	CRKL	CHDC2	CDA	KIF2A
HPCA	RNF7	PHLPP1	RBFOX3	KIF22	LRRC7
NMT2	RTBDN	SPTBN1	TGM3	TSPAN8	WFDC3
KRT36	MPP2	LTBP3	SNCAIP	STX16	GFI1B
CACNA1E	RAI14	TMEM189-UBE2V1	C8orf59	ZNF714	SLC30A10
SOX8	CBLN3	GPR26	FRA10AC1	FN3K	RABGAP1
TMEM70	SLC7A9	TMPRSS11F	GKN2	FCN2	CHRM1
MPP6	ZNF461	FBXL15	HMGN5	C2orf15	HNRNPUL2
SPATS2L	BLMH	C10orf54	UBAC2	SCLT1	MS4A1
ZBED2	PLCH2	SPIN4	UFM1	FAM229B	MGARP
LYPD3	HYKK	DNASE2B	TAS2R13	RGS3	L1TD1
TXNDC2	SLC41A1	IQCK	ABLIM1	CENPU	IL27
KIF3A	DYNLRB2	UGT2B15	ARNTL	NTN3	BTG3
NRD1	KLF2	HTRA1	MEA1	DPYSL4	BCAS1
TSC22D2	EOMES	RIPK3	SERPINB7	SYNE2	RAI2
PTN	ALDH7A1	CHRNA1	SPANXN2	IFIT5	SH3D19
HYI	ZFP36	NME9	GPR116	GLRA1	C4orf27
GPR45	GDF15	CAPZA2	TMEM243	CHI3L1	FCRL5
RTKN2	CYP27C1	RPH3AL	CEPT1	FBXO32	ADC
EXOSC1	QSOX1	RPTOR	KIAA1107	SLC43A3	GPR150
LRRC14	SRMS	HAAO	DLG5	AP4S1	DAOA
ZNF766	DKK2	PCDHB13	MAN2A1	DNAJC6	KIAA0319L
PLAC8L1	ACADSB	L3MBTL2	ZBTB41	TMEM42	ZNF831
RIT2	STC2	CDK15	ASAH1	EIF4E3	GRB14
POLD2	ATP1B3	YME1L1	RELT	CHRM4	BTF3L4
SUV39H1	TFF2	ANTXR1	MEOX2	PCDH18	CLUAP1
TOMM20L	GDF1	NOLC1	CUL7	ZNF69	MCM4
C16orf93	ARIH2	CHST11	FAM168B	DDAH1	URAD
FAM162A	HNRNPH3	CCDC13	IRGQ	KIR2DL3	TMEFF1
RNF6	PTPLB	SERPINH1	TES	FAM50B	PAGE5
PITRM1	CCDC148	CTNNA3	NUDT3	TSPAN9	IKZF2
DNAJC7	CDH7	WBP1L	HGF	SPDYE4	C1orf87
MAFA	TIMM17B	PGBD3	TMEM86B	TNFRSF13B	HAPLN3
BCDIN3D	C14orf166B	TLE4	C11orf35	ZNF527	ASZ1
PRDM15	DMXL1	TROAP	GLUD2	C7orf65	ELF1
FAP	C7orf10	NFU1	PDZD11	ZFP14	UPB1
PHF12	CKAP2	LAMC3	GCNT2	CMTM1	PDZD9
TOMM70A	DCN	CCDC132	EBPL	TRO	MMGT1
IDI2	FLOT2	PBX3	PDXDC1	ATP4B	PPM1B
GPR18	TNFAIP8	NARF	NAA38	CYorf17	TRHDE
SHC4	EPC2	MAN2B1	TRMT10B	MXD1	SMARCA4

MVB12A	TAF1D	ZDHHC21	SDF2	ZNF26	DNAJC19
TMCO6	DNAH10	EVI2A	TMEM154	ALDH1A1	HLA-DQB2
KLHDC7B	SCMH1	ANO10	PHF21B	DIRC1	PSAP
CATSPER3	FAM50A	SPRED2	C9orf72	ESAM	METTL6
CD86	FNDC8	C8orf88	LLPH	PM20D2	CHPT1
CENPP	PGAM5	ARL6	TTPA	CCL18	RBM18
SLC2A13	C22orf23	ST8SIA6	ECHDC3	RNF39	KLHL24
CDH15	CMPK2	ANXA11	CENPV	KXD1	LY96
ARHGAP18	CLGN	GRM5	GPR123	ZNF836	SPINK1
LINS	SMIM20	OLAH	IGSF11	SLC7A6	RPL37
PLEKHN1	EMC8	FGF4	SLC24A2	C14orf178	ARHGEF12
IPMK	MXRA5	DNAJB12	MBNL1	PLK5	ASIC1
ATP5F1	ZDHHC17	METAP1	TBX3	ZNF721	DGAT2L6
FAM120AOS	NRG4	NODAL	ELMSAN1	CALR3	ICOS
PCDHB2	ZNF329	WBP5	TIPRL	DAD1	MROH2B
TATDN1	THAP10	NXNL2	FAIM	TMEM190	POU3F3
DIABLO	C8orf33	HP1BP3	TDRP	SEMA7A	UBA7
COG5	PPM1L	C1GALT1C1	C2orf47	PDPN	TMEM230
NDN	CLRN3	SEMA4G	NRBP1	TSEN15	MKRN1
HIST1H1C	ST3GAL6	SEC11A	SAMD12	FAM169B	ARHGAP19
LCMT2	PRKCA	DPY19L1	MAGEB17	AP3S1	GNAT1
CMTM4	MBTPS2	FAM196A	IQCB1	GUCY2D	USP25
RNF133	DKK4	C14orf39	PTRHD1	USP51	ZNF224
TTC33	AHI1	PDLIM5	INSL6	HRH4	CLDN14
CDK6	PMEP1A	ADAMTS14	CCBE1	TAS2R43	RFX1
LRRC52	MAP1LC3A	KLHL1	R3HCC1	SLC35A3	VCL
RCOR1	PWWP2B	MSMO1	C18orf32	PPP1R2	STAT5A
MSL2	SLC41A2	RFPL3	WASF3	TDRD3	SEZ6
TMEM140	HCLS1	SPINK9	IHH	IRX2	IFLTD1
KLHL40	COL9A2	C4A	PLEKHF2	CLIC2	FXD4
IPO4	CAMK2D	RHOA	PLCL2	FCAMR	SYT15
SLC17A5	CCDC11	THAP2	SVIP	TBL2	RRAGC
SUCLA2	CDK14	SLC25A16	PPP1R3A	TMEM194A	USP43
MX2	SPTSSB	HIGD1A	SSBP2	WISP3	FA2H
C3orf14	CDKL5	CCR2	CD3G	L3MBTL3	LAMTOR2
TXLNG	TRIML1	TMEM65	GRM8	XKR3	DUSP13
PLA2G5	NEDD4L	FOXC1	CORO2A	GMDS	VAMP4
PCDHGC5	ZNF346	CEP104	FMNL3	C1orf54	ZNF33B
DIRAS2	CD3D	PRAM1	TCEB3B	REG3A	TP53AIP1
FRS2	RBBP6	C7orf63	TCEAL4	SMARCD1	SORCS3
ZNF674	KIAA0586	RAB18	AQP11	LRBA	PPP1R14A
STATH	ZNF214	PALM2	ANGPTL3	SLC25A34	CYB5B
HLX	WNK3	FCER1A	MGAT4A	COPS2	PPP3R1
ACSBG1	ZNF625	ZER1	HYAL3	GLI3	ZCCHC24
MIS12	HOXB5	ACBD7	MEIG1	PLEKHO1	THEM5
ITM2C	IQCF5	CEP70	ZNF98	USB1	BET1
C5orf15	HECTD1	CCDC169	CRISPLD1	OPN3	RPGRIP1L
C21orf58	CDHR1	LYN	ENHO	FETUB	TMEM139
MINPP1	CPD	SERPINA9	ZNF573	RAB28	ATP6V1C1
GLOD4	LIPE	COL13A1	BCL2A1	SCPEP1	ALPI
MYOZ1	NSG1	NUDT7	NLRP3	AMZ2	SV2B
ARL14	ZBTB7A	CT45A5	C1orf173	PRDX4	PSMC5
WDR49	SERTAD1	CAAP1	HEPH	ABCC2	WWP1
AGTRAP	GRIN3B	XPNPEP1	SSTR3	CSRP2BP	THTPA
LYSMD3	ASB8	FOXI2	HSBP1L1	CCNI	GKAP1
KLRC4	RTN2	CCDC136	C10orf88	ZNF432	FAM180A
TICAM2	ADRA1B	MTHFD1L	MYOD1	DPP4	ASCL2
ACTR2	FABP2	PPIC	TLR7	CALB1	ADM5

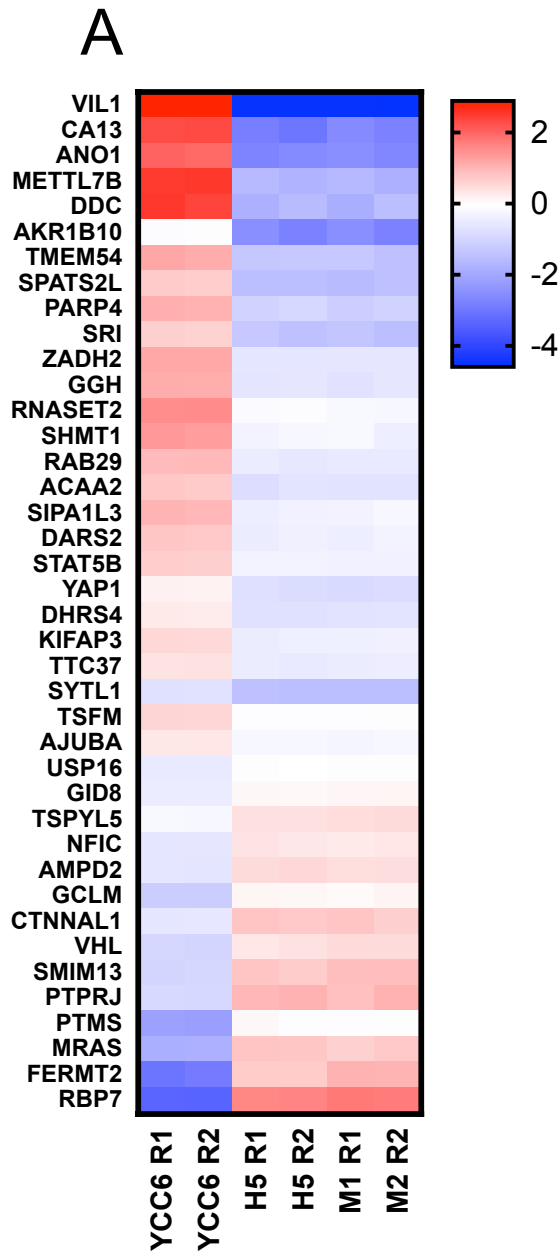
KCNF1	NPY1R	BBIP1	MFSD4	KDELR3	MUM1L1
SCRIB	LSM14B	ODAM	GNG8	TRIM8	MGAT5
VSIG1	EIF4B	HS3ST5	ZNF276	AJUBA	ELP6
C5orf48	ZMYND11	DPY19L4	TPP2	KRTAP12-3	SPN
INS	FZD8	HS3ST3A1	PTPN3	IFI35	PRX
AGAP2	NPTX1	ABCB5	HIST1H3A	FZD4	HSPG2
GFPT2	LRAT	ZNF83	C8orf47	ZNF567	C6orf25
C9orf153	TSNAX	ZNF503	MUSTN1	ARL4A	SSBP4
HYAL1	IL31RA	DUSP5	SLC44A5	NDRG3	HGS
DDX19B	TRIML2	TCP10	EYA1	ZNF596	CARD10
PHTF2	RBM11	SKAP2	CREB3L3	MMAB	C10orf128
ASB9	HPSE	ZNF586	B3GNT3	DEFB132	GPRIN2
ATRNL1	SPEN	TMEM178B	CRELD2	PSMG2	ZNF44
SEC11C	VSIG10L	SLC45A2	ARHGEF19	SLC23A1	SCUBE3
WSB1	AXIN2	ATG3	EAPP	MMP20	FAM133A
GUCA1C	GRK5	PHYHIPL	TEKT4	METTL23	RRAS2
LCE3D	DUS1L	TMEM5	DIRAS1	GLYATL1	CCDC3
SUB1	EXOC3L2	DRD4	FAM45A	POPDC2	ISX
DOT1L	SERPINA11	BEND6	LRRC19	ECHDC2	HCN3
ROR2	ELAVL2	MCMDC2	USP1	ACHE	SCN2B
NUBP1	CHMP4B	ADAM18	BLNK	PAPPA	HMX2
CCDC7	PAX2	TUBAL3	MARVELD2	PDGFC	RHBDD1
RASGEF1B	SIGLEC5	SWT1	VEGFC	TC2N	SH3PXD2B
CSGALNACT2	FAS	DHFR	RNF186	ZNF781	EPDR1
DHTKD1	PCDHB10	ADI1	SPG21	CDR1	SELV
FRMPD2	RFC1	GOT1	LIMD1	FCHO2	ARL14EP
FRAT2	CNTD1	ZNF208	RCN1	C12orf43	LILRB1
ZRANB1	RBMS3	DENR	ARHGEF2	MTCH2	ZNF563
AKIRIN1	ARHGAP5	NMU	MLANA	ALDH4A1	LIPK
ZNF22	GCN1L1	KLRC3	RASGEF1A	BBS5	ZFP42
MMD	ZNF419	C1orf229	AKR7A3	38961	STPG2
SGCD	PHOSPHO1	TXNL1	NFE2L3	TTPAL	C1orf65
PAGE1	RAP1GDS1	FAM21C	TMEM68	PCBD2	LRTM1
SLIT1	HLTF	ADAM12	GPR160	MYL9	ITGAV
ILK	GXYLT1	HEG1	SPEP1	GIMAP4	CUTC
VGLL4	LRPAP1	SLC39A11	AP5Z1	UGP2	NSD1
FKBP8	NXNL1	KNCN	APBB1IP	RNLS	MAPT
FAM170B	C12orf40	PTCHD3	CETN3	TTC12	CYB5A
DNAJC1	CSRP2	PPAPDC1B	ZNF280A	NAB2	OCIAD1
ZNF830	TAF15	TBR1	COMMD3	NUP35	BNIP2
GALNT12	PCP2	MPC2	IL20RB	CLSTN2	REP15
CCDC127	PDCD2L	C10orf129	METTL18	KRTAP26-1	SMAD1
GSTO2	NFX1	FAM122A	EIF6	SC5D	IPCEF1
LTBR	KIAA1239	DLC1	C11orf16	PDZRN3	SLFN13
ZNF239	ZNF557	SHPK	SPINK7	PARD6B	ZNF488
PRF1	APCDD1L	ARHGEF39	NECAB1	IRF7	HOXA7
GALNTL6	NIT2	SNX16	GNPDA1	CSTF2	CST7
PIP4K2A	UTP11L	TMEM260	FAM149B1	TPST2	ENTPD1
VDAC2	CNP	RPS27A	ZC3H12B	GALNT2	
MLLT6	CAP1	PDCL2	SEC31B	SEC14L4	
B3GNT9	KRTAP17-1	ZBTB8A	SPRR1A	IDI1	



Supplementary Figure 1. Mass spectrometry transcriptomic data reveals common differentially expressed proteins in all YCC6 ATRi resistant clones. A. Proteins downregulated in the resistant clones, compared with the YCC6 WT population. Red means high protein expression while blue means low protein expression. **B.** Proteins upregulated in the resistant clones, compared with the YCC6 WT population. Red means high protein expression while blue means low protein expression. Statistical significance means differences in protein expression levels with a FDR corrected Welch's test p-value <0.01 and Log2 fold change differences lower than -0.5 or larger than 0.5. All experiments were performed in two biological replicates.



Supplementary Figure 2. Mass spectrometry transcriptomic data reveals common differentially expressed proteins in H1/H2/H3/H4/H6 YCC6 ATRi resistant clones. A. Top 100 proteins downregulated in the H1/H2/H3/H4/H6 resistant cluster, compared with the YCC6 WT population. Red means high protein expression while blue means low protein expression. **B.** Top 100 proteins upregulated in the H1/H2/H3/H4/H6 resistant cluster, compared with the YCC6 WT population. Red means high protein expression while blue means low protein expression. Statistical significance means differences in protein expression levels with a FDR corrected Welch's test p-value <0.01 and Log2 fold change differences lower than -0.5 or larger than 0.5. All experiments were performed in two biological replicates.



Supplementary Figure 3. Mass spectrometry transcriptomic data reveals common differentially expressed proteins in H5/M1 YCC6 ATRi resistant clones.

A. Proteins up and down regulated in the H5/M1 resistant cluster, compared with the YCC6 WT population. Red means high protein expression while blue means low protein expression. No protein interactions were detected. Statistical significance means differences in protein expression levels with a FDR corrected Welch's test p-value <0.05 and Log2 fold change differences lower than -0.5 or larger than 0.5. All experiments were performed in two biological replicates. No protein interactions were seen.

Resumen en castellano

Introducción y objetivos de esta tesis

El cáncer gástrico (CG) es el quinto cáncer más frecuente a escala mundial y constituye la tercera causa de muertes ocasionadas por cáncer, produciendo alrededor de 800.000 muertes al año. La etiología del CG es compleja, resultando en una combinación de factores genéticos, epigenéticos y ambientales entre los cuales se encuentran la obesidad, la infección por la bacteria *Helicobacter pylori* o el virus Epstein-Barr, así como diversos factores dietarios, consumo de alcohol y tabaco.

A pesar de los avances prometedores en el diagnóstico y tratamiento del CG, la supervivencia global de los pacientes diagnosticados con este tipo de neoplasias sigue siendo extremadamente pobre. El tratamiento actual se plantea como una estrategia multimodal en la que se incluyen la cirugía, la quimioterapia y la radioterapia, sin tener en cuenta las características moleculares de cada tumor. Con ello se ha conseguido mejorar el control local del tumor, así como disminuir la tasa de diseminación o metástasis, pero, el pronóstico de la enfermedad avanzada sigue siendo poco esperanzador. La biología molecular del CG, particularmente, el conocimiento de las vías de señalización implicadas en su patogénesis, y su contribución al desarrollo de nuevas modalidades de terapias dirigidas se halla en una etapa temprana, en comparación a otros tipos de neoplasias.

Alrededor del 95% de los CGs diagnosticados son de tipo adenocarcinoma, los cuales se han clasificado, tradicionalmente, en CG difuso e intestinal, siguiendo las pautas clínico-patológicas propuestas por Lauren en el año 1965. Al igual que la clasificación de Lauren, otras categorizaciones del CG basadas en las características histológicas del tumor han sido utilizadas, las cuales han demostrado muy poco uso pronóstico o clínico hasta la fecha.

No fue hasta hace unos pocos años, cuando se comenzaron a publicar las primeras clasificaciones moleculares en CG, como la del “Cancer Genome Atlas Research”, la cual clasifica el CG en cuatro subgrupos: el CG con inestabilidad cromosómica (CIN, 50%), con inestabilidad de microsatélites (MSI, 22%), genómicamente estable (20%) y con infección del virus Epstein-Barr (EVB, 9%). Esta nueva clasificación, junto con

otras que se han publicado *a posteriori*, ofrecen una visión más amplia del GC, teniendo en cuenta nuevas características genéticas y moleculares que permitirán el descubrimiento de nuevas dianas accionables, que puedan mejorar el pronóstico y supervivencia de los pacientes con CG.

El gen *ARID1A* forma parte del complejo SWI/SNF, encargado de remodelar la cromatina para el control de la expresión génica mediante la remodelación de los nucleosomas en los promotores génicos. Dado a su papel regulador de la expresión génica, las mutaciones en los diversos componentes del complejo SWI/SNF, incluyendo las que ocurren en *ARID1A*, causan la desregulación de diversas rutas metabólicas, muchas de las cuales se han relacionado con el desarrollo del cáncer. De todas las mutaciones descritas en las distintas subunidades del complejo, las ocurrientes en *ARID1A* son las más comunes, detectadas en alrededor del 20% de los cánceres, y en el 20% de los pacientes con CG.

Las mutaciones en *ARID1A* suelen resultar en la pérdida de expresión de la proteína, y se asocian con el subgrupo de CG con inestabilidad de microsatélites, mutaciones activadoras de la ruta PI3K, así como con un genotipo wild-type (WT) para la proteína p53. Diversas funciones, aparte de la regulación de la expresión génica han sido atribuidas a *ARID1A*, incluyendo el mantenimiento de la integridad genética, mediante su interacción con diversas proteínas relacionadas con procesos de reparación del DNA. Así, *ARID1A* ha sido descrita como una proteína clave en el proceso de decatenación del DNA, facilitando su reparación tras una ruptura de doble cadena mediante su interacción con la Topoisomerasa IIA y ATR. En relación con estas observaciones, se ha descrito que el silenciamiento simultáneo de otras proteínas clave en este proceso de reparación, junto con el de *ARID1A* conduce a la muerte celular por medio de un fenómeno denominado "letalidad sintética". La letalidad sintética, es descrita como un escenario en que la pérdida no simultánea de dos genes permite la viabilidad celular, pero la ausencia simultánea de ambos genes causa la muerte de la célula. Así, estudios previos han demostrado que genes relacionados con la reparación del DNA, como es el caso de *EZH2*, *ARID1B*, *PARP* y *ATR*, son letalmente sintéticos con *ARID1A*, y por tanto causan la muerte de las células cancerígenas deficientes en *ARID1A* cuando son inhibidos. Estos estudios han sido realizados principalmente, por medio del uso de modelos cáncer de ovario, en el cual las mutaciones en *ARID1A* son altamente frecuentes (alrededor del 40%

de los casos en el caso de los carcinomas de células claras de ovario). Los fármacos que tienen como diana algunos de estos genes, como los inhibidores de PARP están siendo actualmente utilizados en la práctica clínica para tratar a los pacientes con cáncer de mama, ovario o próstata que presentan mutaciones en los genes *BRCA1* y *BRCA2*, los cuales juegan un papel central en las rutas de reparación del DNA. Asimismo, los inhibidores de ATR (iATR) están comenzando a ser probados en diversos ensayos clínicos, algunos de los cuales pretenden tener cuenta, retrospectivamente, la presencia de mutaciones en *ARID1A* y otros genes que puedan conferir sensibilidad a dichos inhibidores.

Aunque los iATR se han convertido en terapias anticancerígenas prometedoras, los mecanismos de resistencia farmacológica son muchas veces inevitables, lo cual enfatiza la importancia de identificar biomarcadores de respuesta y resistencia a dichos fármacos, con el objetivo de encontrar combinaciones terapéuticas que puedan proporcionar una respuesta clínica más eficaz y a largo plazo.

Es por todo esto, que este proyecto se centra en el estudio de *ARID1A* como un biomarcador potencial de la sensibilidad a los inhibidores de proteínas implicadas en las rutas de reparación del daño al DNA en CG, así como en la búsqueda de biomarcadores de resistencia a los iATR, lo cual nos permitirá diseñar nuevas combinaciones de fármacos que eviten la aparición de mecanismos de resistencia a dichos inhibidores en los pacientes con CG.

Por ello, los objetivos del presente proyecto son:

1. Probar los fármacos inhibidores de proteínas letalmente sintéticas con *ARID1A* en un panel de células tumorales y en modelos isogénicos de cáncer gástrico.
2. Validar las relaciones de letalidad sintética descritas *in vitro* por medio de modelos murinos de cáncer gástrico o PDXs (patient-derived Xenografts).
3. Identificar mecanismos de resistencia a los inhibidores de ATR en cáncer gástrico por medio del uso de tecnologías de cribado genético y creación de modelos de resistencia.

Metodología principal utilizada en esta tesis

Con el ánimo de alcanzar dichos objetivos, se han utilizado múltiples tecnologías comunes en biología celular y genética funcional, siguiendo los protocolos previamente descritos en la literatura (Western Blot, PCR, cultivos celulares, extracción de DNA, RNA y proteínas). A continuación, se describen los materiales y modelos utilizados, así como la metodología más novedosa utilizada en esta tesis, que se basa en la creación de modelos isogénicos y en los experimentos de cribado genético de alto rendimiento.

Modelos usados en esta tesis

Los ensayos *in vitro* se han realizado mediante el uso de un panel de siete líneas celulares de CG (SNU 1, SNU 5, SNU 484, SNU 638, NCI N87, AGS y YCC6), así como la línea celular de cáncer colorrectal isogénica para el gen *ARID1A*, HCT 116. Todos los modelos han sido caracterizados por medio de la secuenciación del exoma, así como por PCR cuantitativa y western blot de los genes y proteínas de interés. Adicionalmente, las líneas celulares han sido caracterizadas para su estatus de inestabilidad de microsatélites. Para los ensayos *in vivo* se han utilizado cuatro modelos murinos derivados de tumores gástricos humanos (PDX) deficientes para el gen *ARID1A*, y tres modelos *ARID1A* WT. Dichos modelos han sido caracterizados por medio de la secuenciación del exoma (DNA), secuenciación del transcriptoma (RNAseq), inmunohistoquímica para la expresión de *ARID1A* (IHQ), y determinación de la inestabilidad de microsatélites (MSI). Los experimentos con ratones han sido realizados por la empresa CrownBio.

Experimentos de respuesta a fármacos

La evaluación de la respuesta de los modelos celulares a los inhibidores probados se ha realizado mediante el uso de los siguientes inhibidores: para iATR, los fármacos VX970, AZD6738 y M4344; para PARP, olaparib y talazoparib; para la ruta PI3K, MK2206 y BKM120; para HDAC6, ACY1215; y para EZH2, GSK126. Así, la eficacia de dichos inhibidores en los diversos modelos utilizados se ha evaluado por medio de experimentos de proliferación celular, en los que se ha medido la capacidad proliferativa de las células tras exponerlas a diversas dosis del inhibidor a lo largo de 5 días, en placas de 384 pocillos. El número de células vivas tras la exposición al fármaco utilizado se ha determinado por medio del uso del reactivo cell titre glo, que

emite una señal fluorescente solamente en el caso de que la célula esté viva.

Experimentos de cribado genético (CRISPR screens):

En el caso de los experimentos de cribado genético se ha utilizado la técnica CRISPR/Cas9, que se basa en la habilidad de la endonucleasa Cas9 de cortar el DNA en una secuencia determinada, dirigida por un RNA guía (gRNA). Así, una vez el enzima Cas9 es dirigido a la secuencia diana, ésta es capaz de cortar ambas hebras del DNA, causando mutaciones que pueden dar lugar a la pérdida de función del gen escogido. En esta tesis, se ha utilizado dicha técnica, no solo para editar el genoma de una manera dirigida (creación de modelos isogénicos para *ARID1A* y otros genes de interés), sino también para la realización de cribados genómicos de alto rendimiento y la identificación de dianas moleculares de relaciones de letalidad sintética con los iATR (“CRISPR screens”). En este caso, y con el objetivo de encontrar biomarcadores de resistencia a los iATR, se han llevado a cabo dos tipos de cribado mediante CRISPR. El primero de ellos, denominado CRISPRn screen, se ha realizado a escala de todo el genoma (GW CRISPR screen, con gRNAs para alrededor de unos 20,000 genes), y consiste en la simultánea producción de mutaciones de pérdida de función del gen a lo largo de todo el genoma en una población de células, en la que cada célula es mutada en sólo uno de los genes. Ésta población es pues sometida a altas dosis del fármaco iATR (VX970 en éste caso), bajo las cuales, solamente las células con mutaciones en genes que confieren una ventaja selectiva son capaces de sobrevivir y proliferar. La secuenciación del DNA extraído de las células resistentes (Next-Generation Sequencing) y el correcto análisis de los resultados, permite conocer los gRNAs que se encuentran sobre-representados en dicha población resistente y, por tanto, los genes que, al ser mutados confieren resistencia a los iATR. El otro tipo de CRISPR screen utilizado es el llamado CRISPRx, en el cual se utiliza un enzima Cas9 sin capacidad endonucleasa, que retiene la habilidad de unión al DNA en una secuencia específica, por medio de la dirección del gRNA. Es entonces, cuando la adición de enzimas editoras del DNA (desaminasas), capaces de causar sustituciones de bases en la secuencia diana (por medio de su unión con la Cas9), son transfectadas al interior de la célula. Así, se consiguen realizar sustituciones de aminoácidos en la zona circundante a la secuencia complementaria al gRNA, sin realizar roturas de la doble hélice de DNA. Esta variante del CRISPR, permite evaluar los efectos que

determinadas mutaciones puntuales tienen sobre la funcionalidad de la proteína diana. En esta tesis, esta tecnología ha sido utilizada para realizar sustituciones de aminoácidos del gen *ATR* a lo largo de toda su secuencia, ya que éste es un gen esencial en la célula, y las mutaciones troncales (que eliminan completamente *ATR* de la célula) no pueden ser evaluadas de una manera funcional.

Silenciamiento de genes

Los experimentos de silenciamiento de genes han sido llevados a cabo por medio de la transfección inversa de las células con RNAs silenciadores (siRNAs).

Creación de modelos isogénicos de resistencia a los iATR

La creación de las líneas celulares resistentes a los iATR se ha realizado por medio de la exposición progresiva a dosis ascendientes del fármaco VX970 en un periodo de 4-6 meses. Así, se han generado los clones H1, H2, H3, H4, H5, H6 y M1, que han sido sometidos a la secuenciación del proteoma por medio de técnicas de espectrometría de masas.

Ciclo celular

La medición del ciclo celular ha sido llevada a cabo por medio de técnicas de citometría de flujo, tras la tinción de las células con yoduro de propidio (marcador de la cantidad de DNA en cada fase del ciclo) y EdU (marcador de la síntesis del DNA).

Análisis estadístico

Todos los análisis estadísticos han sido llevados a cabo por medio del programa GraphPad Prism, excepto el análisis de los resultados de los CRISPR screens, en cuyo caso se ha utilizado el programa R.

Resultados principales de esta tesis

1. *ARID1A* y *ATR* son sintéticamente letales *in vitro*

En la primera parte de la tesis, se ha llevado a cabo la caracterización de un panel de líneas celulares de CG, y se ha probado su sensibilidad a diversos inhibidores que han sido previamente definidos como efectivos en modelos deficientes en *ARID1A*, en otros tipos de cáncer (inhibidores de *ATR*, *PARP*, *PI3K*, *HDAC6* y *EZH2*). De todos

los inhibidores probados, se ha observado que las líneas celulares con mutaciones en *ARID1A* son especialmente sensibles a los iATR, tanto en el caso del panel de líneas celulares de CG, así como en el modelo isogénico HCT 116. Esto se ha observado fundamentalmente en los casos en los que las líneas celulares presentaban niveles nulos de expresión de *ARID1A*. Con el objetivo de validar estas observaciones, se han realizado tanto experimentos de silenciamiento de *ARID1A* en líneas celulares resistentes para los iATR por medio del uso de siRNAs, así como la generación de una línea celular de CG isogénica para *ARID1A*. En ambos casos, el silenciamiento del gen o la represión de la expresión de la proteína *ARID1A* ha causado un incremento en la sensibilidad de las células cancerígenas a los iATR, demostrando que *ARID1A* y *ATR* son sintéticamente letales en las líneas celulares de CG.

2. *ARID1A* y *ATR* son sintéticamente letales *in vivo*

Para validar las observaciones descritas en las líneas celulares, se han utilizado siete modelos murinos derivados de tumores gástricos humanos, en los cuales se ha probado la respuesta al iATR M4344 en modelos deficientes para *ARID1A*, así como en modelos WT. Consecuentemente con lo que hemos observado *in vitro*, los ratones con tumores deficientes para *ARID1A* han demostrado ser exquisitamente sensibles a los iATR, comparados con el grupo control. En el caso de dos de los tres modelos de PDX *ARID1A* WT, se ha observado que el tratamiento con M4333 es capaz de reducir la proliferación del tumor, a una escala mucho menor que en los casos deficientes para *ARID1A*. Sorprendentemente, uno de los modelos *ARID1A* WT ha resultado ser altamente sensible a M4344, indicando que *ARID1A* no es el único determinante de sensibilidad a iATR en CG. En este último caso, y con el objetivo de determinar las causas de la sensibilidad detectada en este modelo, se han recogido los tumores resultantes al final del experimento, para su caracterización molecular y la determinación de nuevos biomarcadores de sensibilidad a los iATR. Adicionalmente, se ha probado el tratamiento combinatorio de M4344 con un inhibidor de PARP (talazoparib), con el objetivo de observar si la combinación de ambos fármacos es capaz de mejorar la respuesta en los modelos murinos. En este caso, hemos observado como la combinación de M4344 y talazoparib tiene un impacto incluso mayor en el tamaño del tumor en varios de los modelos usados, pero esto parece ser independiente del estatus de expresión de *ARID1A* en dichos modelos.

3. Determinación de biomarcadores de resistencia a los inhibidores de ATR

Aunque los iATR prometen ser un tratamiento efectivo para los cánceres con defectos genéticos en las proteínas reparadoras del DNA, los pacientes que reciben tratamientos en monoterapia corren el riesgo de sufrir resistencias terapéuticas a largo plazo. Es por ello por lo que las combinaciones de fármacos suelen ser más efectivas a la hora de detener el desarrollo de las células tumorales de una forma efectiva. Para determinar los fármacos que pueden potenciar el efecto de los iATR y evitar la aparición de resistencias, es importante detectar los genes implicados en el desarrollo de dichas resistencias. Para ello, hemos seguido tres aproximaciones: CRISPR screens de todo el genoma “genome-wide (GW) CRISPR screens”, generación de modelos isogénicos resistentes a los iATR y CRISPRx screens.

3.1. GW CRISPR screens:

La realización de un GW CRISPR screen en la línea de CG YCC6, nos ha permitido detectar una larga lista de biomarcadores potenciales de la resistencia a los iATR, por medio de la selección de las células resistentes a altas dosis del fármaco, tras producir en ellas mutaciones individuales a lo largo de todo el genoma (una mutación por célula).

Al probar una lista de alrededor de 20.000 genes, un análisis riguroso y meticuloso de los datos debe ser llevado a cabo para poder descartar los resultados verdaderos de los falsos positivos y falsos negativos. Adicionalmente, es necesaria la realización de diversos experimentos de validación de los descubrimientos por medio del uso de formatos y modelos ortogonales. Con este objetivo, se ha realizado un subsecuente mini-CRISPR screen, en el que se ha probado un número reducido de genes seleccionados, escogiendo los que resultaron tener una mayor significatividad estadística en el estudio inicial. De esta forma, hemos podido validar el papel de los genes *CDC25B*, *HUWE1*, *HNRNPF*, *CARD10*, *SMG8*, *SMG9*, *IRF9*, *STAT1* y *STAT2* en la resistencia a los iATR. Además, se han creado modelos isogénicos de algunos de los genes validados, con el objetivo de llevar a cabo experimentos funcionales que permitan determinar el mecanismo por el cual estos genes causan resistencia a los iATR.

3.2. Los modelos isogénicos resistentes a los iATR han permitido definir una lista de determinantes de resistencia terapéutica

Con el objetivo de obtener los modelos relevantes, que nos permitan determinar nuevos biomarcadores de resistencia a los iATR, se han generado diversos clones de células resistentes a los iATR a partir de la línea celular de CG, YCC6. Estos clones han sido caracterizados para la expresión del proteoma (por medio de la medición de la expresión más de 9.000 proteínas), a través de técnicas de espectrometría de masas. Así, se han podido evaluar los cambios significativos de expresión de proteínas, potencialmente ligados a la aparición de la resistencia terapéutica. Sorprendentemente, varios de los clones resistentes presentan un cambio en la morfología celular, pasando de ser células originalmente epiteliales, a células con una morfología más mesenquimal, indicativa de un elevado potencial metastático de las células cancerígenas. Esto se ha correlacionado con el hecho de que diversas proteínas, implicadas en la adhesión celular, adhesión a la matriz extracelular y en la definición del citoesqueleto se encuentran desreguladas en dichos clones resistentes. Entre estas proteínas se encuentran las codificadas por los genes *CDH1*, *n-CAM*, *KRT7*, *KRT19*, *SMAD4*, *PIK3CB*, *SPTBN1*, *ITGB4*, *PARD6B*, *ROCK2*, *RHOB*, *PAK1*, *ECM1*, *MLLT4*, *EZR*, *VIM*, *ARHGAP21* y *CD2AP*.

Aparte de la desregulación de las proteínas implicadas en la determinación de la morfología celular, otras proteínas, también potencialmente relevantes en los fenómenos de resistencia a los iATR han sido detectadas. Éstas incluyen proteínas ampliamente relacionadas con cáncer como son *MET*, *HRAS*, *PIK3CB*, *NF1*, *TYK2* y *STAT5B*.

Llamativamente, la proteína *SMG1* se encuentra sobreexpresada en los clones resistentes, cuando son comparados con las células parentales. *SMG1* es una proteína quinasa central en el mantenimiento de la estabilidad genómica de la célula, por medio de la degradación de los RNAs mensajeros defectuosos. *SMG1* es negativamente regulada por el heterodímero formado por las proteínas *SMG8* y *SMG9*, las cuales han sido definidas en la sección anterior como causantes de resistencia a los iATR. Es por esto por lo que, tras validar que la proteína *SMG1* esta sobreexpresada en los clones resistentes por medio de western blot, hemos realizado experimentos de silenciamiento de *SMG1* utilizando siRNAs. Estos experimentos han demostrado que al silenciar *SMG1*, las células resistentes vuelven a ser sensibles a los iATR. Esto nos indica el interés de probar la combinación de

los iATR con los inhibidores de SMG1 en ensayos clínicos, con el objetivo de evitar resistencias a los iATR en CG.

3.3. Las mutaciones en el dominio FAT de ATR causan resistencia a los iATR (CRIPRx screens)

Finalmente, con el mismo objetivo de determinar los procesos genéticos por los cuales las células cancerígenas pueden resultar resistentes a los iATR, hemos modificado genéticamente la línea celular YCC6, causando mutaciones a lo largo de toda la secuencia del gen *ATR*. Esto nos ha permitido determinar qué zonas de la proteína son relevantes a la hora causar resistencias a su inhibición en nuestros modelos. Tras el evento de mutagénesis, se han seleccionado las células resistentes por medio del tratamiento con altas dosis de los iATR y secuenciado el gen *ATR*, para determinar cuáles son las mutaciones causales de dicha resistencia. Así, hemos detectado que las mutaciones en el dominio FAT de *ATR* son capaces de transformar las células cancerígenas, previamente sensibles, en células resistentes a los iATR. Con el objetivo de validar estas observaciones, se pretende crear modelos isogénicos mutados para esta zona del gen *ATR*, en los que podamos determinar si las causas de esta resistencia son estructurales (debidas al bloqueo de la unión del inhibidor a la molécula de *ATR*) o funcionales (por la función anormal de *ATR* en la célula).

Implicaciones biológicas e importancia de los resultados presentados en esta tesis

En este estudio, se ha demostrado por primera vez que *ARID1A* es un candidato valioso como biomarcador de sensibilidad a los iATR en CG, tanto por medio de modelos celulares (en el panel de células y en modelos isogénicos de CG) como en modelos animales (PDXs). Debido al hecho de que *ARID1A* se encuentra mutado en alrededor del 20% de los CGs, se plantea el interés del diseño de ensayos clínicos que permitan probar los iATR en pacientes con CG deficiente para *ARID1A*. Esto podría mejorar el pronóstico y la supervivencia de dichos pacientes. Asimismo, se abre la puerta a la valoración del uso de dichos inhibidores en cánceres provenientes de otras histologías, ya que las mutaciones en *ARID1A* son comunes en muchos otros tipos de cánceres.

Por otro lado, en esta tesis se han identificado y validado una lista de biomarcadores de resistencia a ATRi, lo cual abre la posibilidad a probar nuevas combinaciones de fármacos que puedan incrementar el éxito del uso de los iATR por medio del detenimiento de la aparición de metástasis, la mejora de la supervivencia y calidad de vida de los pacientes con CG.

Finalmente, se resalta la importancia de evaluar a los pacientes seleccionados para su tratamiento con los iATR en ensayos clínicos, para las mutaciones en el gen *ATR*, ya que estas pueden evitar una respuesta farmacológica completa al tratamiento, por medio del bloqueo de la unión del inhibidor a la proteína o, por medio de la alteración de la función de ATR en la maquinaria celular. De esta forma, será posible mejorar la selección del inhibidor a utilizar y la prevención de posibles resistencias al tratamiento.

Conclusiones

Como parte de las conclusiones de la tesis presentada, se ha:

1. Demostrado que la inhibición de ATR causa letalidad sintética en los cánceres gástricos con deficiencias en el gen *ARID1A*. Esto se ha evaluado por medio del uso de un panel de líneas celulares, modelos isogénicos celulares y modelos murinos derivados de tumores humanos.
2. Propuesto que los genes *HUWE1*, *HNRNPF*, *IRF9*, *SMG8*, *SMG9*, *CARD10*, *CDC25B* y *STAT2*, deben ser evaluados como potenciales biomarcadores de la resistencia a los inhibidores de ATR en pacientes con cáncer gástrico.
3. Descrito que la sobreexpresión del gen *SMG1*, consecuencia de la pérdida de expresión de sus reguladores *SMG8* y *SMG9* conduce a la resistencia a los inhibidores de ATR en cáncer gástrico.
4. Identificado una lista de potenciales biomarcadores de resistencia a los inhibidores de ATR en cáncer gástrico por el medio de la creación de modelos isogénicos terapéuticamente resistentes.

5. Descrito que mutaciones en el dominio FAT del gen *ATR* causan resistencia a los inhibidores de ATR y por tanto debe considerarse su evaluación a la hora de someter a los pacientes de cáncer gástrico a dicho tratamiento en los ensayos clínicos.

